A COMPREHENSIVE STUDY OF DRINKING WATER COAGULATION WITH ALUMINUM SULFATE

by

Amir Younis Alansari

A dissertation submitted to the faculty of
The University of North Carolina at Charlotte
in partial fulfillment of the requirements
for the degree of Doctor of Philosophy in
Civil Engineering

Charlotte

2021

Approved by:

_____
Dr. James E. Amburgey

_____
Dr. Olya Keen

_____
Dr. Mei Sun

_____
Dr. Jordan C. Poler

_____
Dr. Terry T. Xu

ABSTRACT

AMIR Y. ALANSARI. A Comprehensive Study of Drinking Water Coagulation with Aluminum Sulfate. (Under the direction of DR. JAMES E. AMBURGEY)

Coagulation is usually the first and most important step in conventional drinking water treatment processes. The efficiency of all downstream processes is directly dependent on the effectiveness of the coagulation stage. Coagulants such as aluminum sulfate (alum) have been used for treating drinking water for over a century now. Since the early 1900s, researchers have been studying coagulants in hopes of understanding the mechanisms by which they help remove contaminants from water. Despite the significant contributions and breakthroughs by many researchers, we still rely on a trial-and-error process (jar testing) to optimize coagulation. Accurately modeling the coagulation process has been nearly impossible because water is a chemically complex medium that varies spatially and temporally. There are also many competing and interacting factors that influence how coagulants interact with contaminants and the resulting overall treatment efficiency.

This research aimed to develop an accurate computer model for coagulation with aluminum sulfate with practical, real-world applications. The study identified and addressed five primary challenges related to the study and modeling of coagulation. The five challenges were as follows: (1) independently control water quality parameters, (2) isolate the effects of coagulation dose and pH, (3) standardize the jar test procedure, (4) identify performance metrics that are scalable and independent of jar test mixing parameters, and (5) establish effective optimization strategies. A design of experiments approach was used to create 16 synthetic waters based on four water quality factors (dissolved organic carbon (DOC), specific ultraviolet absorbance (SUVA), alkalinity, and

turbidity) at two discrete levels. An extensive dataset was built by measuring the performance at 1,632 unique combinations of water quality and coagulation conditions where all relevant coagulation factors – water quality, coagulation conditions, and mixing parameters – were tightly controlled. The measured performance metrics were settled and filtered water turbidity, DOC, UV_{254}, zeta potential, and total chemical costs.

Efforts to predict turbidity removals using simple regression models were unsuccessful. The regression models considered ranged from linear regression models with varying complexity to more advanced regression models based on machine learning such as support vector machines and gaussian process regression. When tested on a new water (i.e., one that was not used to train the model), the root-mean-square error (RMSE) of the predicted turbidity ranged between 28 – 37%, while the R^2 values ranged between 0.41 – 0.64. It was apparent that regression models could not model all the complex underlying non-linear behaviors of the coagulation process.

On the other hand, a deep neural network (DNN) trained on the same dataset produced acceptable results. The RMSE and R^2 values of the trained neural network (on the test dataset) were 9.6% and 0.88, respectively. The user input parameters were only DOC, SUVA, alkalinity, and turbidity of the raw water. More importantly, the trained neural could generate a contour plot (a process that requires 17 jar tests to produce experimentally) that correctly predicted the size and shape of the effective coagulation boundaries with acceptable accuracy. Similarly, the model correctly predicted the behavior of the coagulation process to changes in water quality conditions (e.g., an increase in SUVA). The trained neural network could also predict full-scale filtered turbidity removals within ±1.4% at 11 different drinking water treatment plants under cold and warm water conditions. It should be emphasized that these results were obtained simply by providing raw water quality parameters. The model was only trained to predict filtered water

turbidity removals using synthetic waters. It can be concluded that deep neural networks are ideally suited for modeling complex drinking water treatment problems such as coagulation, a task in the past considered to be virtually impossible.

ACKNOWLEDGEMENTS

I would like to express my sincere gratitude to my committee chair and advisor, Dr. James Amburgey. I am grateful for his guidance, patience, trust, motivation, and friendship over the last twelve years. Under his mentorship, I was always able to freely follow my curiosity and work on challenges to grow my skillsets as a researcher and an engineer. No words can describe the profound influence that Dr. Amburgey had in all of my accomplishments throughout the years. I would also like to thank my committee members, Dr. Olya Keen, Dr. Mei Sun, Dr. Jordan Poler, and Dr. Terry Xu, for their valuable time and feedback.

I would like to extend my appreciation to Dr. Benjamin Radford, who's guidance and assistance were paramount in my efforts to model the coagulation process. I would like to thank Dr. James Edzwald who generously offered his time and invaluable expertise on more than one occasion. I would also like to thank Mark Hahn for always taking the time out of his busy schedule to send me data from utilities around the state. I am especially grateful to Brian Wilson at the City of Newton water treatment plant. Brian was always willing to provide me with access to raw water samples and full-scale data. Knowing that I am always eager to learn new things, Brian has even invited me on several occasions to explore inside tanks, flocculation basins, and sedimentation basins, and many more process while they were being cleaned or maintained.

I was extremely fortunate to have received the full financial support of the government of the U.A.E. in my pursuit of a higher education. Their backing allowed me to completely dedicate myself towards my education and research.

I was blessed to have the unconditional love and support of my parents and family. They always encouraged me to follow my dreams and be the best version of myself that I could be. Last, I couldn't have done this without the love and encouragement of my best friend and partner, Nathalia.

TABLE OF CONTENTS

LIST OF TABLES

LIST OF FIGURES

LIST OF ABBREVIATIONS

°C	degrees Celsius
µeq/L	microequivalent per liter
µeq/mg	microequivalent per milligram
µm	micrometer
µS/cm	micro Siemens per centimeter
µg/L	micrograms per liter
Abs	absorbance
Al^{3+}	aluminum ion
$Al(OH)_3$	aluminum hydroxide
Alum	aluminum sulfate
$CaCO_3$	calcium carbonate
DBP	disinfection by-products
DI	deionized
DOC	dissolved organic carbon
EDL	electrical double layer
ft	feet
FI	flocculation index
gpm	gallons per minute
L	liter
L/mg · m	liter per milligram per meter
M	molar
m^2	meter squared

mg/L	milligram per liter
mL	milliliter
mM	millimolar
mm	millimeter
mV	millivolts
n	number of samples
N	normal
nm	nanometer
NOM	natural organic matter
NTU	nephelometric turbidity units
ppm	parts per million
rpm	revolutions per minute
SUVA	specific ultraviolet absorbance
SCM	streaming current monitor
T	temperature
UV	ultraviolet
UVA_{254}	ultraviolet absorbance at 254 nm
WTP	water treatment plant
Z	valency

PREFACE

Coagulation is defined herein as the process of adding chemicals to destabilize contaminants in the water treatment process, which is a topic that has been widely studied for over a century. Thanks to the contributions of drinking water treatment researchers such as Langelier, Black, O'Melia, Amirtharajah, Edzwald, and countless others, we have a basic understanding of the mechanisms and factors that are involved. They developed tools that made it possible to monitor and optimize coagulation and published hundreds of peer-reviewed articles and multiple textbook chapters on the topic. Yet, coagulation is often still described as more of an art than a science. Coagulation exists in two discrete realms – theory and practice. Unfortunately, as water treatment theory was developed, it was often necessary to oversimplify this complex phenomenon by making assumptions to fit rudimentary models to facilitate understanding some of the mechanisms at play but have little to no practical, real-world applications. When it comes to practice, the best tool we have at our disposal is based on trial-and-error, which has largely remained unchanged since jar testing was first introduced more than a century ago by Langelier. Many questions about coagulation remain unanswered. However, interest in and research funding for coagulation has been low for decades. To make matters worse, many of the great coagulation teachers and innovators are either deceased or retired, which means there will be a lack of guidance for future researchers and practitioners.

This document will review what is known about coagulation from a practical perspective leaving out some of the theory and adding new research results in an attempt to provide the reader with a clearer and more useful understanding of coagulation. The goal was to bridge the gap between coagulation theory and coagulation practice. In this comprehensive study, well-established practical guidelines and theories were scrutinized, compared, and tested. This study

was limited to a single coagulant – aluminum sulfate (or alum). Hopefully, the same principles and approaches presented in the following pages can be directly applied to many other coagulants used to treat water.

Although this document is being submitted as a doctoral dissertation, it does not read like one or follow the typical format. The document was written in the form of a comprehensive textbook chapter or a manual on coagulation.

CHAPTER 1: COAGULATION

1.1. Why is coagulation key to water treatment?

Coagulation is typically the first step in most conventional surface water treatment plants (Figure 1.1). To a casual observer visiting a treatment facility, this step would probably be the least noticeable or impressive process at the entire facility. In essence, all that is occurring in this step is the addition of a chemical, the coagulant, at a concentration measured in parts per million in water undergoing treatment. However, this seemingly simple step is, in fact, the cornerstone of modern surface water treatment. The success of every single subsequent process after coagulation is directly dependent on the efficiency of this stage. Without coagulation, particles would be too small to settle and too stable to filter. Disinfection would be less efficient and typically lead to the production of higher concentrations of carcinogenic disinfection by-products.

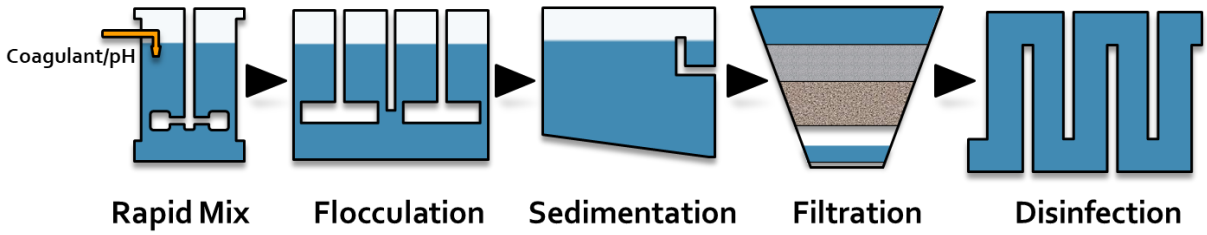

Figure 1.1. A schematic of a conventional surface water treatment plant

In April of 1993, roughly 400,000 residents of Milwaukee, WI suffered from severe nausea, stomach cramps, and watery diarrhea for an average of 7-10 days each. The cause was determined to be the presence of a protozoan pathogen called *Cryptosporidium parvum* in the distribution system (Fox and Lytle 1996). Officials conducted an investigation to determine the cause of the outbreak and found that the treatment plant had elevated filtered turbidity levels for several days leading up to the outbreak (Figure 1.2a). Chlorination is practically ineffective against

Cryptosporidium; therefore, the primary barrier was filtration. Elevated filtered water turbidity levels increase the probability that *Cryptosporidium* will be able to pass through the treatment process. Figure 1.2b shows the direct correlation between turbidity and *Cryptosporidium* removals (LeChevallier and Norton 1992). The removal rate of filters can be improved either by increasing the contaminant's size where it would be too large to pass through the pores or modify the naturally negative surface charge on the contaminant such that it would attach to the negatively charged surfaces of the filter media.

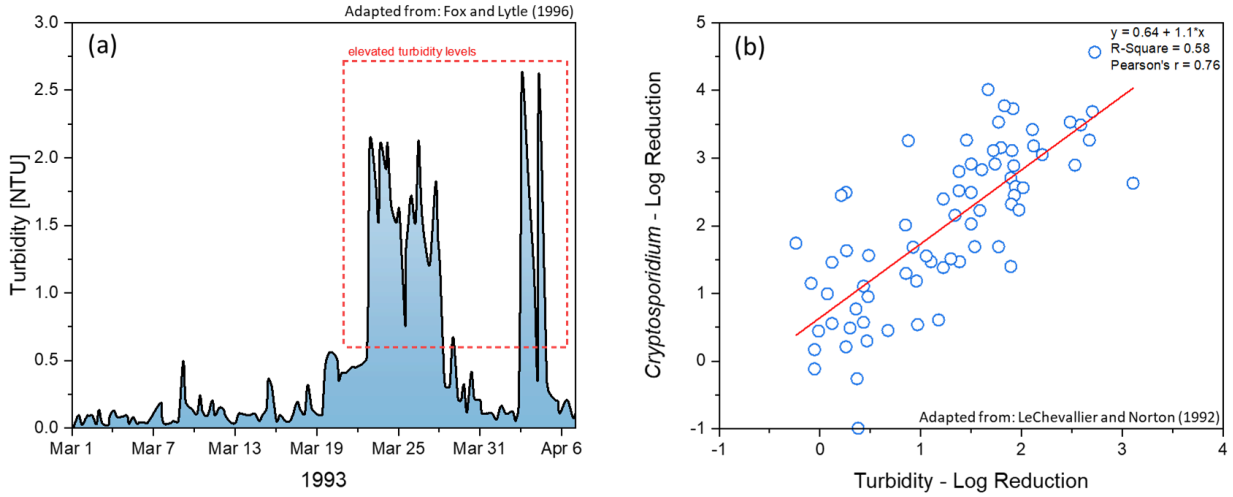

Figure 1.2. (a) Milwaukee filtered turbidity removals (b) Relationship between *Cryptosporidium* and turbidity removals

The purpose of adding a coagulant is to increase the likelihood that a downstream engineered process, such as filtration, would efficiently remove a contaminant of interest. When done correctly, the natural negative surface charge on the *Cryptosporidium* would be modified and result in its aggregation with other particles to form floc that is large enough to settle and close enough to neutrally charged to overcome the electrostatic repulsion forces and attach to the negatively charged filter media. The incident in Milwaukee was quite simply a failure of the

coagulation process, which impacted filtration removals and ultimately allowed *Cryptosporidium* to pass through the treatment system and enter the distribution system at elevated concentrations.

The importance of coagulation is not limited to the removal of chlorine-resistant pathogens such as *Cryptosporidium*. Coagulation reduces the concentration of dissolved natural organic matter (NOM), which is a precursor of carcinogenic disinfection by-products (DBPs) such as chloroform (Reckhow and Singer 1984). Coagulation has also been shown to improve the performance of low-pressure membrane filters by reducing membrane fouling and removing contaminants that are smaller than the membrane's pores (Alansari et al. 2015; Alansari et al. 2016). Coagulation has even been shown to effectively remove microplastics from drinking water (Skaf et al. 2020).

1.2. The Nature of Contaminants

There are many ways to classify contaminants in water. Contaminants may be dissolved, particulate, suspended, colloidal, soluble, insoluble, organic, inorganic, microbial, regulated, unregulated, emerging, anthropogenic, point source, non-point source, or a combination of the above classifications. Classifications could be based on a set of operational criteria or how a given contaminant impacts the water quality. An example of an operational classification is when a water sample is filtered through a 0.45μm membrane filter to determine whether a contaminant is dissolved or particulate. The fraction of the sample that passes through the filter is classified as being dissolved, while the remainder is classified as being particulate. The United States Environmental Protection Agency (USEPA) classifies a contaminant as any physical, chemical, biological, or radiological substance in water.

In surface water treatment, contaminants are generally referred to as particles. Particles of concern are typically in the range of 0.001 – 10μm, including physical, chemical, biological, or radiological substances. Figure 1.3 compares the sizes of some of these particles. A common classification of particles in drinking water treatment is whether particles are suspended or colloidal. Particles larger than 1μm are typically classified as suspended, while particles smaller than 1μm are classified as colloidal. With minimal turbulence, suspended particles eventually settle out of the water, whereas colloidal particles remain in suspension indefinitely. As a result, the removal of colloidal contaminants such as bacteria, viruses, clays, and NOM by sedimentation/settling is expected to be negligible. Thus, the primary barrier against such contaminants would be expected to be filtration.

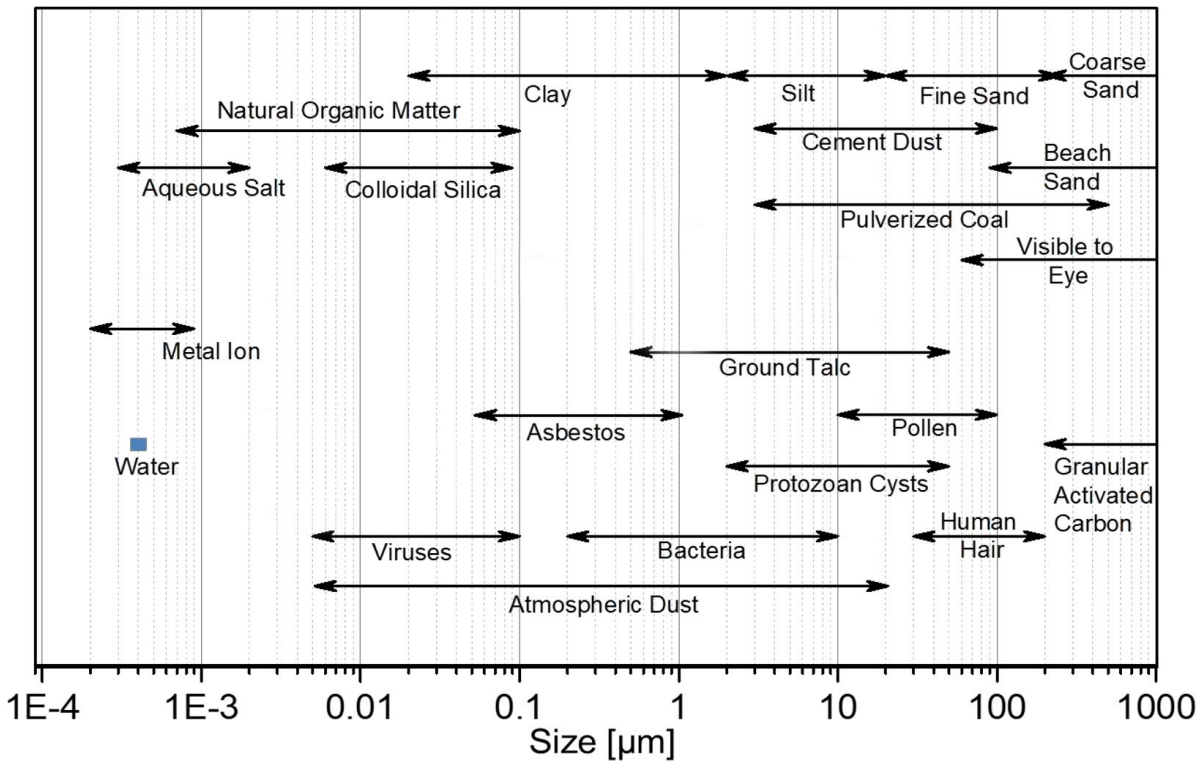

Figure 1.3. Size spectrum of common particles

Membrane filters can consistently produce water free of particles larger than the membrane pores regardless of the incoming raw water quality. Microfiltration membranes can remove particles as small as 0.1μm while ultrafiltration membranes can remove particles as small as 0.001μm. However, the small pores require a relatively high energy input (i.e., pressure) to push the water through the pores, especially as the membrane filter begins to clog. On the other hand, the pores in a sand filter are approximately 50-75μm, which is large enough to be operated by gravity (i.e., static head). Compared to membrane filtration, granular media (sand) filters are cheaper to operate and maintain; however, the large pores also make it possible for all colloidal particles and many of the smaller suspended particles to pass through the filter grains and remain in the treated drinking water supply. Unfortunately, this includes most of the particles of concern, such as protozoan cysts, bacteria, viruses, and NOM. Nevertheless, the preferred filtration method for most surface water treatment plants in the United States has been granular media filtration. So, how does a filter with 75-μm holes remove 5-μm *Cryptosporidium* oocysts or smaller particles?

In layman's terms, the particles must increase in size and/or become stickier. Consequently, the larger particles would be more likely to settle in the sedimentation process or become too large and/or sticky to pass through the filter. It is possible to create larger particles by combining several smaller ones. This process is typically called flocculation, and the aggregate particles are called flocs. For this process to occur, particles must first collide with one another, and their collisions must subsequently result in their sticking together to form a floc. Flocculation, in the context of drinking water treatment, does not occur naturally. Most particles in water have a negative surface charge; therefore, repulsive forces exist between the negatively charged particles that repel them and prevent the formation of floc. The origin of the negative surface charge is of little to no practical significance to the application of coagulation in drinking water treatment. Still, this

information is generally agreed upon and available from multiple sources (Gregory 2005; Bratby 2016; Hendricks 2016). However, it is crucial to understand how surface charge plays a role in the coagulation process.

1.3. Water Treatment Destabilization Mechanisms

Colloidal particles remain in suspension primarily due to their small size and remain separated due to their negatively charged surface. In this state, the particles are referred to as being stable or existing in a stable suspension. Thus, coagulation aims to destabilize these particles, and the process is called particle destabilization. Particle destabilization can be achieved by four mechanisms: (1) compression of the electrical double layer; (2) adsorption and charge neutralization; (3) adsorption and interparticle bridging; and (4) enmeshment in a precipitate (Amirtharajah and Mills 1982; Letterman, Vanderbrook and Sricharoenchaikit 1982; Amirtharajah and Trusler 1986). Bratby (2016) summarized destabilization mechanisms as (1) a reduction of the effective surface charge, (2) a reduction of the zone of influence of the surface charge, and (3) a reduction of the number of adsorbed water molecules.

The predominant mechanisms involved during coagulation for water treatment purposes (represented by the arrows in Figure 1.4) are charge neutralization of negatively charged particles by adsorption of positively charged metal species and sweep flocculation where particles are enmeshed into solid precipitates (Dennett et al. 1996; Johnson and Amirtharajah 1983; Pernitsky and Edzwald 2006). The dominant coagulation mechanism usually depends on the coagulant dose and pH during coagulation. This will be discussed in the subsequent sections.

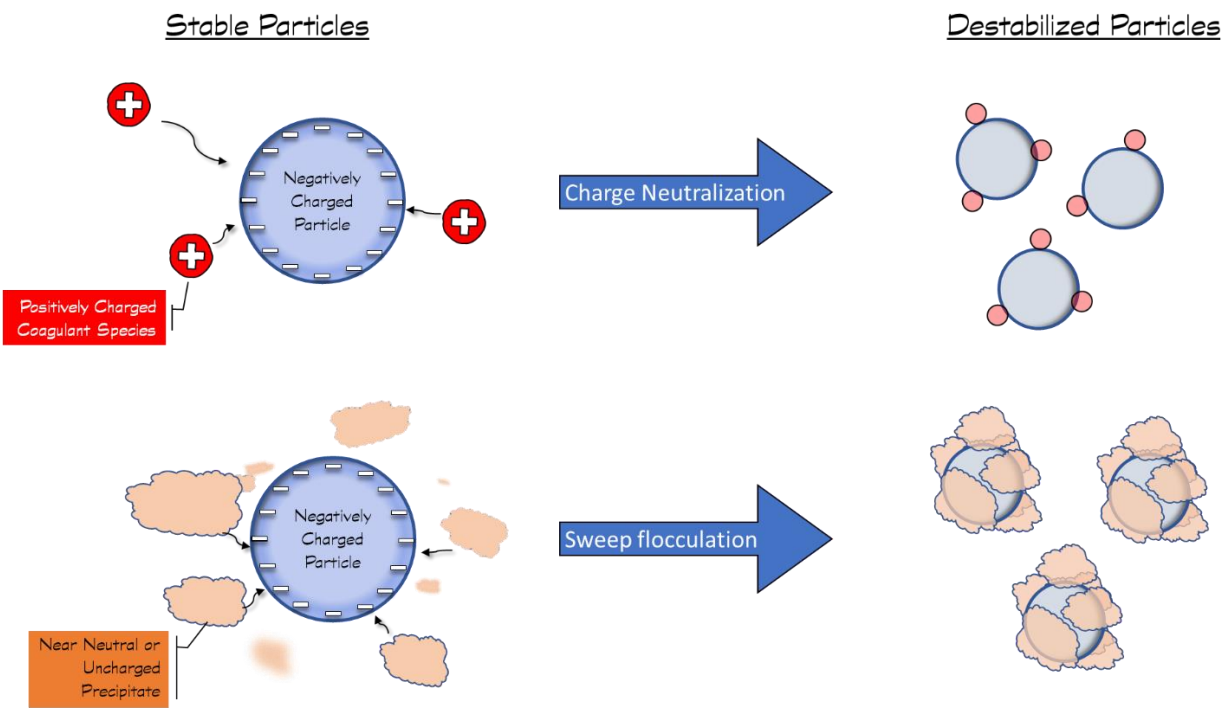

Figure 1.4. Water treatment destabilization mechanisms (after Dennett et al. (1996))

Destabilization of negatively charged particles can be achieved with nearly any metal salt, i.e., one that contains positively charged ions (e.g., sodium chloride or magnesium sulfate). However, researchers more than a century ago discovered that the effectiveness of a metal coagulant was related to its valence (charge number). Specifically, the concentration of cations required to destabilize a negatively charged particle decreases by a factor of $1/z^6$, where z is the valency of the metal coagulant. In other words, the required dose of a +3 coagulant would be roughly 730 times lower than the dose required for a +1 coagulant. This phenomenon is known as the Schulze-Hardy rule.

Figure 1.5 demonstrates the Schulze-Hardy effect with different metal coagulants; however, a careful examination of the results would reveal that the trend does not quite follow the $1/z^6$ ratio (Smith 1920). As quoted by most drinking water treatment textbooks, this is to be expected as the Schulze-Hardy rule is an overly simplistic model of destabilization. The intent here

is simply to demonstrate that trivalent (+3 charge) salts are more effective than divalent (+2 charge) salts followed by monovalent (+1 charge) salts. Again, while monovalent salts can be used to destabilize contaminants in water, the concentrations required would approach seawater levels. For this reason, metal coagulants used in drinking water treatment are generally trivalent types.

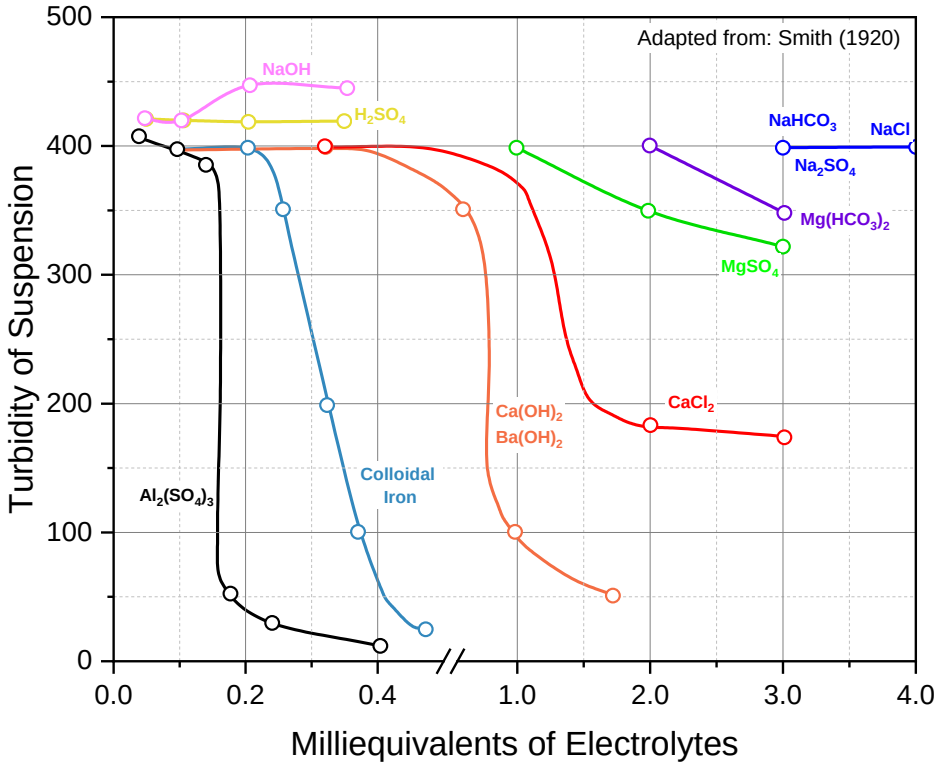

Figure 1.5. Effect of electrolytes on the coagulation and settling of clay suspensions after 1-hour of settling. From (Smith 1920)

1.4. Surface Charge Measurement

Surface charge measurement techniques generally fall under two categories: streaming potential and electrophoresis. The key difference between the two phenomena is whether the liquid is moving relative to the particle (streaming potential) or vice versa (electrophoresis). The phenomena are covered in detail by Gregory (2005).

Most particles in water are negatively charged; however, the suspension as a whole (water and particles) has a net zero charge. Figure 1.6 shows a diagram of a negatively charged particle in solution. Negatively charged particles attract positively charged ions (counterions) to form a rigid layer that surrounds the particle called the Stern layer. The Stern layer is considered to be rigid (fixed) because counterions are adsorbed onto the surface of the negatively charged particle and remain with the particle as it moves relative to the fluid. However, electroneutrality (i.e., zero net charge) is typically not satisfied at the Stern layer; therefore, the field of attractive and repulsive forces extends beyond the Stern layer until electroneutrality is satisfied. As a result, another distinct layer of loosely bound counterions surrounds the particle. The second layer's outer-boundary is called the diffuse layer (also known as the Gouy-Chapman diffuse layer). Ions can freely move between the diffuse layer and the bulk solution. This particle model, along with the layers, is collectively known as the electrical double layer (EDL).

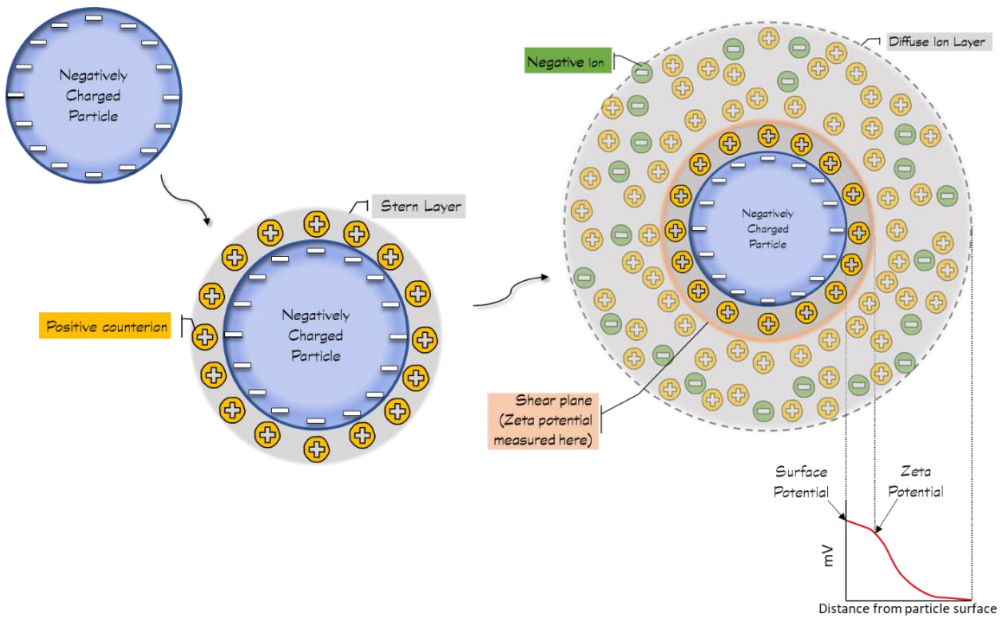

Figure 1.6. The electrical double layer

As noted above, when a particle moves relative to the fluid, the Stern layer moves with the particle while the diffuse layer does not, and those ions can be interchanged with those in the bulk solution. A separation boundary develops between the two layers, known as the shear plane. Measurements of a particle's surface charge cannot be made directly; therefore, most quantifications of a particle's surface charge are made approximately at the shear plane. The potential at the shear plane is called the zeta potential. Zeta potential is measured in units of millivolts (mV). Zeta potentials of particles typically found in water are shown in Table 1.1.

Table 1.1. Zeta potential of particles in water

Particle Type	Zeta Potential [mV]
Clays (kaolinite, montmorillonite)[1]	-15 to -20
Viruses[2]	-15 to -53
Bacteria[2]	-5 to -50
Protozoan Cysts[1,2]	-7 to -40
Algae[1]	-3 to -30
Ottawa Sand at pH 7.0[3]	-100

[1] Hendricks, 2016; [2] Polaczyk et al. 2020; [3] Truesdale et al. 1998

1.4.1. Streaming Current Monitor

A streaming current monitor (SCM) is an instrument that relies on the streaming potential phenomenon. One of the perks of SCM is that readings are immediately available (similar to placing a pH electrode in water) and are representative of the bulk solution. As a result, SCMs have been mostly utilized as continuous (online) monitors to monitor coagulant dosing and maintain optimal performance at drinking water treatment plants (Dentel, Thomas and Kingery 1989). The signal measured by the SCM is proportional to the charge on the surface of the particles (i.e., zeta potential); however, the magnitude and units of the measurement are relative and instrument-specific.

While the SCM has been marketed as a coagulation control strategy, it is essential to note that the SCM signal can be influenced by many factors besides the surface charge of the water. Dentel and Kingery (1989) reported that the plant flow rate, coagulant type and strength, the concentration of solids, pH, conductivity, temperature, detention time, and sensor fouling are all relevant factors that affect the SCM readings. Therefore, a change in the SCM reading should not always be interpreted as a change in coagulation requirements. Manufacturers of online SCMs recommend optimizing coagulation conditions using a jar tester to establish a setpoint.

1.4.2. Zeta Potential

Electrophoresis is a phenomenon that occurs when an electric field is applied to a liquid containing charged particles. Particles travel towards the oppositely charged electrode at a velocity that is a function of their charge, the viscosity of the fluid, and the applied voltage gradient (Black and Hannah 1961; Riddick 1961). Operationally, this phenomenon is quantified in terms of electrophoretic mobility. In early coagulation studies, the process involved microscopically observing a particle and recording the time the particle covered a given distance under an applied voltage (Black and Smith 1962). Compared to streaming current, early electrophoretic measurement techniques had the disadvantage of being relatively lengthy and subjective as it required both the selection and observation of individual particles (Bratby 2016). However, modern advancements in light scattering measurement techniques and instrumentation have primarily addressed these issues.

As noted above, electrophoretic mobility is directly related to the surface charge of the particle, i.e., its zeta potential. Several equations have been proposed for calculating the zeta potential from the experimentally determined electrophoretic mobility (Polaczyk 2010). The

appropriate equation depends on the thickness of the double layer, commonly referred to as the Debye length (κ^{-1}), and the radius of the particle. Most modern instruments allow the user to define or select a zeta potential model for their analyses. Polaczyk et al. (2020) compared five different models used to calculate zeta potential from electrophoretic mobilities of fifteen different microorganisms under simulated surface water conditions. The microorganisms investigated and their recommended zeta potential models are shown in Table 1.2. Additionally, the authors presented a simple graphical guideline for selecting the appropriate zeta potential model (Figure 1.7).

Table 1.2. Recommended zeta potential models for microorganisms in water

Microbe Class	**Organism Name**	**Recommended Model**
Bacteriophages	MS2	Modified Booth
	phi X174	Modified Booth
Human Viruses	HAV HM-175	Henry
	Echovirus 1	Henry
	HAdV2	Henry
	HadV40	Modified Booth
Vegetative Bacteria	F. *tularensis*[a]	Helmholtz-Smoluchowski
	Y. *pestis*[a]	Helmholtz-Smoluchowski
	E. *faecalis*	Helmholtz-Smoluchowski
	S. Typhimurium[a]	Helmholtz-Smoluchowski
	E. *coli*[a]	Helmholtz-Smoluchowski
Bacterial Endospores	B. *atrophaeus*	Helmholtz-Smoluchowski
	B. *anthracis*	Helmholtz-Smoluchowski
Surrogates	Microspheres[b]	O'Brien-Hunter
Parasites	C. *parvum*	Helmholtz-Smoluchowski
	G. *intestinalis*	Helmholtz-Smoluchowski

[a] gram-negative
[b] Carboxylate modified 4.5 μm Fluoresbrite™ YG, Polysciences, Inc

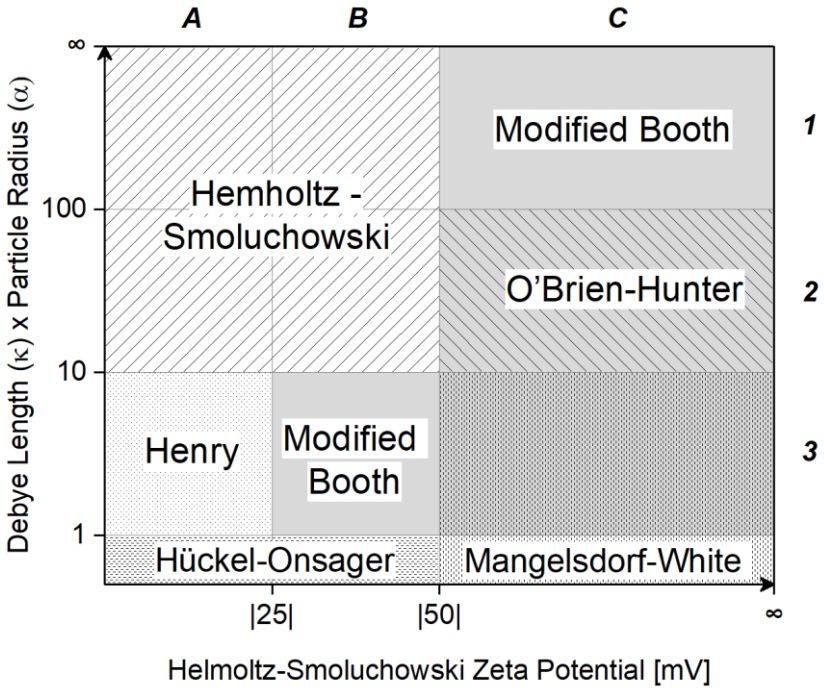

Figure 1.7. Zeta potential model zone chart

1.5. The Zeta Potential Paradox

It is generally accepted that good turbidity removal can be achieved with a post-coagulation zeta potential between ± 5 – 10 mV (Riddick 1961; Pernitsky et al. 2011). Figure 1.8 shows a contour plot of the average zeta potential measurements from a series of jar tests using a synthetic water. The figure was constructed using a total of 102 data points ranging from 3 – 100 mg/L as alum-14 and pH 5.0 – 8.0, represented by the black data points. Post-coagulation zeta potential samples were collected at the end of a one-minute rapid mix stage. The overlaid pattern in Figure 1.8 represents the boundary where the measured filtered turbidity removals were below 0.3 NTU (the current filtered turbidity standard in the United States).

According to Figure 1.8, turbidity removals were generally achieved between pH 6.0 and pH 8.0 above 20 mg/L as alum-14. A close examination of the results revealed that while effective

turbidity removals generally coincided with the recommended zeta potential range, the zeta potential value itself was not a good predictor of turbidity removals. For example, the measured zeta potentials at Conditions A and B (Figure 1.8) were –2.38 (±3.44 mV) and –2.48 mV (±4.05 mV), respectively. Based on the rule of thumb on zeta potential, both conditions would be expected to achieve high filtered turbidity removals; however, the actual filtered turbidity removals were 94% at pH 6.0 at Condition A and –40% at pH 5.5 at Condition B. This suggests that there may be other forces involved in the coagulation process besides the simple electrostatic interactions, as noted by others (Johnson and Amirtharajah 1983).

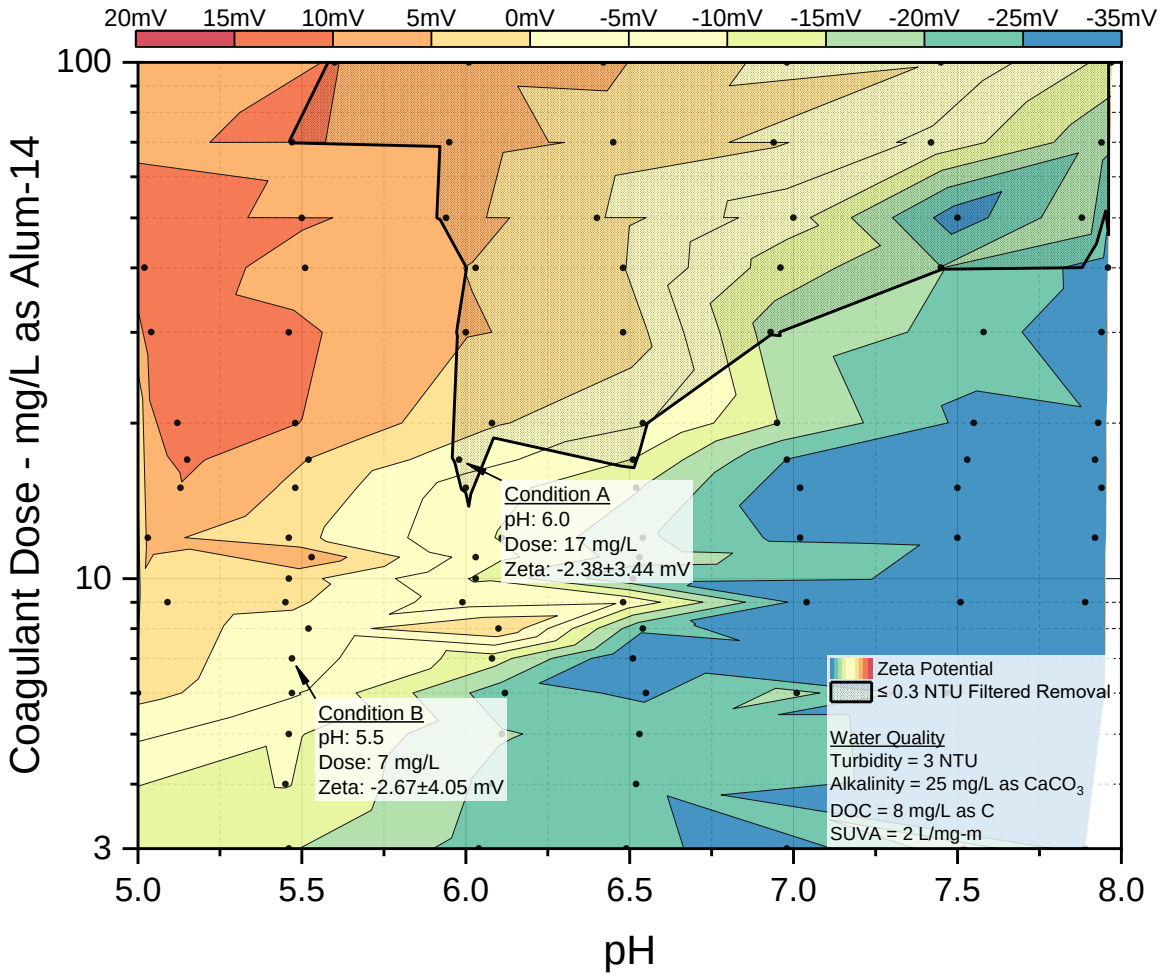

Figure 1.8. Contour plot of average zeta potential measurements

The range of effective zeta potential values leading to good removals may depend on the specific coagulant dose and coagulation pH. Figure 1.9 shows the post-coagulation zeta potential measurements from a series of jar tests with 16 different waters. Details of the jar test procedure and investigated waters will be discussed in subsequent chapters. The post-coagulation zeta potentials were plotted as a function of the applied dose and measured post-coagulation pH. The color of the symbols corresponded to the selected coagulant dose range. For example, blue symbols correspond to conditions where the applied coagulant dose was between 15 and 30 mg/L as alum-14, while red symbols correspond to conditions where the dose was over 30 mg/L as alum-14. The entire range of zeta potential measurements (n=1,632) was plotted in the top panel, whereas only conditions that resulted in a filtered water turbidity of $\leq$ 0.3 NTU were plotted in the bottom panel.

A visual pairwise comparison of the results in the top and bottom panels would provide an estimate of the effective zeta potential range for a given dose and pH. For example, the zeta potential measurements of the low dose conditions (yellow symbols: 3 – 15 mg/L as alum-14) at pH 6.5 ranged from approximately -40 to 5 mV in the top panel; however, a filtered water turbidity below 0.3 NTU was primarily achieved with conditions that had a zeta potential of approximately -20 to 5 mV. Similarly, at pH 6.5, almost all the high dose conditions (red symbols) in the -20 to 10 mV achieved a filtered water turbidity below 0.3 NTU. At pH 6.0, the effective zeta potential range for the high dose conditions increased to 0 to +15 mV.

Figure 1.9 could potentially be used as a guide for selecting a zeta potential range that would likely result in satisfactory removals based on the applied coagulation conditions. However, a close examination of the results would reveal that filtered turbidity removals are not simply a function of the applied dose and measured zeta potential (shown in Figure 1.8), particularly in the

low pH and below 30 mg/L as alum-14 range. For example, approximately 85% of the cases in the range of -10 to 0 mV and pH 5.0 did not achieve a filtered turbidity removal below 0.3 NTU.

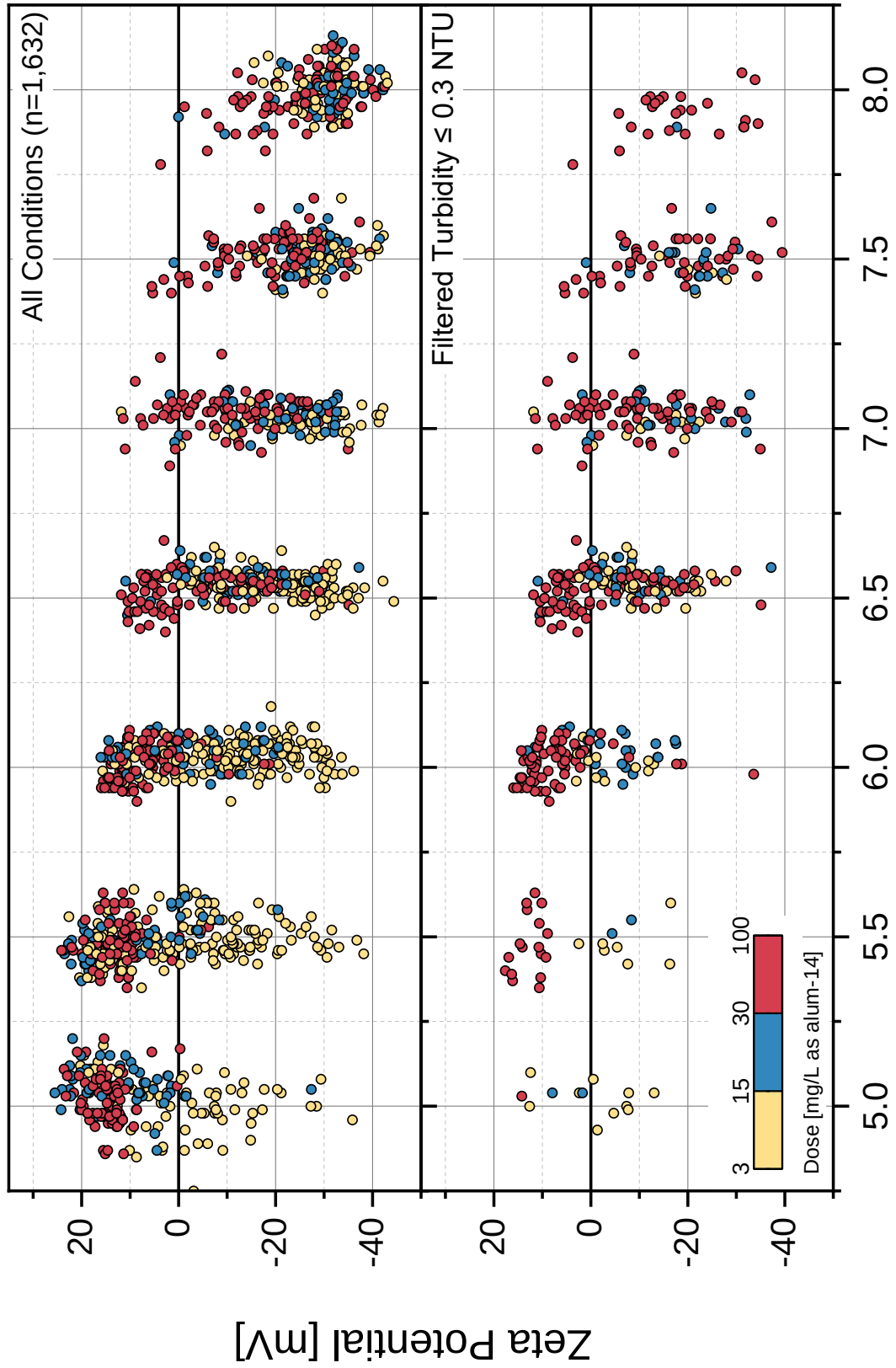

Figure 1.9. Zeta potential measurements of coagulated waters as a function of pH and dose

1.6. Coagulants

Coagulants used in drinking water treatment can be classified as being either metal salts, inorganic polymers, or organic polymers. The third class of coagulants, referred to as natural coagulants, has recently received extensive research interest; however, full-scale applications of these type of coagulants is still very limited. Metal coagulants (also known as inorganic coagulants) have been the preferred coagulant type primarily due to their relatively low cost and high availability. Organic polymers are typically used as coagulant aids. Metal coagulants in drinking water treatment generally fall under two categories: (1) aluminum-based and (2) iron-based. Both types of coagulants are typically available in the form of chlorides (e.g., ferric chloride) and sulfates (e.g., aluminum sulfate). Total chemical costs are usually the primary factor that dictates the selection of a suitable coagulant; however, it can sometimes depend on the type of water being treated and the facility's specific treatment goals (Haarhoff and Cleasby 1988; Crozes, White and Marshall 1995).

Aluminum sulfate (better known as alum) is the most commonly used coagulant in the United States. Alum is available in both dry and liquid form; however, utilities are increasingly choosing the latter form since it is more convenient to use and easier to control the product's quality. The general chemical formula of alum is $Al_2(SO_4)_3 \cdot \text{n}\ H_2O$, where n refers to the degree of hydration and is in the range of 14 – 18. Unfortunately, there is no official standard unit for reporting alum concentrations in the field of water treatment. Liquid alum used in treatment plants is typically in the form of $Al_2(SO_4)_3 \cdot 14\ H_2O$ (also known as dry alum) and is typically reported in parts per million (ppm) units while reagent grade alum used in most research laboratories is typically in the form as $Al_2(SO_4)_3 \cdot 18\ H_2O$ and is typically reported as mg/L as Al.

Calculating the concentration of alum used would require knowledge of the chemical formula, percentage of that chemical, specific gravity of the coagulant, and the treatment plant's flow rate. Coagulants should be supplied with an accompanying Certificate of Analysis (COA) or a technical data sheet that contains information regarding the chemical composition of the product. The stock solution concentration can usually be calculated in units of mass per volume based on the information provided. Alternatively, the coagulant's Safety Data Sheet (SDS) could contain information regarding the chemical composition.

An example of an SDS is shown in Figure 1.10. Equation 1 can be used to calculate the concentration of the alum based on the provided specific gravity and product strength:

$$Concentration\left[\frac{mg}{L}\ as\ product\right] = \%\ [as\ product]\ x\ Specific\ Gravity\ x\ 10{,}000 \qquad (1)$$

9. PHYSICAL AND CHEMICAL PROPERTIES

Appearance	No information available
Color	Clear, light green or amber
Chemical Formula	48.5% Al2 (SO4)3 * 14H2O in water
Odor	Odorless
Odor Threshold	No information available
Physical State	Liquid
pH	~3.5 (1% solution)
Flash Point:	Not flammable
Autoignition Temperature	Not applicable
Boiling Point/Range	101 °C
Melting Point/Range	-16 °C
Flammability Limits in Air	No information available
Explosive Properties	No information available
Oxidizing Properties	No information available
Evaporation Rate	Not determined
Vapour Pressure	Not applicable
Vapour Density	Not applicable
Specific Gravity	1.335
Solubility	No information available
Partition Coefficient (n-octanol/water)	No information available
Viscosity	No information available
Molecular Weight	~594 for Al2 (SO4)3 * 14H2O
Water Solubility	100
VOC Content(%)	~50

Figure 1.10. Example of a SDS for liquid alum (from General Chemical)

In this case, the supplier specified that the product is in units of % as $Al_2(SO_4)_3 \cdot 14\ H_2O$; therefore, the calculated concentration will have a similar unit. Using equation 1, the concentration of the stock liquid alum in this example is thus:

$$Concentration = 48.5\ [\%\ as\ Al_2(SO_4)_3 \cdot 14\ H_2O]\ x\ 1.335\ x\ 10{,}000$$
$$= 647{,}475\ \left[\frac{mg}{L}\ as\ Al_2(SO_4)_3 \cdot 14\ H_2O\right]$$

In some cases, the coagulant's strength is expressed in a different unit than what is required. For example, the strength of the coagulant could be reported as % Al_2O_3 while what is required is the equivalent concentration reported as % $Al_2(SO_4)_3 \cdot 14\ H_2O$. Equation 2 can be used to convert any given coagulant concentration to an equivalent concentration with a different unit provided that the chemical formula is known:

$$Conc.of\ B\ [B\ units] = Conc.of\ A\ [A\ units]\ x\ \left(\frac{MW\ of\ B}{MW\ of\ A}\right) \quad (2)$$

MW = molecular weight [g/mol]

For example, the concentration of the liquid alum solution shown in Figure 1.10 is approximately 725,957 mg/L as $Al_2(SO_4)_3 \cdot 18\ H_2O$ (MW=666 g/mol). Similarly, the concentration of the liquid alum solution is 111,183 mg/L as Al_2O_3 (MW=102 g/mol).

Regardless of the unit selected to represent the coagulant's concentration, what matters is the actual amount of the "active ingredient," in this case aluminum, that is being added and not necessarily the bulk product itself. Figure 1.11 compares the proportions of aluminum, sulfate, and water in the three different forms of alum. It is evident that aluminum only makes up less than 10% of the total amount of liquid alum added. If the same volume of each coagulant solution was added to a water sample, then the actual concentration of aluminum that was added would be different in each of the three samples. The total aluminum concentration would be highest in the water sample that was dosed with alum measured in units of mg/L as $Al_2(SO_4)_3 \cdot 14\ H_2O$ and

lowest in the water sample that was dosed with alum measured in units of mg/L as $Al_2(SO_4)_3 \cdot 18\ H_2O$. To avoid confusion or error, the preferred method of reporting coagulant concentrations in the scientific literature has been in terms of its metal content (e.g., 1.3 mg/L as Al).

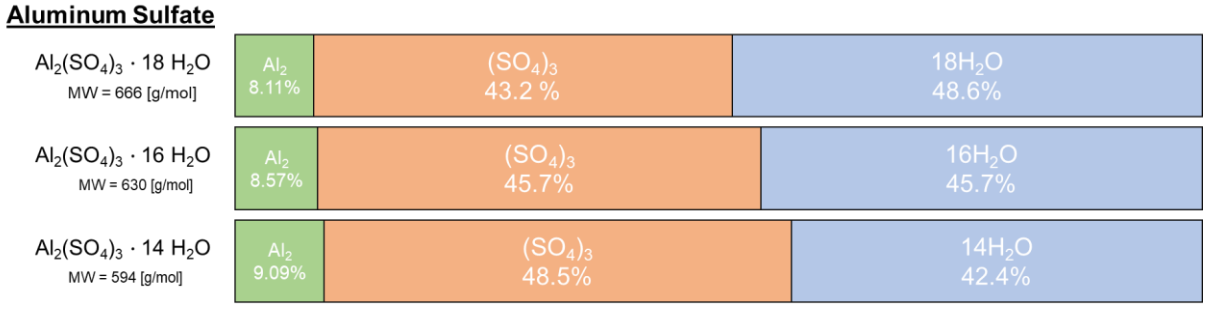

Figure 1.11. Proportions of aluminum, sulfate, and water

By reporting the coagulant concentration in these units, an equivalent amount of any other strength or type of aluminum-based coagulant could be added by a simple unit conversion. Equation 3 can be used to calculate the metal content of a coagulant reported in any form or unit.

$$Conc.[units\ as\ metal] = Conc.[units\ as\ product]\ x\ \left(\frac{MW\ of\ metal\ portion}{Total\ MW\ of\ product}\right) \quad (3)$$

For example, the concentration of the liquid alum from Figure 1.11 can be reported as mg/L as Al by using Equation 3:

$$\frac{mg}{L}as\ Al =$$
$$647{,}475\ \left[\frac{mg}{L}as\ Al_2(SO_4)_3 \cdot 14\ H_2O\right]\ x\ \left(\frac{27\left[\frac{mg}{L}as\ Al\right]x\ 2}{594\left[\frac{mg}{L}as\ Al_2(SO_4)_3 \cdot 14\ H_2O\right]}\right) = 58{,}861\left[\frac{mg}{L}as\ Al\right]$$

Note that in the above example, the molecular weight of aluminum (MW = 27 g/mol) was multiplied by 2 since each compound of aluminum sulfate is comprised of two aluminum atoms; therefore, the total molecular weight of the aluminum portion is 54 g/mol. Table 1.3 provides the conversion factors for reporting the coagulant concentration in different units.

Table 1.3 Alum conversion table

Multiply mg/L of:	by	To obtain:
Al^{3+}	1.000	mg/L as Al^{3+}
Al_2O_3	0.530	
$Al_2(SO_4)_3$	0.158	
$Al_2(SO_4)_3 \cdot 14\ H_2O$	0.091	
$Al_2(SO_4)_3 \cdot 16\ H_2O$	0.086	
$Al_2(SO_4)_3 \cdot 18\ H_2O$	0.081	
$AlCl_3$	0.202	
$AlCl_3 \cdot 6\ H_2O$	0.112	
Multiply:	**by**	**To obtain mg/L as:**
mg/L as Al^{3+}	1.000	Al^{3+}
	1.888	Al_2O_3
	6.333	$Al_2(SO_4)_3$
	11.00	$Al_2(SO_4)_3 \cdot 14\ H_2O$
	11.67	$Al_2(SO_4)_3 \cdot 16\ H_2O$
	12.33	$Al_2(SO_4)_3 \cdot 18\ H_2O$
	4.939	$AlCl_3$
	8.939	$AlCl_3 \cdot 6\ H_2O$

Contrary to all that was discussed in the last paragraph, the coagulant concentration henceforth will be reported in units of mg/L as $Al_2(SO_4)_3 \cdot 14\ H_2O$. Alum concentrations reported in this form are more intuitive since it is widely used in the water treatment industry. The abbreviation “alum-14” will be used instead of $Al_2(SO_4)_3 \cdot 14\ H_2O$ for brevity.

CHAPTER 2: COAGULATION REACTIONS

2.1. Alum Coagulation Diagram

In 1982, Amirtharajah and Mills performed an extensive review of the literature to generalize regions on the alum solubility diagram where coagulation would be effective. The 1982 version of the coagulation diagram originally included only three distinct coagulation zones; however, Edwards and Amirtharajah (1985) later included a fourth zone based on the removal of color-causing compounds in the pH 4.0 – 5.0 range (Figure 2.1). The zones shown in Figure 2.1 represent the operational boundaries of both coagulation mechanisms – i.e., charge neutralization or sweep flocculation – with respect to the alum dose and pH.

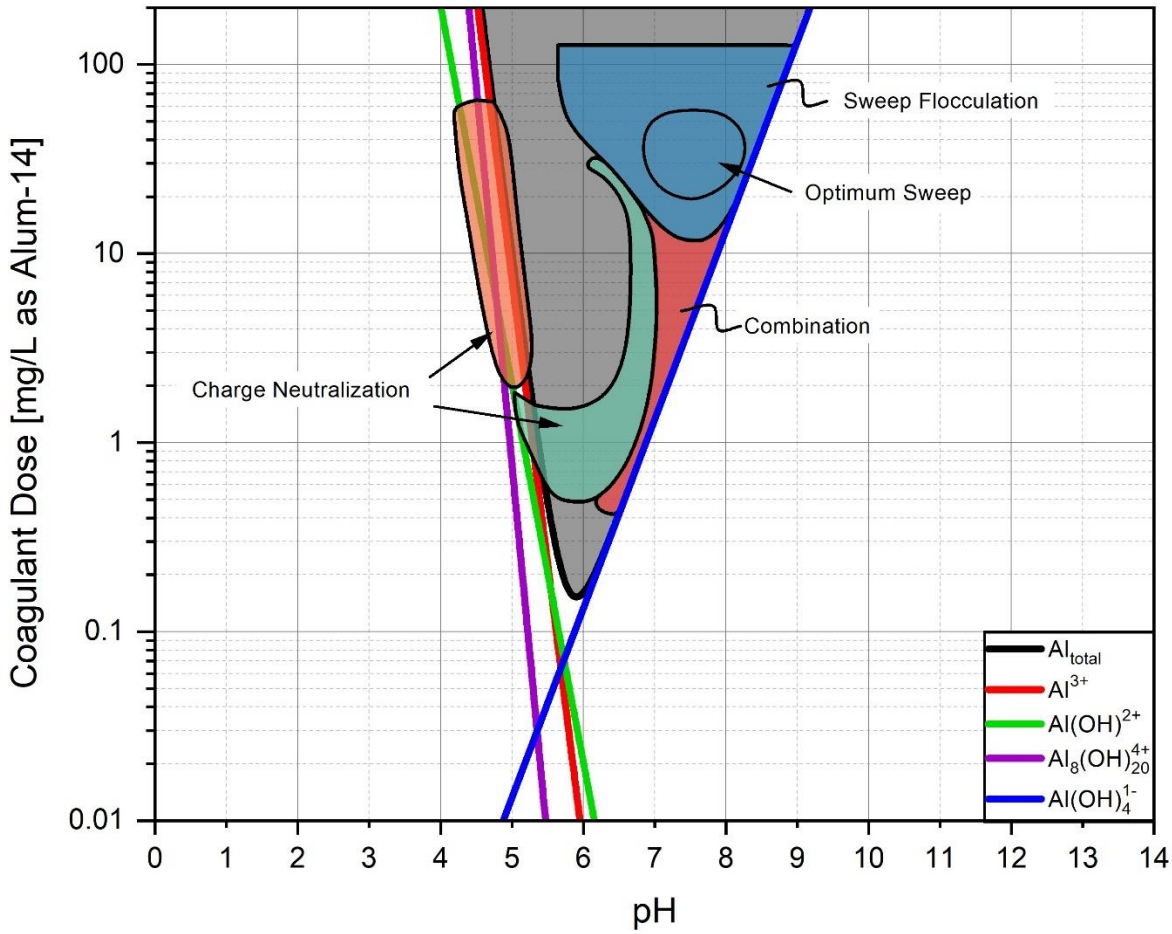

Figure 2.1. Alum coagulation diagram at 25°C (Edwards and Amirtharajah, 1985)

In general, charge neutralization zones tend to be dominant under low alum doses and pH values, while sweep flocculation tends to be dominant under high alum doses and pH values. It is also possible for both coagulation mechanisms to occur sequentially as the pH drops with alum addition. Edzwald (2013) stated that charge neutralization conditions are typically restricted to doses below 11 mg/L as alum-14 (1 mg/L as Al) and pH 6.0 or less. The exact limits of the charge neutralization mechanism will vary based on factors such as water quality and temperature; however, a more general criterion for charge neutralization is that it tends to be predominant under conditions that favor the formation of soluble positively charged species (as opposed to the amorphous precipitate). Some researchers stated that charge neutralization is achieved by the adsorption of positively charged hydrolysis species onto the surface of the contaminants (e.g., Amirtharajah and Mills (1982) and Van Benschoten and Edzwald (1990a)) while others have argued that charge neutralization is preceded by the formation and adsorption of positively charged $Al(OH)_{3(am)}$ (e.g., Dentel and Gossett (1988) and Dempsey (1988)).

Amirtharajah and coworkers (1982; 1985) intended for the diagram to have practical, real-world applications where one would be able to select optimum coagulation conditions directly from the diagram. In reality, the diagram simply outlines the boundaries where coagulation is expected to be effective and should not be interpreted as a universal roadmap that applies to all water qualities and temperatures. Several key limitations prevented the original alum coagulation diagram from being directly applicable to the real world. Besides being an oversimplification of the coagulation process, some of the limitations were: 1) the boundaries were based mainly on past studies on alum coagulation in either DI water or waters containing only clays, 2) the impact of natural organic matter on turbidity removals were not considered, 3) the referenced studies used to create the diagram employed different criteria for what constituted effective coagulation, and 4)

the impact of temperature on coagulation was not considered. Nevertheless, the diagram has been paramount in advancing coagulation theory and practice by capturing the complexities of coagulation in a single diagram. For this reason, the coagulation diagram has become a common figure in coagulation chapters since the time of its publication. The coagulation diagram will be deconstructed and updated incrementally in the subsequent sections to reflect the research progress since its publication in 1985.

2.2. Aluminum Hydrolysis Reactions

When aluminum (in the form of alum) is added to water, it typically dissociates into different soluble aquo aluminum species called hydrolysis products. Like all chemical reactions, aluminum hydrolysis reactions are governed by thermodynamic equilibrium (balance) forces that determine what form the aluminum ions would exist and how much it would remain soluble. The process depends largely on the type and quantity of constituents present in water and the temperature of the water. Alum stock solutions generally have a very low pH, typically in the range of pH 2.0 – 3.0. Below pH 3.0 (at 20°C), the predominant form of the aluminum ion is $Al(H_2O)_6^{3+}$. Each aluminum ion forms a bond (called a ligand) with six water molecules (Figure 2.2).

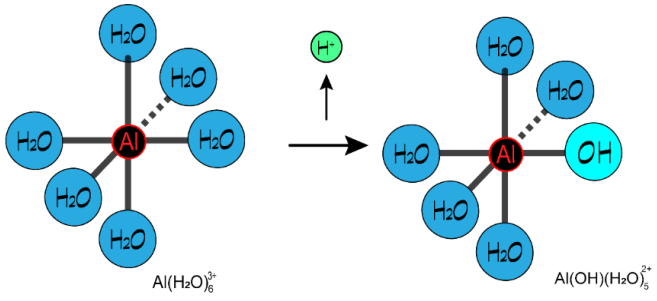

Figure 2.2. Hydrated aluminum ion followed by initial hydrolysis reaction

For brevity, many sources simply use Al^{3+} instead of including the water molecules in the chemical formula. Above pH 3.0, a hydroxyl group (OH^-) replaces one of the water ligands on the

hydrated aluminum ions to form $Al(OH)(H_2O)_5^{2+}$ (or simply $Al(OH)^{2+}$). As the pH increases further, different monomeric (one aluminum ion) and polymeric (multiple aluminum ions) hydrolysis products begin to form sequentially. However, it is believed that polynuclear species do not play a significant role under most conditions encountered in drinking water treatment with alum (Van Benschoten and Edzwald 1990a; Jiao et al. 2015). Above pH 6.5 (at 20°C), aluminum hydrolysis products predominantly exist in the form of $Al(OH)_4^-$. If the total amount of aluminum in the system exceeds the thermodynamic solubility limit at a given pH, the soluble hydrolysis species will precipitate (come out of solution). Under conditions typically encountered in drinking water treatment, the solid precipitate would primarily be in the form of amorphous aluminum hydroxide $Al(OH)_{3(am)}$ (Hayden and Rubin 1973).

Table 2.1 lists the sequential aluminum hydrolysis reactions and their corresponding equilibrium expressions. The double arrows in the chemical reactions indicate that the reactions can occur in either direction to maintain equilibrium. The equilibrium expressions were re-arranged such that the concentration of each hydrolysis product can be calculated given the pH. Table 2.2 presents equations for calculating the equilibrium constants (K_i values) for each reaction as a function of temperature. Equilibrium constants provided by Nordstrom and May (1996) and Brown and Ekberg (2016) are fairly similar (<1% difference) except for the $Al(OH)_2^{1+}$ species (<6% difference). In their review of the literature, Brown and Ekberg (2016) questioned the reliability of the data previously provided by some of the studies on $Al(OH)_2^{1+}$.

Table 2.1. Sequential aluminum hydrolysis reactions

Reaction	Equilibrium Expression
$Al(OH)_{3(am)} \leftrightharpoons Al^{3+} + 3OH^-$	$[Al^{3+}] = \frac{10^{K_{so}}}{[OH^-]^3}$
$Al^{3+} + H_2O \leftrightharpoons Al(OH)^{2+} + H^+$	$[Al(OH)^{2+}] = \frac{10^{K_{11}} \cdot [Al^{3+}]}{[H^+]}$
$Al^{3+} + 2H_2O \leftrightharpoons Al(OH)_2^{1+} + 2H^+$	$[Al(OH)_2^{1+}] = \frac{10^{K_{12}} \cdot [Al^{3+}]}{[H^+]^2}$
$Al^{3+} + 4H_2O \leftrightharpoons Al(OH)_4^{1-} + 4H^+$	$[Al(OH)_4^{1-}] = \frac{10^{K_{14}} \cdot [Al^{3+}]}{[H^+]^4}$
$H_2O \leftrightharpoons H^+ + OH^-$	$[OH^-] = \frac{10^{K_w}}{10^{-pH}}$

Note: $[H^+] = 10^{-pH}$

Table 2.2. Equations for calculating equilibrium constants given temperature

Equilibrium Constant	Nordstrom and May (1996)	Brown and Ekberg (2016)
K_{so}	$(-7.333x10^{-4}T^2) + (0.4676T) - 105.73^a$	-[b]
K_{11}	$4.771 - \frac{2899.05}{T}$	$4.83 - \frac{2923}{T}$
K_{12}	$88.5 - \frac{9391.6}{T} - 27.121 * \log T$	$8.78 - \frac{5788}{T}$
K_{14}	$40.875 - \frac{10908.4}{T} - 11.041 * \log T$	$67.2 - \frac{12474}{T} - 8.47 * \ln T$
K_w	$(-1.896x10^{-4}T^2) + (0.1462T) - 40.74^a$	

T = temperature [°K] (note: °K = 273.15 + °C)
[a] Equation was derived using a polynomial fit of values provided by Pernitsky and Edzwald (2006)
[b] No equation provided by the authors

In charge neutralization, destabilization of the negatively charged contaminants occurs by positively charged coagulant species. It would, therefore, be useful to determine the conditions under which positively charged aluminum hydrolysis species would predominate. Figure 2.3 compares the distribution of the aluminum hydrolysis products as a function of pH at 20°C using the equations provided in Table 2.1 and Table 2.2. The top and bottom panels represent the distributions calculated using the Nordstrom and May (1996) and Brown and Ekberg (2016) constants, respectively. Based on the Nordstrom and May (1996) constants, the positively charged hydrolysis products are the dominant species between pH 5.10 and pH 6.6 would be $Al(OH)_2^{1+}$. On the other hand, positively charged hydrolysis products are the dominant species only between

pH 5.2 and 6.25 based on the Brown and Ekberg (2016) constants. The effects of temperature on the species distribution can be visualized using an online interactive dashboard called “Alum Equilibrium” (Alansari 2020b).

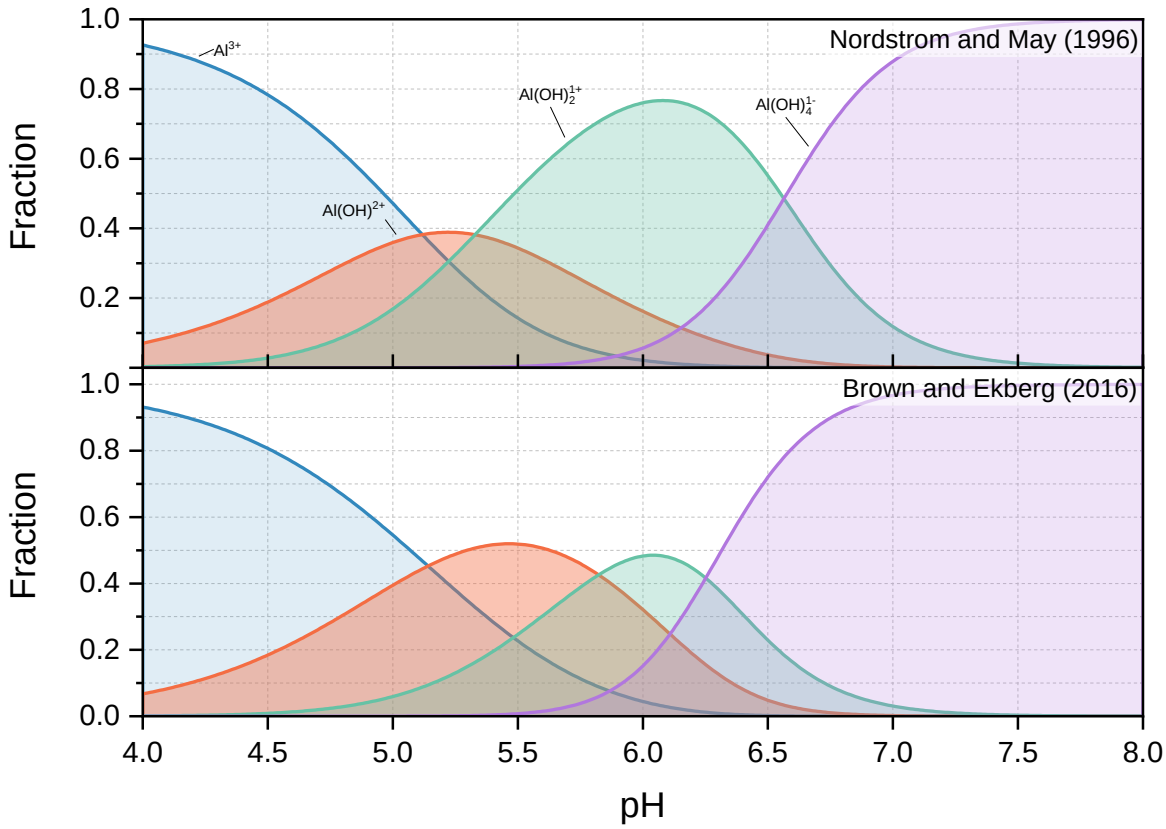

Figure 2.3. Distribution of aluminum hydrolysis products at 20°C

2.2.1. Alum Coagulation Diagram: Updating Species and Equilibrium Constants

The first step in revising the coagulation diagram was to update the aluminum hydrolysis species that are in equilibrium with the amorphous precipitate and use the most recent and widely accepted equilibrium constants. As noted earlier, Van Benschoten and Edzwald (1990a) showed that $Al(OH)_{3(am)}$ was only in equilibrium with three soluble monomeric aluminum species: Al^{3+}, $Al(OH)^{2+}$, and $Al(OH)_4^-$. Figure 2.4 shows the updated coagulation diagram using three monomeric aluminum species and the Nordstrom and May (1996) equilibrium constants.

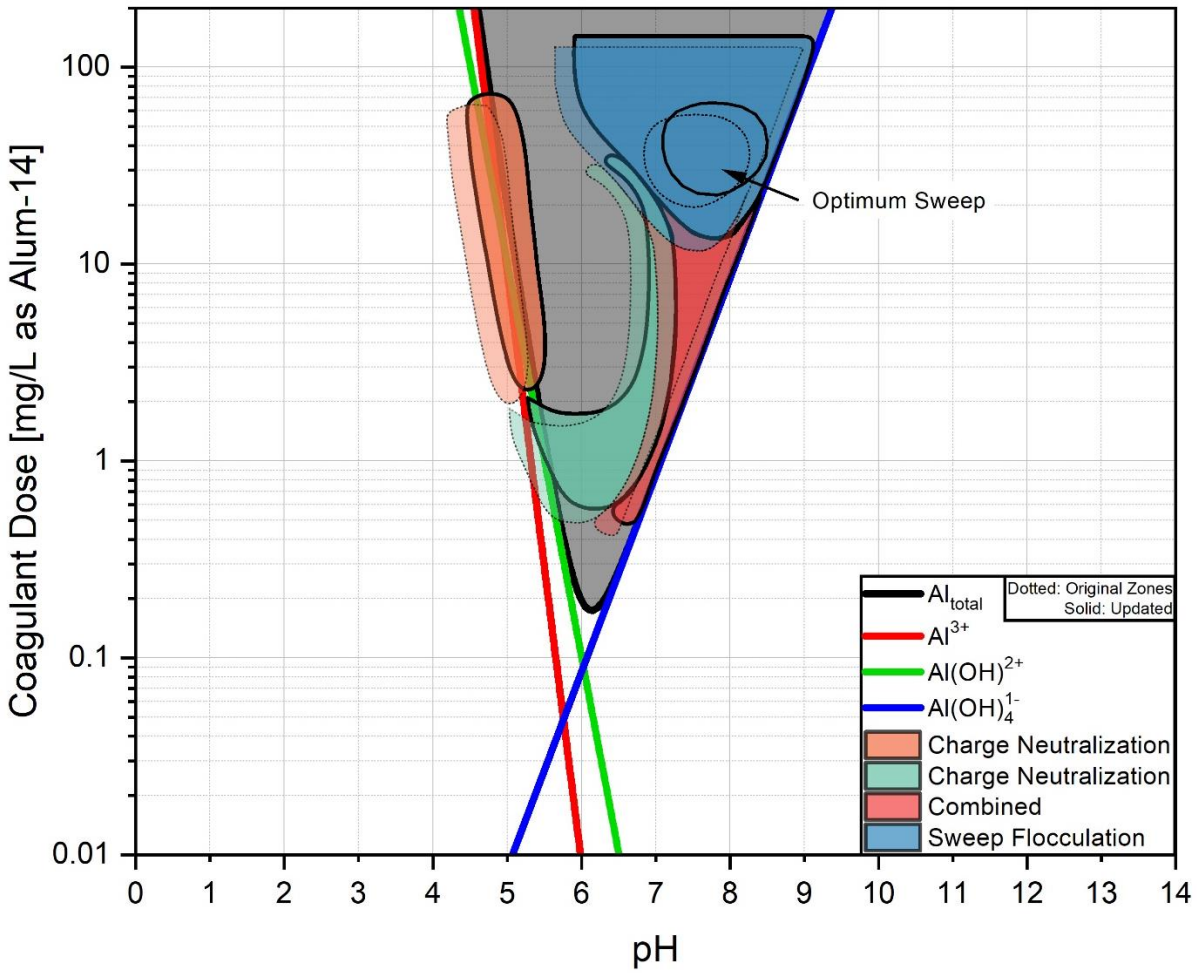

Figure 2.4 Coagulation diagram with updated species and equilibrium constants

Updating the species and constants increased the pH of minimum solubility from approximately 5.90 to 6.14. Similarly, the concentration of soluble alum increased from 0.15 to 0.17 mg/L as alum-14. It was assumed that the position of the coagulation zones was relative to the solubility line; therefore, the coagulation zones were moved accordingly. The dotted coagulation zones in Figure 2.4 represent the zones from the original diagram whereas the solid zones represent the updated zones.

2.2.2. Aluminum Solubility and Temperature

Optimum coagulation conditions for turbidity removals typically occur under conditions where the formation of the amorphous aluminum hydroxide precipitate, $Al(OH)_{3(am)}$, are favored. Amirtharajah and coworkers (1982; 1985) based their coagulation diagram on three monomeric species (Al^{3+}, $Al(OH)^{2+}$, $and\ Al(OH)_4^{1-}$) and one polymeric specie ($Al_8(OH)_{20}^{4+}$); however, Van Benschoten and Edzwald (1990a) showed that $Al(OH)_{3(am)}$ was only in equilibrium with three soluble monomeric aluminum species: Al^{3+}, $Al(OH)^{2+}$, and $Al(OH)_4^-$. Figure 2.5 shows the solubility diagram of aluminum sulfate at 25°C (left-panel) and 5°C (right-panel). The solubility diagrams were created using the equilibrium constants provided by Nordstrom and May (1996) in Table 2.2.

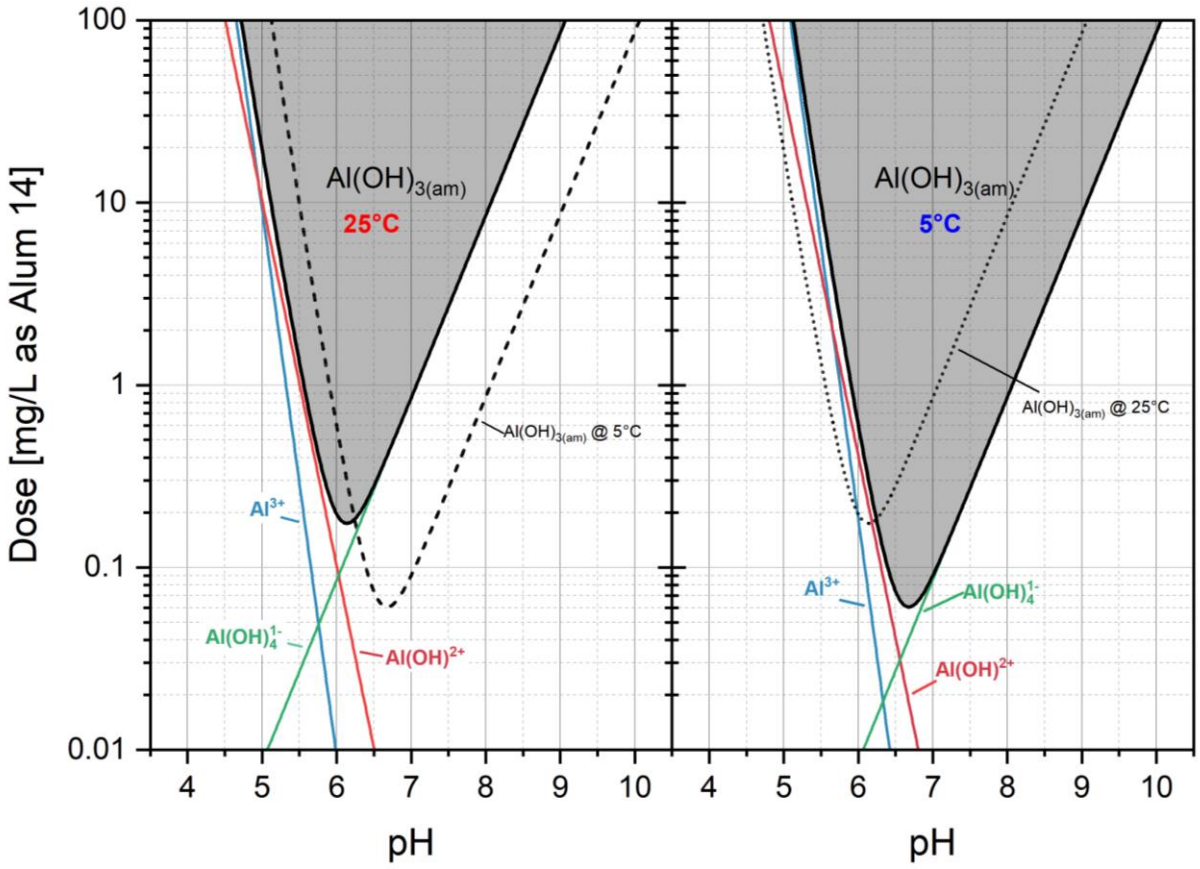

Figure 2.5. Alum solubility diagram at 25°C (left-panel) and 5°C (right-panel)

The sum of the three monomeric species, at a given pH, creates the black solid line representing the solubility limit of aluminum. For example, at pH 7.0 and 25°C, any amount of alum added up to approximately 0.8 mg/L as alum-14 (the solubility limit at that condition) would be soluble. If 10 mg/L as alum-14 were added, then, in theory, 0.8 mg/L as alum-14 would be soluble, and the remaining 9.2 mg/L as alum-14 would precipitate. The solubility of the coagulant would also be controlled by temperature. At the same pH but at 5°C, the solubility limit of aluminum decreases to approximately 0.1 mg/L as alum-14, i.e., the coagulant becomes less soluble with decreasing temperature. The pH at which the coagulant would be the least soluble is called the pH of minimum solubility. The pH of minimum solubility at 25°C and 5°C is 6.27 and 6.68, respectively; therefore, the pH of minimum solubility increases as the temperature decreases. The effect of temperature on the solubility of the alum can be visualized in the "Alum Equilibrium" dashboard (Alansari 2020b).

Van Benschoten and Edzwald (1990a) found that the effects of temperature on the solubility of $Al(OH)_{3(am)}$ in deionized water could be accounted for by the changes in the OH^- concentration. This would imply that the concentration of OH^- in the water would change with temperature if the pH was held constant. Using pOH instead of pH would ensure that the concentration of OH^- is always the same; thus, mitigating the effects of temperature on the solubility or performance of alum. Using the ion product of water (pK_w, Table 2.2), the pH could be adjusted to various temperatures by keeping pOH constant. For example, a water with a pH of 6.5 at 25°C has an approximate pOH of 7.5, based on a pK_w of 14. At 4°C, the pK_w is approximately 14.8; therefore, the adjusted pH of the water would be 7.3 for a constant pOH value.

Figure 2.6 shows jar test results from Van Benschoten (1988) with alum in DI water at 4°C and 25°C. The coagulant dose in all cases was 13.5 mg/L as Al (~149 mg/L as alum-14). The general appearance of both plots was fairly similar, except, the colder temperature results were simply shifted by approximately 0.8 - 0.9 pH units to the right (higher pH). The dashed series represents the results from the experiments performed at 4°C, but the pH was adjusted to 25°C based on a constant pOH value. The pH at which particles first appeared and the peaks between 25°C and 4°C results were in agreement. Thus, it could be concluded that temperature effects can largely be accounted for by the concentration of OH^- which is a function of temperature and the equilibrium constant ($pK_w = pH + pOH$).

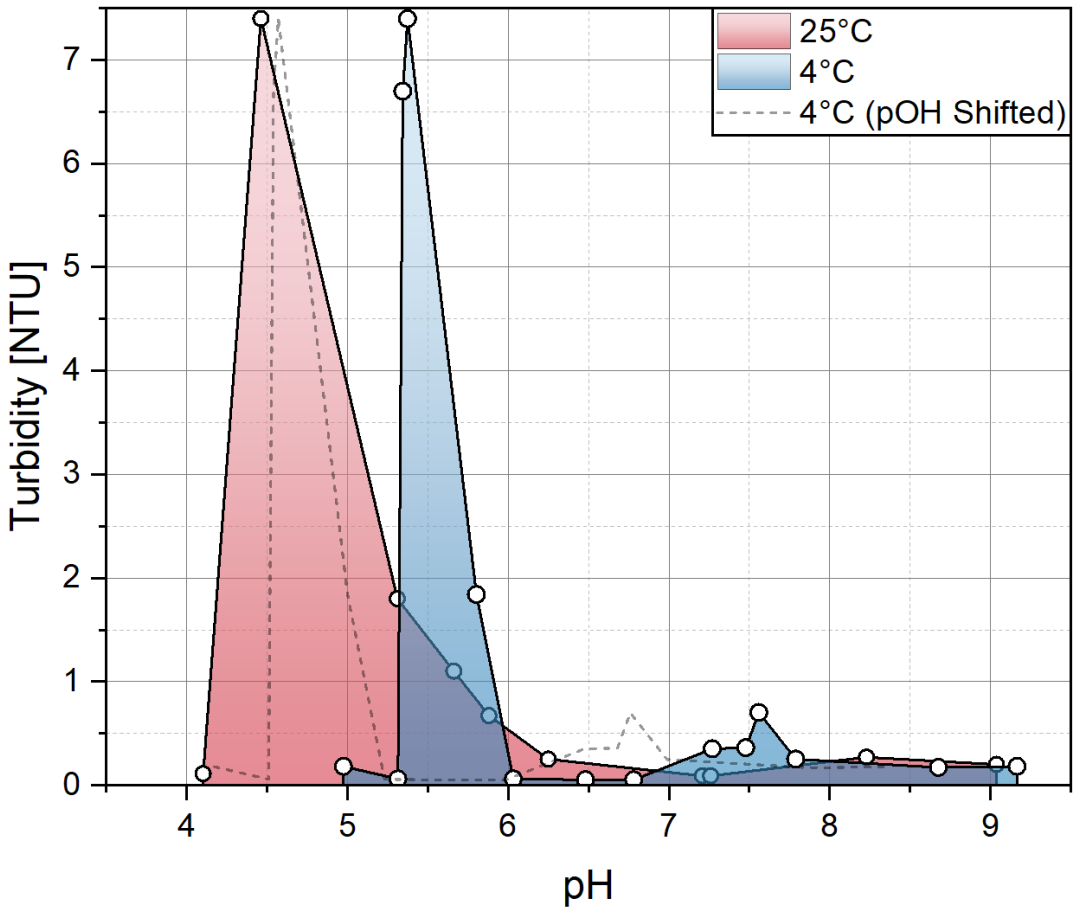

Figure 2.6 Jar tests with alum in DI water at two temperatures (from Van Benschoten 1988)

2.2.2.1. Residual Dissolved Aluminum

Elevated residual aluminum levels in the treated water can potentially cause adverse health effects in humans (Letterman and Driscoll 1988). Edzwald (2020) proposed that regulatory limits for residual aluminum should be reduced from 0.2 mg/L as Al (the current USEPA limit) to 0.05 mg/L as Al (0.55 mg/L as alum-14) for plants using aluminum-based coagulants. Figure 2.7 shows the pH boundaries for the 0.05 and 0.2 mg/L as Al limits for temperatures ranging from 5 to 30°C. For example, at pH 7.0, a plant can expect to maintain residual aluminum levels below the new proposed limit as long as the water temperature is below 20°C. Operating at or near the minimum solubility line of aluminum (green line) would minimize residual aluminum levels in the treated water. Equations for calculating the upper and lower pH boundaries given temperature are provided in Table 2.3. Alternatively, an interactive dashboard version of Figure 2.7 was also developed to allow users to quickly and easily calculate the pH boundaries based on their own operating conditions (Alansari 2020a).

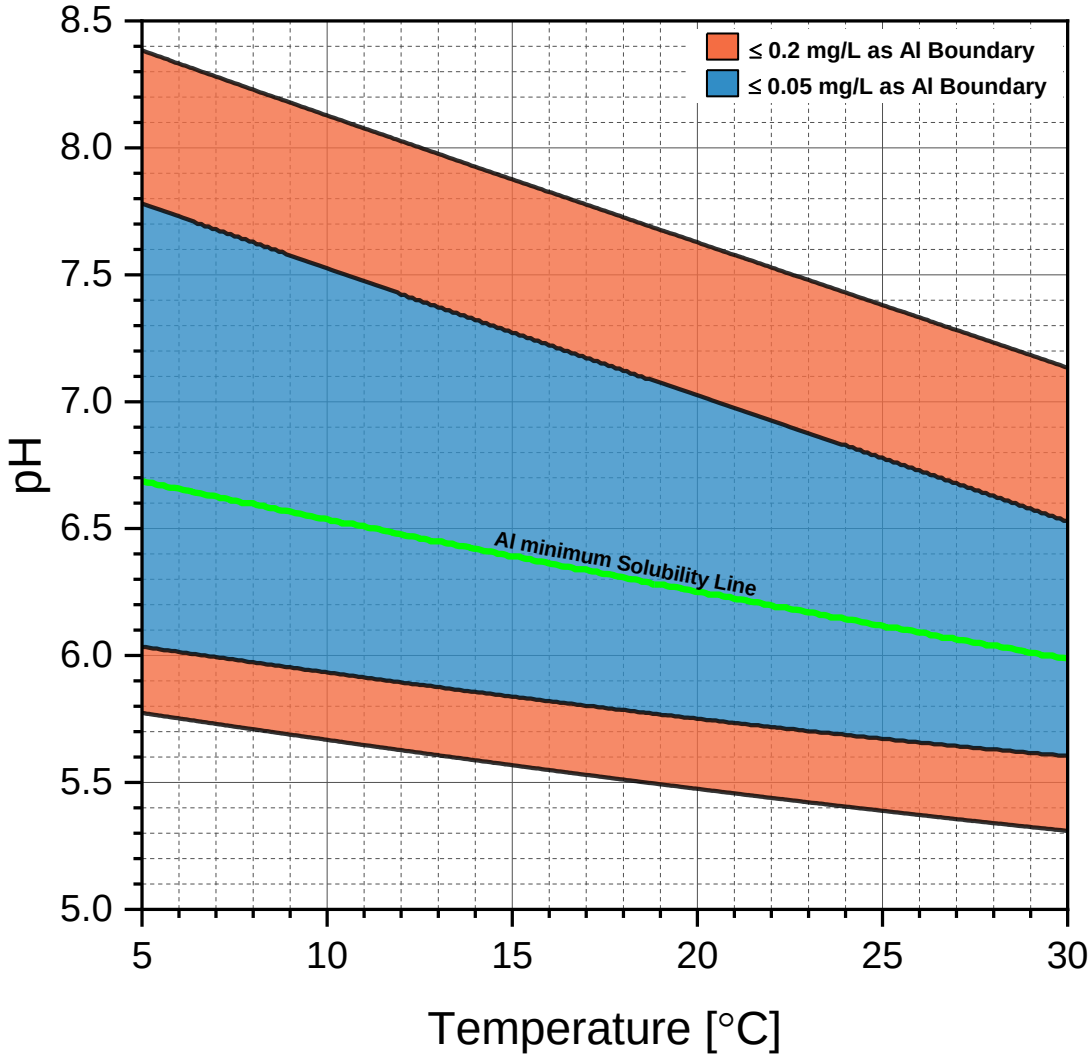

Figure 2.7. Dissolved aluminum boundaries with respect to pH and temperature

Table 2.3. Equations for calculating dissolved aluminum pH boundaries

Parameter		Empirical Equation
0.05 mg/L as Al	Lower Boundary	$pH = (1.65x10^{-4})x^2 - 0.0231x + 6.146$
	Upper Boundary	$pH = (4.15x10^{-5})x^2 - 0.0514x + 8.036$
0.2 mg/L as Al	Lower Boundary	$pH = (1.35x10^{-4})x^2 - 0.0234x + 5.887$
	Upper Boundary	$pH = (4.72x10^{-5})x^2 - 0.0515x + 8.638$
Minimum Solubility		$pH = (9.73x10^{-5})x^2 - 0.0314x + 6.840$

2.2.3. Alum Coagulation Diagram: Incorporating Temperature Effects

As discussed earlier, the alum solubility lines would move down diagonally with a reduction in temperature and vice versa; therefore, it is also expected that the coagulation zones would change or move with changing water temperatures. Figure 2.8 shows the effects of reducing the temperature from 25°C to 5°C on the coagulation zones using two possible scenarios. In the left-panel, it was assumed the location of the coagulation zones was relative to the solubility line; therefore, a reduction in temperature would move the zones down and to the right. In the right-panel, it was assumed that the coagulation zones would move based on a constant pOH value as described by Van Benschoten and Edzwald (1990a). In the first case, a decrease in temperature would suggest that "effective" coagulation could theoretically be achieved at a much lower dose since the zones moved lower while in the second case, a decrease in temperature would simply move the zones to the right.

Unfortunately, almost all the research on the effects of temperature on coagulation has been focused either on the solubility of the coagulant or simply on the effects of temperature on the overall treatment process. It is unclear at this point exactly how the coagulation zones would respond to temperatures changes. The more conservative approach would be to assume that the coagulation zones would move according to the concentration of OH^- as suggested by Van Benschoten and Edzwald (1990a) as shown in the right panel of Figure 2.8.

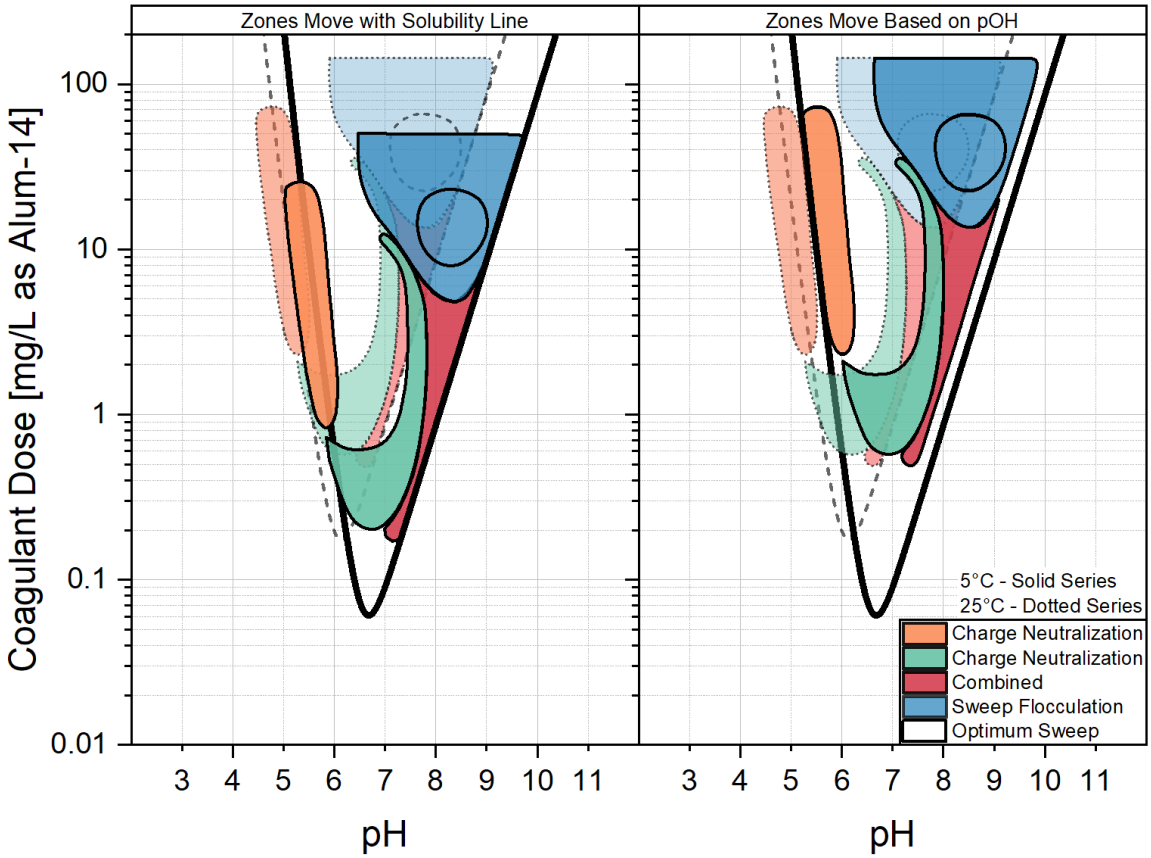

Figure 2.8. Temperature effects on coagulation diagram

2.3. Calculating the Total Charge Demand

In a simplistic model of charge neutralization, the total negative charge from the contaminants must be met by an equivalent positive charge for destabilization to occur successfully. The total negative charge, i.e., charge demand, depends on the nature and concentration of contaminants in the water. This will be discussed in more detail later. The total charge is usually expressed in terms of equivalents per mass or volume. For example, Al^{3+} has a charge of +3 eq/mol; therefore, dividing the charge by molar mass of aluminum (27 g/mol) yields an equivalents per mass of 0.111 eq/g or 111 µeq/mg of Al (Edzwald and Tobiason 1999). Using this approach, the total available positive charge can be estimated from the species distribution. Table 2.4 provides the equivalent values for the positive mononuclear hydrolysis species.

Table 2.4. Charge of aluminum hydrolysis species

Species	Charge [eq/mol]	[µeq/mg of Al]
Al^{3+}	3	111
$Al(OH)^{2+}$	2	74
$Al(OH)_2^{1+}$	1	37

Figure 2.9 shows a contour plot of the total positive charge as a function of pH and alum dose. The data was generated using Visual MINTEQ 3.1 (a chemical equilibrium modeling software). The default aluminum equilibrium constants of the software were modified to match the Nordstrom and May (1996) constants for consistency. At the model's conditions, the results showed that there was little to no positive charge above pH 7.25. Below pH 7.0, the total positive charge increased with decreasing pH and increasing alum dose. Suppose a water has a total negative charge demand of 30 µeq/L at pH 6.0. In theory, destabilization of the contaminants would occur with an equivalent positive charge at a dose of 10.5 mg/L as alum-14 at the same pH as shown by the dotted lines in Figure 2.9. The underlying assumption of this simplistic model is that one negative charge reacts with one positive charge and the end-result is a destabilized particle. In reality, the interactions are more complex and less efficient. The purpose of Figure 2.9 is simply to provide a visual illustration of the total charge distribution as a function of the coagulant dose and pH and highlight the conditions under which charge neutralization would theoretically be possible.

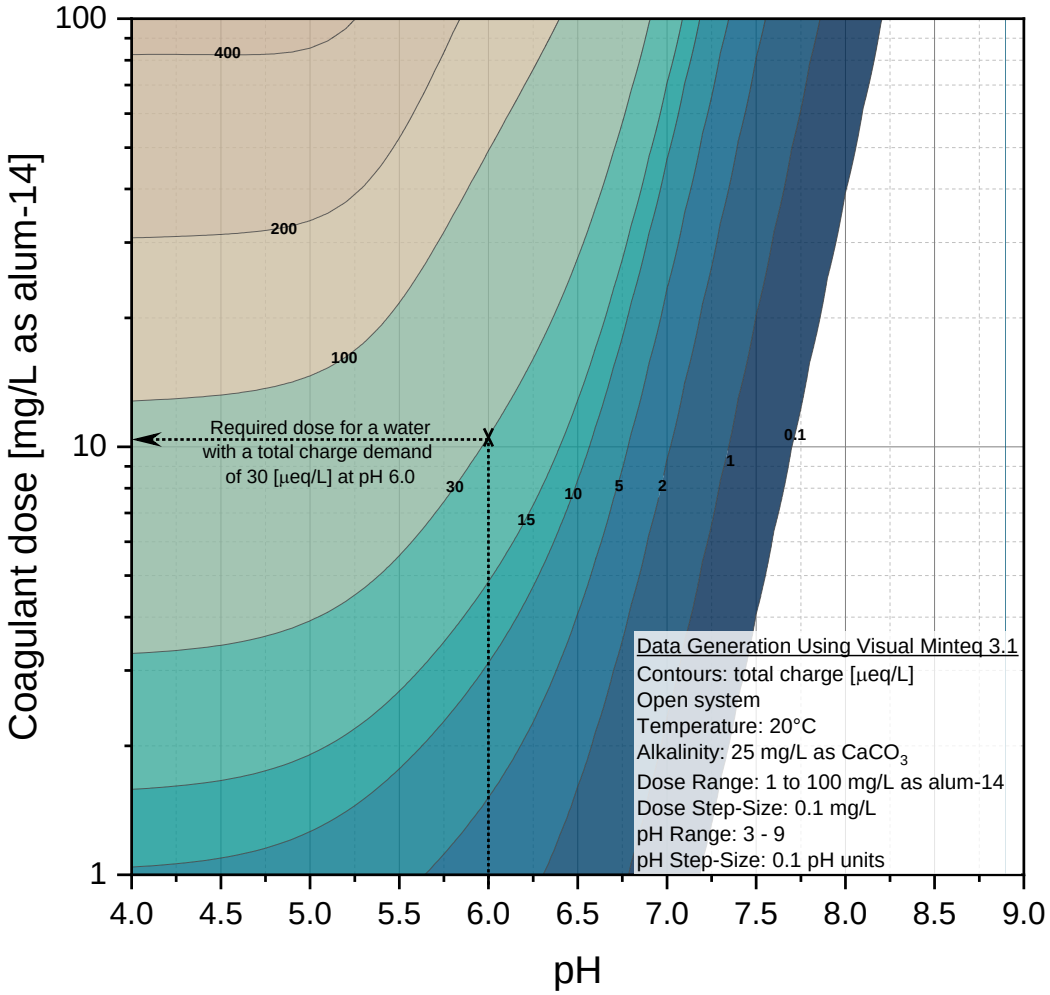

Figure 2.9. Contour plot of total positive charge

2.4. Transitioning Between Ideal and Real Water Samples

Thus far, it was assumed that aluminum was added directly to deionized (DI) water and the only ligand that reacted with the aluminum was OH^-. In natural waters, aluminum forms aluminum-ligand complexes with several other ions that are typically present, such as F^-, SO_4^{2-}, PO_4^{3-}, CO_3^{2-} and the functional groups on NOM. Just like aluminum hydrolysis species, aluminum complexes are soluble; therefore, the solubility of the coagulant would largely depend on the type and concentration of ionic species present in the water. Driscoll and Letterman (1988) found that the presence of fluoride increased the solubility of the alum (i.e., higher residual aluminum concentrations) due to the formation of soluble aluminum-fluoride complexes. Similarly, Vik and coworkers (1985) reported that residual aluminum levels increased under suboptimal coagulation conditions due to aluminum complexation with NOM.

2.4.1. Alum and Alkalinity

Alum behaves like an acid when added to water due to the release of hydrogen ions during hydrolysis reactions (Figure 2.2). As a result, the water's pH after alum addition decreases primarily as a function of the alum dose, raw water alkalinity, and temperature. Alkalinity is a measure of a water's acid neutralization (buffering) capacity. In drinking water treatment, alkalinity is usually reported in units of mg/L as $CaCO_3$. Figure 2.10 illustrates the effects of the sequential addition of alum on the pH of DI water with alkalinity ranging from 10 to 200 mg/L as $CaCO_3$. All experiments were performed with DI water at 20±1°C.

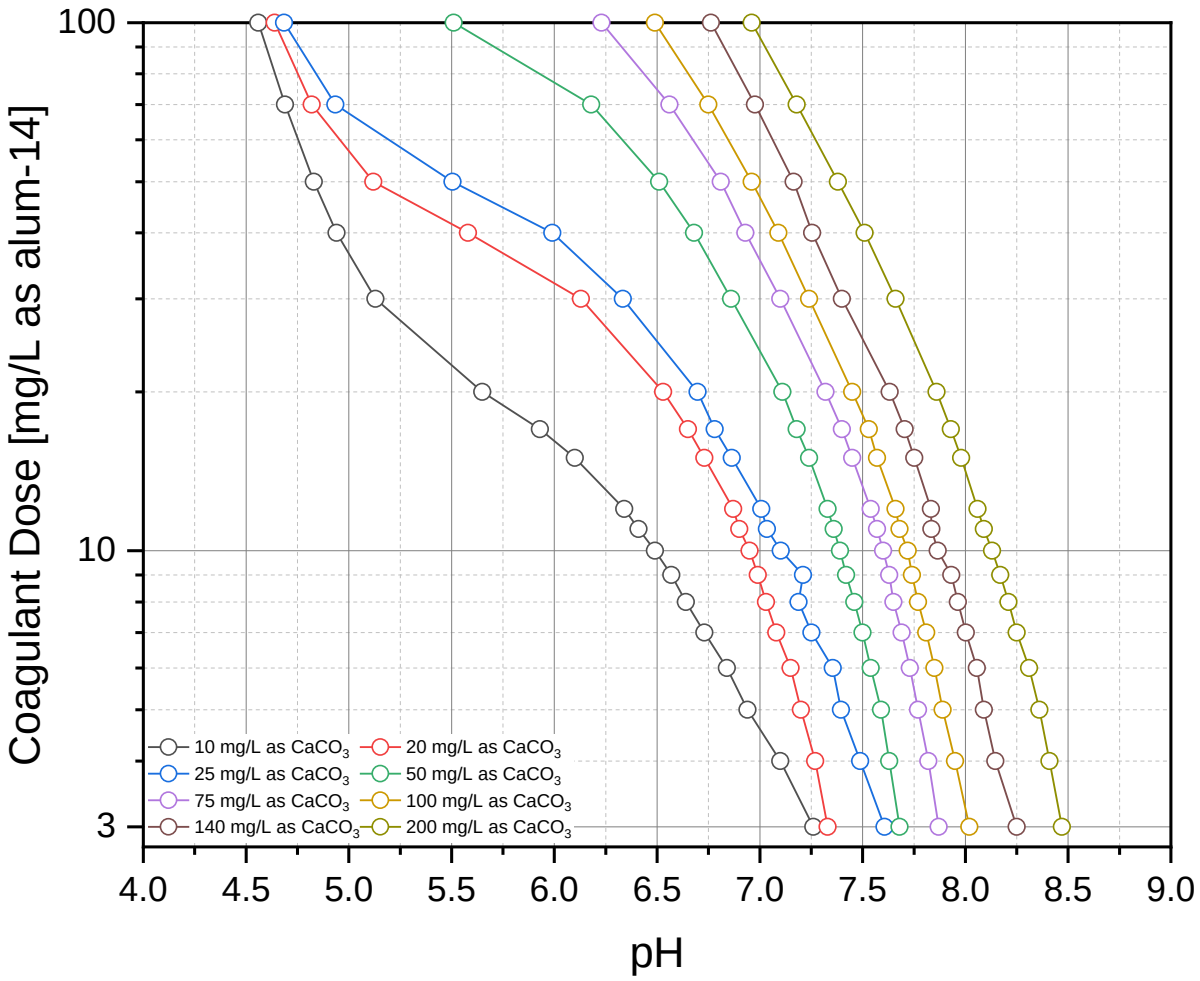

Figure 2.10. Addition of alum to deionized water containing various levels of alkalinity

In general, alum's capacity to depress the pH is hindered the greater the alkalinity of the raw water. For example, a dose of 20 mg/L as alum-14 reduced the pH to 5.65 and 7.45 with an alkalinity of 10 and 100 mg/L as $CaCO_3$, respectively. Treatment facilities that treat low alkalinity waters (e.g., 10 mg/L as $CaCO_3$) typically cannot operate at high alum doses (without adding a strong base with the alum) because the pH after coagulant addition can exceed the solubility boundary of $Al(OH)_3$. Figure 2.11 shows jar test settled water turbidity removals from a water treatment facility that treats low alkalinity water. The “alum only” line shows the water's pH when alum was added without any pH adjustment. Operating to the right of the alum only line would

require the addition of a base while operating to the left of the line would require the addition of an acid. The overlaid heatmap shows the region where the treatment plant typically operated – darker regions correspond to higher frequencies. It was evident that caustic or base addition was critical at this facility since the alum titration line did not pass through the greater than 70% removal zone by sedimentation. Therefore, any increase in alum dose has to be supplemented with an increase in the base (caustic) dose to remain within the removal region for this water.

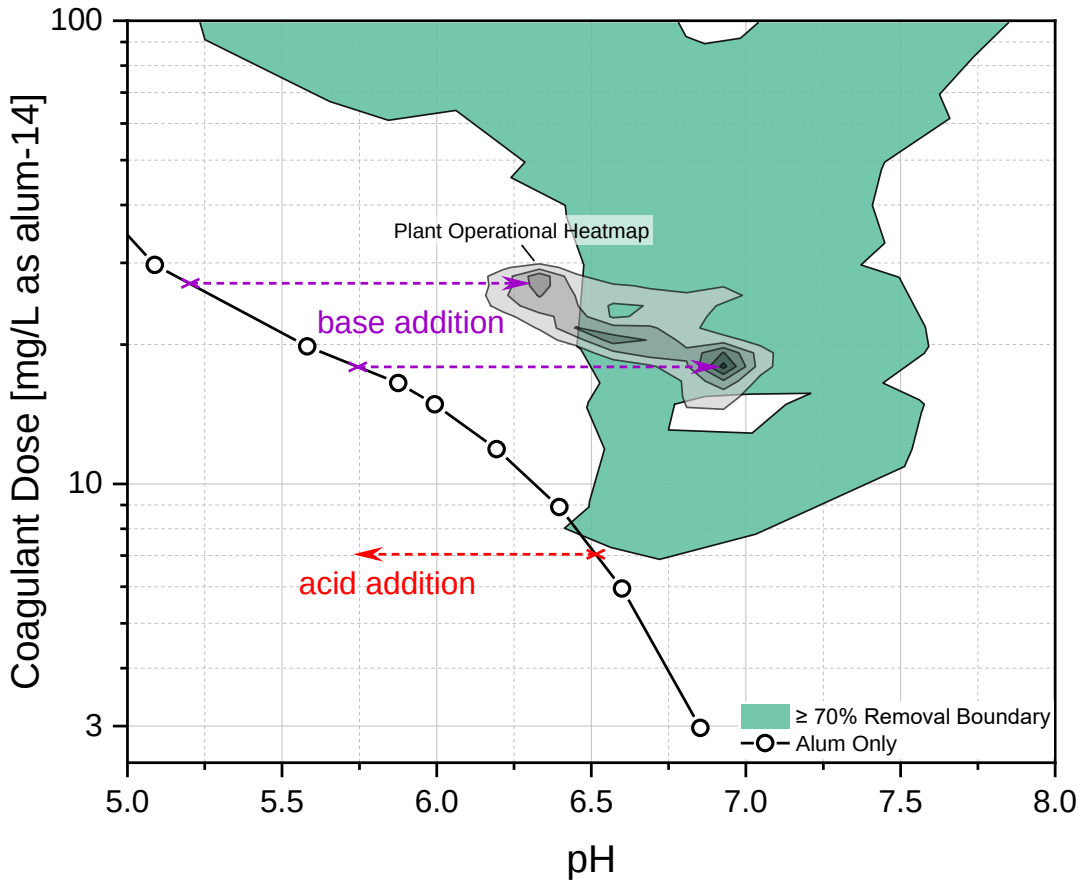

Figure 2.11. Low alkalinity water settled water turbidity jar test results

On the other hand, high raw water alkalinity would make it difficult for plants to operate in zones where charge neutralization is the predominant coagulation mechanism. According to Figure 2.9, soluble positively charge aluminum hydrolysis species are available in sufficient amounts near pH 6.5. Without the means to adjust the pH, a plant treating high alkalinity water

would need to add very high alum concentrations to reduce the pH to the point where positively charged species are likely to form. This is particularly relevant to treatment plants that rely on surface charge measurement techniques (zeta potential or streaming current) to monitor or optimize coagulation.

2.4.2. Influence of Dissolved Organics

Figure 2.12 shows how dissolved organic carbon (DOC) can impact the total dissolved aluminum concentration in a low alkalinity water. The chemical equilibrium models were performed using Visual MINTEQ 3.1. In all cases, the concentration of aluminum in the system was set to 1.363 mg/L as Al (≈15 mg/L as alum-14) and the alkalinity to 25 mg/L as $CaCO_3$. Alkalinity was added to the model in the form of sodium bicarbonate ($NaHCO_3$). The only possible solid phase in equilibrium was limited to amorphous aluminum hydroxide. Below pH 5.1 and above pH 8.2, the aluminum in the system in all cases was completely dissolved – which was consistent with the theoretical aluminum solubility diagram (Alansari 2020b). DOC was included in the equilibrium model based on the NICA-Donnan model parameters for humic substances (Milne et al. 2003). It was assumed that the DOC comprised of 60% fulvic acids. The minimum dissolved aluminum concentration with alum and alkalinity alone (black line) was 0.018 mg/L as Al (0.2 mg/L as alum-14) and occurred at a pH of 6.14. Adding 2 mg/L as DOC to the model (red line) increased the dissolved aluminum concentration and pH of minimum solubility to 0.15 mg/L as Al (1.65 mg/L as alum-14) and 6.5, respectively. Finally, increasing the DOC to 8 mg/L (blue line) increased the dissolved aluminum concentration to 0.35 mg/L as Al and the pH of minimum solubility to 6.91.

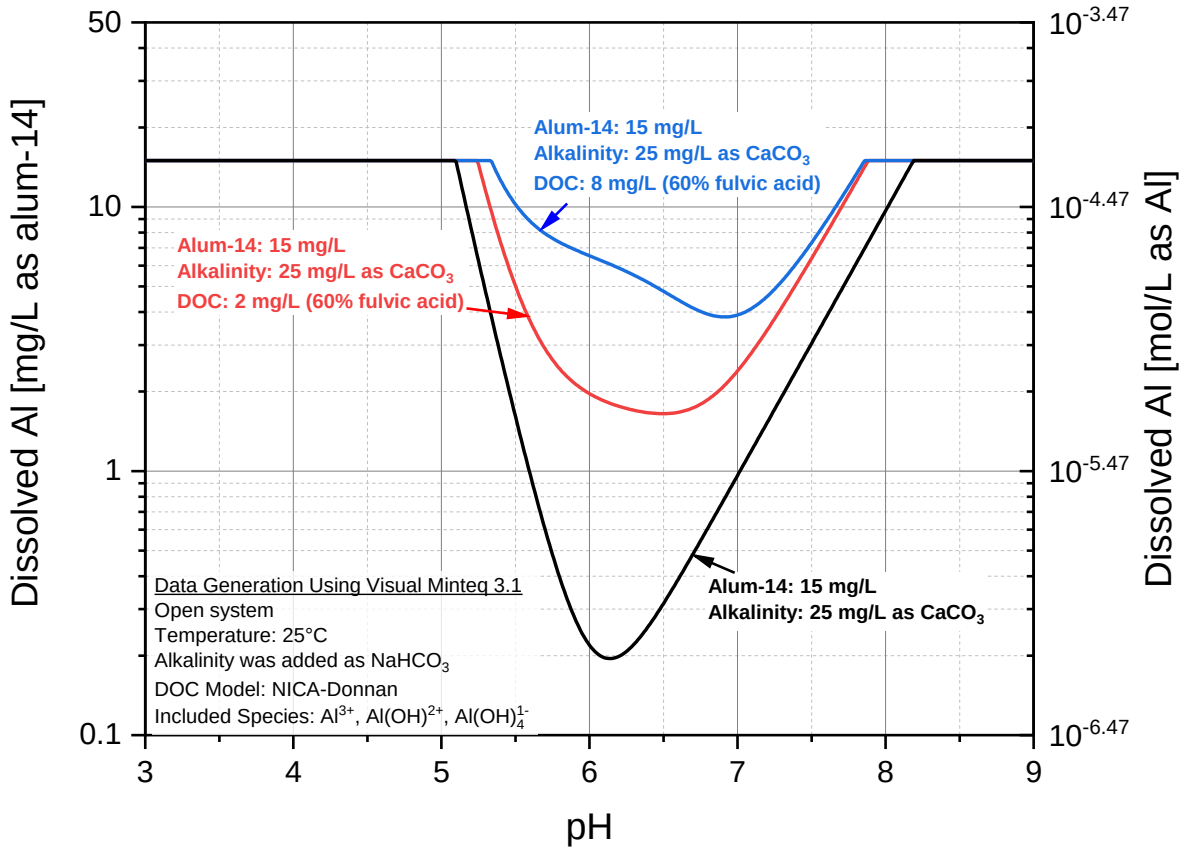

Figure 2.12. Effect of complexation on total dissolved aluminum concentration

2.4.3. Alum Coagulation Diagram: Including DOC

The original coagulation diagram was based mainly on past studies on alum coagulation in either DI water or waters containing only clays. Figure 2.12 showed that the presence of DOC (as in most natural surface waters) increased the solubility of the coagulant, i.e., higher doses of alum would be required to produce the amorphous precipitate at a fixed pH. As a result, the coagulation diagram and coagulation zones would have to be updated to conform with real-world conditions (e.g. NOM in water). Figure 2.13 combined the coagulation diagram (from Figure 2.4) with the total aluminum solubility at varying levels of DOC (from Figure 2.12). The solubility curves for waters containing DOC were calculated using a similar approach as described in the previous section.

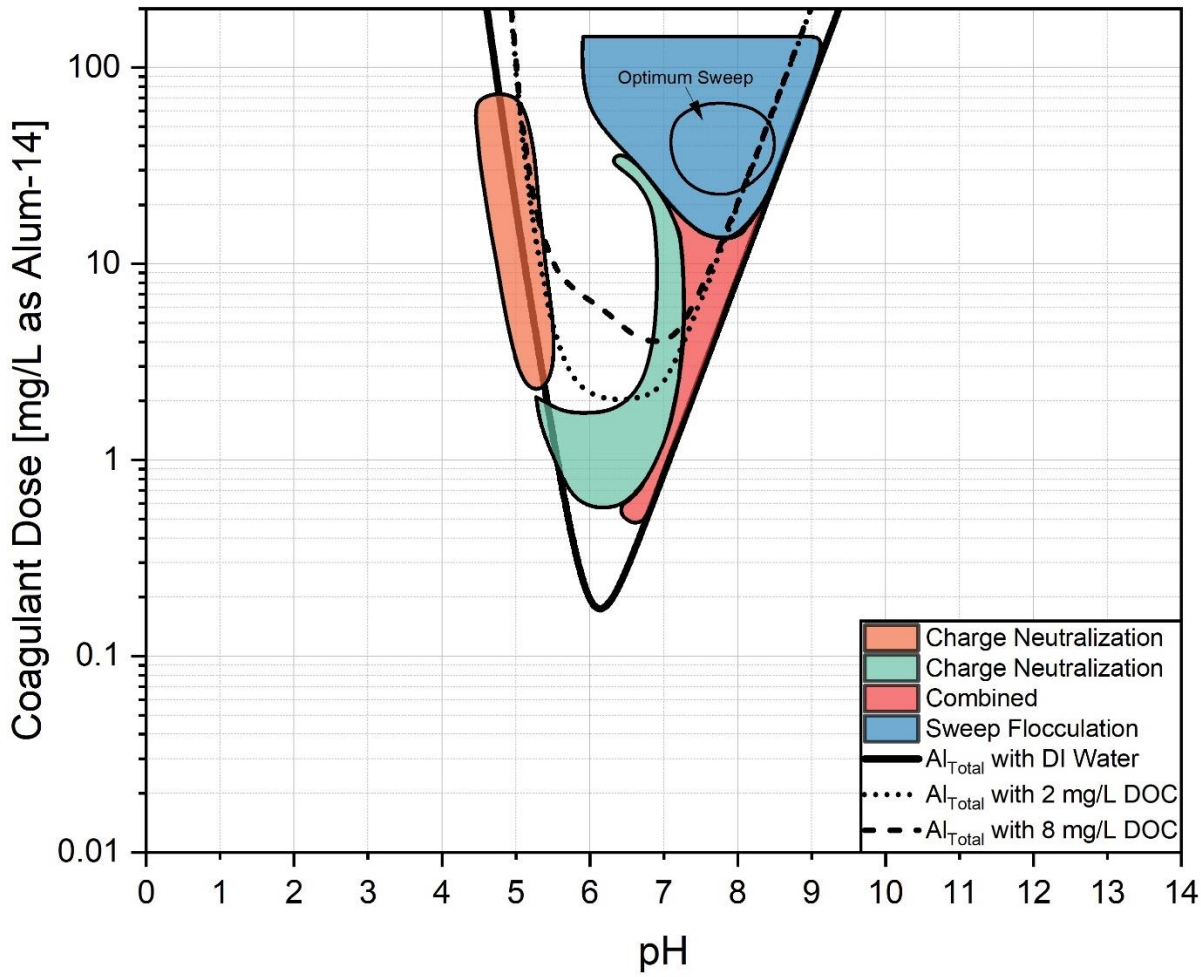

Figure 2.13 Coagulation diagram with waters containing DOC at 25°C

Figure 2.13 showed that a significant portion of the charge neutralization and combined zones occur under conditions where effective coagulation would likely not be possible with real waters. Figure 2.15 only shows the areas where effective coagulation would likely be possible with real waters. The areas where coagulation is unlikely to be effective was colored in grey. Effective coagulation (in terms of turbidity removal) below 2 mg/L as alum-14 would likely not be possible with waters containing DOC, particularly above pH 6; therefore, all conditions below 2 mg/L as alum-14 were excluded. Above pH 6.0 at 25°C, the primary coagulation mechanism is expected to be via sweep flocculation, which relies on the formation of amorphous hydroxide precipitate.

The presence of DOC would increase the solubility of the coagulant; thus, minimizing the formation of the precipitate required for sweep flocculation. As a result, only conditions that fall inside the solubility limits (in the presence of DOC) could be realistically considered.

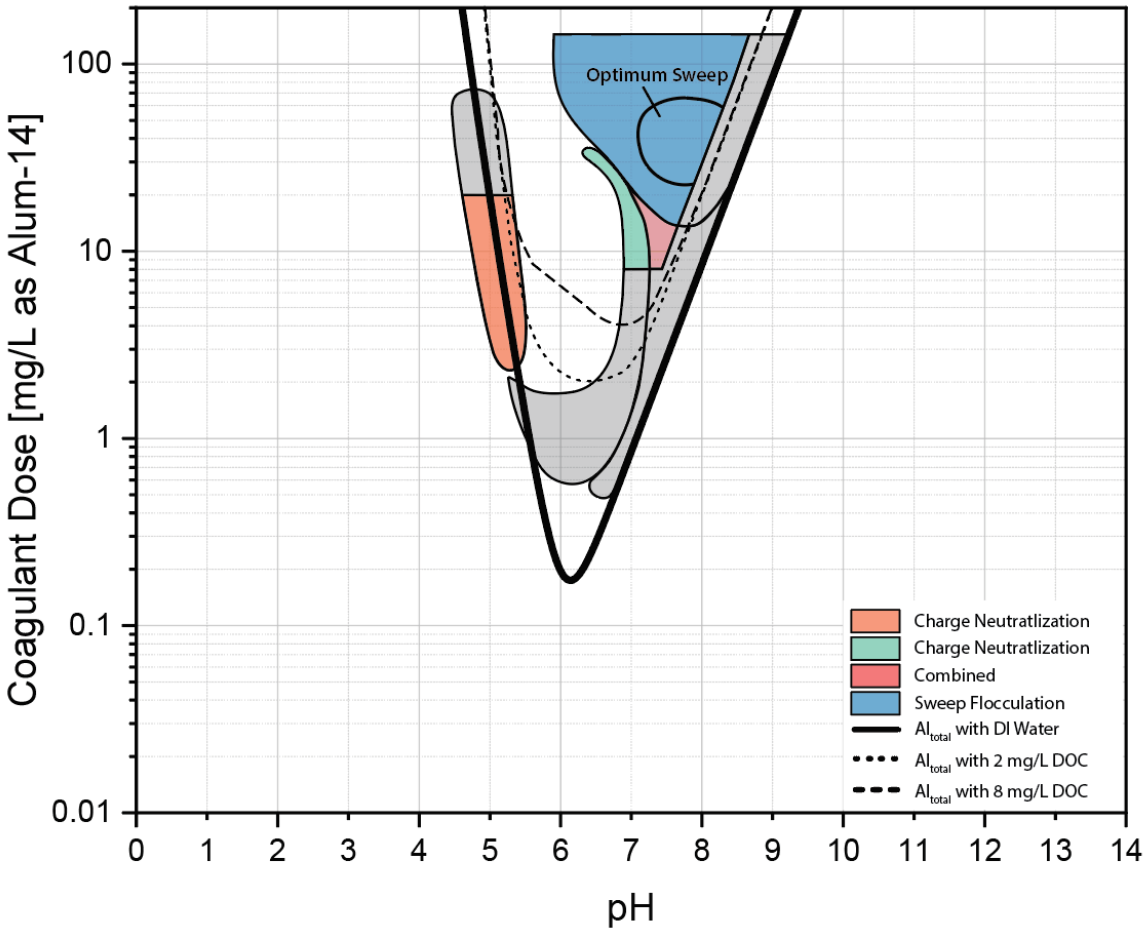

Figure 2.14 Zones where effective coagulation is likely possible

Based on Figure 2.9, effective coagulation above 20 mg/L as alum-14 in the orange charge neutralization region (below pH 5.5) would likely not be possible due to the high total available positive charge relative to the total charge demand of most waters. On the other hand, it is unlikely that charge neutralization would be possible in the lower portion of green charge neutralization region (above pH 7.0) due to the very low total available positive charge relative to the total charge demand of most waters. Ultimately, the coagulation zones would need to be modified to reflect a

more realistic view of coagulation with real waters. The scales of the coagulation diagram were adjusted to only include the typical operating range of most treatment plants in Figure 2.15.

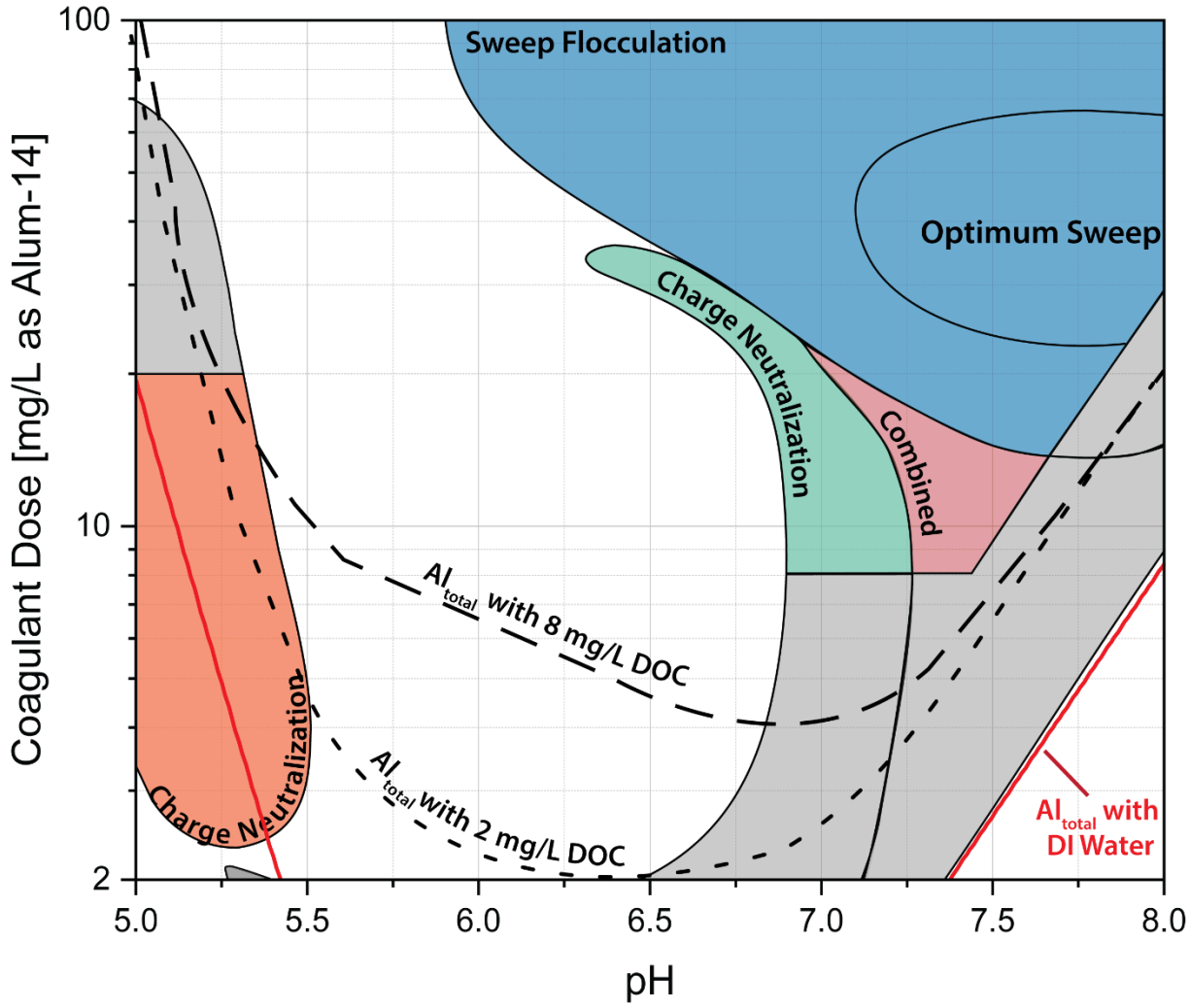

Figure 2.15 Zoomed in coagulation diagram

2.5. New Coagulation Diagram

Thus far, only updates were made to the original coagulation diagram. In this section, a new coagulation diagram will be presented that addersses many of the shortcomings of the original coagulation diagram that limited its applications to the theoretical rather than real-world study of coagulation. Primarily, the new coagulation diagram incorporates the effects of different water quality parameters on the shape, size, and location of the coagulaiton boundaries. The new diagram will be presented incrementally beginning with an update of the coagulation zones (Figure 2.16).

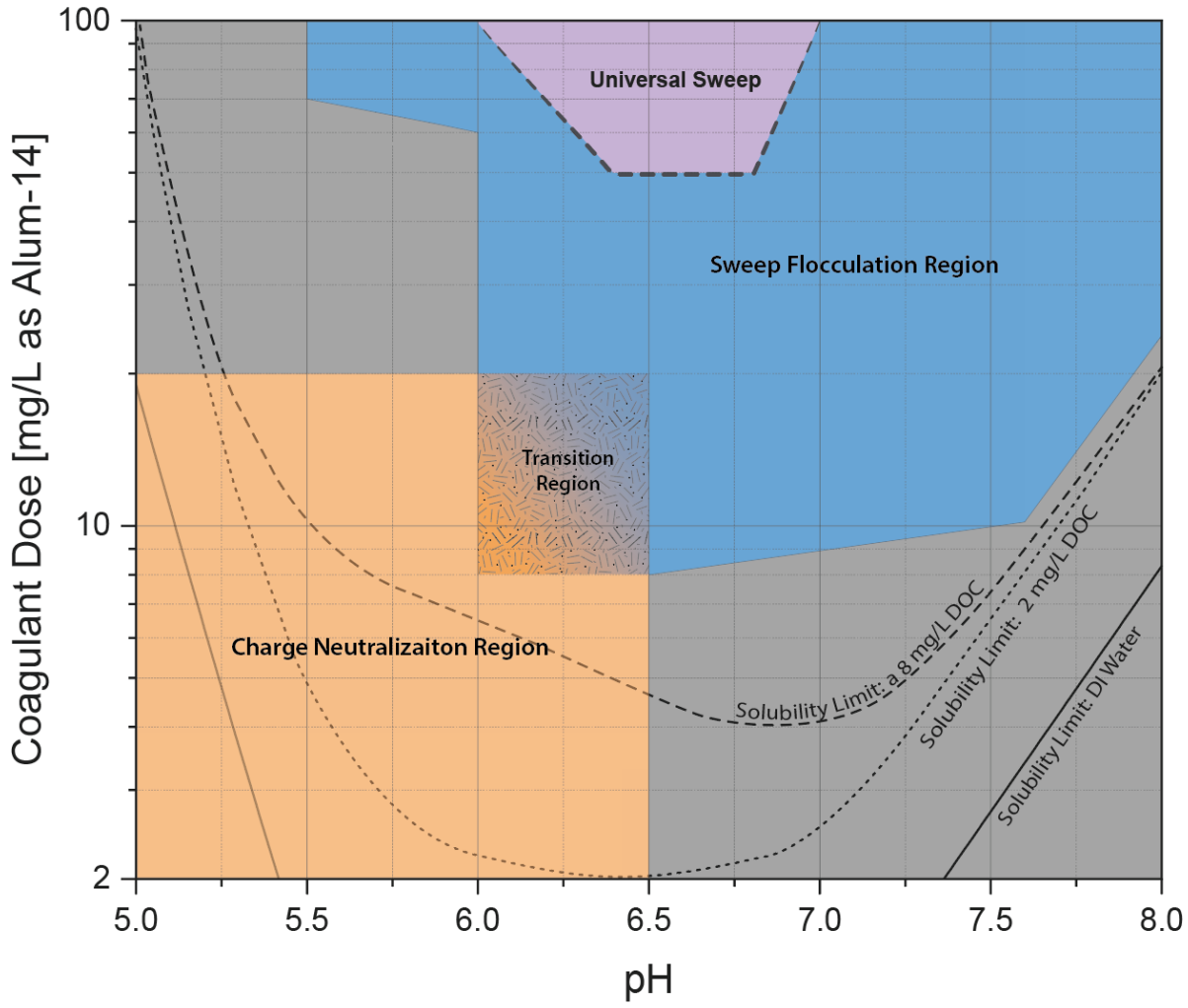

Figure 2.16 New alum coagulation diagram with general coagulation regions

The new coagulation diagram is comprised of 4 primary regions: 1) charge neutralization, 2) transition region, 3) sweep flocculation, and 3) universal sweep. These regions represent conditions where effective coagulation in terms of filtered turbidity removal would be possible, depending on the raw water quality conditions. The new boundaries were based on a series of carefully controlled jar tests with 16 different waters (discussed in Chapter 5). The conditions tested ranged from pH 5 – 8.0 and 3 to 100 mg/L as alum-14.

Coagulation in the lower-left region of the coagulation diagram would occur via the charge neutralization mechanism (shown in orange). The charge neutralization region ranges from pH 5 to 6.5 and from 2 to 20 mg/L as alum-14. Effective coagulation in the upper-left and lower-right regions would likely not be possible due to either an excess of total available positive charge which would restabilize the contaminants or conditions that would not be suitable for the formation of floc. Coagulation via the sweep flocculation mechanism occurs in the upper-right region of the new coagulation diagram (shown in blue). A "transition" region would exist between pH 6.0 and 6.5 and 8 to 20 mg/L as alum-14 where it would be difficult to distinguish the primary coagulation mechanism. It could be possible that both mechanisms are occurring simultaneously in the transition region. Finally, the universal sweep region represents the coagulation conditions that are likely to be effective with practically any water, i.e., independent of water quality.

Figure 2.17 shows the new coagulation diagram with the effects of raw water DOC and alkalinity on the effective coagulation zones. In general, the DOC concentration of the raw water would control the location of the effective coagulation boundary while alkalinity only affects the slope of the boundaries as the pH increases. For example, the lower dose limit of the effective coagulation boundary for a low DOC and low alkalinity water would be found at approximately 8 mg/L as alum-14. Increasing the DOC of the raw water would cause the boundary to move up and

to the left (i.e., higher dose and lower pH). A sharp cut-off boundary would also be observed in the conditions above 20 mg/L where the applied coagulant dose would rapidly transition (~0.1 – 0.2 pH units) from being ineffective to effective due to a transition from charge neutralization to sweep flocculation. The pH at which the sharp boundary would be observed would depend primarily on the DOC and alkalinity of raw water but would range from approximately pH 6.0 (high DOC/alkalinity) to pH 6.5 (low DOC/alkalinity). Alkalinity would generally only impact high pH (pH > 7.0) conditions by increasing the slope of the right-edge of the effective coagulation boundary; however, an effect would only be observed with a large change in raw water alkalinity.

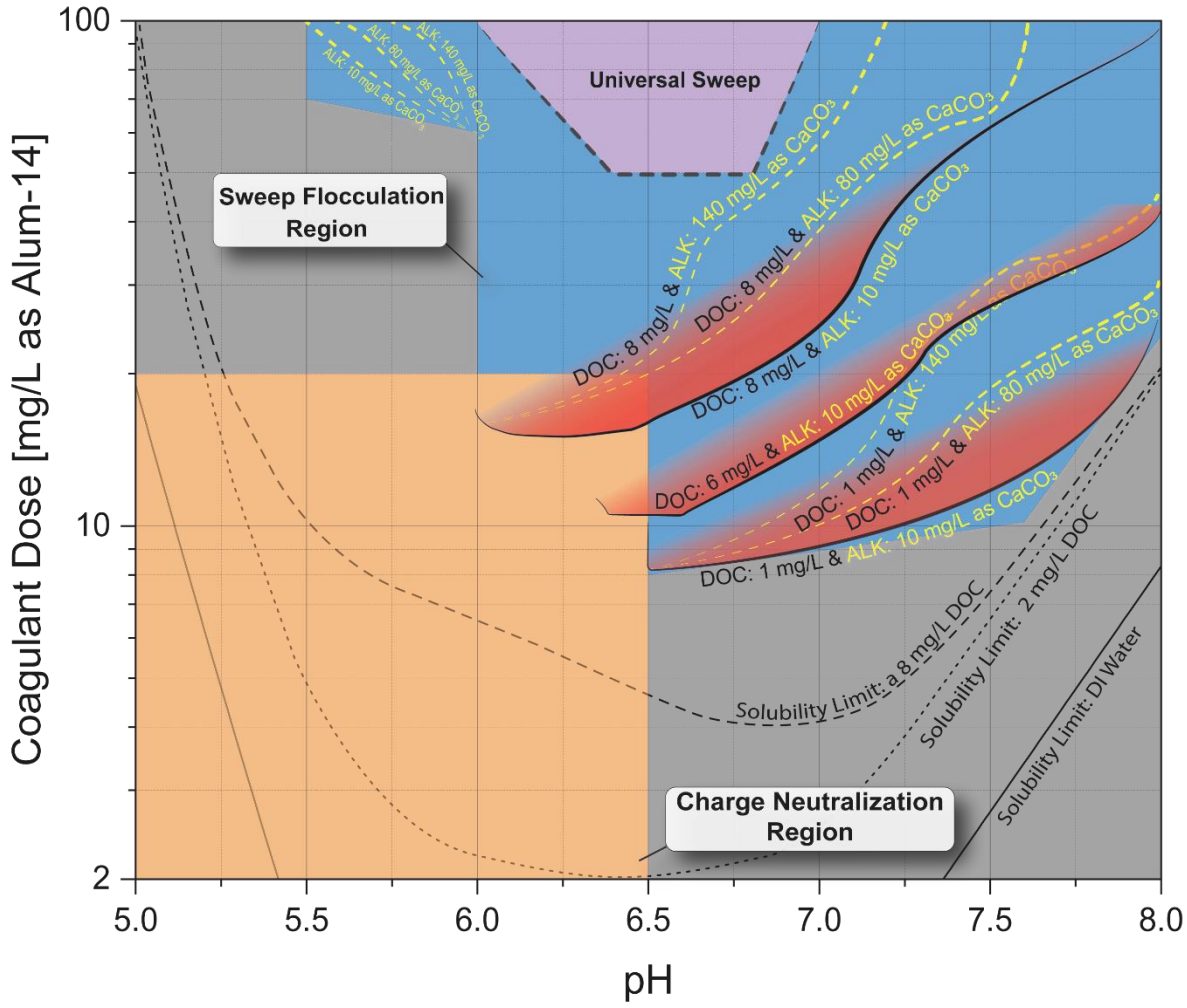

Figure 2.17 Coagulation diagram with DOC and alkalinity effects

Figure 2.18 shows the final coagulation diagram which includes the combined effects of raw water DOC and specific ultraviolet absorbance at 254nm (SUVA). In general, SUVA impacts conditions in the charge neutralization region. The effective coagulation boundary would extend further into the charge neutralization region the higher the SUVA of the raw water. The green and purple boundaries represent waters low and high in DOC, respectively. The SUVA boundaries are meant to only show where effective coagulation conditions might be located. The stoichiometric nature of the charge neutralization mechanism makes it difficult to generalize the shape and location of an effective coagulation zone; however, in most cases the zones are expected to be small and disconnected due to the stoichiometric nature of the charge neutralization mechanism, particularly with waters low in DOC.

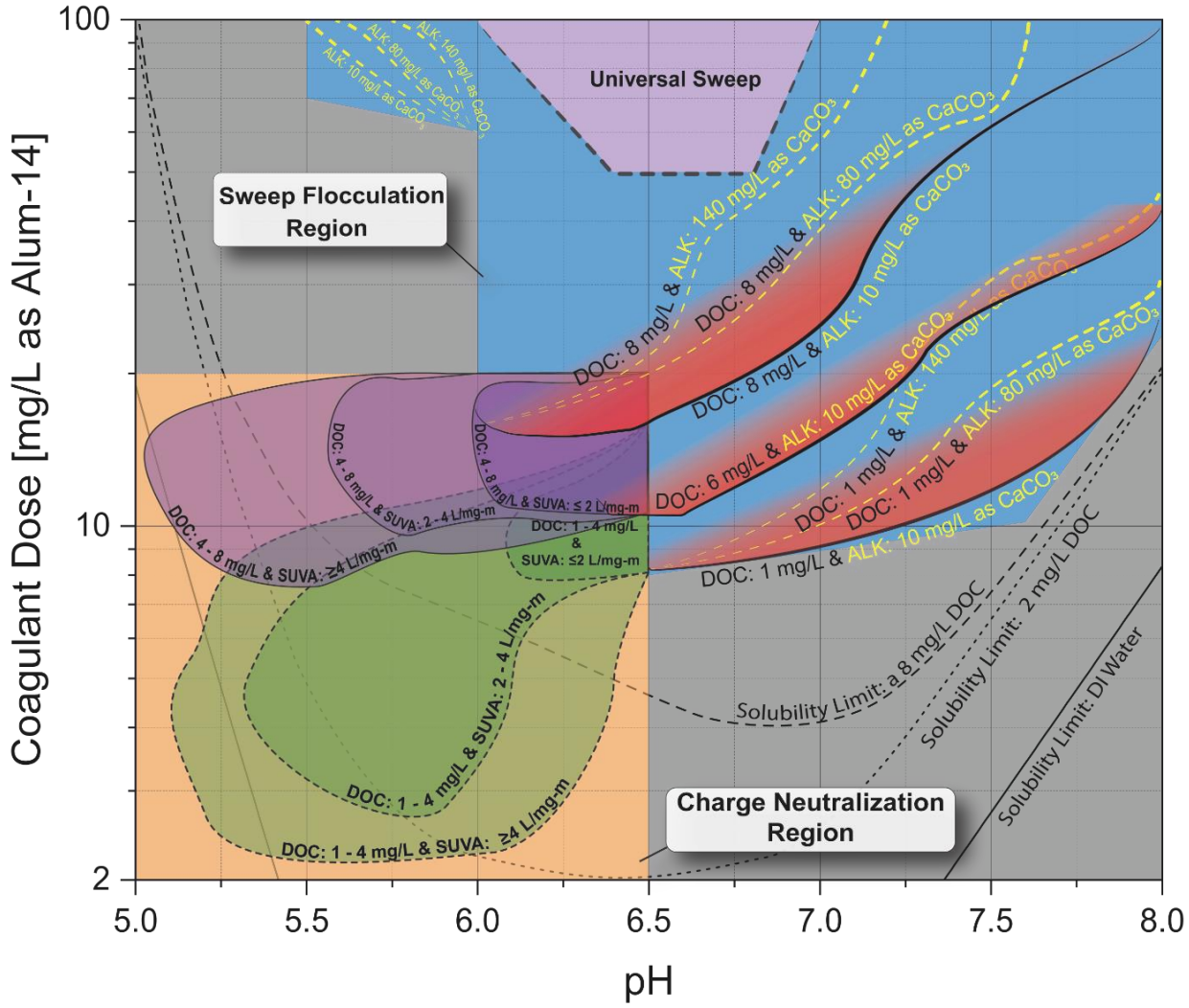

Figure 2.18 Final alum coagulation diagram

Ultimately, the goal of updating the coagulation diagram was to provide a diagram with practical real-world applications. The addition of the water quality boundaries would make it possible for operators and engineers to quickly identify optimal coagulation conditions based on their own water quality conditions as originally intended by Amirtharajah and coworkers (1982, 1985).

CHAPTER 3: COAGULATION OPTIMIZATION

It is often said that drinking water treatment is an art as much as it is a science (Kawamura 1975). This notion was based on the fact that most drinking water treatment practice has been guided by experience and empirical knowledge rather than on a fundamental understanding of the underlying processes. In addition, every water is different, and every drinking water treatment plant is unique in its design and operation. Unfortunately, the former approach is the only viable option for optimizing processes such coagulation. Optimization is essentially an experimental process; therefore, it is essential that the experimenters (operators and engineers) plan and conduct these experiments strategically and effectively. Thus, it is even more critical that the experimenters have developed a fundamental understanding of the coagulation process and the relationships between the input and output parameters. The following section will mainly focus on the process of optimizing coagulation.

Coagulation can be visualized as a simple process with inputs and outputs, as shown in Figure 3.1. Some input parameters or factors can be controlled (e.g., the coagulant dose), whereas most factors are uncontrollable (e.g., raw water quality parameters). The efficiency of the process can be quantified by measuring the response of a given variable with respect to the input factors. To optimize the coagulation process, operators and engineers must clearly define their objectives and then, through experimentation, select a combination of controllable inputs that would produce the best possible outcome based on their desired set of goals.

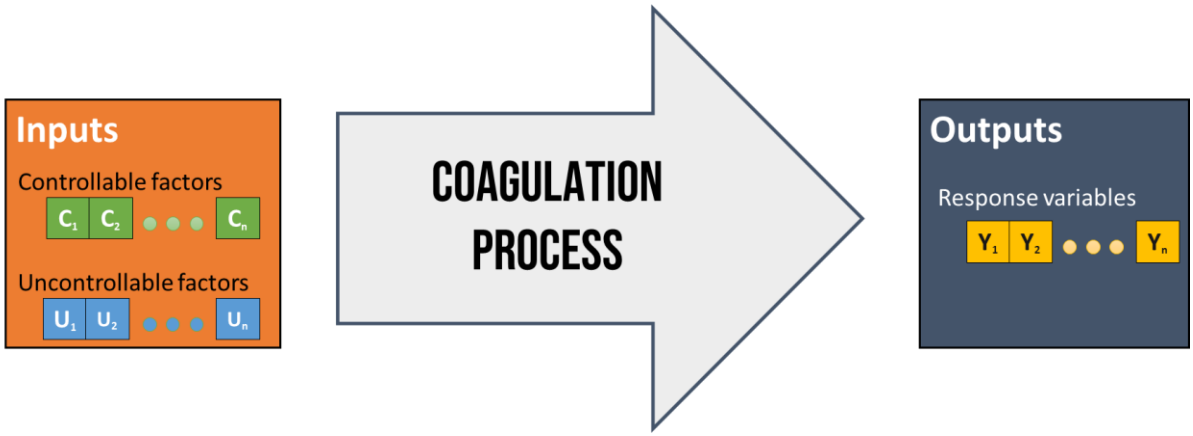

Figure 3.1. A simple model of the coagulation process

The objective of coagulation was earlier stated as being to destabilize contaminants in water to be effectively removed via a downstream engineered process such as sedimentation and/or filtration. By this definition, the efficiency of the process could be assessed by quantifying the removal of the contaminant(s) of interest. Consequently, optimization would imply maximizing the removal of the contaminants in the overall treatment process while also considering the amount of treatment chemicals being used (i.e., minimizing the cost of treatment chemicals). For example, the input parameters of the process include the raw water quality (e.g., turbidity), coagulation conditions (e.g., dose, type, and pH), and plant design parameters (e.g., flow rate or the number of mixing stages). In most instances, coagulation conditions could be the only controllable factors. The output parameters or response variables include the quality of the filtered water and the total cost of treatment chemicals used.

Drinking water treatment plants are designed as a series of continuous-flow reactors (basins) – where there is a continuous flow of water flowing into and out of the treatment facility. It commonly takes between 4 – 12 hours for the water to travel from the point of coagulant addition to the point of filtration; therefore, quantifying the performance of the coagulation stage just based on the removal of contaminants after filtration is impractical in full-scale treatment facilities both

in terms of resources and associated risks to public health. For this reason, operators must rely on an assortment of direct and indirect metrics for quickly assessing the efficiency of their coagulation stage. In 2002, Logsdon and his colleagues published a report which included a survey of 37 drinking water treatment plants and their practices in selecting their coagulation conditions and measuring their performance (Figure 3.2). More than 60% of the plants reported that they used at least four or more different coagulation metrics to assess the performance of their coagulation process. The most prevalent strategy employed by the surveyed plants was the use of historical plant data (records) in their decision-making process.

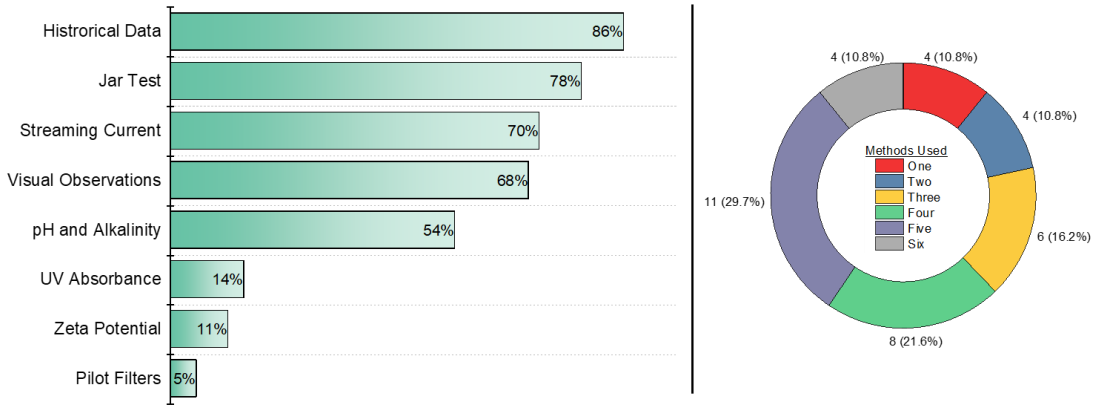

Figure 3.2. Methods used for monitoring coagulation performance (from Logsdon et al. (2002))

3.1. Historical Data

Modern drinking water treatment plants generate enormous amounts of data from daily/hourly log sheets, online instrumentation, and supervisory control and data acquisition (SCADA) systems. Any tool or system that facilitates access to this data is instrumental in allowing the staff to be more proactive in their day-to-day operations. For example, operators could use a spreadsheet to log and plot hourly plant data versus time which could reveal trends that may not be obvious when presented in a table format. However, data visualization is only one part of the

equation. The key is in how the information is analyzed and interpreted by the user. Historical records can help provide insights that can help the staff make informed decisions and minimize the potential risks associated with using a trial-and-error approach; however, care should always be taken when analyzing and interpreting historical plant data.

3.1.1. Correlation versus Causation

A common pitfall in analyzing data is interpreting correlations as causation. For example, Figure 3.3a shows a correlation between the alum dose and settled water turbidity – i.e., settled water turbidity generally decreased with increasing alum dose; therefore, one can conclude that lower settled water turbidity can be achieved by simply increasing the coagulant dose. The same results are plotted versus time in Figure 3.3b, and at first glance, it appears as though the initial conclusion was valid. However, there was also a correlation between the temperature of the raw water and settled water turbidity. In general, sedimentation basins perform better at warm temperatures; thus, it was also possible that the lower settled water turbidity over time was the result of the warmer temperatures (Morris and Knocke 1984). At the same time, temperature affects aluminum hydrolysis reactions and the solubility of the precipitate. As a result, it is difficult to determine with certainty whether the lower settled water turbidity values were the direct result of the increased coagulant dose, increased raw water temperature, or a combination of both factors changing simultaneously. The example shown in Figure 3.3 highlights one of the many difficulties associated with the study of coagulation and the optimization of this process. Many competing factors can impact the efficiency of the coagulation process; however, the problem remains that these factors also influence each other. The effects of different factors on coagulation will be discussed further later.

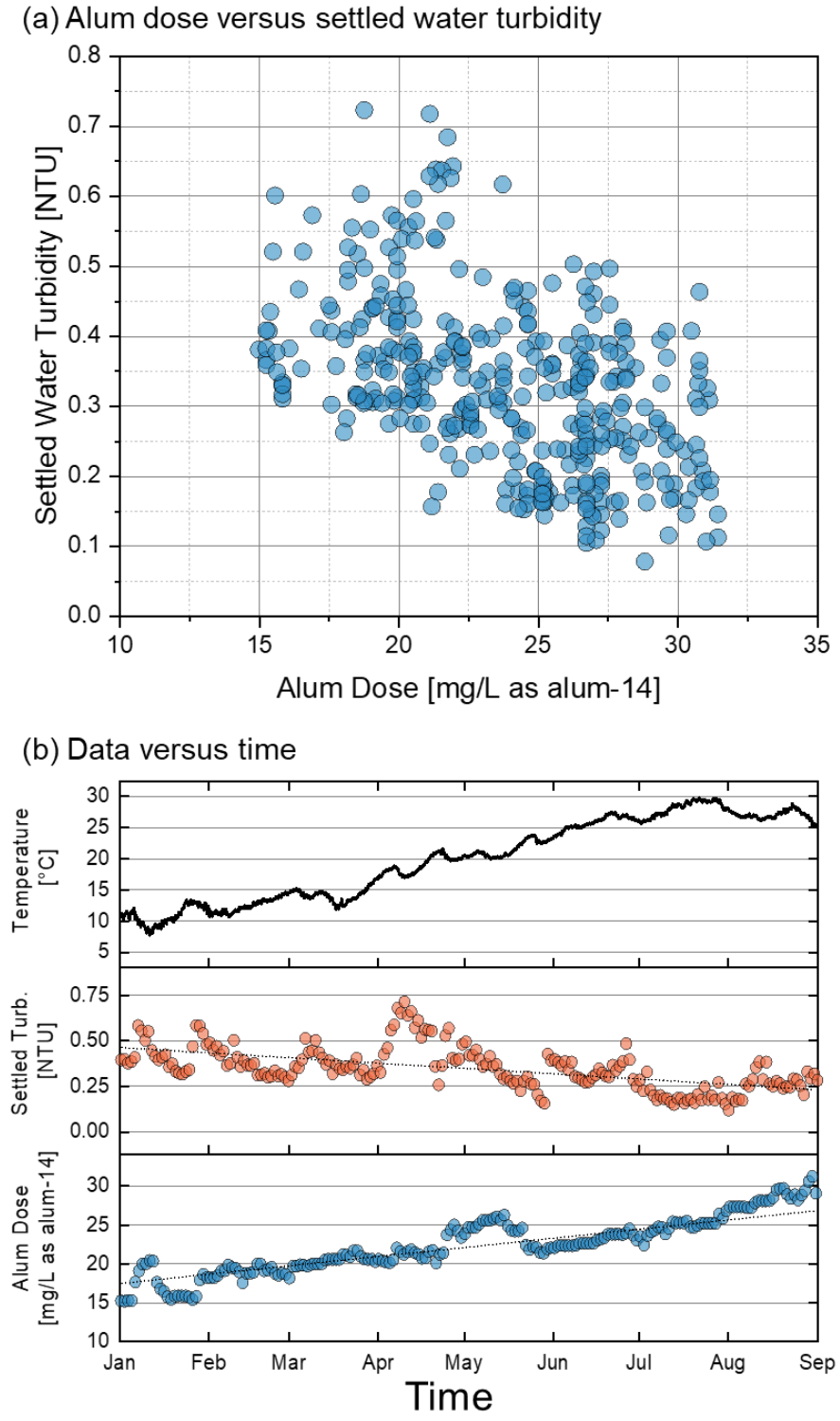

Figure 3.3. Plant historical data

3.1.2. Data Limitations

Historical data often contains limited water quality information necessary for a full assessment of coagulation requirements. Ultraviolet absorbance at 254 nm (UV_{254}) and DOC provide an indication of the characteristics and concentration of the natural organic matter in the raw water, which is often the controlling parameter of coagulation requirements (Edzwald 1993; Edzwald and Tobiason 1999). The treatment plant whose data were shown in Figure 3.3 did not continuously measure UV_{254} and DOC levels of the raw water, which may have contained some additional clues to explain the observed trend. Additionally, historical data typically lacks contextual factors such as the events or factors that triggered the operator to change the coagulant dose.

3.1.3. Assumptions Hidden in Historical Data

In addition to historical plant data, many treatment plants rely on quantitative and qualitative measurements that relate to the efficiency of the coagulation stage. Except for visual observations, measurements are performed either in real-time using online instrumentation or as grab samples using benchtop equipment. The underlying assumption is that there exists a direct or indirect correlation between the measured parameter and the efficiency of the coagulation process (e.g., removal of contaminants from water). For example, operators visually evaluating the clarity of their sedimentation basins are, in effect, assuming that their basins' clarity is a function of their selected coagulant dose and pH. Surface charge measurement techniques are based on the assumption that the removal of contaminants would be maximized when coagulation is performed at a near-neutral contaminant surface charge (e.g., ±10 mV). Similarly, the reduction of UV_{254} is expected to reduce the formation of potentially harmful disinfection by-products in the finished water.

3.2. Pilot Filters

Some treatment plants monitor the performance of their coagulation process by filtering a fraction of the coagulated water using a pilot-scale filter that is equipped with an online turbidimeter (Conley and Evers 1968). Visible floc is not expected to form due to the relatively short detention times (<10 minutes) after coagulant addition. The primary purpose of a pilot or lab filter is not to accurately predict the filtered water turbidity of the full-scale process but rather to simply provide a baseline from which changes in coagulation requirements can be captured/quantified over time. The short detention time is ideal for detecting early signs of deteriorating treated water quality due to suboptimal coagulation. Compared to surface charge and UV_{254} measurements, pilot-filters hypothetically offer a better approximation of the expected full-scale results since they are based on a direct measurement of the "treatability" of the water (i.e., turbidity removal) rather than a correlation.

Figure 3.4 shows results from a case study where a lab-scale filter was used to directly filter coagulated water and monitor the performance of the coagulation stage. In this case, one of the primary goals of the treatment plant was to maintain a settled water turbidity value below 1.0 NTU in 95% of the samples measured. Operators observed that the lab-scale filter predicted the response of the settled water to changing water quality conditions approximately 4 – 6 hours in advance.

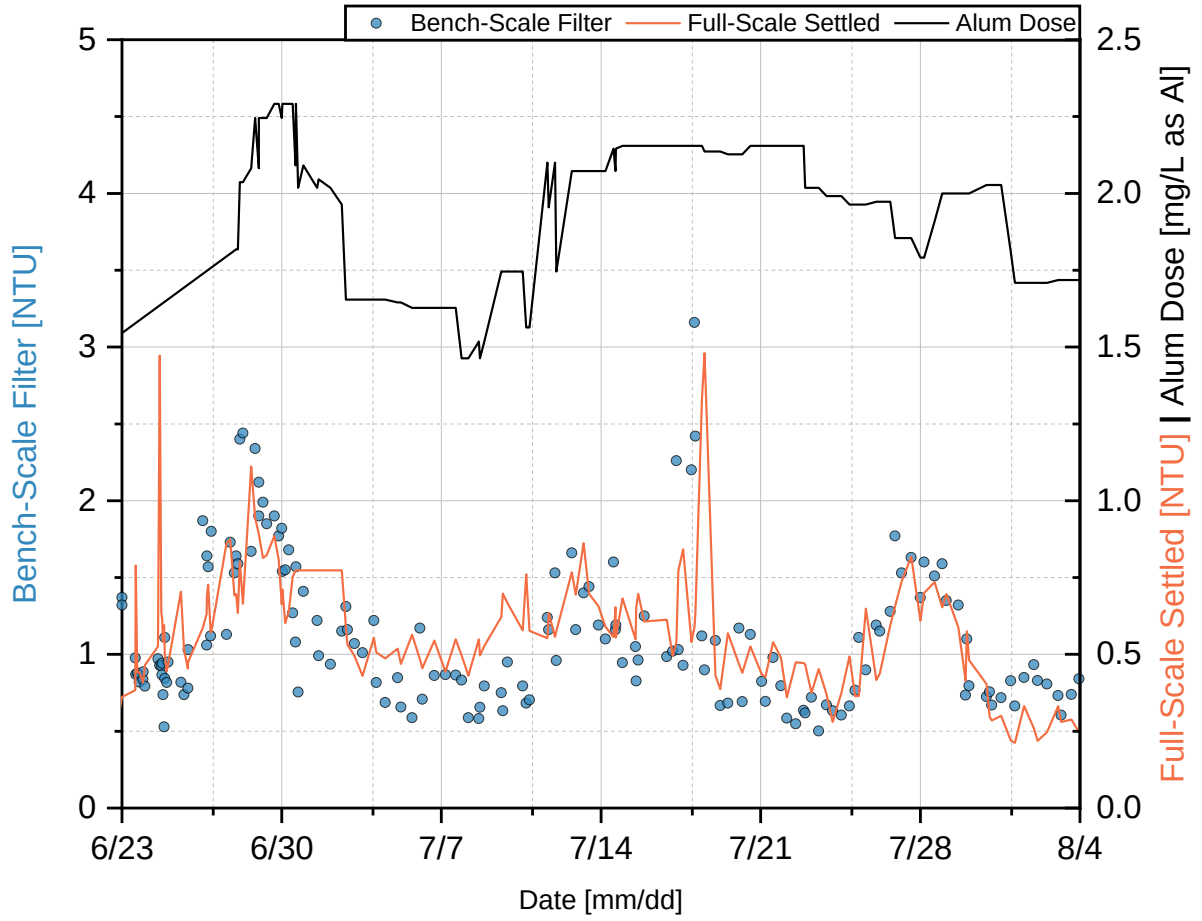

Figure 3.4. Bench-scale filter results

3.3. The Conventional Jar Test Procedure

Even though the measurement techniques mentioned so far help monitor coagulation, the consequences of using a trial-and-error approach to optimize the process at the full-scale prevent them from being useful as optimization tools. Experimentation and optimization of the coagulation process should be performed using bench- and pilot-scale systems that simulate the physical and chemical processes in the full-scale treatment process. Jar testing is regarded as the most reliable and widely used bench-scale tool to optimize coagulation conditions in drinking water treatment (Black et al. 1957; Hudson and Wagner 1981). The jar tester is a simple bench-scale apparatus with four to six identical jars or beakers equipped with overhead mixers. The jar tester was invented by Wilfred Langelier, who originally built the apparatus to demonstrate the effects of mechanical mixing on coagulation efficiency; however, he later recognized its potential use as a tool for investigating the effects of water quality parameters (e.g., alkalinity and pH) in the coagulation process (Langelier 1921; Langelier 1982). The overall design and operation of the jar test apparatus has largely remained the same since its invention in 1918 by Langelier (Figure 3.5).

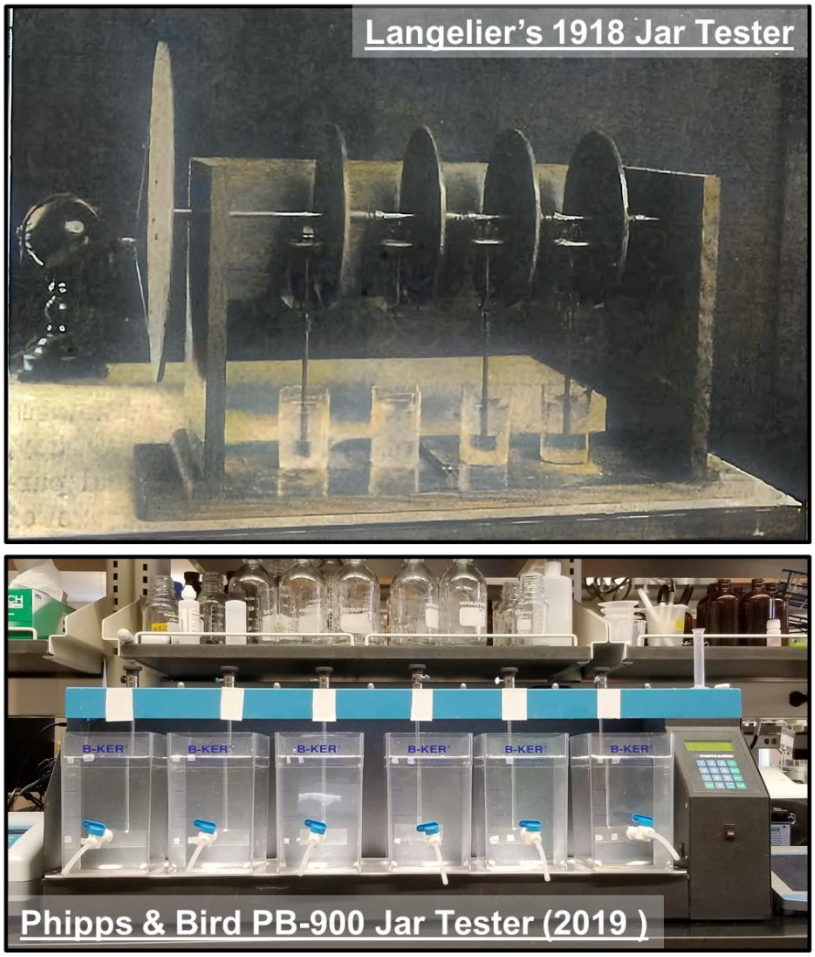

Figure 3.5. Comparison between a modern jar test apparatus and one developed by Langelier

The general approach of jar testing is usually to start with a high-intensity mixing stage to rapidly disperse the coagulant and/or chemicals (rapid mix), followed by a low-intensity mixing stage to allow the contaminants to aggregate (flocculate) and finally, a particle separation stage to separate the floc from water. The jar tester has gradually evolved into a tool that can be used to optimize coagulation and as a tool that can aid engineers in designing and optimizing drinking water treatment processes (Griffith and Williams 1972). Singley (1981) stated that jar tests can be used to perform the following tasks: (1) selection of suitable coagulant type, (2) optimization of coagulation dose and pH, (3) determination of order of pH adjusting chemical addition, (4)

optimization of mixing parameters (e.g., intensity, time, or the number of stages), and (5) selection and optimization of coagulant aids (Amirtharajah and O'melia 1990).

Before the 1950s, it was a common and accepted practice to evaluate coagulation performance in jar tests based on a visual evaluation of floc formation. The underlying assumption was that a large floc or floc that formed rapidly was indicative of optimum coagulation conditions (Brown 1936). Langelier and Ludwig (1949) observed that low settled water turbidity – collected after a constant settling period – always corresponded with “high quality” floc. By the 1970s, settled water turbidity became the standard metric by which coagulation performance was evaluated in bench-scale experiments. Settled water turbidity was considered the most convenient and easily reproducible method of objectively quantifying coagulation efficiency (Black and Vilaret 1969). Jar test procedures based on settled water turbidity measurements were commonly referred to as conventional jar tests (TeKippe and Ham 1970).

3.3.1. Controllable Factors in A Conventional Jar Test

The factors involved in the coagulation process can be grouped into three categories: water quality parameters (e.g., raw water turbidity or alkalinity), coagulation conditions (e.g., coagulant type or dose), and mixing parameters (e.g., duration of rapid mix or number of flocculation stages). Operators and engineers are practically only able to control and optimize coagulation conditions and mixing parameters. In this case, it is also assumed that the sample volume and container dimensions are constant variables. In a conventional jar test procedure, the dependent or response variable would be settled water turbidity. Experimenters would be able to quantify the effect of any of the controllable factors (e.g., coagulant dose) on the coagulation process by measuring the

turbidity of the water at the end of the settling stage. Figure 3.6 shows a general model of the controllable factors involved in a conventional jar test procedure.

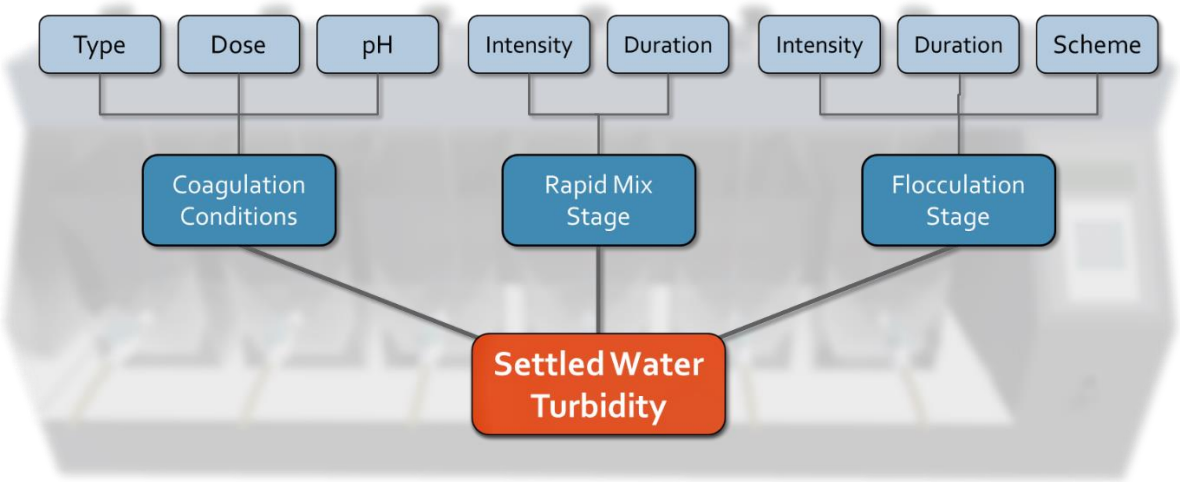

Figure 3.6. Controllable factors in a conventional jar test

3.3.2. The Standardization Debate

Black and coworkers (1957) noted that "...there are about as many individual variations in (jar test) procedures as there are individuals carrying out the test." Researchers have long debated over the need for a standardized jar test procedure. On the one hand, the jar tester was promoted as a tool for operators and engineers to replicate the full-scale drinking water treatment process. On the other hand, the lack of a standardized procedure meant that jar test results obtained using different procedures could not be compared directly.

Graham (1939) stated that "jar tests will have little meaning unless stirring conditions match those of the plant closely." This view has been endorsed by many researchers, engineers, and authorities over the years, including ones that expressed the need for a standardized jar testing procedure. Treatment plant operators are expected to match their jar test mixing parameters as close as possible to their unique treatment plants by calculating their basins' theoretical mixing

intensities and detention times. It is often the case that even when full-scale treatment plant conditions are precisely replicated, jar test results would not match the results observed in the full-scale process; thus, operators would have to go through a tedious trial-and-error process to tweak their jar test procedure until their results matched (Hudson and Wagner 1981; Teefy, Farmerie and Pyles 2011). Some sources refer to this process as "calibrating" the jar test procedure to an individual treatment plant (Budd et al. 2004).

The commercialization of the jar tester and the publication of industry guidelines such as the American Water Works Association's (AWWA) M37 manual has somewhat reduced the variability of the selected sample volumes and container dimensions. Settled water turbidity has since become the preferred industry metric for objectively quantifying coagulation efficiency; however, there is still some discrepancy in the selected duration of the settling stage and sampling protocols (e.g., depth at which the sample is collected). Several researchers also noted that floc characteristics and settled water turbidity were highly sensitive to jar test mixing parameters (Griffith and Williams 1972; Ives 1979; Bernhardt and Schell 1993); therefore, minor variations in the procedure could produce markedly different results.

A key factor in the standardization of the jar test procedure is the performance metric selected to evaluate the efficiency coagulation in the jar test procedure. A suitable performance metric that facilitates the standardization of jar testing must have the following characteristics: (1) it should be based on a reproducible and objective measurement, (2) it should be independent of mixing parameters, and (3) it should be directly scalable and representative of full-scale results. Settled water turbidity would meet the first criterion by being a reproducible and objective measurement; however, it fails to meet the second and third criteria. Metrics based on dissolved contaminants such as natural organic matter (e.g., UV_{254} and DOC) would be suitable since they

would meet the first and second criteria; however, they cannot be used exclusively since they do not give any indication of the extent of turbidity removal – which is arguably the primary metric by which the performance of the full-scale process is evaluated.

3.4. Jar Test Filtration

Some researchers recommended using membrane filters or filter papers to reproduce full-scale granular media filtration results (e.g., Hudson and Wagner (1981) and Herman (1984)). Membrane/paper filters and granular media filters (such as sand) rely on different mechanisms of removing contaminants from water. In membrane filtration, particles are removed via size exclusion or sieving whereas, in granular media filtration, removal occurs via contact and attachment between particles and the surfaces of individual media grains. As a result, granular media filtration relies on media depth where water is forced to travel through a tortuous path, thereby increasing the likelihood of collisions between the particles and the media. The attachment efficiency of stable particles is expected to be low due to the same repulsive forces that keep two particles apart; therefore, chemical pretreatment (i.e., coagulation) is required to destabilize the particles and enhance their attachment efficiency. This implies that a greater burden is placed on the efficiency of the coagulation stage instead of floc size since the pores in a granular media filtration are orders of magnitude larger than most contaminants. Compared to granular media filtration, some drawbacks of using membrane filtration include an increased risk of floc breakage due to sampling and additional recurring expense of filters.

Researchers have also explored the idea of quantifying coagulation efficiency using filtered water turbidity. Hannah et al. (1967) developed a bench-scale granular media filter which was used to measure filtered water turbidity. In their procedure, the authors collected a sample of settled water and poured into the filter column. Their column could be operated at either 2 or 8 gpm/ft^2.

In general, Hannah et al. (1967) found that the results obtained from a small bench-scale granular media filter column were comparable to the results obtained from a pilot-scale filter. TeKippe and Ham (1970) used a somewhat similar approach; however, the filtration rate in their filter was set to 20 gpm/ft^2 (approximately 10 times the recommended rate) to evaluate the strength of the floc. The authors reported a good correlation between settled water turbidity and filtered water turbidity. Brink and coworkers (1988) developed a jar test procedure based on granular media filtration instead of settling specifically for direct filtration plants (i.e., without a sedimentation stage) or plants that treated low turbidity waters where it was challenging to form settleable floc. The authors found that jar test filtered turbidity results were scalable and closely matched plant results. Dentel et al. (1988) developed a bench-scale filter apparatus that could quantify floc filterability and estimate filter run times and head loss. Their results were mostly in good agreement with the full-scale process. Bernhardt and Schell (1993) developed a mixing/filtration apparatus in which the coagulated water could be directly filtered (i.e., without pouring), thereby minimizing the possibility of breaking the formed floc. Bernhardt and Schell found that filtration was a better metric than settled water turbidity when optimizing mixing parameters.

Ultimately, filtration-based jar tests were historically not considered as anything more than a solution for plants that do not produce a settleable floc. Researchers who investigated bench-scale filtered turbidity as a performance metric observed the close similarity between the bench-scale and full-scale results; yet, failed to note its significant implications as a performance metric in the optimization of coagulation conditions and mixing parameters.

3.5. Next-Generation Jar Test Procedure

A new (next-generation) jar test procedure was developed that had three key advantages over conventional jar test procedures. First, the new jar test procedure uses a standardized mixing program. This means that operators and engineer do not need to match their jar test mixing program to their process or spend time calibrating their procedure to match their jar test results with the full-scale process. Figure 2.10 showed that alum behaves like an acid, which means that the pH will vary as a function of the coagulant dose and the raw water alkalinity. In the case of optimizing coagulation conditions, either the pH or the coagulant dose must be held constant as the other factor is varied across the jars. As a result, the procedure uses a single-variable optimization approach where all coagulation variables are controlled (fixed) to study the effects of a single parameter of interest (e.g., coagulant dose) on the overall process. Last, optimization is based on granular media filtration instead of settling. A custom-built filtration stand that houses six identical bench-scale filters is used to directly filter treated or settled water at the end of the experiment. Experiments performed by King (2017) showed that the combination of a relatively shallow media depth and high filtration rate ensured that sub-optimal coagulation conditions would not be falsely identified as optimal; therefore, the water was filtered by gravity at a rate of approximately 4.5 – 5 gpm/ft^2. A summary of the next-generation jar test procedure is provided in Appendix A; however, readers are strongly encouraged to refer to the videos and step-by-step guides freely available online (Alansari 2020d). The advantages of the next-generation jar test procedure over a conventional jar test procedure will be demonstrated in the subsequent sections and chapters.

3.5.1. Coagulation Optimization with The Next-Generation Jar Test Procedure

The following experimental result and discussion presented herein were intended to allow a comparison of results obtained from a conventional jar test procedure and results obtained from the next generation jar test procedure. The objective of this study was to identify zones of effective treatment in terms of settled and filtered water turbidity removal and to identify optimal charge neutralization and sweep flocculation conditions. The optimal charge neutralization and sweep flocculation conditions were selected for an investigation of mixing parameters in the following chapters.

3.5.1.1. Synthetic Water Preparation

Water quality is a primary factor that influences coagulation requirements and floc characteristics; therefore, water quality parameters need to be tightly controlled for this investigation. A synthetic raw water was created by combining DI water and surrogates for natural turbidity, alkalinity, DOC, SUVA. This ensured that the variability in the raw water quality was minimized; hence, excluded as a factor in the analyses of data. Details on the preparation of the synthetic water can be found in Appendix B. A water that had a low turbidity, DOC and SUVA, and low-mid alkalinity was selected since previous studies have shown that these conditions are typically less than ideal for the formation of floc (Letterman, Tabatabaie and Ames Jr 1979; Brink, Choi, Al-Ani and Hendricks 1988; Edzwald and Tobiason 1999; Jarvis, Jefferson and Parsons 2006). Table 3.1 presents a summary of the synthetic water quality parameters.

Table 3.1. Synthetic raw water quality parameters

Parameter	**Average *(± SD)*** [a]
Turbidity [NTU]	3.0 *(± 0.17)*
Dissolved organic carbon [mg/L as C]	2.0 *(± 0.21)*
Specific ultraviolet absorbance [L/mg-m]	2.3 *(± 0.098)*
Zeta potential [mV]	−26.3 (±9.77)
Alkalinity [mg/L as $CaCO_3$]	27.4 *(± 2.5)*

[a] Sample size = 102

3.5.1.2. Sedimentation Versus Filtration

A total of 17 jar tests (with 6 jars each) were performed where the investigated coagulant dose ranged from 3 to 100 mg/L as alum-14 while the pH ranged from 5 – 8 in 0.5 pH increments. Figure 3.7 shows the investigated coagulant dose and pH conditions. The X-symbols represent the target pH values, while the dot-symbols represent the measured pH values at the corresponding coagulant doses. The pH after coagulation was measured by collecting a 200 mL sample from each jar at the end of the rapid mix stage. In general, a difference of ±0.2 from the target pH was considered acceptable. Settled water turbidity samples were collected at the end of a 20-minute settling period. Filtered turbidity samples were collected by directly filtering the settled water using a set of bench-scale filters.

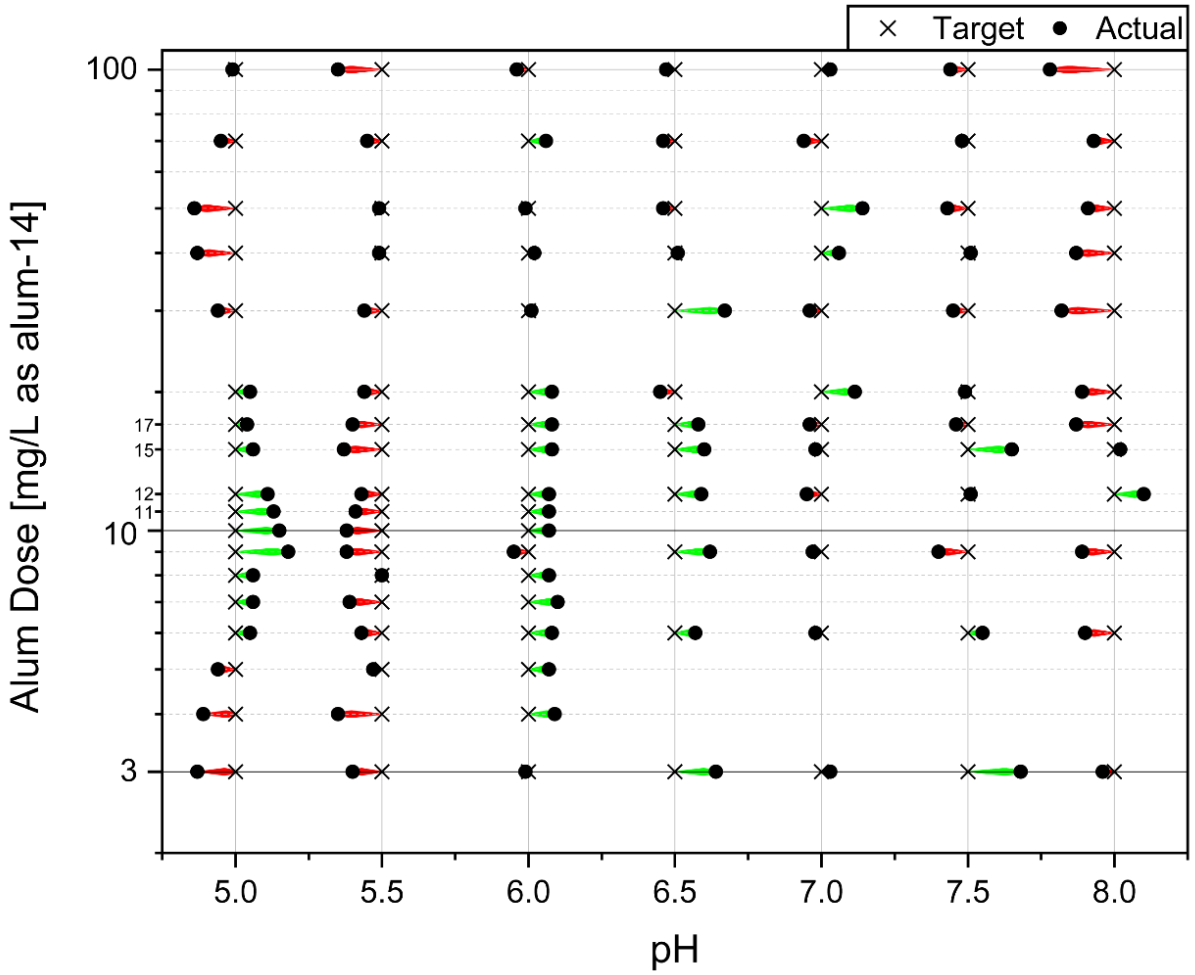

Figure 3.7. Investigated coagulation conditions (102 data points)

Settled and filtered water turbidity removals were plotted on contour graphs shown in Figure 3.8. The average raw water turbidity was 3.0 NTU; therefore, a filtered turbidity removal above 90% would correspond to a turbidity below 0.3 NTU (the current turbidity standard in the United States for full-scale water treatment facilities). It is worth noting that the jar test filters are producing this turbidity with only 3-inches of filter media at a flow rate of 4 – 5 gpm/ft^2, so a full-scale facility would reasonably expect a turbidity lower than 0.3 NTU under these coagulation conditions. There are currently no regulatory limits for settled water turbidity; hence, an "optimum" can only be selected based on the relative turbidity between the jars. Some states do participate in optimization programs that encourage utilities to achieve a reduced settled water

turbidity of less than or equal to 1.0 or 2.0 NTU (depending on the average raw water turbidity) and a filtered water turbidity less than or equal to 0.1 NTU (Barr 2007; GLUMRB 2018).

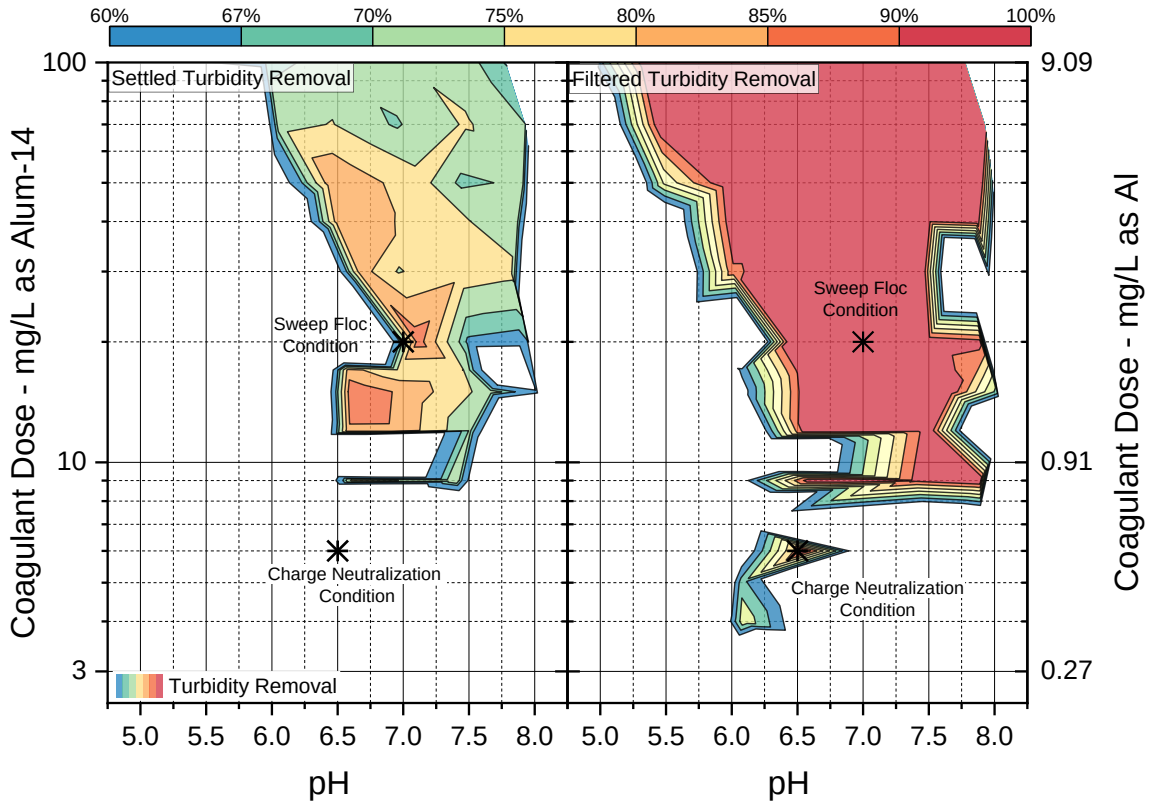

Figure 3.8. Settled (left) versus filtered (right) jar test results

The zones of highest settled turbidity removals (>80%) were small relative to filtered water turbidity zones and appeared to be sensitive to minor changes in coagulant dose and pH. The optimum settled turbidity removal zone was between pH 6.5 – 7.25 and 12 – 15 mg/L as alum – 14. The advantages of optimizing coagulation conditions based on filtration, instead of settling, become apparent when comparing the two plots in Figure 3.8 in terms of both size and consistency of optimal zones. The largest effective filtered turbidity removal zone (>90%) extended diagonally from approximately pH 5.5 to 7.75 between 9 – 100 mg/L as alum-14. Also, a small distinct zone was identified where the filtered turbidity removal exceeded 90% at a relatively low dose of 6

mg/L as alum-14 and pH 6.5 (whereas the settled turbidity removals showed no similar indication of optimal treatment).

The charge neutralization condition was selected at a coagulant dose of 6 mg/L as alum-14 (0.55 mg/L as Al) and a pH of 6.5. At this condition, the coagulant exhibited a stoichiometric behavior in terms of turbidity removal (Shin, Spinette and O'Melia 2008). Edzwald (2013) suggested that the charge neutralization mechanism is restricted to a coagulant dose below 1 mg/L as Al (11 mg/L as alum-14) and a pH approximately six or less. The selected condition met the dose criterion; however, the selected pH was slightly higher than the proposed pH limit. According to Figure 13, positively charged aluminum species were present in varying proportions at the investigated condition; therefore, the selected charge neutralization condition was considered acceptable (Edzwald and Tobiason 1999). The jar test settled and filtered turbidity removals at the selected charge neutralization condition were 47 and 93%, respectively (indicating that the optimal charge neutralization conditions would likely not be identified by the conventional jar test methods based on sedimentation only). The sweep flocculation condition was selected at a dose of 20 mg/L as alum-14 (1.82 mg/L as Al) and a pH of 7.0. The selection of the sweep flocculation condition was based on its central location on the filtered turbidity removal contour plot. This condition coincided with the sweep flocculation zone identified by Edwards and Amirtharajah (1985). The jar test settled and filtered turbidity removals at the selected sweep flocculation condition were 87 and 97%, respectively.

The difference between optimizing coagulation conditions using settled water turbidity and filtered water turbidity results can be even more substantial. Figure 3.9 shows the results of the same experiment performed with a water with the same raw water turbidity and alkalinity but different levels and characteristics of dissolved organics. At pH 6.5, the settled water turbidity

optimum dose was approximately 55 mg/L as alum-14 (based on the >80% removal criterion), while the filtered water turbidity criterion (>90% removal) was achieved with roughly 50% less alum. Optimization based on filtered turbidity showed that even further reductions of the coagulant dose would be possible by operating at a lower pH (e.g., 9 mg/L as alum-14 and pH 5.0). This pattern of different optimum conditions was consistently observed with 14 other waters. An online dashboard was created to visualize and compare settled and filtered water turbidity results (Alansari 2021b).

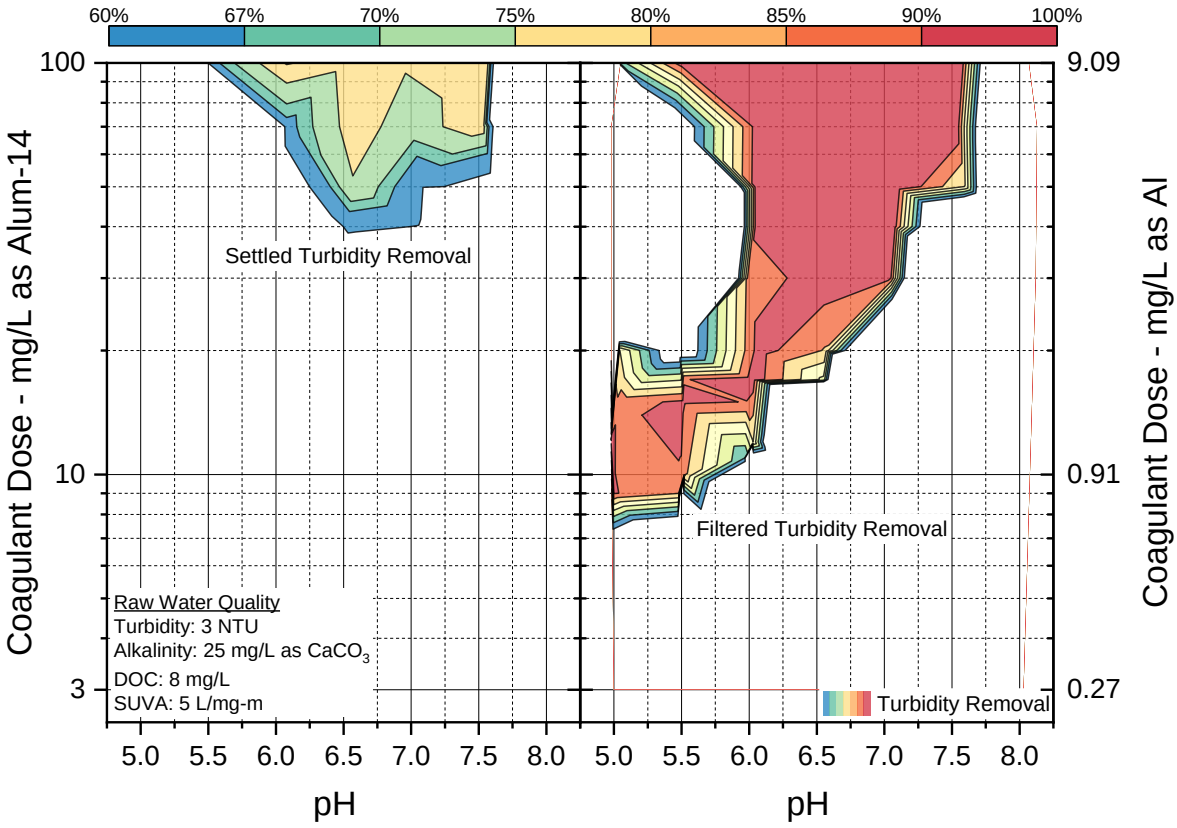

Figure 3.9. Settled (left) versus filtered (right) jar test results, case 2

3.5.1.3. Floc Characterization

Floc characterization was performed using a photometric dispersion analyzer (PDA2000, Rank Brothers Ltd.). The PDA measures the intensity of a light beam as it passes through a flowing suspension. The ratio of the fluctuations in beam intensity to the average of the beam intensity, which is related to the turbidity of the suspension, was used as an indicator of the state of aggregation of the suspension. This ratio is typically referred to as the flocculation index (FI). An increase in the FI is an indication of aggregation (flocculation), while a decrease is caused by disaggregation (floc break-up). An in-depth description of the instrument's theory and operation can be found in an article published by Gregory (2009). A description of the experimental setup is provided in Appendix C. Floc formation characteristics were quantified in terms of the maximum observed FI and floc formation times. In this study, floc formation times were defined as the time required for the FI to increase by 10% ($t_{10\%}$) and 90% ($t_{90\%}$) of the maximum observed FI value. In general, the FI has been shown to correlate with floc size directly; therefore, it could be reasonably assumed that a higher FI value corresponded to a larger floc size (McCurdy, Carlson and Gregory 2004).

Experiments using the PDA were performed at the predetermined charge neutralization and sweep flocculation conditions to establish baseline values with the standardized mixing program (Figure 3.10). Although the filtered turbidity removals of the two coagulation conditions were within 4% of each other, their floc formation characteristics and settled turbidity removals were markedly different (as shown in Figure 3.8). Floc appeared relatively early in the first flocculation stage under sweep flocculation, while floc did not appear until the second stage of flocculation with charge neutralization. Consequently, the time for the FI to increase by 10% was approximately 2 minutes with sweep flocculation compared to 9 minutes with charge

neutralization. The FI reached a plateau by the third flocculation stage with sweep flocculation (≈11 minutes). Under charge neutralization, the FI trend remained linear for the duration of the charge neutralization experiment, which implied that the floc size was still increasing at the end of this experiment. The difference in the rate of formation between the two mechanisms can be attributed to the difference in the concentration of particles (as a result of different coagulant doses) and perhaps the collision-attachment efficiencies of the respective coagulation mechanisms (Matsui et al. 1998; Crittenden et al. 2012b).

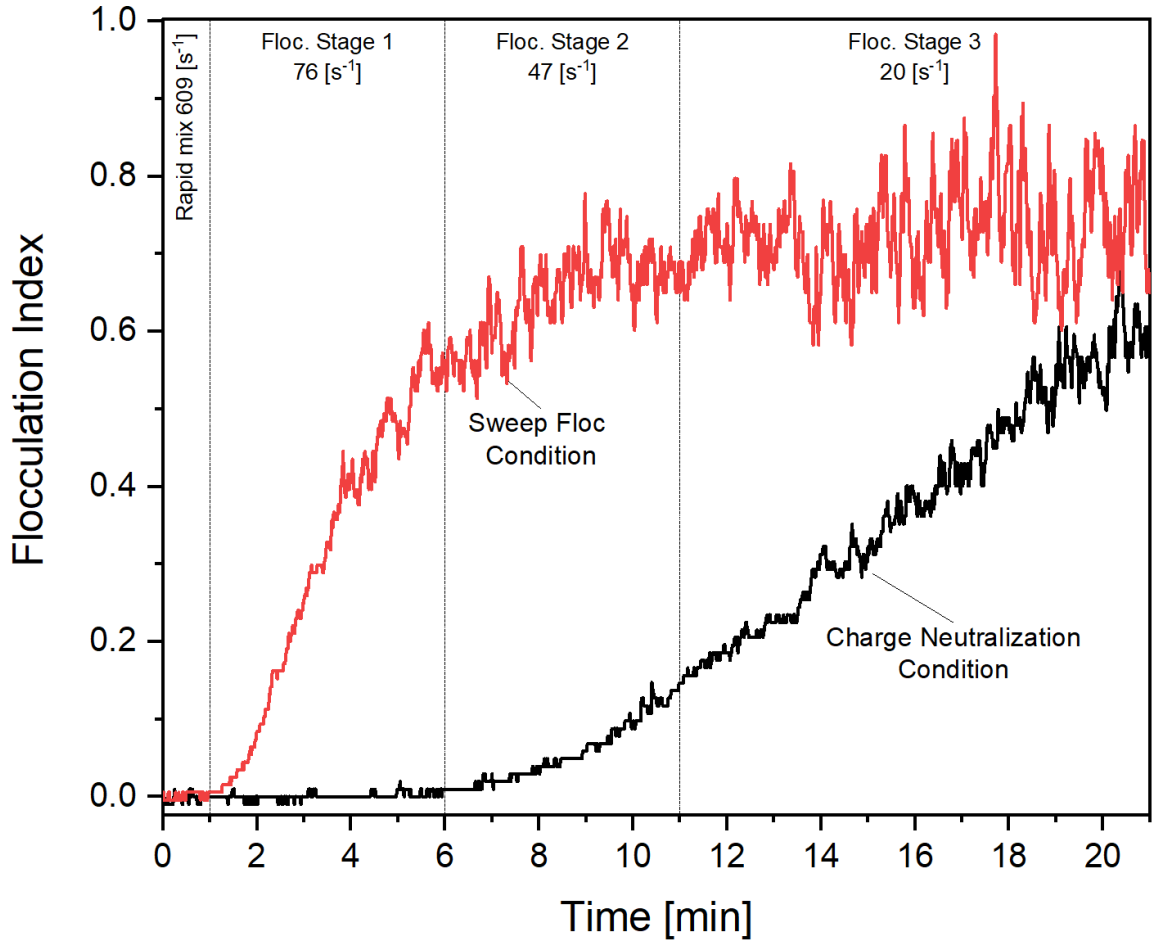

Figure 3.10. Baseline PDA experimental results

3.6. Advanced Coagulation Optimization

Turbidity is often regarded as the primary performance metric for optimizing coagulation conditions in jar tests. However, coagulation conditions for optimal turbidity removals may not always overlap with other treatment goals, such as the reduction precursors of disinfection by-products. For example, Randtke (1988) stated that the optimum pH for the removal of organics is typically in the range of pH 5.0 – 6.0. On the other hand, the optimum pH for the removal of turbidity is typically reported as being in the range of pH 6.0 – 7.0 (Budd, Hess, Shorney-Darby, Neemann, Spencer, Bellamy and Hargette 2004). Modern treatment plants usually have to meet multiple treatment goals to produce safe drinking water; thus, jar test procedures should also incorporate these goals in the optimization process. Figure 3.11 shows some of the typical output parameters that can be used to optimize coagulation conditions. However, before discussing how to optimize for multiple output parameters, it is important to first examine how an optimum coagulation based on a single parameter might be identified.

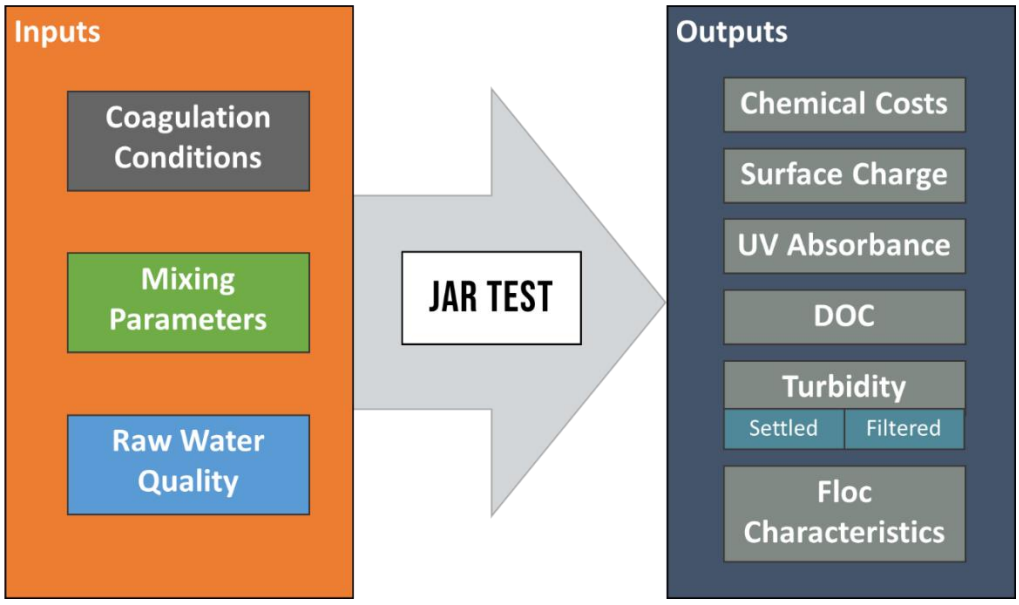

Figure 3.11. Output parameters of the coagulation process

3.6.1. Optimizing Based on Total Chemical Costs

From an operational point of view, an optimum coagulation condition must also consider the cost of treatment chemicals used and maximize the removals of the contaminants of interest. Thus, the process of optimizing the coagulation stage becomes a multi-parameter optimization problem. Experimenters can incorporate the total chemical costs in their jar tests by scaling up the volumes of the coagulant and pH adjusting chemicals used at each investigated coagulation condition. Figure 3.12 shows a contour graph of the total chemical costs to treat a million gallons of water as a function of the coagulant dose and coagulation pH. The costs for alum (48.5%), sodium hydroxide (50%), and sulfuric acid (93%) were assumed to be $319, $500, and $160 per dry ton, respectively. The method of scaling up the volumes of chemicals used and calculating their total cost is outlined in Appendix D. Although the estimated costs may vary by location and vendor, the fact that the chemical costs are expected to change with respect to changing coagulation conditions would remain the same.

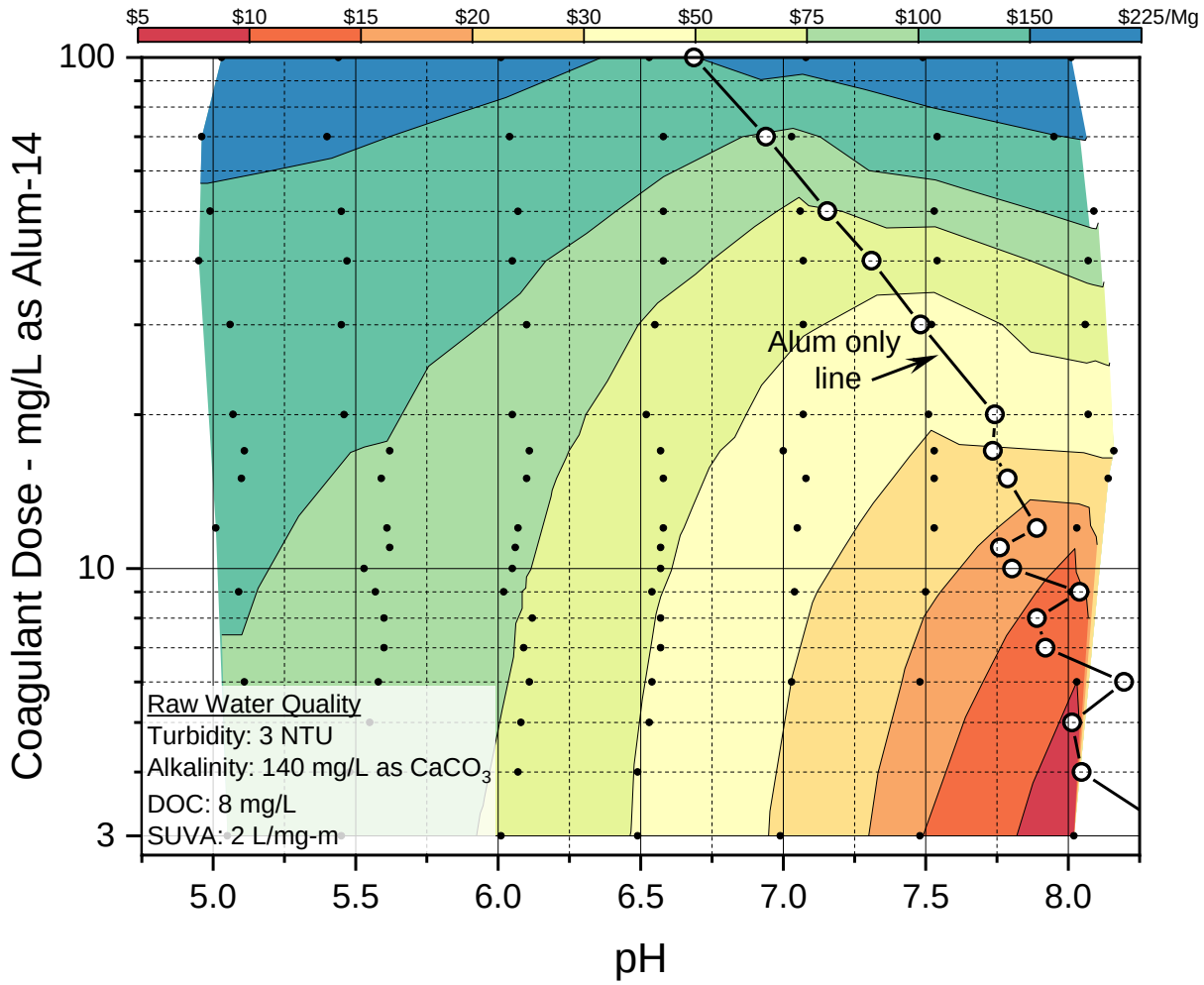

Figure 3.12. Chemical costs of treating 1 million gallons of water

3.6.2. Optimization Algorithms

Selecting an optimum coagulation condition based on cost and the removal criterion for a given contaminant depends on the specific optimization goals. For example, the goal might be to minimize the total cost while also meeting the minimum removal requirement. Alternatively, one might want to identify a robust coagulation condition that is not sensitive to minor water quality changes while also being cost-effective. Figure 3.13 demonstrates two approaches (or algorithms) for selecting an optimum coagulation condition from a contour plot. The top algorithm minimizes

chemical costs based on a specified removal criterion, while the bottom one maximizes robustness with respect to chemical costs.

In summary, a search grid is generated from a contour plot of the parameter being optimized. In this example, the grid ranged from pH 4.7 to 8.2 in increments of 0.05 pH units (i.e., 70 points in total) and ranged from 3 to 100 mg/L as alum-14 in increments of 0.5 mg/L as alum-14 (i.e., 194 points in total). The algorithm first excluded all datapoints where the removals were below the specified criterion. Minimum target removals are achieved by operating within the optimum contour boundaries of a given metric (e.g., >97% filtered turbidity removal). The algorithm then sorts the filtered dataset based on total chemical costs and selects the cheapest condition as the optimum condition to minimize costs. Minimizing based on chemical costs typically yields to conditions that are near or at the boundaries of the removal zones. Minor changes in water quality parameters could potentially shift the selected optimum point outside the optimal removal boundary. To increase robustness, the robust algorithm finds all datapoints that would still meet the removal criterion if the pH were shifted by $\pm$0.25 units and the dose was shifted by $\pm$ 3 mg/L as alum-14. The cheapest condition is then selected as the optimum robust condition.

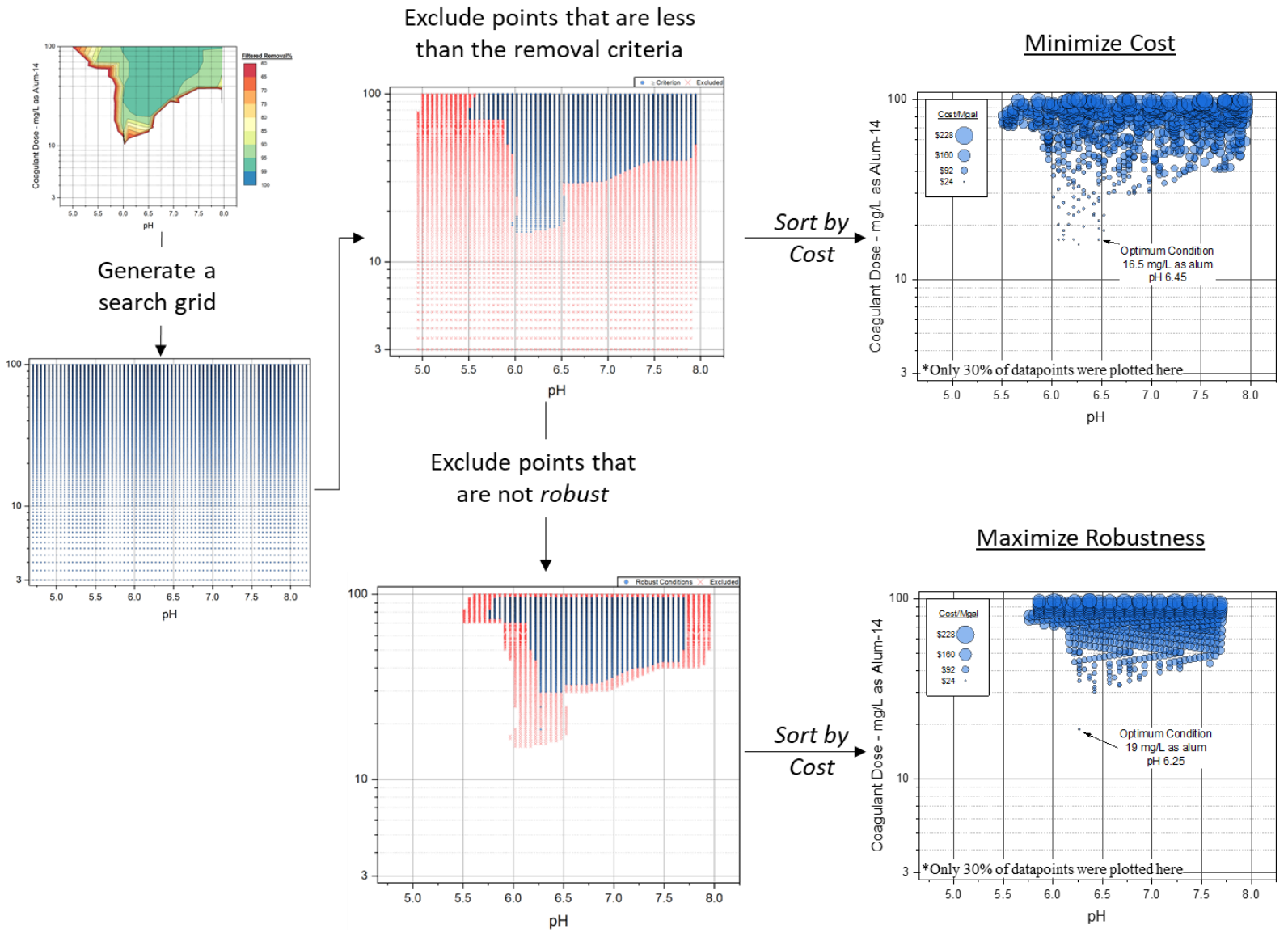

Figure 3.13. Optimization algorithms

3.6.3. Combining Multiple Optimization Criteria

Multiple removal goals are achieved when the boundaries of different performance metrics overlap. For example, to optimize for both settled and filtered water turbidity, a plant would have to operate in the region where the optimum settled turbidity zone overlaps with the optimum filtered turbidity zone. If DOC were also considered, then the plant would need to operate in the region where the optimum DOC zone overlaps with the optimum settled turbidity zone and optimum filtered turbidity removal zone. The most basic optimization approach is a one-level optimization scenario where a single water quality parameter (e.g., settled water) is optimized. Figure 4.4 shows how a total of 11 different optimization scenarios can be considered using four performance parameters for each of the optimization algorithms discussed above. Multi-level optimization scenarios consider multiple parameters (up to four) simultaneously. All multi-level optimization scenarios included filtered turbidity removals since it was the only parameter currently regulated by the US Environmental Protection Agency (USEPA).

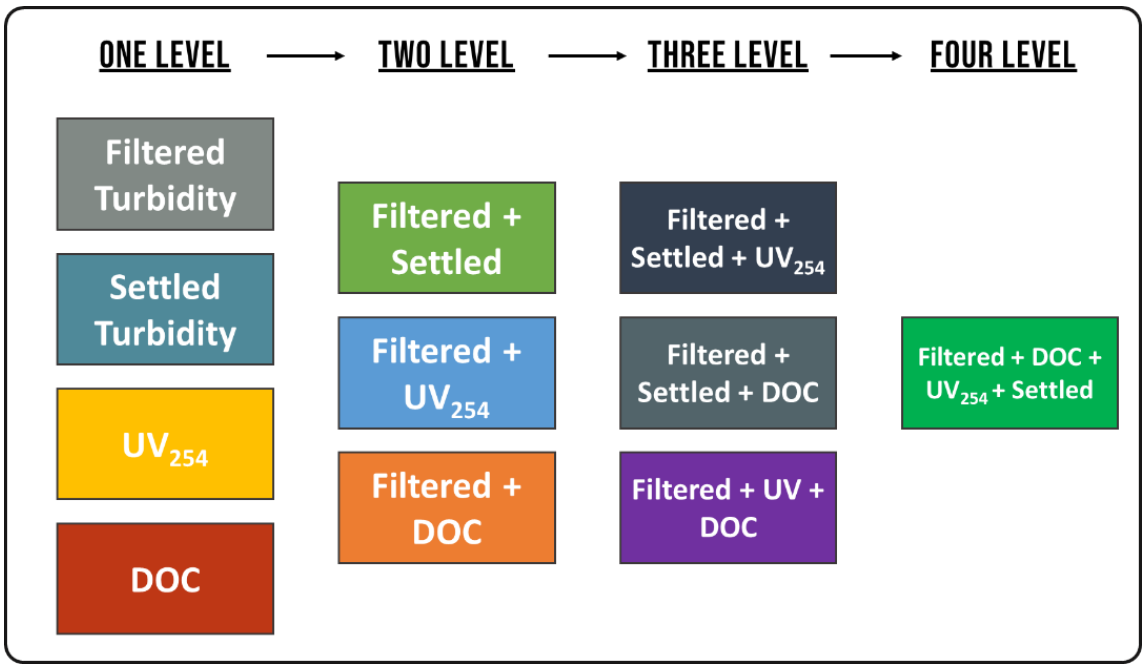

Figure 3.14. Optimization scenarios

Figure 3.15 compares optimum removal boundaries for settled water turbidity, filtered water turbidity, UV_{254}, and DOC. Settled water turbidity limits were based on the USEPA's Area-Wide Optimization Program (AWOP) limits, i.e., less than 1 NTU for waters with an average raw water turbidity below 10 NTU and less than 2 NTU for waters with an average raw water turbidity above 10 NTU (Barr 2007). Filtered turbidity limits were based on the USEPA's filtered turbidity limit of less than 0.3 NTU (USEPA 2002). UV_{254} removal criteria were selected based on the 3rd quartiles of the measured removals. DOC removal criteria were based on the USEPA's Stage 1 TOC removal requirement (USEPA 1998). Edzwald and Tobiason (1999) claimed that DOC makes up about 90 – 99% of the TOC fraction; therefore, setting the limits based on DOC removals provided a more conservative goal.

The water used in this example could generally be classified as challenging to treat due to the combination of a relatively high raw water alkalinity and DOC. The "alum only" line revealed that without any pH adjustment, the filtered turbidity target would only be achieved when the coagulant dose exceeded 50 mg/L as alum-14. Additionally, the settled water turbidity limit could not be achieved without a pH adjustment since the alum-only titration line did not cross the removal boundary. As a result, it was evident in this case that pH adjustment (acid addition) was necessary to meet both turbidity goals. The chemical costs contour plot shown in Figure 3.12 would make it possible to select the optimal coagulation condition based on the optimization algorithms described above as well. The optimum conditions identified using the cost-minimizing algorithm are shown in Figure 3.15a, while the optimum conditions identified using the robust algorithm are shown in Figure 3.15b.

a) Cost-Minimizing Algorithm

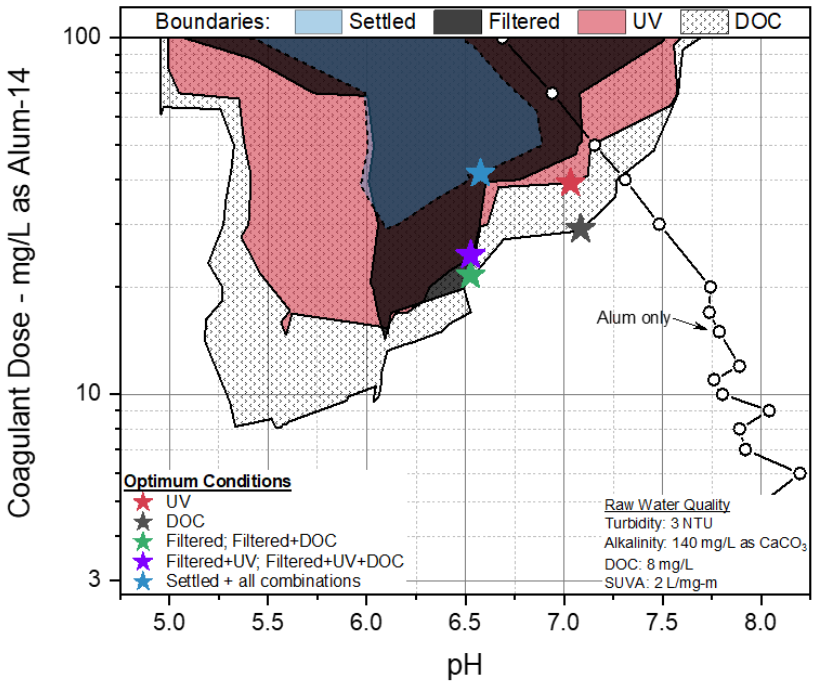

b) Robust Algorithm

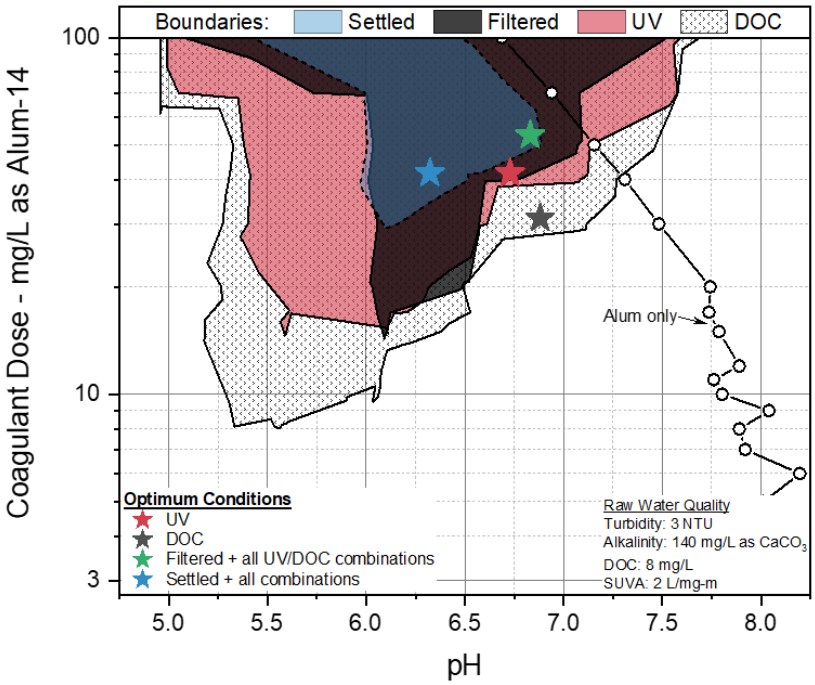

Figure 3.15. Optimum removal boundaries

The cost-minimizing algorithm identified five different optimum conditions (indicated by the star-symbols) depending on the selected optimization scenario. The optimum coagulation conditions were generally located between pH 6.0 and 7.0 and above 30 mg/L as alum-14. Even though significantly lower doses were identified for some of the parameters (e.g., 9 mg/L as alum-14 at pH 5.5 for DOC removal), the amount of acid required to operate at the low pH conditions was cost-prohibitive. For example, the total chemical costs at the low dose (9 mg/L as alum-14 and pH 5.5) and optimum DOC removal condition were approximately $93 and $50 per million gallons of water treated, respectively. In general, the total chemical cost increased proportionally the further away the coagulation condition was from the alum-only line. As a result, all the conditions identified in Figure 3.15a were located at or near the optimum boundaries and as close to the alum-only line as possible for the respective output parameters. Operating at or near boundaries could potentially be risky if the boundaries shift in the wrong direction with minor water quality changes. The goal of the second optimization algorithm was to identify optimum conditions that would be relatively less susceptible to minor water quality changes. In general, the optimum coagulation conditions identified using the robust algorithm were at a lower pH and/or higher dose than the conditions identified by the first algorithm (Figure 3.15b). Again, the second algorithm considers the total cost of the treatment chemicals; thus, the optimum conditions close to the alum-only line instead of being in a more central location relative to the optimum boundary.

Table 10 shows the optimum coagulation conditions at all the considered optimization criteria. All the conditions identified using the cost-minimizing algorithm were cheaper compared to the same criteria identified using the robust algorithm. For example, the total chemical cost for the filtered turbidity condition increased by approximately 22% by using the robust algorithm. An interesting observation to note is that the most expensive conditions were always when settled

water turbidity was included as an optimization criterion. This implies that optimizing for settled water turbidity in a jar test would potentially lead to increased chemical costs without any significant benefit to the overall treatment process.

Table 3.2. Optimum coagulation conditions

Algorithm	Optimization Criteria [a]	pH	Coagulant Dose [b]	Cost/Mgal [$]
Cost Minimizing	DOC	7.1	29	$ 50
	UV_{254}	7.0	39	$ 62
	Filtered	6.5	22	$ 66
	+ DOC	6.5	22	$ 66
	+ UV_{254}	6.5	25	$ 69
	+ UV_{254} + DOC	6.5	25	$ 69
	Settled	6.6	42	$ 84
	+ Filtered	6.6	42	$ 84
	+ Filtered + UV_{254}	6.6	42	$ 84
	+ Filtered + DOC	6.6	42	$ 84
	+ Filtered + UV_{254} + DOC	6.6	42	$ 84
Robust	DOC	6.9	31	$ 60
	UV_{254}	6.7	42	$ 77
	Filtered	6.8	53	$ 85
	+ DOC	6.8	53	$ 85
	+ UV_{254}	6.8	53	$ 85
	+ UV_{254} + DOC	6.8	53	$ 85
	Settled	6.3	42	$ 95
	+ Filtered	6.3	42	$ 95
	+ Filtered + UV_{254}	6.3	42	$ 95
	+ Filtered + DOC	6.3	42	$ 95
	+ Filtered + UV_{254} + DOC	6.3	42	$ 95

[a] Optimum conditions sorted by treatment cost
[b] mg/L as alum-14

The method described above is suitable for selecting optimum conditions from contour plots; however, contour plots require a wide matrix of coagulant dose and pH conditions, an extensive experimental process, and special software. Operators usually have limited time and resources; thus, they require a rapid and efficient method of identifying optimum coagulation conditions. King (2017) proposed using an alternating single-variable optimization method to identify optimum coagulation conditions. King demonstrated that a global optimum coagulation condition based on filtered turbidity removal could be identified with 2 – 3 jar tests. Users are

encouraged to use *JTWizard* in conjunction with a single-variable optimization approach such as the one developed by King (2017). *JTWizard* an interactive excel-based jar testing program that guides and assists users in performing jar tests (Alansari 2020d). The software includes the optimization algorithms discussed earlier, where the “best” jars are automatically selected.

CHAPTER 4: JAR TEST MIXING PARAMETERS

Jar testing has traditionally been recommended as a tool for design engineers to determine appropriate mixing intensities (G-values) and detention times. Current design guidelines generally recommend the rapid mix stage have a short detention time (10 – 60 s) with mixing intensities (G-values) in the range of 300 – 1000 s^{-1} (Baruth 2004; Hendricks 2016). For flocculation, authorities generally recommend a tapered flocculation design with a minimum detention time of 20 minutes at maximum flow and G-values in the range of 20 – 75 s^{-1} (Baruth 2004; Crittenden, Trussell, Hand, Howe and Tchobanoglous 2012b). In a recent revision, the "10 states" standards (2018) recommended a minimum detention time of 30 minutes with a flow-through velocity of 0.5 to 1.5 ft/min and agitators with peripheral velocities between 0.5 to 3.0 ft/s. Edzwald (2014) provided a history of mixing applications in drinking water treatment. While it is not clear how the mixing guidelines were developed, it can be reasonably assumed that many of the guidelines were primarily based on conventional jar test procedures (i.e., settling in a jar). For example, Amirtharajah and Mills (1982) used a conventional jar test procedure to demonstrate that intense rapid mixing (high G-values) was only required for effective coagulation under charge neutralization conditions.

4.1. Rapid Mix

The premise for rapid mixing, particularly for high-intensity rapid mixing, was based on the notion that the coagulation reactions are completed within 7 seconds (Letterman, Quon and Gemmell 1973; Amirtharajah and Mills 1982; Committee 1989). Thus, in theory, intense rapid mixing would ensure that the aluminum hydrolysis products are rapidly formed and available for absorption by all contaminants. Researchers have recently begun questioning the role and

significance of rapid mixing in drinking water treatment. Edzwald (2013) argued, based on the article published by Amirtharajah and Mills (1982), that most treatment plants operate under sweep flocculation conditions where intense mechanical rapid mixing (as per design guidelines) was not necessary. In a series of jar tests, Vadasarukkai and Gagnon (2015) found that rapid mix stage G-values had no impact on TOC removals but a significant impact on settled water turbidity removals under both optimum charge neutralization and sweep flocculation mechanisms. However, the authors reported that the G-value requirements for effective turbidity removals were markedly lower than the current design guidelines. In a later publication, these authors reported that the observed differences in settling performance ultimately became negligible when floc was given enough time to settle (Vadasarukkai and Gagnon 2017). Allerdings and colleagues (2015) reported that there was no significant impact on turbidity removals in a full-scale facility after several incidents of rapid mixer equipment failures. Malinaro et al. (2019) presented similar findings from case studies where the rapid mixer was not operated either due to equipment failure or operator error. This constitutes significant evidence that rapid mixing might not be required in some or all water treatment facilities.

4.2. Flocculation

Floc formation occurs when destabilized particles collide and attach. The process is kinetically governed where collisions between particles are thought to occur primarily by three mechanisms: fluid shear (mixing), differential settling (gravity), and Brownian motion (random motion of particles). Early theories describing the rate of collisions between the particles (collision frequency functions) used a simplistic approach where changes in fluid motion and short-range forces were ignored (Lawler 1993). In this view, fluid shear becomes the dominating collision mechanism for a wide range of particle sizes. As a result, many of the flocculation design

guidelines and practices, even to this day, are based mainly on fluid shear, i.e., mixing. In 1992, Han and Lawler published a noteworthy research paper in which they incorporated the effects of changes in fluid motion (hydrodynamic retardation) and short-range forces in particle collisions. In their view, collisions primarily occurred by Brownian motion instead of fluid shear, while minimal mechanical mixing ($G \approx 20\ s^{-1}$) was only required to keep particles in suspension. This model indicates that most flocculation systems in water treatment facilities could be significantly overdesigned. An excellent and comprehensive explanation of both theories and their governing equations was provided by Benjamin and Lawler (2013). Although Han and Lawler's 1992 article has been cited more than 200 times, many of the citing papers were concerned with the specifics of their mathematical model concerning flocculation and not primarily with the practical implications of their conclusions. An online interactive data visualization dashboard was created to compare the two prevailing flocculation models (Alansari 2020c). The app plots the dominant regions for each collision mechanism as a function of G-value ($10 – 120\ s^{-1}$), temperature ($5 – 40$ °C), and particle density ($1 – 2.5\ g/cm^3$).

4.3. The Optimization Problem

Researchers have demonstrated that the coagulation mechanism (Letterman, Quon and Gemmell 1973; Amirtharajah and Mills 1982; Jarvis, Jefferson and Parsons 2005; Li et al. 2006; Jiao et al. 2017), rapid mix parameters (Rossini, Garrido and Galluzzo 1999; Li, Zhu, Wang, Yao and Tang 2006; Yu et al. 2011), and flocculation parameters (Matsui, Yuasa, Furuya and Kamei 1998; Spicer et al. 1998; Yu, Gregory, Campos and Li 2011) can impact coagulation and flocculation efficiency. In addition to affecting optimum coagulation conditions (e.g., dose and pH), water quality has also been shown to impact optimum mixing parameters (Griffith and Williams 1972; Kawamura 1973). Unfortunately, the actual coagulation process is even more

complex because coagulation conditions and mixing parameters have a combined interactive effect (Kan, Huang and Pan 2002; Gregory and Carlson 2003). This implies that to optimize coagulation conditions, mixing conditions would have to be kept constant and the optimized coagulation conditions would only apply to the selected set of mixing parameters and vice versa (Figure 4.1). Therefore, it should not be surprising that many researchers considered the standardization of the jar test as a futile endeavor.

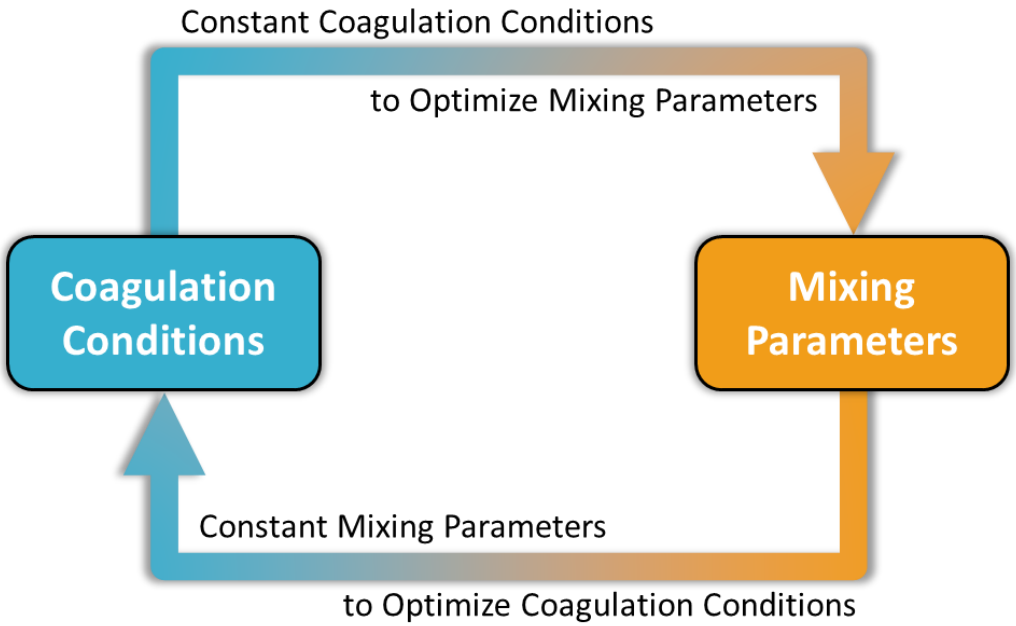

Figure 4.1. The optimization problem

4.4. Optimizing Jar Test Mixing Parameters

While using filtered instead of settled water turbidity in jar testing can offer operational and cost advantages to water treatment facilities, the effects on rapid mix and flocculation parameters on floc characteristics (e.g., size and formation times) and turbidity removals under optimized charge neutralization and sweep flocculation conditions are a separate matter. The following experimental results and discussion presented herein were intended to allow a

determination of the degree by which mixing intensity and time impact turbidity removal efficiency during the conventional drinking water treatment process. The specific focus here was on the effects of jar test mixing parameters on floc formation (time and size) and treated water turbidity (settled and filtered). Figure 4.1 showed that coagulation conditions could only be optimized under constant mixing parameters and vice versa. As a result, the coagulation conditions were fixed by using the optimum charge neutralization and sweep flocculation conditions identified for the low-turbidity and low-organics water studied in Chapter 3.

Rapid mix factors included the duration and the intensity of the rapid mix stage, while flocculation factors included the flocculation scheme (i.e., single-stage or tapered flocculation) and the duration and intensity of the flocculation stage. Ideally, a full-factorial experimental design (or similar approach), where all the mixing factors are varied, would have provided a complete picture of the main and interacting effects between the investigated mixing variables. However, this would have required over 1,400 experiments (without replications) based on the number of factors and their respective levels considered in this study. This was by no means practical due to time and resource limitations. Nevertheless, these effects could still be quantified, to an extent, by comparing the results to a set of baseline values using a single-variable optimization approach. In this case, the baseline conditions were established using the standardized mixing program from the next-generation jar test procedure (Figure 3.10). A total of 82 experiments were performed in which the effects of rapid mix and flocculation factors on turbidity removals and floc formation characteristics were measured (Table 4.1)

Table 4.1. Investigated mixing parameters[a]

Experiment	Rapid mix		Flocculation	
	Duration [s]	G-Value [s^{-1}]	Duration [min]	G-Value [s^{-1}]
Rapid Mix Duration	5, 15, 30, 60, 120, 300	609	50	SS: 20
Rapid Mix Intensity	60	0[b], 300, 609, 1200	50	SS: 20, 76 T: 76→ 47 → 20
Flocculation Duration	60	609	20, 30, 40, 50	SS: 20
Flocculation Intensity	60	609	50	SS: 20, 47, 76, 120 T: 76→ 47 → 20

SS = single-stage flocculation; T = tapered flocculation
[a] All experiments were performed under charge neutralization and sweep flocculation conditions
* Rapid mix G-value = Flocculation G-value

4.5. Effects of Flocculation Parameters

4.5.1. Duration of Flocculation

The baseline experiment (Figure 3.10) showed that with the selected charge neutralization condition, the flocculation index was still increasing and did not reach a plateau after 20 minutes of flocculation. Here, a single-stage flocculation scheme was used at a G-value of 20 s^{-1}, as this represented the "worst-case scenario" condition in terms of floc formation time with just enough mixing energy to keep the floc from settling. Experiments were performed with the flocculation stage duration ranging from 20 to 50 minutes in 10-minute increments (Figure 4.2). The results showed that it took approximately 35 minutes for the FI to reach a plateau under the selected charge neutralization condition and only 11 minutes with the sweep flocculation condition, which was the same as with the 3-stage tapered flocculation experiment.

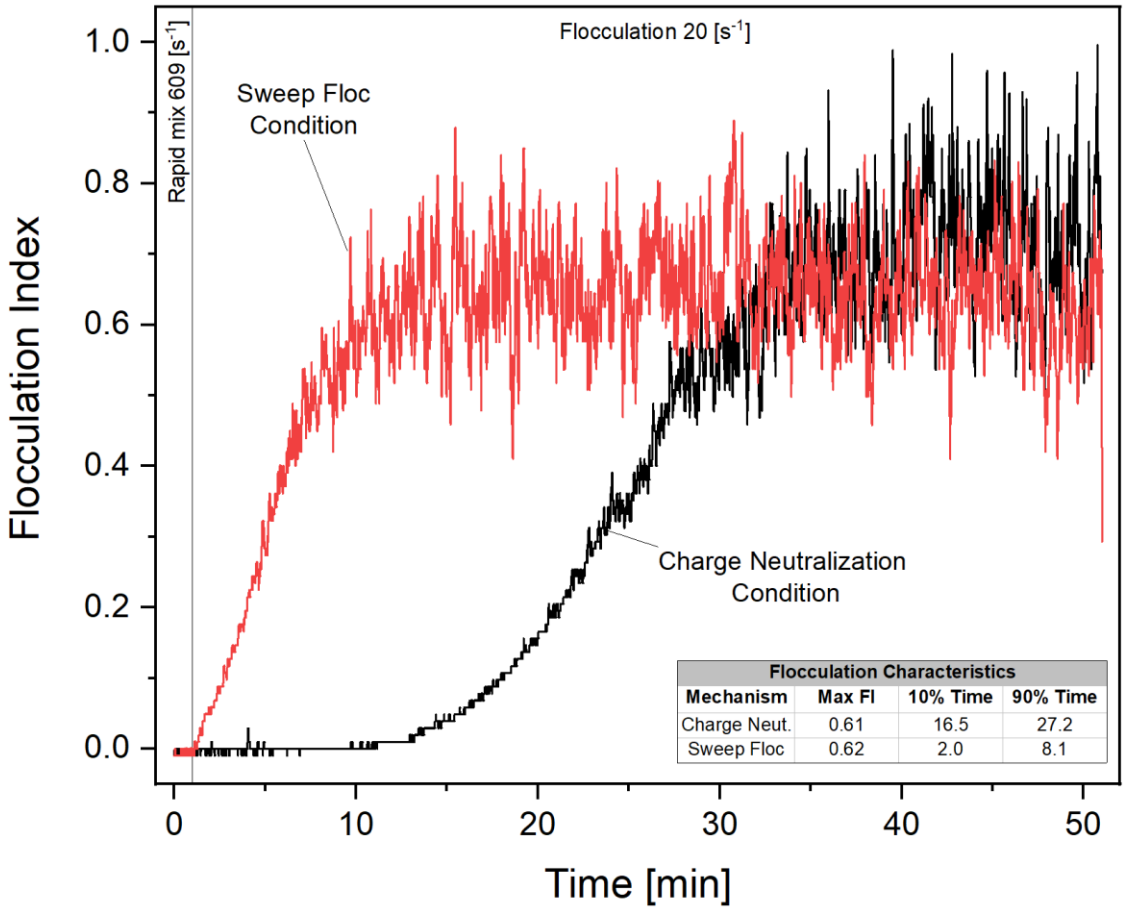

Figure 4.2. PDA results of experiments at 20 s-1 and floc stage duration of 50 minutes

Figure 4.3 shows a plot of the settled and filtered turbidity removals versus the duration of the flocculation stage at a G-value of 20 s^{-1}. Settled water turbidity samples were collected after a 20-minute settling period. The water was filtered immediately after settling, and samples for filtered water turbidity were collected 2 minutes after the start of filtration. Under both coagulation mechanisms, settled turbidity removals were proportional to the length of the flocculation stage up to 50 minutes. This supports (and is likely the basis for) current flocculator designs in water treatment facilities. Flocculation time, under charge neutralization, had a more pronounced effect on settled water turbidity removals where the removals increased from -11 to 71% as time increased from 20 to 50 minutes, respectively. A similar trend was observed with sweep

flocculation; however, the effect was relatively less pronounced where the removals only increased from 67 to 90% in the same time range. Under charge neutralization, the correlation between floc size (based on the FI data shown in Figure 4.2) and settled turbidity removals was apparent. However, it is unclear why settled water turbidity removals increased with flocculation time under sweep flocculation conditions since all samples were collected after the FI reached a plateau.

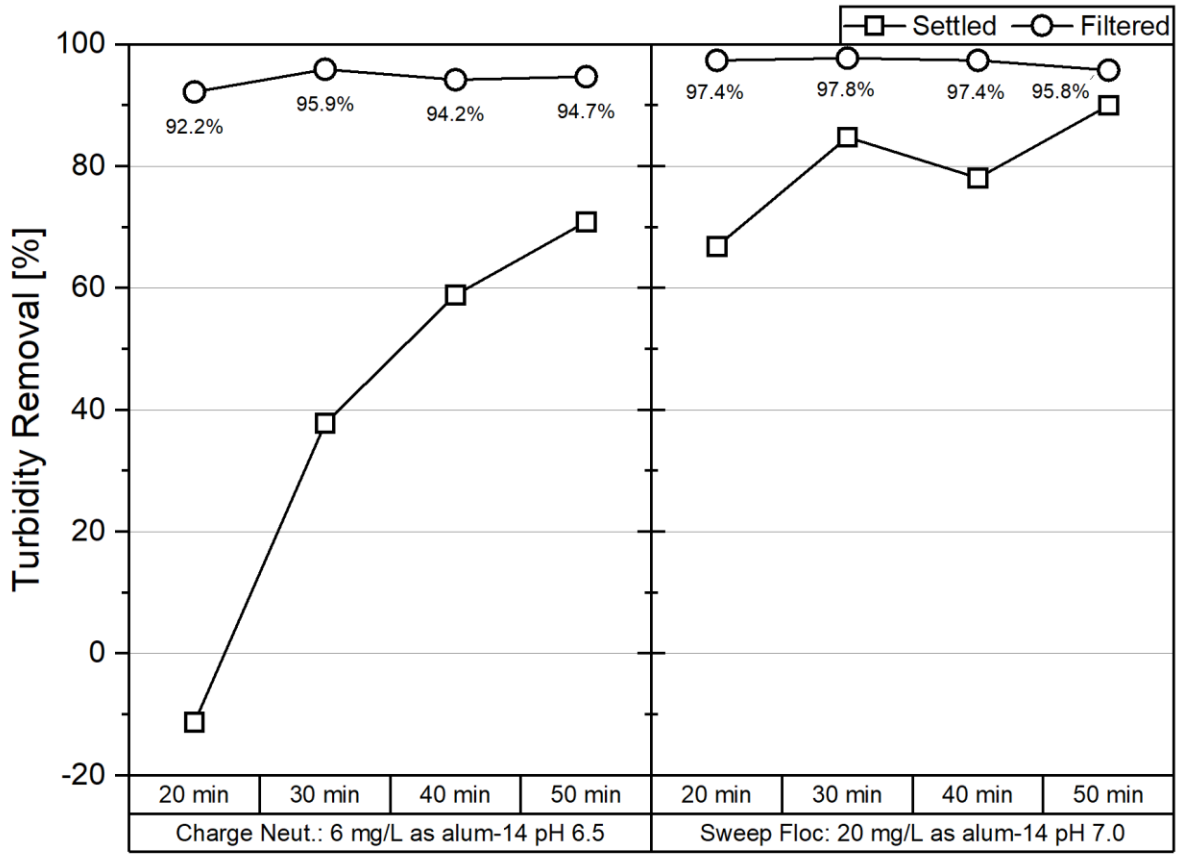

Figure 4.3. Effect of flocculation stage (20 s^{-1}) duration experiments on turbidity removals

Filtered turbidity removals in Figure 4.3 appeared to be relatively independent of flocculation time or floc size. The removals were within 4% for each coagulation mechanism and showed no apparent trend over time for all the investigated conditions. Greater than 90% filtered turbidity removals were consistently achieved despite the settled turbidity removals ranging from -11 to 90%. One possible explanation could be that, even at the shortest flocculation time (20

min.), the floc was both properly charged and large enough to filter efficiently but perhaps not large enough to settle. Filtered turbidity removals of samples collected earlier in this experiment could have been considerably lower. As a result, these experiments were repeated, but this time the water was filtered directly (without settling).

4.5.1.1. Direct Filtration

Samples for the direct filtration experiments were collected immediately after rapid mix, before and during the growth phase, and after the FI plateau for each coagulation condition. The results of this experiment showed that flocculation time only had an impact on filtered turbidity removals in the charge neutralization case (Figure 4.4). Under sweep flocculation, greater than 95% filtered turbidity removals were achieved immediately after rapid mix (609 s^{-1} or 300 rpm for 1 minute). With charge neutralization, the filtered turbidity removal immediately after the rapid mix stage was approximately 70%; however, the removals increased to above 90% with only 9 minutes of mixing at 20 s^{-1}. In these cases, floc was not visible to the naked eye until about 5 minutes with sweep flocculation and 20 minutes with charge neutralization. These data suggest that while there might not be a minimum flocculation time for sweep flocculation, there might be a minimum amount of flocculation required for charge neutralization (circa 9 min. at a G-value of 20 s^{-1}) for this water. These results support the hypothesis that flocculation time or floc size was not a primary factor when optimizing coagulation conditions using granular media filtration instead of settling in a jar test since optimal filtered turbidities were achieved while floc was not yet visible to the naked eye provided that there was at least 9 minutes of flocculation after rapid mix at a G-value of 20 s^{-1}.

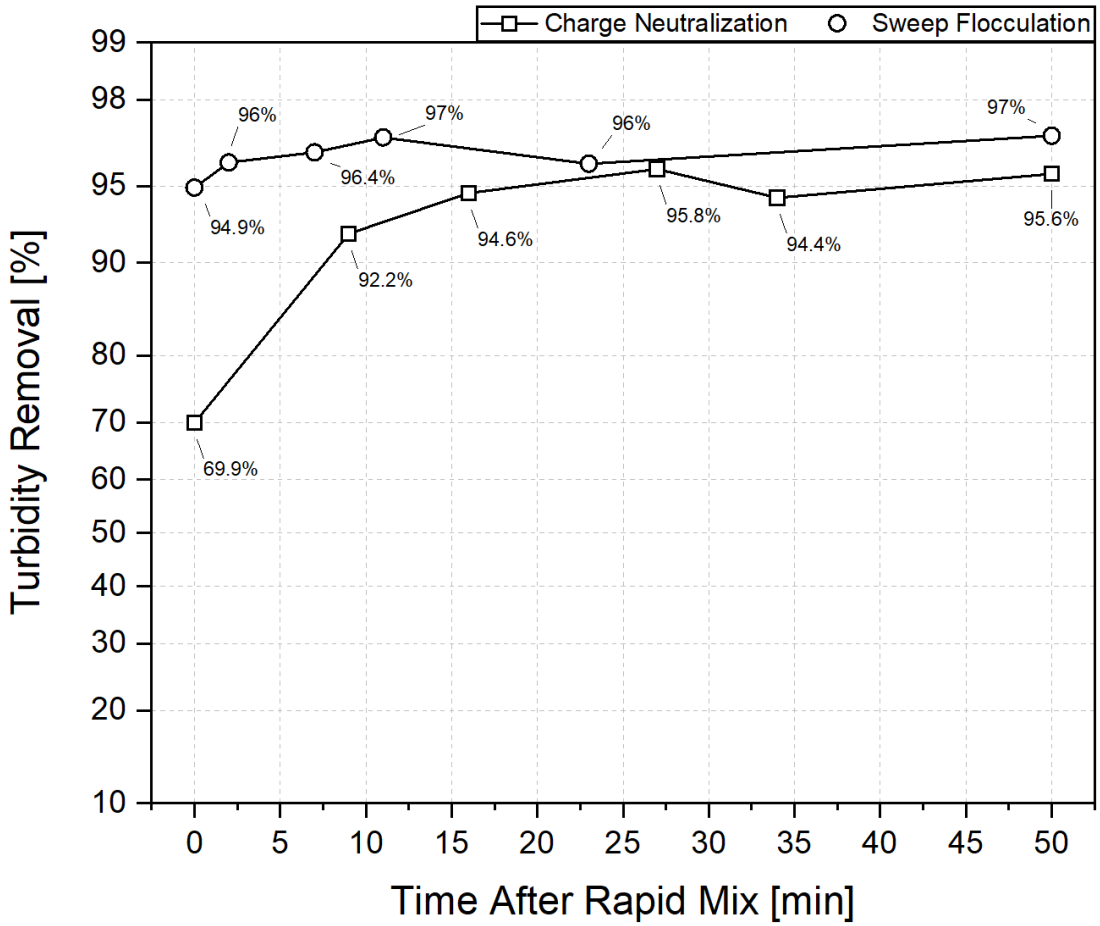

Figure 4.4. Direct filtration turbidity removals

4.5.2. Flocculation Intensity

For subsequent experiments, a fixed flocculation stage duration of 50 minutes where floc size, or FI, was no longer a function of time was selected. This permitted the exclusion of time as a factor when measuring the effects of other mixing variables, such as flocculation intensity. When tapered flocculation was used as the flocculation scheme, the time of the final stage was set to 50 minutes (60 minutes total).

Experiments were performed where the G-value of the flocculation stage was varied from 20 to 120 s^{-1}. Figure 4.5 shows the floc intensity experimental results under charge neutralization and sweep flocculation. Generally, floc appeared earlier as the flocculation stage's mixing intensity

increased; however, the effect was more noticeable under charge neutralization compared to sweep flocculation (Table 4.2). Under charge neutralization, the $t_{10\%}$ was 6.5 minutes at 120 s^{-1} compared to 16.5 minutes at 20 s^{-1}, whereas under sweep flocculation, the $t_{10\%}$ was only 1.5 minutes at 120 s^{-1} compared to 2 minutes at 20 s^{-1}.

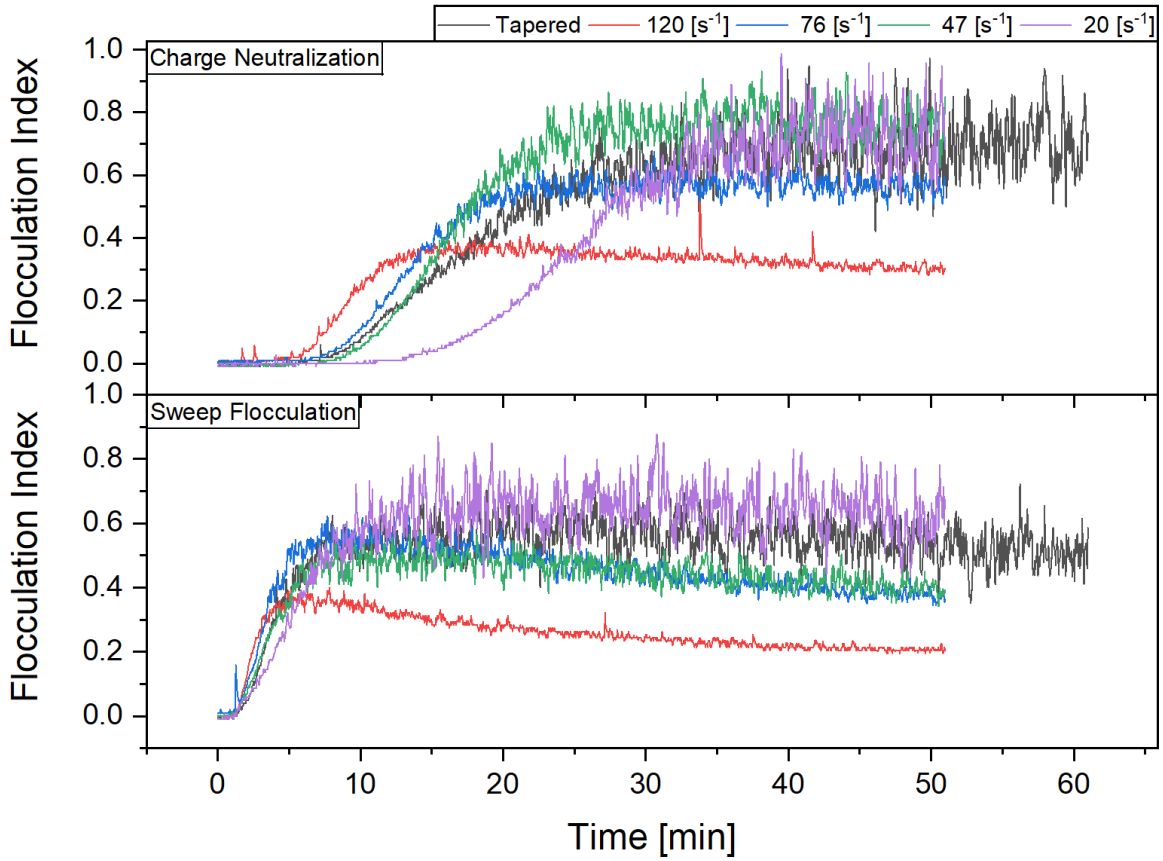

Figure 4.5. Flocculation stage G-value PDA experiments

Table 4.2. Floc formation times

Coagulation Mechanism	Flocculation G-Value [s^{-1}]	$t_{10\%}$ [min]	$t_{90\%}$ [min]	$t_{90\% - 10\%}$ [min]
Charge Neutralization	20	16.5	27.2	10.7
	47	10.4	21.2	10.8
	76	9.0	17.8	8.8
	120	6.5	11.1	4.6
	76→ 47 → 20	9.6	21	11.4
Sweep Flocculation	20	2.0	8.1	6.1
	47	1.7	5.4	3.7
	76	1.7	3.5	1.8
	120	1.5	2.6	1.1
	76→ 47 → 20	2.2	6.1	3.9

Similarly, the time for the floc size to increase from 10 to 90% decreased as the flocculation G-value increased. It should be noted that although the $t_{10\%}$ values were within 30 seconds for all the sweep flocculation experiments, the $t_{90\%}$ values ranged from 2.6 to 8.1 minutes as the G-value decreased from 120 s^{-1} to 20 s^{-1}, respectively. The size of the floc (max FI), to some extent, was also a function of the G-value. In general, the floc's maximum size decreased with increasing G-value, likely due to the higher shear forces (Ching, Elimelech and Hering 1994). The results also highlighted the benefits of tapering flocculation. With tapered flocculation, floc appeared earlier (as was also observed with high-intensity mixing), and the floc grew relatively larger (as was also observed with low-intensity mixing). These trends agreed with the findings published by several authors (Matsui, Yuasa, Furuya and Kamei 1998; Spicer, Pratsinis, Raper, Amal, Bushell and Meesters 1998; Yu, Gregory, Campos and Li 2011).

Results of the settled and filtered water turbidity removals at the investigated flocculation G-values for 50 minutes were plotted in Figure 4.6. Settled turbidity removals were proportional to floc size (max FI) and inversely proportional to the flocculation stage's mixing intensity. Mixing intensity had a noticeable impact on settled water turbidity, under both sets of optimized coagulation conditions, with settled turbidity removals ranging from 25 to 90%. On the other hand,

filtered turbidity removals were relatively independent of the mixing intensity during flocculation. At least 95% filtered turbidity removals were achieved regardless of the applied mixing intensity.

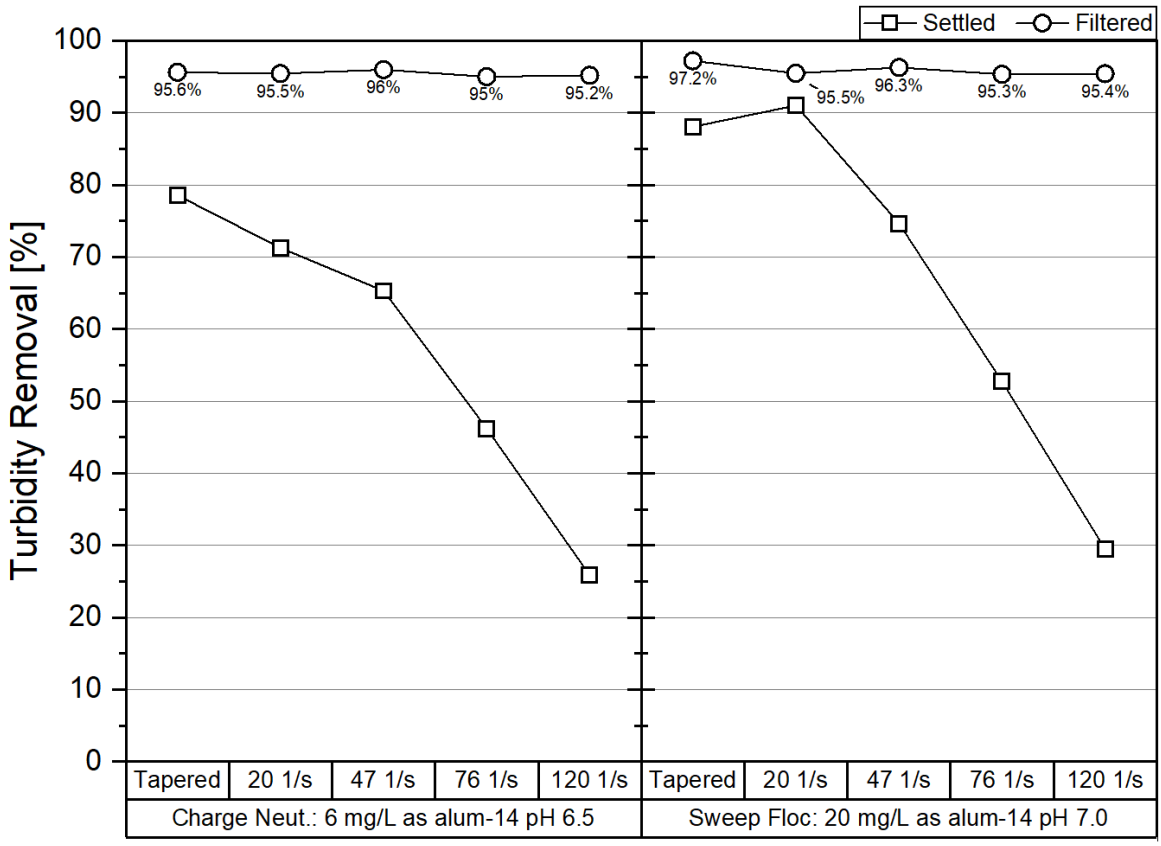

Figure 4.6. Flocculation stage intensity experiments

The mixing intensity during the flocculation stage impacted both the floc size and floc formation time. When using settled water turbidity as a performance metric, these observed differences in floc characteristics appeared to have a noticeable effect on treatment efficiency. As a result, it may seem that Han and Lawler's proposed theory that flocculation G-value is insignificant was not accurate since there was a measurable performance difference. Nevertheless, the G-value Han and Lawler proposed (20 s^{-1}) resulted in the largest floc size and highest settled water turbidity removals when using a single-stage flocculation scheme. However, it should be noted that even if mixing conditions in the jar test are such that the same size flocs are formed in

a jar as in the full-scale flocculator, sedimentation is not a process that can be directly scaled down from the full-scale process to a jar. When results are compared in terms of filtered water turbidity removals, which is a directly scalable treatment process, mixing intensity of the flocculation stage becomes insignificant to overall treatment efficiency (provided there is at least 20 s^{-1} of mechanical mixing), as concluded by Han and Lawler (1992).

4.6. Effects of Rapid Mix

4.6.1. Intensity of Rapid Mix

These experiments aimed to determine the effects of the rapid mix G-value on floc formation characteristics and turbidity removals under optimum charge neutralization (6 mg/L as alum-14 at pH 6.5) and sweep flocculation conditions (20 mg/L as alum-14 at pH 7.0). The investigated rapid mix G-values were 0, 300, 609, and 1200 s^{-1}. The 0 s^{-1} condition was performed by setting the rapid mix G-value equal to the G-value of the subsequent flocculation stage (76 or 20 s^{-1}). The duration of the rapid mix stage was fixed at 60 seconds. Each set of experiments was performed with two separate single-stage flocculation G-values (76 and 20 s^{-1}) and the standard tapered flocculation scheme (76, 47, and 20 s^{-1}) to assess the potential interactions of rapid mix and flocculation G-values. The duration of the flocculation stage was fixed at 50 minutes for all experiments. Figure 4.7 shows a plot of the time required for the FI to increase by 10% at all the investigated conditions.

For any given mixing condition, floc always appeared earlier under the sweep flocculation condition compared to charge neutralization. Except for one case (charge neutralization, G-value=1200 s^{-1}), the time required for the floc size to grow by 10% generally decreased with increasing rapid mix intensity. In general, the difference between the 10% growth times between

lowest and highest intensity experiments was small (≈2.7 minutes) in all but one case. Under charge neutralization, increasing the flocculation intensity from 20 to 76 s^{-1} or using a tapered flocculation scheme resulted in a considerable reduction in the time required for the floc to appear. Under sweep flocculation, the time for the floc size to grow by 10% was longer only when a relatively low rapid mix intensity was followed by low flocculation stage intensity.

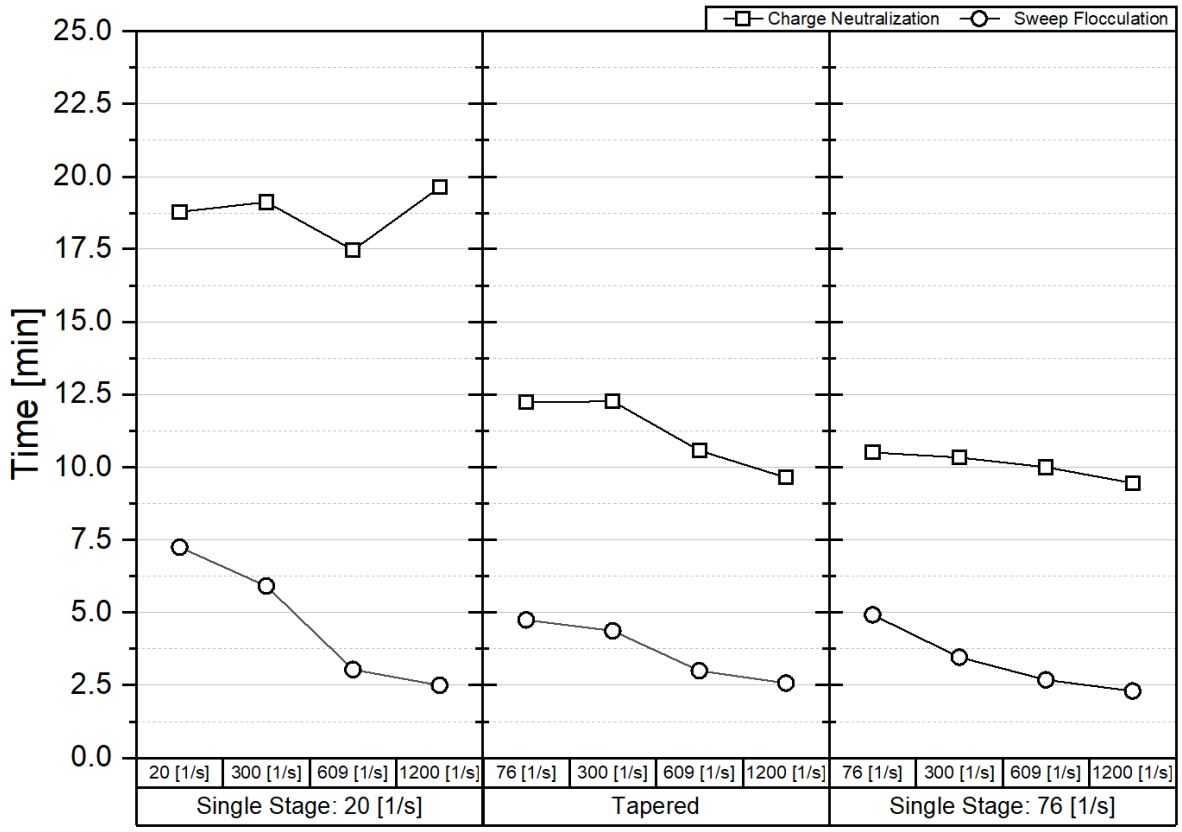

Figure 4.7. Time for floc to grow by 10% versus rapid mix G-value (top row) at the investigated flocculation conditions (bottom row)

Figure 4.8 compares the maximum measured FI values in all the investigated conditions. Relatively larger floc was formed with the low intensity (20 s^{-1}) single-stage flocculation and with the tapered flocculation scheme compared to the high intensity (76 s^{-1}) single-stage flocculation. Overall, no clear trends could be discerned from the maximum FI results. In some cases, the floc

size decreased with increasing rapid mix intensity while in others, increasing the rapid mix intensity had the opposite effect.

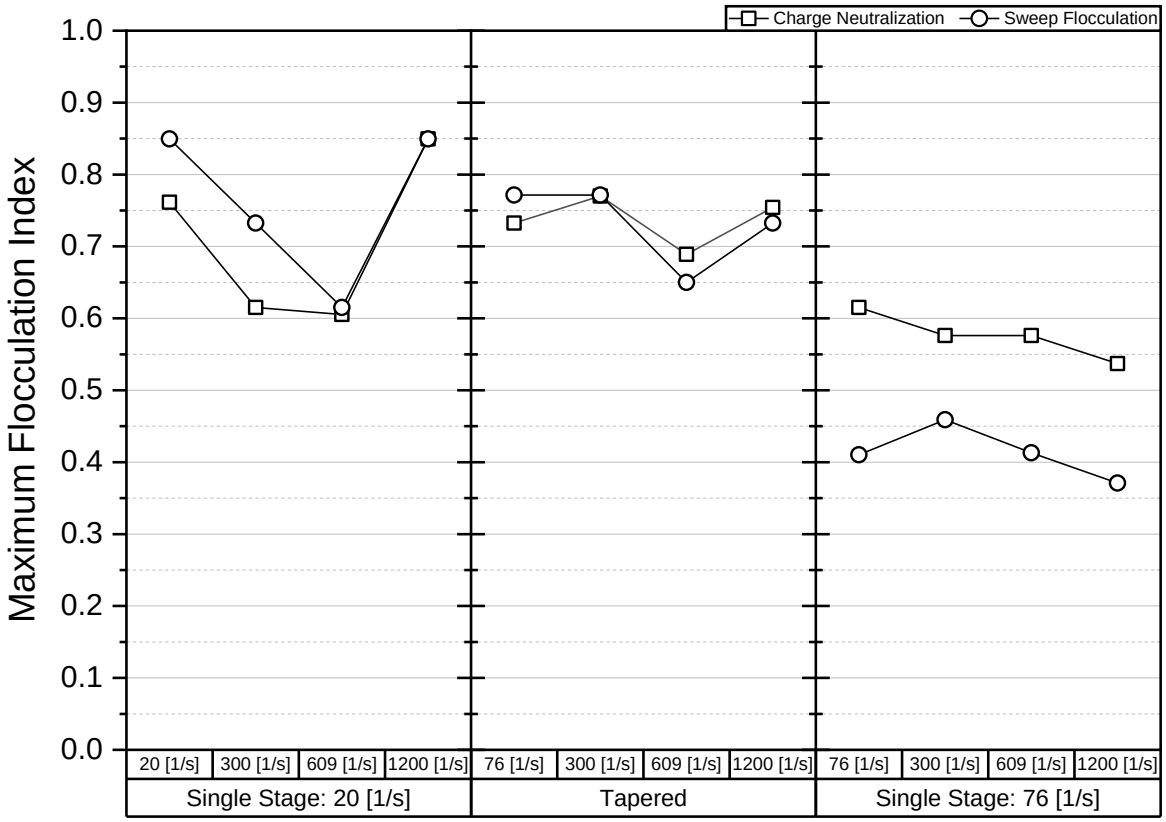

Figure 4.8 Maximum flocculation index versus rapid mix G-value (top row) at the investigated flocculation conditions (bottom row)

Amirtharajah and Mills (1982) claimed that intense rapid mixing was only required when operating under charge neutralization conditions. The authors based their analyses on settled water turbidity removals in a conventional jar test. Figure 4.9 compares the turbidity removals of all the investigated rapid mix intensity conditions. Settled turbidity removals ranged from approximately 20 – 88%, with no distinct pattern in the removals. In some cases, the settled water turbidity removals decreased with increasing rapid mix intensity (e.g., when flocculation=76 s^{-1}), while in others, increasing the rapid mix intensity had the opposite effect (e.g., when flocculation=20 s^{-1}).

The highest settled water turbidity removals were observed in only one out of six cases where the G-value of the rapid mix stage was highest. It was also interesting to note that the lowest settled turbidity removals coincided with only two out of the six instances where there was no rapid mix (i.e., the rapid mix G-value was set equal to the subsequent flocculation stage G-value). However, the removals of these two instances were only within 5% of the following data point. Also, the settled water turbidity removals were consistently high in all cases where tapered flocculation was used. This agrees with the general design recommendation for tapering the flocculation process. Settled water turbidity removal results were somewhat random; however, despite this observed variability with the settled turbidity removals, filtered turbidity removals were between 94 and 97% for all investigated conditions. Therefore, it could be concluded that the intensity of the rapid mix stage had no impact on turbidity removals when the results were compared in terms of filtered turbidity removals, regardless of the coagulation mechanism.

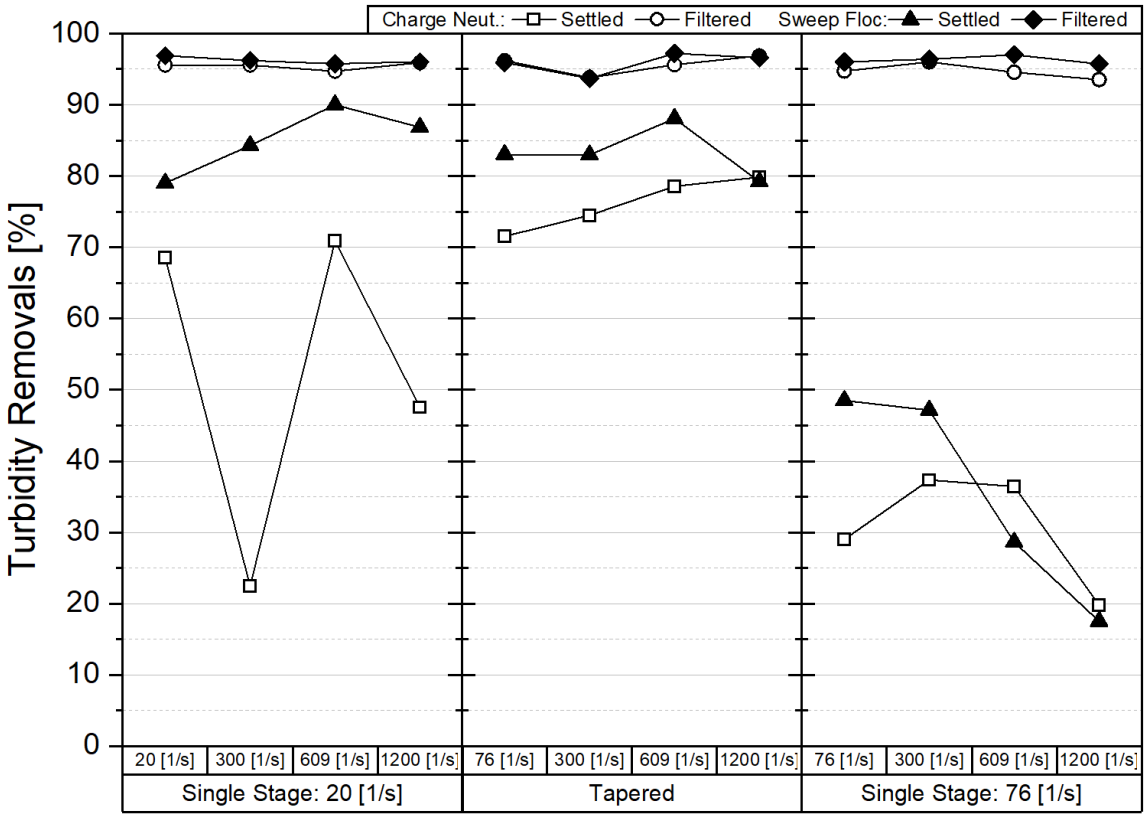

Figure 4.9. Effect of rapid mix G-value (top row) and flocculation conditions (bottom row) on water turbidity removals

4.6.2. Duration of Rapid Mix

The goal of the next set of experiments was to determine the effects of the duration of rapid mix on floc formation characteristics and turbidity removals. The G-value of the rapid mix stage was fixed at 609 s^{-1} – the default setting in the next-generation jar test procedure. The investigated rapid mix durations were 5, 15, 30, 60, 120, and 300 seconds. Experiments were performed using a single-stage flocculation G-value of 20 s^{-1} for a duration of 50 minutes. The results of the PDA experiments at the investigated conditions are shown in Figure 4.10. In general, the time required for the floc to appear was inversely proportional to the duration of the rapid mix stage – i.e., floc appeared earlier, the longer the duration of the rapid mix stage.

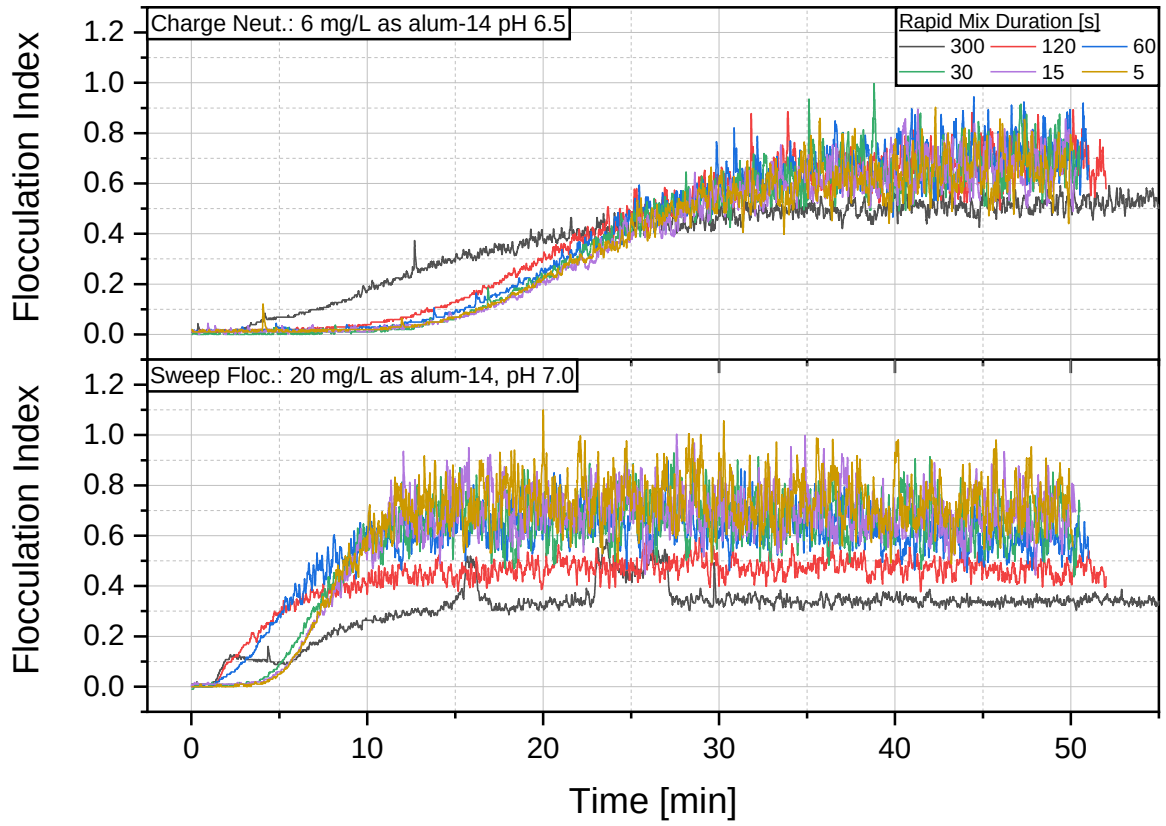

Figure 4.10. Effect of rapid mix duration

Under charge neutralization, increasing the rapid mix duration from 5 to 120 s reduced the time for floc to appear by 2.8 minutes (17%-time reduction) without impacting the maximum floc size (Figure 4.11). On the other hand, increasing the duration to 300 s for charge neutralization also reduced the time for the floc to appear by approximately 11 minutes (or a 70%-time reduction); however, the maximum floc size was reduced by approximately 20%. Increasing the rapid mix duration under sweep flocculation conditions had a more pronounced effect on floc size and formation times. Increasing the duration from 5 to 60 s reduced the time for the floc to appear by approximately 3 minutes (54%-time reduction) and reduced the maximum size of the floc by 16%, whereas increasing the duration to 120 or 300 s reduced the time by up to approximately 4 minutes (72%-time reduction) and reduced the maximum size of the floc by more than 50%.

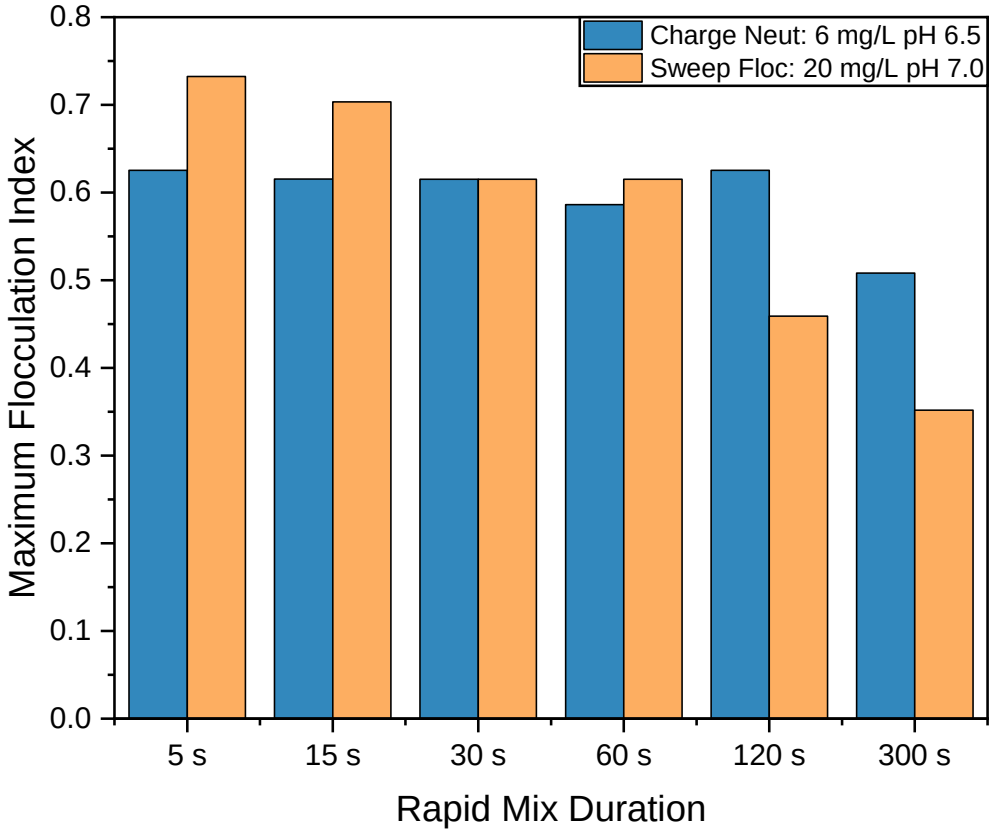

Figure 4.11. Effect of rapid mix duration on maximum flocculation index

The impact of rapid mix duration on floc formation times and size, particularly under sweep flocculation conditions, could most likely be attributed to floc appearing during the rapid mix stage (Figure 4.12). The figure was constructed by incrementally offsetting the y-axis of each set of rapid mix duration experiments by a value of 0.5 units on the flocculation index. Floc appearing during the rapid mix stage was subjected to high shear forces. This ultimately resulted in a relatively lower max FI (floc size), as seen with the 120 s (sweep flocculation) and 300 s (charge neutralization and sweep flocculation) experiments. The extent to which the duration of the rapid mix stage impacted floc characteristics could be attributed to the strength of the floc produced under the two coagulation mechanisms. Floc produced under alum charge neutralization conditions is thought to be stronger and less susceptible to breakage than floc produced under sweep flocculation

conditions (Li, Zhu, Wang, Yao and Tang 2006; Yu, Gregory, Campos and Li 2011; Jiao, Fabris, Chow, Drikas, van Leeuwen, Wang and Xu 2017).

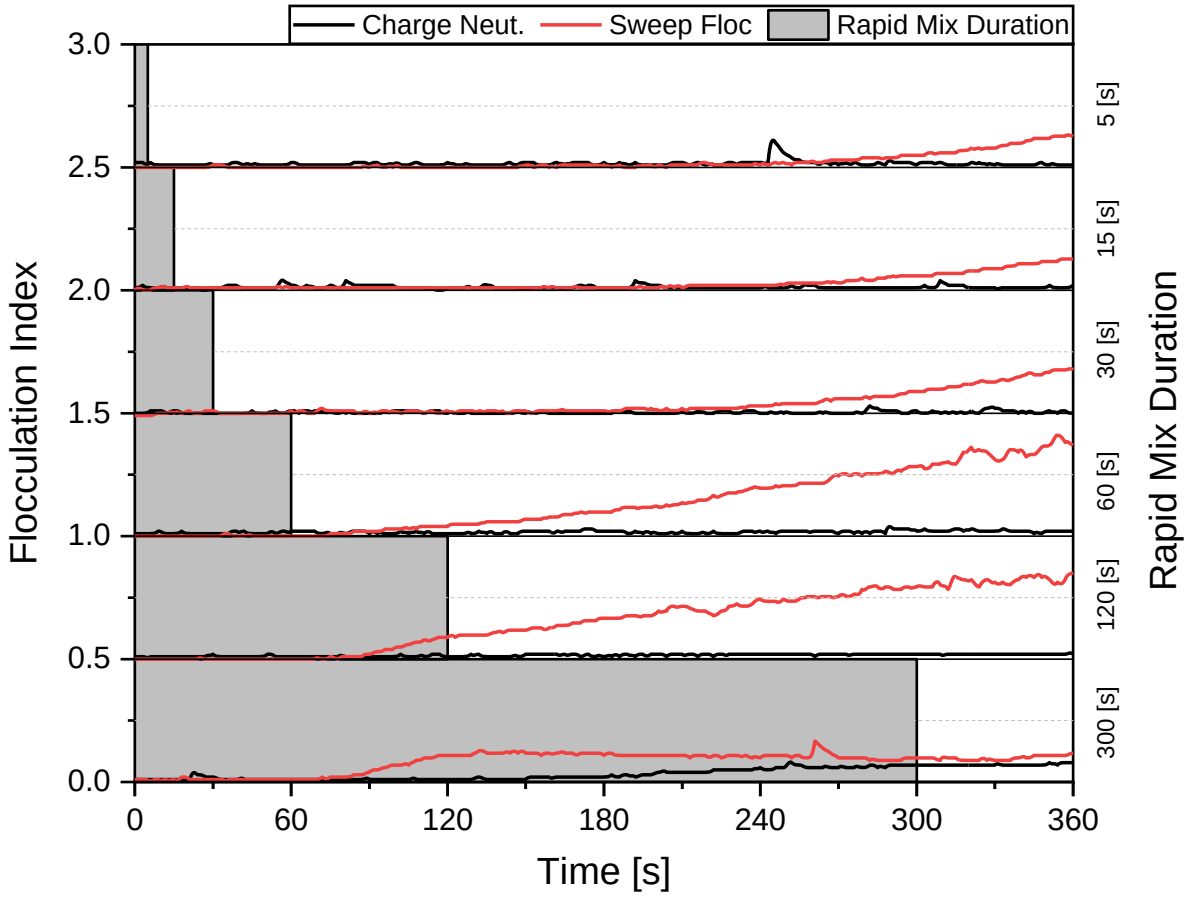

Figure 4.12. Flocculation index versus time under charge neutralization and sweep flocculation conditions. Bars denote the duration of the rapid mix stage

Figure 4.13 shows the settled water and filtered water turbidity removals at the investigated rapid mixing durations. Settled turbidity removals generally increased as the rapid mix stage duration decreased from 300 s to 30 s. A further decrease in the duration had little to no effect on the settled turbidity removals. Without considering the filtered turbidity removal data, it would appear as though rapid mix duration has, to some extent, a sizeable impact on floc formation characteristics and settling performance, thus suggesting an optimum rapid mix duration exists as

shown by Letterman and co-workers (1973). An extended rapid mix stage duration would result in the floc forming during periods of high-intensity mixing, ultimately leading to smaller and less settleable floc due to breakage. Despite these observed differences in floc formation characteristics and settled turbidity removals, the duration of the rapid mix stage had little to no effect on filtered turbidity removals (or overall treatment efficiency). The variability in the filtered turbidity removals was less than 4% for all investigated cases, and the removals were all greater than 90% with only 3 inches of filter media.

Most drinking water treatment plants operate well below their designed capacity (maximum daily flow) most of the time; therefore, the theoretical detention times (tank volume/flow rate) in their basins would be longer than the designed detention times. Additionally, only 63% of the contents in an ideal continuous-flow stirred tank reactor (e.g., rapid mix basin) would exit the reactor in a single theoretical detention time; therefore, the average detention time of the reactor would be greater than the theoretical detention time (Hendricks 2016). Nevertheless, many treatment plants are operating without difficulties meeting filtered turbidity limits despite having rapid mix basins with long detention times where floc might be negatively impacted. The results of this experiment suggest that as long as coagulation conditions (i.e., coagulant dose and coagulation pH) are optimized, the floc would be filtered efficiently regardless of the size and its settleability. Rapid mix times longer than 2 or 5 min tended to impact sedimentation negatively, but rapid mix times as short as 5 s showed no negative impacts. These results suggest that rapid mix times should have maximum detention time instead of the minimum values currently required by many states.

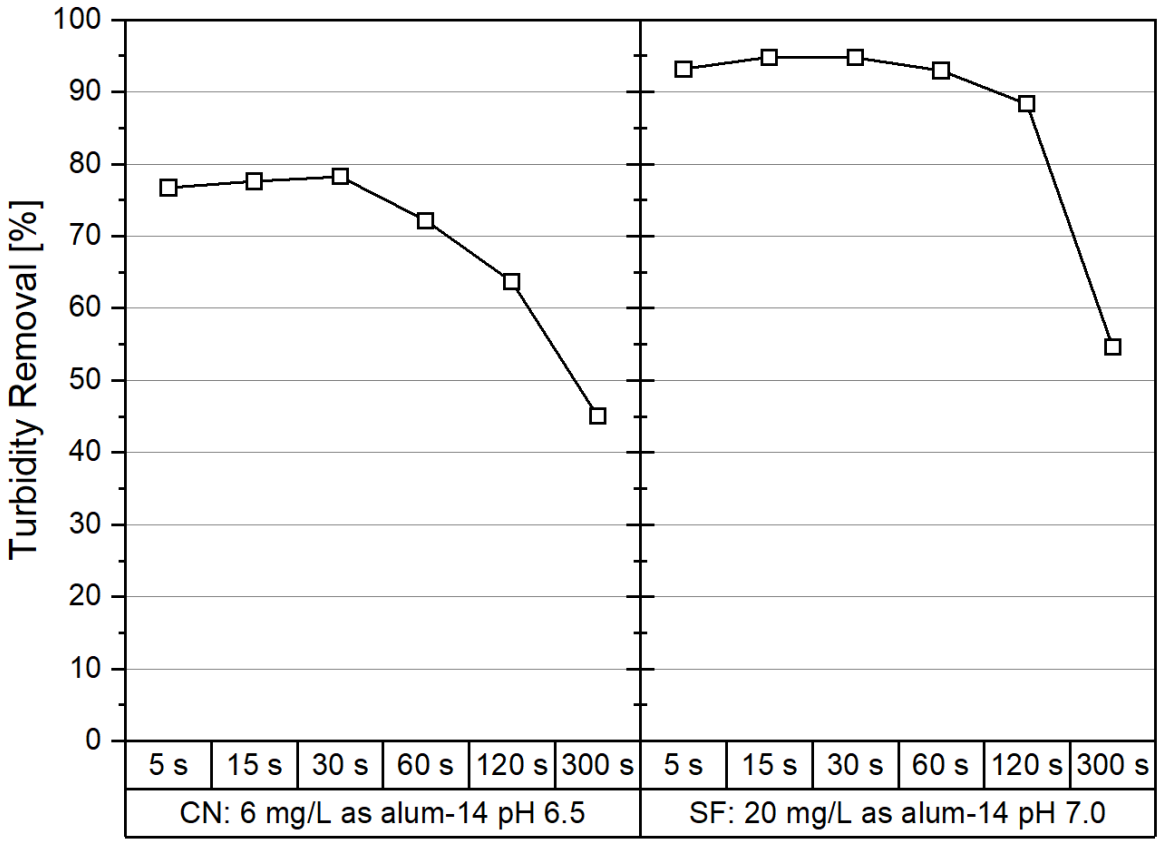

Figure 4.13. Effect of rapid mix duration on settled water turbidity removals

4.7. Rapid Mix Case Study

This section presents results from a case study of a conventional surface water treatment plant that was forced to operate without a rapid mixer for a period of 2 weeks while they waited for parts to repair the drive. At the time of the study, the coagulant was dosed in the 30" raw water supply pipe 140 ft upstream of the plant's only rapid mixer. A base was fed immediately before the rapid mix basin to increase the coagulated water pH. The water exiting the rapid mix basin passed through a Parshall flume followed by a 140 ft horizontal-flow baffled channel before entering the 2-stage flocculation basin. The volume of the rapid mix basin was approximately 5,000 gallons. The calculated theoretical detention times were 55 s, 110 s, and 144 s at the plant's designed capacity, average daily flow, and minimum daily flow, respectively. A model of the rapid mix basin is shown in Figure 4.14.

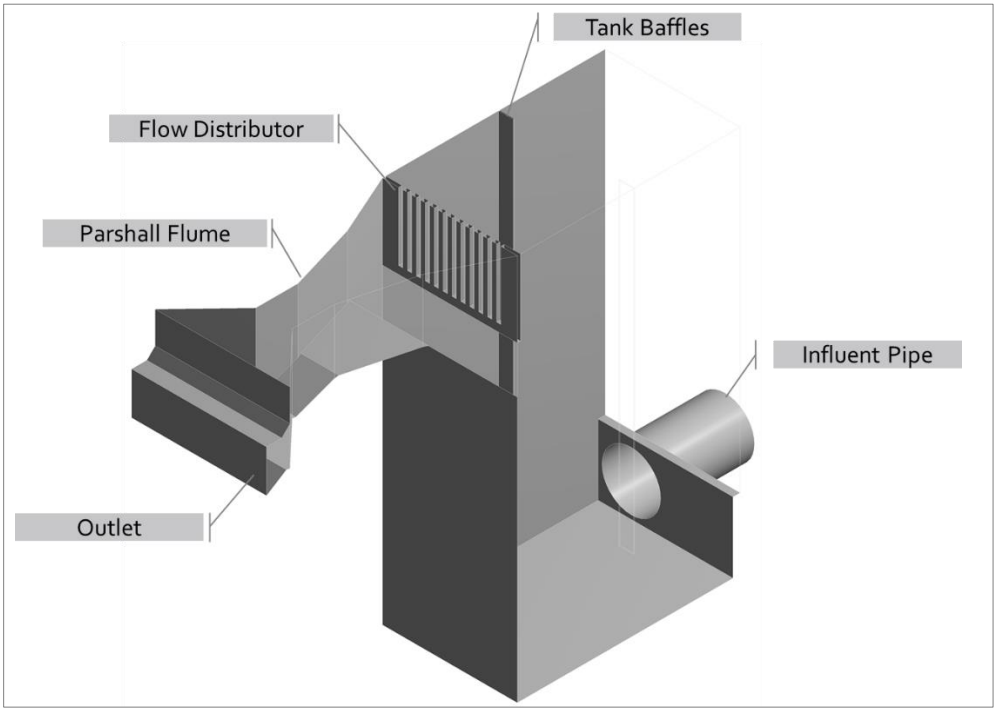

Figure 4.14. Model of rapid mix basin

A series of computational fluid dynamics (CFD) simulations of the stages leading up to the flocculators were performed to estimate average G-values in the inlet pipe, the rapid mix basin (without the mixer), Parshall flume, and baffled channel. Additionally, a simulated tracer was injected into the model, using the step injection method, to estimate the actual detention time in the system and visualize flow paths. Aluminum sulfate was used as the tracer in the simulation. The concentration of the tracer at the coagulant inlet pipe was adjusted to achieve a final concentration of 28 mg/L at steady-state. The simulations were performed at the plant's minimum daily flow since it provided the least amount of energy to the system (in the form of turbulence, entrance/exit losses, etc.). Ultimately, the goal was to determine whether shutting off the mixer would negatively affect floc settleability and filterability.

It should be noted that the case study presented here resulted from an unplanned repair and was not in the original scope of this research study; therefore, a comprehensive set of experiments to validate the accuracy of the model was not performed. Albeit this approach was a better estimate of the actual conditions in the plant instead of using calculated theoretical values for the jar test mixing parameters (Hudson Jr 1975; Teefy 1996). Figure 4.15 shows the results of the simulated tracer study performed at the plant's minimum daily flow. The average detention time between the point of coagulant addition and the outlet of the Parshall flume was found to be approximately 7.3 minutes (i.e., 3 times longer than the calculated theoretical detention time); however, it took roughly 22 minutes for the average concentration of the tracer to reach a steady-state value.

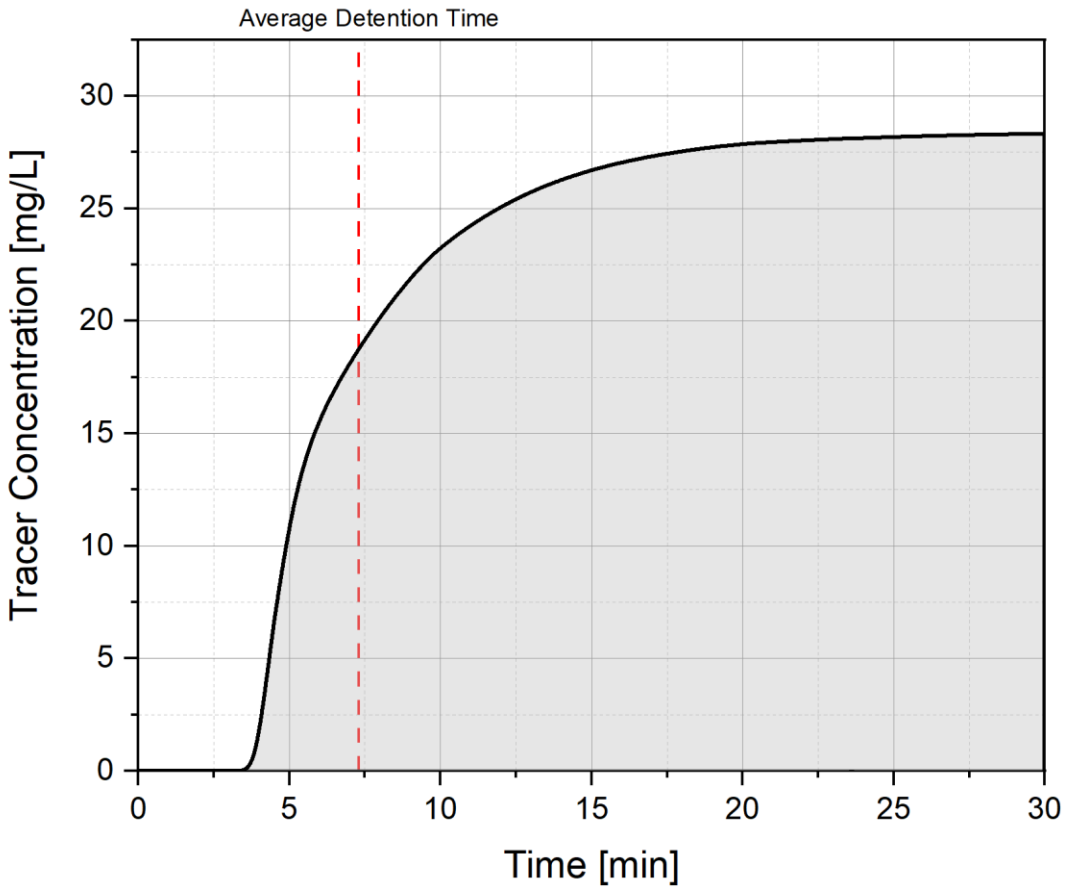

Figure 4.15. Tracer study results

A PDA experiment was performed with a raw water sample collected from the treatment plant using the G-values and detention times estimated from the CFD simulations. The CFD results showed that average G-values in the pipe, flash mixer + Parshall flume, and the baffled channel were approximately 20 s^{-1}, 200 s^{-1}, and 30 s^{-1}, respectively. The time for the tracer's concentration to get to steady-state in the simulated tracer study of the baffled channel was approximately 90 minutes. Figure 4.16 shows the results of the PDA experiment performed with alum at a dose of 15 mg/L as alum-14 and pH 7.0 (the plant's coagulation conditions at the time of sample collection). The flocculation index remained relatively unchanged in the first 5 minutes after coagulant addition; however, within approximately 2 minutes of adding the base to the water, floc started appearing.

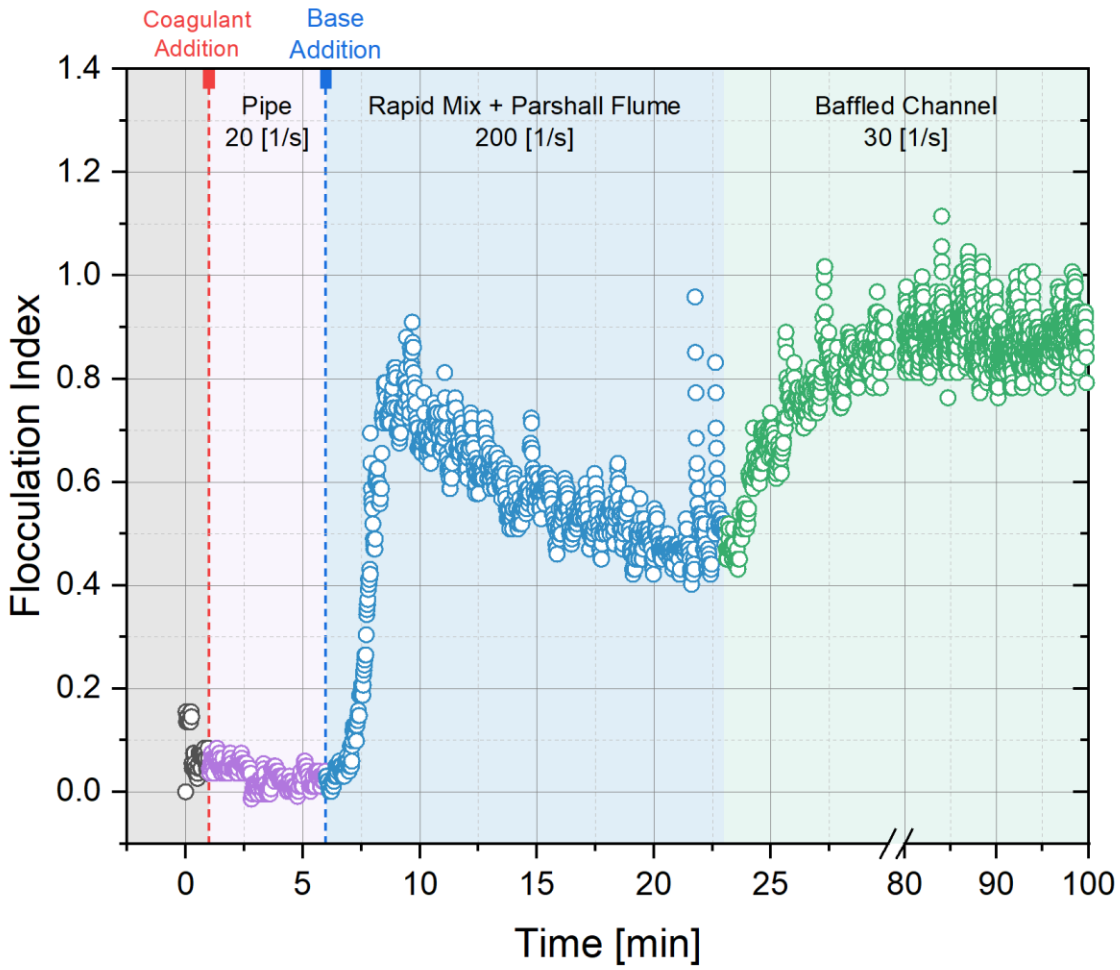

Figure 4.16. PDA experiment based on CFD results (alum dose = 15 mg/L as alum-14, pH = 7.0)

Two hypotheses were considered to explain the lack of floc formation in the rapid mix basin during the first 5 minutes of the PDA experiment. Coagulation reactions are normally considered to be complete with seven seconds of coagulant addition in water treatment facilities (Amirtharajah and Mills 1982; Committee 1989). The first hypothesis considered that the delayed floc formation was related to mixing conditions in terms of the duration and mixing intensity. The first hypothesis claimed that the rate of flocculation was so slow (as shown in Figure 3.10) that it took approximately 6 minutes for the floc to appear after coagulant addition and that the appearance of floc after base addition was merely a coincidence. The alternate hypothesis

considered that the problem was related to unfavorable coagulation conditions (at pH 6.0) in the pipe before the rapid mix stage. Figure 4.17 shows the optimum treatment boundary (≤0.3 NTU filtered turbidity) obtained from jar tests performed with the plant's raw water. The pH of the water with alum only (i.e., without pH adjustment) was approximately 6.0, which did not fall within the optimum boundary. However, adjusting the pH from 6.0 to 7.0 shifted the coagulation conditions from suboptimal to optimal, which subsequently resulted in floc formation.

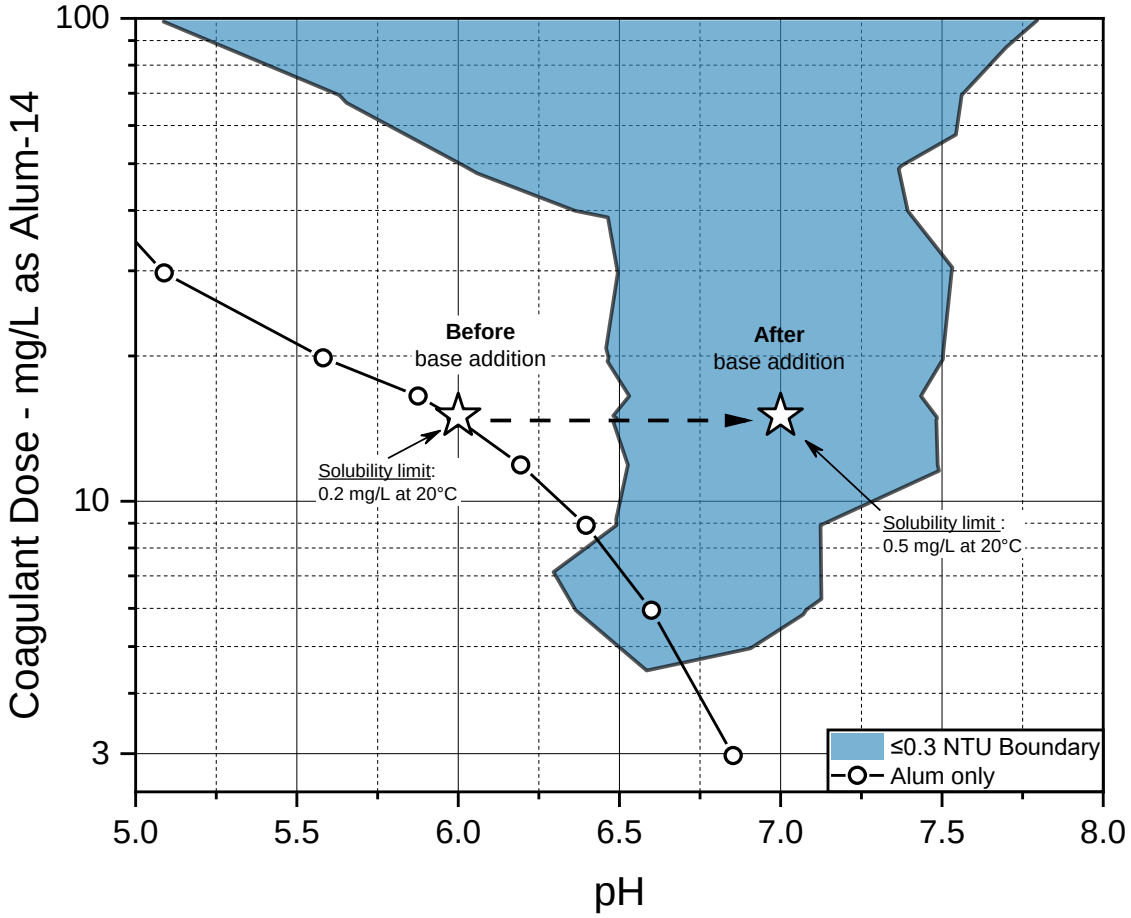

Figure 4.17. Treatment plant's filtered turbidity jar test results

To test these hypotheses, two new experiments were performed where the duration of the 20 s^{-1} mixing stage was extended to 60 minutes. In the first case, coagulation was performed at pH 6.0 (i.e., sub-optimal conditions) with the pH unchanged for the 60-minute duration, while in the

second case, the pH was adjusted to 7.0 after 30 minutes of mixing. In both cases, the coagulant (15 mg/L as alum-14) was added at the start of the experiment. Another set of experiments was performed with similar conditions, except the G-value was increased to 200 s^{-1} to determine if G-value was a factor in floc formation.

The water's average zeta potential increased from -37.7±6.0 mV at pH 7.5 before coagulant addition to 14.4±6.0 mV at pH 6.0 after coagulant addition. Neither extending the mixing time to 60 minutes nor G-value (20 or 200 s^{-1}) resulted in floc appearing under sub-optimal coagulation conditions (Figure 4.18, left panel). When the water's pH was adjusted from 6.0 to 7.0, the zeta potential decreased from 14.4±6.0 mV to -16.8±9.8 mV. Floc appeared approximately 2 and 5 minutes after base addition with the 200 s^{-1} and 20 s^{-1} experiments, respectively (Figure 4.18, right panel). Floc appeared earlier with the high G-value experiment but grew larger with the low G-value experiment. This pattern was consistent with trends observed previously. The results presented in Figure 4.18 confirm the hypothesis that floc appearance in Figure 4.16 was due to a shift from suboptimal to optimal coagulation conditions with a change in pH.

These results also challenge the classic coagulation theory that suggests coagulation is effectively over in 7-seconds (Amirtharajah and Mills 1982; Committee 1989). In this case, it was possible to not only form floc a full 30 minutes after the addition of the coagulant but also using an extremely low G-value (20 s^{-1}) for both rapid mix and flocculation. These bench-scale results predicted that flocculation would theoretically occur in the full-scale process without an operational rapid mixer and not experience any noticeable difference in filtered water turbidity removals.

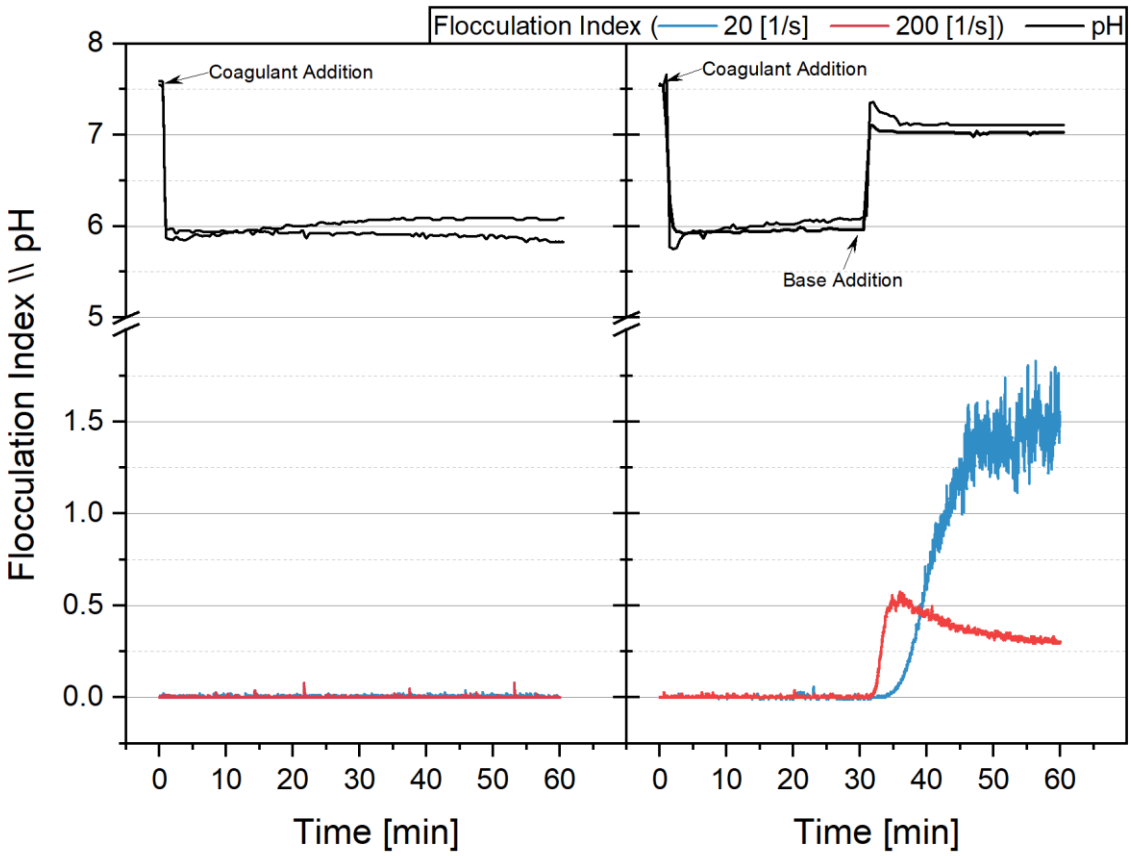

Figure 4.18. Coagulation performed at pH 6.0 (left-panel) versus pH 7.0 (right-panel)

The mixer at the treatment facility was turned off for a period of 2 weeks. Figure 4.19 shows the coagulant dose, raw water, settled water, and finished water turbidities obtained from the plant's records. Data from 10 days prior to the mixer being turned off showed that the plant's settled water turbidity initially ranged between 0.2 to 0.3 NTU and later increased to approximately 0.6 NTU as the raw water turbidity gradually increased from about 7 to 11 NTU. On the other hand, the finished water was consistently less than 0.1 NTU. The plant maintained an average alum dose of approximately 20 mg/L as alum-14 throughout the study. With the mixer off after day 10, the plant did not observe any noticeable difference in their settling and filtration performance. The plant also did not observe any impact on their filter run times (126 hours, on average). The plant could still maintain settled turbidity in the 0.2 to 0.3 NTU range and filtered turbidity less than 0.1

NTU even when the raw water turbidity spiked to 23 NTU. The results presented here were consistent with the findings reported by Allerdings and coworkers (2015) and Malinaro and coworkers (2019). As Edzwald (2013) suggested, intense rapid mixing was not necessary in this case, and the hydraulic energy in the system was sufficient to mix the coagulant and form floc without any discernable impact on performance.

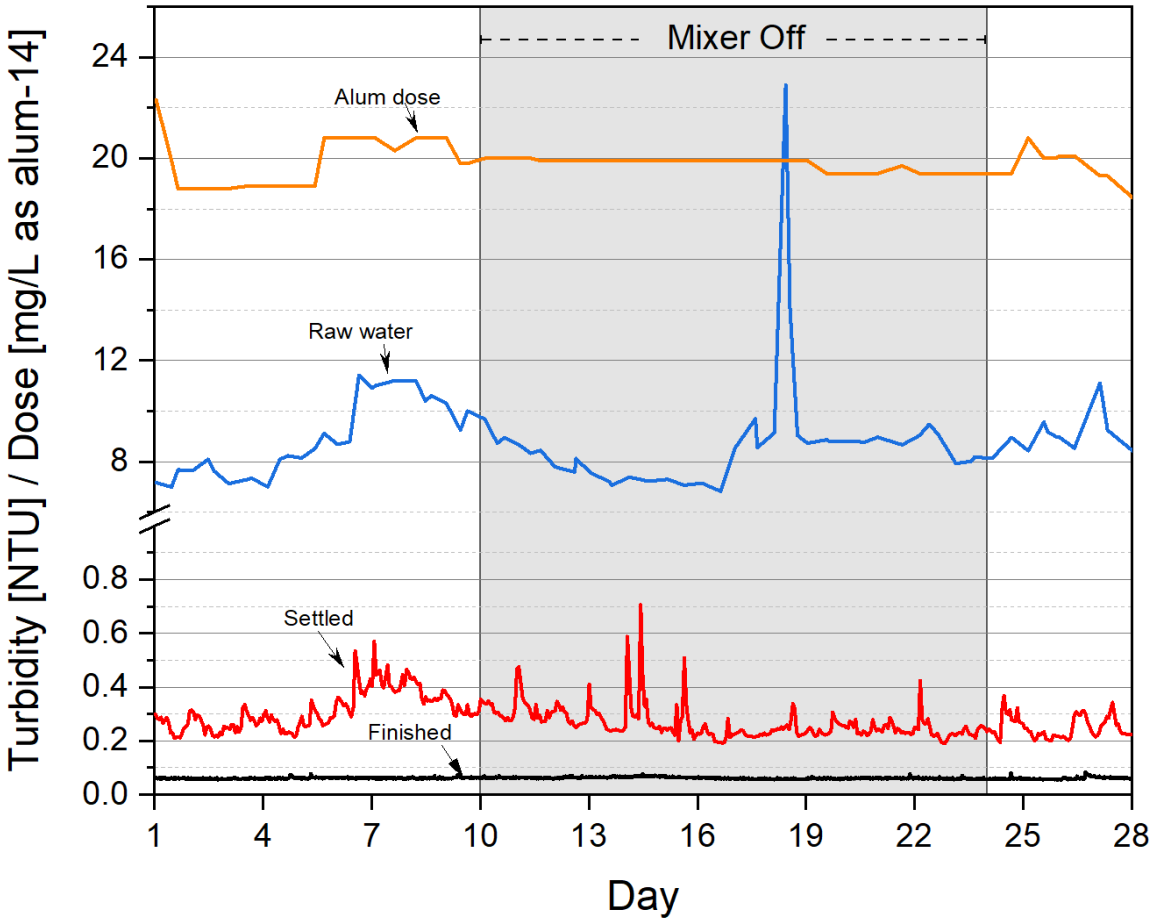

Figure 4.19. Full-scale results from rapid mixer shutdown

4.8. Sedimentation Versus Filtration

It was evident from the results presented in Chapter 3 that using settled water turbidity in a jar as a performance metric could lead to higher alum dosages being identified as being optimal without any added benefit to the filtered water quality. When filtration was used as a performance metric, the effective treatment zones included a wider range of coagulant dosages and were less sensitive to pH. Additionally, effective treatment zones in the region commonly attributed to charge neutralization were only identifiable with filtration. Based on the results presented in this chapter, mixing conditions generally appeared to be significant factors when floc formation characteristics or settled water turbidity removals in a jar were used as metrics of performance. Figure 4.20 compares the settled, and filtered water turbidity removals at all the investigated mixing conditions. The investigated mixing parameters were different in all the experiments performed, but only two optimum coagulant dosages were chosen for this particular raw water. Depending on the selected mixing parameters, settled water turbidity removals ranged from -11 to 80% under the charge neutralization optimum and 18 to 90% under the sweep flocculation optimum. In other words, using jar test settled water turbidity removals varied widely despite using only predetermined optimum coagulation conditions. In contrast, filtered turbidity removals were between 92 – 97% under the optimum charge neutralization and 94 – 98% under the optimum sweep flocculation conditions. While the formation rate and size of floc tended to be influenced by the rapid mix and flocculation parameters, the floc characteristics in jar tests seemed to impact settled water turbidity markedly, although not filtered water turbidity.

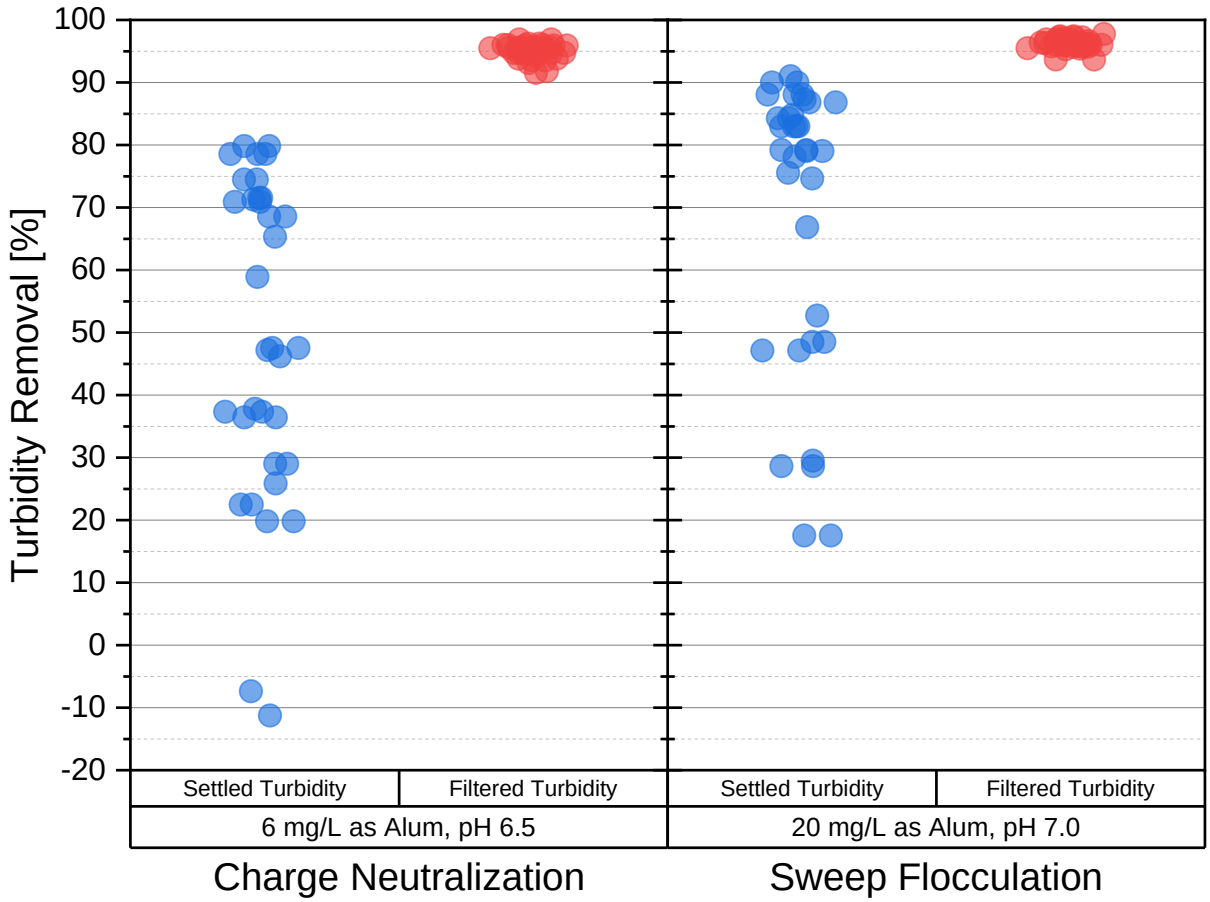

Figure 4.20. Summary of mixing experiments

The importance of rapid mix could not be verified experimentally based on filtered turbidity removals. In fact, rapid mixing only impacted floc size in a negative manner, which occurred when the rapid mixing duration exceeded a threshold (e.g., 120 s). Based on the results presented here and by others (Edzwald 2013; Allerdings, Forster, Vasyukova and Uhl 2015; Malinaro, Rhoades, Pennock and Gutierrez 2019), the necessity or even utility of rapid mixing needs to be established in full-scale facilities.

Flocculation conditions (intensity, duration, and scheme) appeared to be significant factors influencing treatment efficiency when floc formation characteristics or settled water turbidity removals in a jar were used as metrics of performance. However, when the results were compared

in terms of filtered turbidity removals, mixing conditions became insignificant factors on performance provided that there were at least 9 minutes of mixing time with a G-value of 20 s^{-1}.

Based on floc characteristics and settled turbidity removals, the advantages of tapering flocculation were three-fold and consistent with prior research. Relatively large floc was formed with relatively short mixing times; thus, resulting in higher overall energy efficiency. However, there were no practical advantages to using a tapered flocculation scheme instead of a single-stage scheme (e.g., G-value of 20 s-1) when the performance was compared based on filtered turbidity removals. The necessary duration of flocculation was found to be less than 10 minutes, based on the maximum flocculation index (or floc size) under sweep flocculation conditions in this study. This appeared to be significantly less than the minimum duration that is currently recommended by many states (20 – 30 minutes). For charge neutralization, flocculation times for maximum floc size were typically on the order of 30 minutes or less under the studied conditions, but filtered turbidity was not impacted provided there were at least 9 minutes of mixing time with a G-value of 20 s^{-1}.

It is plausible that the importance of mixing in drinking water treatment has been overestimated since many of the past studies based their analyses entirely on settling in jars, which is widely accepted to not accurately scale up to the full-scale process (Hendricks 2016). This in no way implies that sedimentation in the full-scale process is not necessary. Based on this investigation, we should begin to reevaluate current mixing design guidelines and re-emphasize the importance of optimizing coagulation conditions (in terms of both coagulant dose and pH because many water utilities currently lack the capability to adjust pH in one or both directions prior to coagulation). We should revisit whether rapid mixing basins with mechanical mixers should be required or used if already in place since it could negatively impact floc size. We might

also revisit regulatory flocculation requirements because current minimum flocculation times and G-values could drastically exceed the minimum required values identified in this study. Perhaps charge neutralization flocculation requirements should be separately regulated in the future. It is important to remember that the present findings are based on a single set of raw water quality parameters at one temperature using bench-scale laboratory equipment.

Ultimately, this investigation showed that optimization based on granular media filtration is ideal for jar testing to identify optimal coagulation conditions since the results are independent of the mixing parameters used. Thus, as shown in Figure 4.21, the only relevant parameters in the optimization process are the coagulation conditions of the experiment. If the jar test procedure also fixed either the coagulant dose or pH as the other was varied, then the jar test procedure could genuinely be considered as a single variable optimization approach (assuming the coagulant type is also fixed).

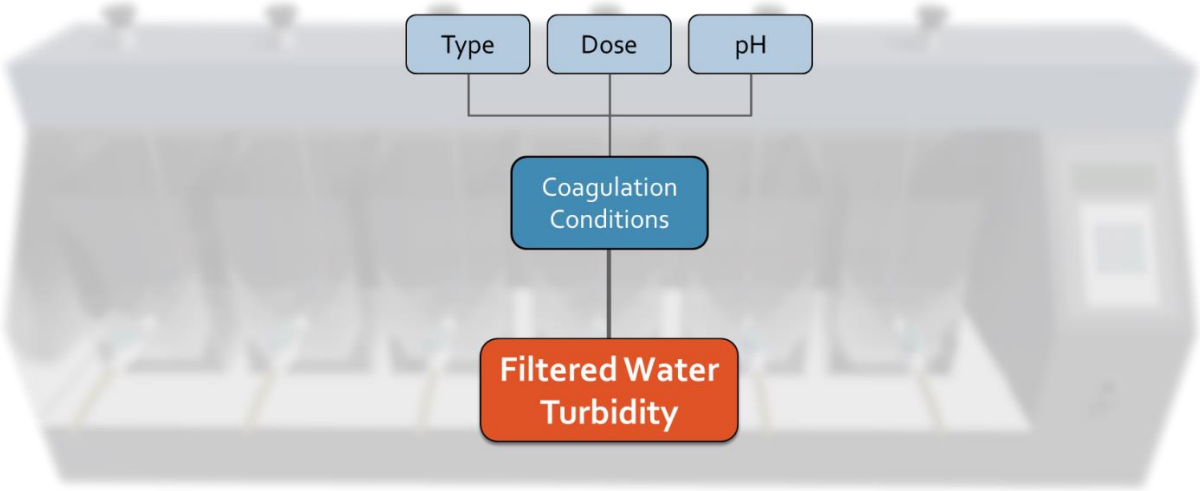

Figure 4.21. Controllable factors in next-generation jar test procedure

CHAPTER 5: WATER QUALITY IMPACTS ON COAGULATION

5.1. The Effects of Water Quality According to The Literature

Most modern drinking water treatment plants continuously monitor aggregate raw quality parameters (such as turbidity) to proactively respond to changes in water quality parameters, which could potentially impact the efficiency of their coagulation stage and subsequent treatment processes. Researchers have demonstrated that coagulation requirements can be influenced by the type and concentration of particles (Langelier and Ludwig 1949; Black and Hannah 1961; Stumm and O'Melia 1968), type and concentration of organics (Vik, Carlson, Eikum and Gjessing 1985; Semmens and Staples 1986; Edzwald 1993; White et al. 1997; Shin, Spinette and O'Melia 2008), presence of ions (Wagner and Hudson 1982; Tseng, Segal and Edwards 2000; Davis and Edwards 2017), and temperature (Morris and Knocke 1984; Knocke, West and Hoehn 1986; Van Benschoten and Edzwald 1990b).

Stumm and O'Melia (1968) suggested that coagulation efficiency was a function of the concentration of particles and the applied coagulation conditions (i.e., dose and pH). The authors quantified coagulation efficiency in terms of turbidity reduction in a jar test. Specifically, they proposed a simple model where particles are destabilized and restabilized based on the total surface area (concentration) of the particles in the raw water and the coagulation conditions. The conceptual model is illustrated in Figure 5.1. Zone 1 corresponds to conditions where the coagulant dose is insufficient to destabilize the contaminants; therefore, no turbidity reduction would be expected. Zone 2 represents the region where destabilization of the contaminants would be achieved via charge neutralization; hence, a reduction in turbidity is observed. The zeta potential of water samples collected in zone 2 would likely be close to in the range of ±10 mV; therefore, a

further increase in the coagulant dose would eventually reverse the charge on the particles. The particle restabilization zone is referred to as zone 3. Zone 4 corresponds to the sweep flocculation zone where destabilization is achieved by the addition of additional coagulant such that the contaminants/particles are enmeshed.

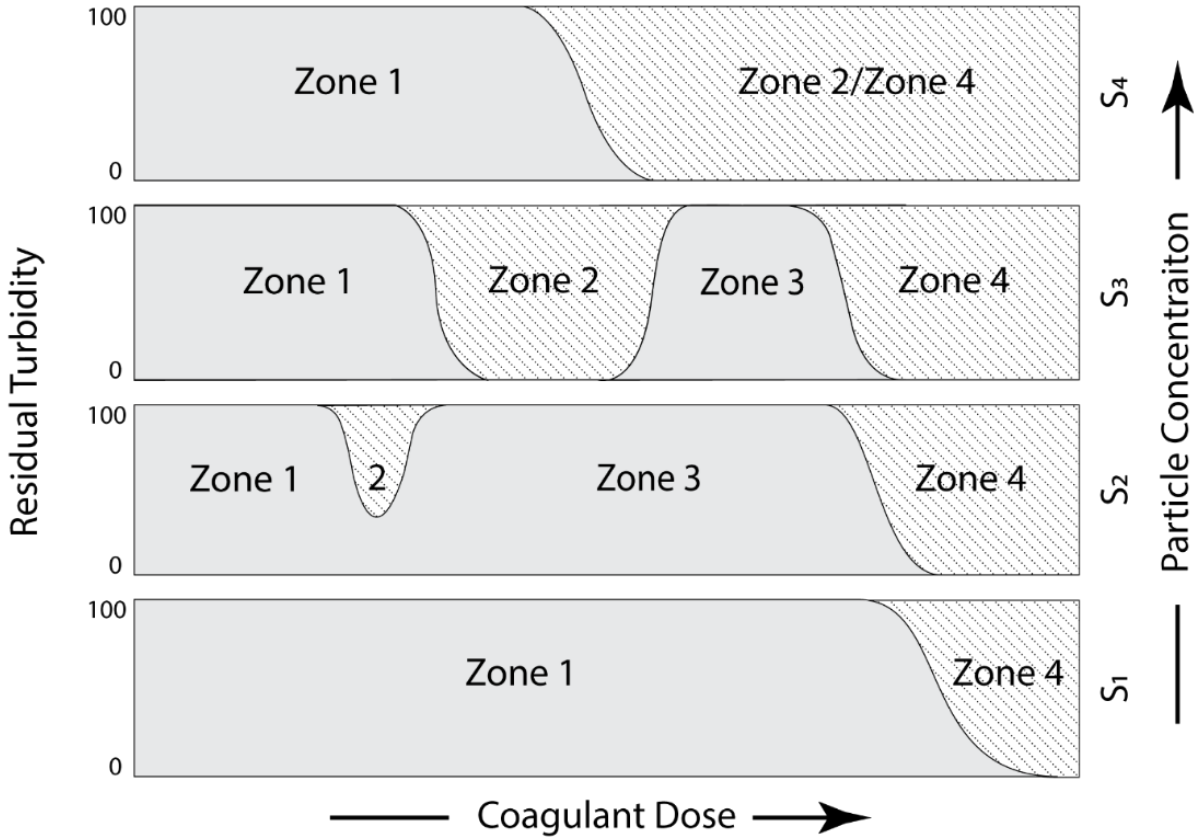

Figure 5.1. Turbidity removal as a function of coagulant dose and particle concentration at a constant pH (adapted from (Stumm and O'Melia 1968))

A detailed analysis of the conceptual diagram in Figure 5.1 was provided by Crittenden et al. (2012a). In summary, Figure 5.1 illustrates that waters with a high concentration of particles would be relatively easier to treat than waters with a low concentration of particles. Comparing the two extremes, S_1 and S_4, it was evident that the coagulant dose required to reduce the turbidity effectively was considerably lower when the concentration of particles was highest (i.e., S_4). Stumm and O'Melia (1968) proposed that particle collisions (i.e., flocculation) would be limited

and likely not to occur in a reasonable time for effective turbidity reduction. As a result, turbidity reduction would only be possible under sweep flocculation conditions where sufficient particles are added to the system by the formation of precipitate. Moderate particle concentrations (S_2 and S_3) would theoretically provide ample contact opportunities for coagulation to occur via the charge neutralization mechanism in zone 2. Increasing the coagulant dose further would restabilize the particles (zone 3) up to the point where coagulation can occur via the sweep flocculation mechanism (zone 4).

Edzwald and Van Benschoten (1990) argued that the effective coagulant dose is usually controlled by the concentration of DOC and not the concentration of particles (i.e., turbidity). Figure 5.2 compares jar test results performed by those authors using water samples collected from the Missouri River and Myrtle Beach. The authors selected these sources for their vastly contrasting water quality characteristics. The sample collected from the Missouri River was classified as being a moderately hard water (150 mg/L as $CaCO_3$), high in turbidity (670 NTU), and relatively low in DOC (3 mg/L). The Myrtle Beach water sample was classified as being a soft water (< 50 mg/L as $CaCO_3$), relatively low in turbidity (30 NTU), and high in DOC (20 mg/L). The authors found that even though the raw water turbidity of the Missouri River was more than 20 times higher than Myrtle Beach, the required coagulant dose to treat the river water was approximately 10 times lower than the required dose for Myrtle Beach (at pH 7.0).

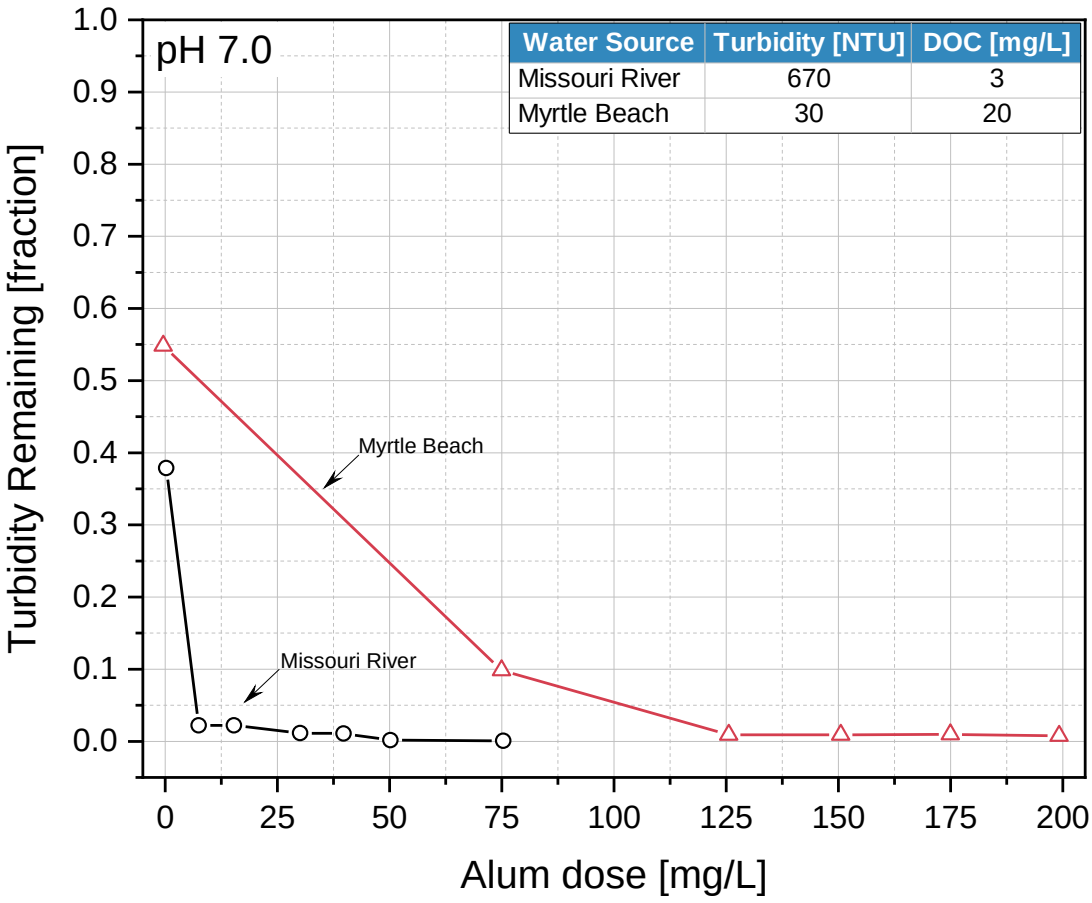

Figure 5.2. A comparison of jar tests with two water sources at (adapted from (Edzwald 1993))

Edzwald and Van Benschoten (1990) attributed the drastic difference between the coagulation requirements to the total charge demand of the two water sources. Clay particles typically have a cation exchange capacity (a function of the total negative charge on the surface of particles in water) in the range of 0.1 to 1 µeq/mg of clay, while the total charge on the functional groups of NOM is typically in the range of 10 to 15 µeq/mg of DOC (Thurman 1985; Edzwald and Van Benschoten 1990; Van Benschoten and Edzwald 1990b). This implies that the total charge demand from 1 mg of DOC could be between 10 to 150 times greater than the total charge demand from 1 mg of clay. It is worth mentioning that turbidity is a simple aggregate measurement that is a function of the concentration, size, and light scattering properties of colloidal particles suspended

in water. Both inorganic particles and organic particles can scatter light; however, it is generally assumed that most of the particles that contribute to turbidity are inorganic clays.

Shin, Spinette, and O'Melia (2008) measured the individual and combined effects of particles and organics on the minimum effective alum dose under carefully controlled experimental conditions. The authors defined the minimum effective alum dose as the point where an additional increase in the alum dose did not significantly improve filtered water turbidity – i.e., the point of diminishing returns. Filtered water turbidity was measured using a 1.2 µm glass fiber filter following a 60-minute settling period. Figure 5.3 compares the minimum effective alum dose as a function of the concentration of colloidal silica particles (Snowtex-ZL, Nissan Chemical Industries, Tokyo, Japan) and DOC at pH 6.0 and 7.0.

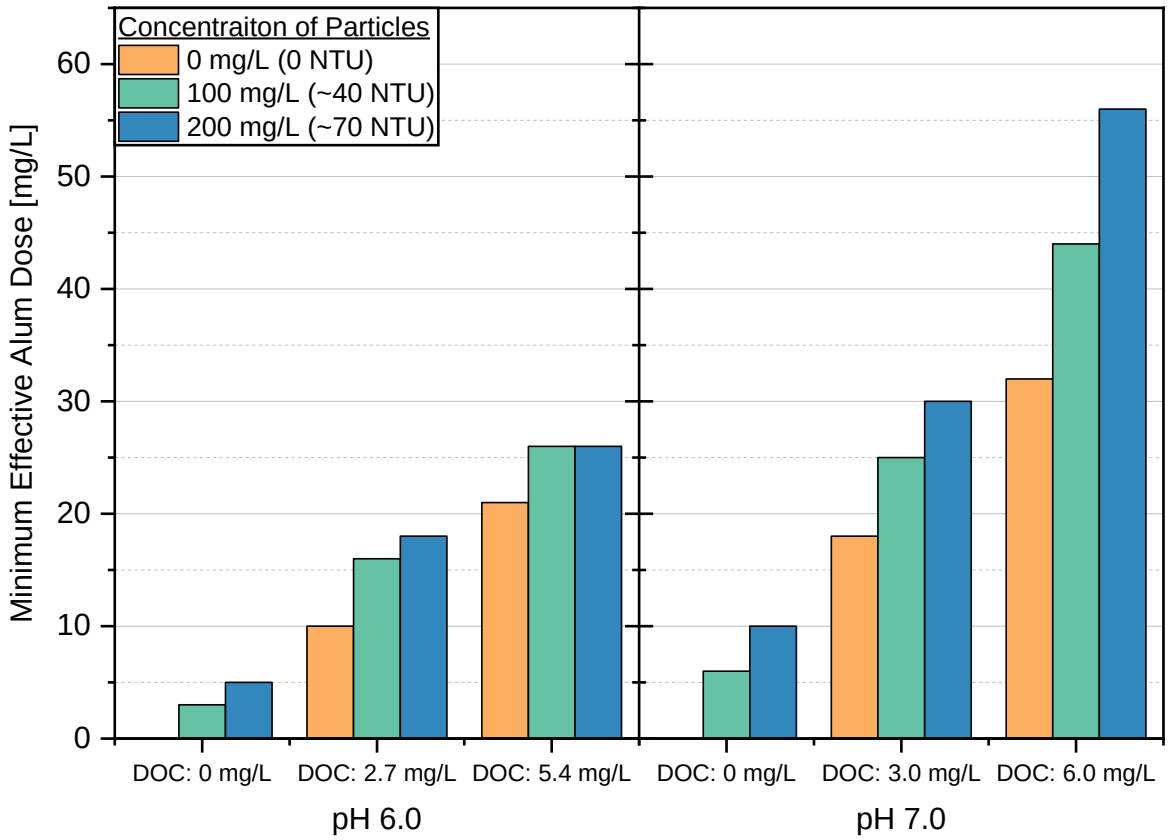

Figure 5.3. Combined effects of particles and DOC at pH 6.0 and 7.0 (adapted from (Shin, Spinette and O'Melia 2008))

The most notable observation was that the minimum effective alum dose was higher in all cases that included DOC compared to the cases without DOC. For example, the effective alum dose for the sample that contained 200 mg/L of colloidal silica and no DOC was 5 mg/L as alum at pH 6.0 compared to 10 mg/L as alum at pH 6.0 for the sample that only contained 2.7 mg/L of DOC and no particles. Increasing the particle concentration from 0 to 100 mg/L increased the required dose by approximately 20 – 35%. On the other hand, increasing the DOC from 0 to 3 mg/L (for a fixed particle concentration) increased the required coagulant dose by approximately 65 – 80%. The results presented by Shin, Spinette, and O'Melia (2008) confirmed the conclusions of Edzwald and Van Benschoten (1990) – i.e., the coagulant demand or minimum effective dose is primarily controlled by the DOC concentration. Moreover, Shin, Spinette, and O'Melia (2008) showed that the effect of increasing the concentration of particles and DOC on coagulation requirements was also dependent on the coagulation pH (Figure 5.3). In general, the impact on coagulation requirements due to increasing particle and DOC concentrations was lower at pH 6.0 than pH 7.0. Increasing the pH from 6.0 to 7.0 has a combined effect of reducing the total available positive charge on the aluminum hydrolysis species (Figure 2.9) and increasing the negative charge on the contaminants (Shin, Spinette and O'Melia 2008).

Besides the concentration of organics, the type of organics present in the raw water also impacts the effective coagulation conditions (Sillanpää, Matilainen and Lahtinen 2015). The type of organics refers to the relative fractions of the NOM present (e.g., humic acids, fulvic acids, etc.). Further classifications of these compounds can be made depending on the fractionation techniques used (Thurman 1985). A significant fraction of the NOM compounds are aromatic or have conjugated double bonds, which absorb light in the UV wavelength region. With regards to drinking water treatment, aggregate parameters such as UV_{254}, DOC, and SUVA are generally

sufficient for estimating the type of organics present and their relative impact on coagulation requirements. Absorbance measurements at 254 nm are proportional to the amount of DOC present in the water (Singer et al. 1981; Edzwald, Becker and Wattier 1985; Edzwald and Kaminski 2009). SUVA is a parameter that is obtained by normalizing the UV_{254} measurement by the amount of DOC present. The parameter (SUVA) was first introduced, at least for drinking water applications, by Edzwald and Van Benschoten (1990). The authors reported that the SUVA provides information on whether a given water sample is low or high in aquatic humic compounds. White and coworkers (1997) investigated the influence of SUVA on the alum dose required to remove DOC for 25 waters in the US and found that, in general, the higher the SUVA of the raw water, the lower the coagulant dose requirement would be to remove DOC. Edzwald and Tobiason (1999) provided a table that generalizes NOM composition and expected coagulation performance as a function of SUVA (Table 5.1).

Table 5.1. Guidelines on nature of NOM and expected DOC removals

SUVA [L/mg-m]	Composition	Coagulation	DOC Removals
> 4	Mostly aquatic Humics, High Hydrophobicity, High MW	NOM controls, Good DOC Removals	>50% for alum
2 - 4	Mixture of Aquatic Humics and Other NOM, Mixture of Hydrophobic and Hydrophilic NOM, Mixture of MWs	NOM Influences, DOC Removals Should be Fair to Good	25-50% for alum
< 2	Mostly Non-Humics Low Hydrophobicity. Low MW	NOM Has Little Influence Poor DOC Removals	< 25% for alum

Adapted from Edzwald and Tobiason (1999)

5.2. Revisiting Water Quality and Coagulation

To date, most coagulation studies focused on the effects of only one or two parameters changing at a time. In the real world, all coagulation factors (variables) interact with one another at all times. When researchers try to measure the effects of a single factor on the coagulation process, they measure that factor's effects plus its interactions with all of the other factors. For example, Shin and coworkers (2008) did not observe any impact on the minimum effective dose when they increased the concentration of colloidal silica from 100 to 200 mg/L at the highest DOC concentration at pH 6.0 (Figure 5.3). On the other hand, they observed an impact on the effective dose for the same change in particle concentration at a lower DOC concentration or higher pH. It is possible that the effects of increasing turbidity on the minimum effective coagulant dose is, in this case, a function of the initial turbidity, DOC concentration, and coagulation pH. Generally, the more factors that are included or considered (e.g., SUVA, alkalinity, or temperature), the more complex the problem becomes. The contributions from the past researchers were undoubtedly critical to advance the body of knowledge on coagulation; however, there is a general lack of understanding of how the factors interact with each other and how their interactions impact the coagulation process. More importantly, how the interacting factors impact different treatment goals (e.g., turbidity removal versus DOC removal) has not been established.

5.3. Interactions Between Coagulation Parameters

Figure 5.4 presents a simplified conceptual visualization of the interactions between the factors involved in the coagulation process. The purpose of the diagram was to merely emphasize that all the factors are either directly or indirectly connected to one another. For simplicity, the factors were connected using a basic line; however, it is important to note that not all connections are bidirectional – e.g., mixing factors are highly unlikely to influence the water temperature. It is

helpful to imagine that the relative position of a factor in the two-dimensional space of Figure 5.4 as being its value or magnitude. A factor moving in space (i.e., its value changing) can influence other factors' position due to their connections (i.e., interactions). Moving factors would likely alter the balance (i.e., equilibrium) of the system – i.e., influence the performance of the overall process.

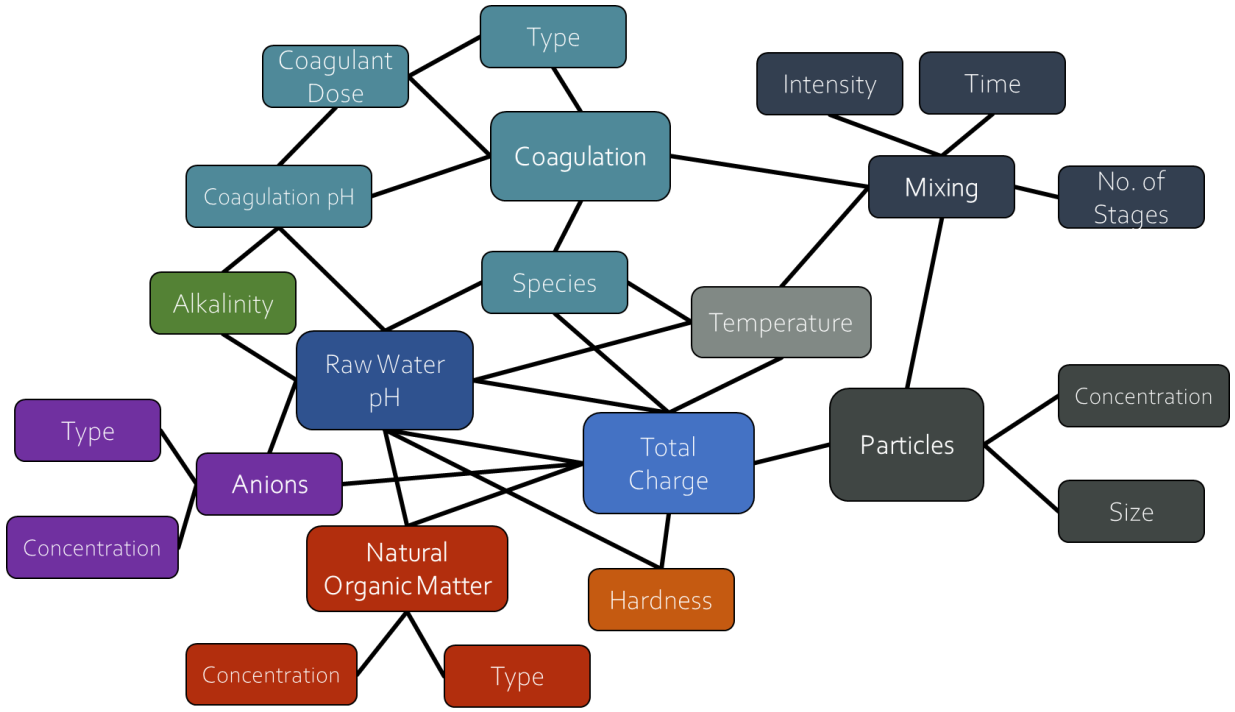

Figure 5.4. Conceptual diagram of interacting coagulation factors

5.4. Isolating the Effects of Water Quality Parameters

The effects of water quality parameters of interest on coagulation efficiency can be quantified if controlled. For this reason, most studies on the chemistry and mechanisms of coagulation were performed using synthetic or model waters where the water quality parameters could be controlled. Appendix B presented a novel procedure for creating synthetic waters based on a target DOC concentration, SUVA, turbidity, and alkalinity. A typical design of experiments (DOE) approach is to perform all possible combinations of each factor at a set of discrete levels

and measure the response of the process using a suitable performance metric. For example, the effects of turbidity and temperature (factors) at three levels (e.g., low, mid, and high) on the coagulation process can be quantified using filtered water turbidity removals. In this case, a total of 9 experiments would be required to perform the experiments at all the possible combinations of the factors at their respective levels. This design is called a full factorial experimental design. The core principles of all DOE methods are based on designing statistically sound experiments (Czitrom 1999; Montgomery 2017). Table 5.2 shows a total of 16 unique waters that were generated using a full factorial experiment design to study the effects of DOC, SUVA, turbidity, and alkalinity on coagulation performance. Each factor included two levels (low and high).

Table 5.2. Investigated waters

Water	**DOC [mg/L as C]**	**SUVA [L/mg-m]**	**Turbidity [NTU]**	**Alkalinity [mg/L as $CaCO_3$]**
Water 1	2	2	3	25
Water 2	2	2	3	140
Water 3	2	2	30	25
Water 4	2	2	30	140
Water 5	8	2	3	25
Water 6	8	2	3	140
Water 7	8	2	30	25
Water 8	8	2	30	140
Water 9	2	5	3	25
Water 10	2	5	3	140
Water 11	2	5	30	25
Water 12	2	5	30	140
Water 13	8	5	3	25
Water 14	8	5	3	140
Water 15	8	5	30	25
Water 16	8	5	30	140

Each water was treated with 12 – 18 dosage levels of alum at seven different pH levels (represented by the red dots in Figure 5.5). The coagulant dose ranged from 3 to 100 mg/L as alum-14 (12 – 18 levels), while the pH ranged from 5 – 8 in increments of 0.5 pH units. Datapoints can

be considered as nodes containing input and output data. In this case, input data included the coagulant dose, target pH, temperature, raw water quality parameters (DOC, SUVA, UV_{254}, alkalinity, turbidity, zeta potential, and pH), type and volume of pH adjusting chemical (acid or base), the pH of the water with coagulant only, and the pH of the water with the pH adjusting chemical only. Output data or response variables included the actual/measured pH of coagulation, pH at the end of the experiment, coagulated water quality parameters (UV_{254}, DOC, SUVA, zeta potential, and settled and filtered water turbidity), and total cost of chemicals.

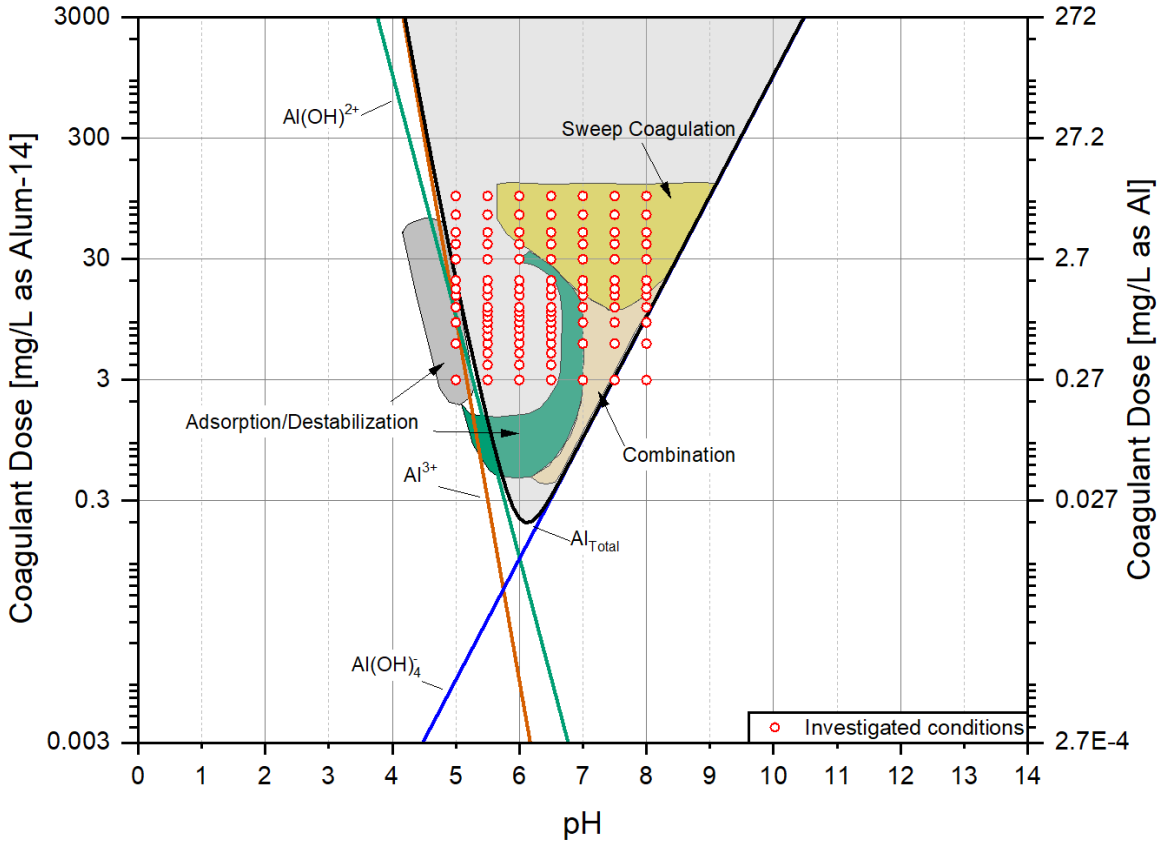

Figure 5.5. Investigated coagulation conditions superimposed on the coagulation diagram (source: Amirtharajah and Mills (1982))

In total, 272 jar tests (17 per raw water) were performed using the next-generation jar test procedure described in Appendix A. As discussed earlier, the advantages of the next-generation jar test procedure were three-fold. First, optimization in the next-generation procedure was based

on granular media filtration instead of settling. Filtration was found to be only dependent on the destabilization efficiency of the coagulation process (Figure 4.21) and relatively independent of the floc size and applied mixing parameters that heavily influence sedimentation removals. Additionally, jar test filtered turbidity results were found to be directly scalable to the full-scale process. Second, the next-generation procedure used a standardized mixing program and does not need to be calibrated to one specific full-scale facility. This was only possible because optimization was based on filtration, which did not depend on the applied jar test mixing parameters (Figure 4.20). Third, the next-generation jar test procedure uses a single-variable optimization approach where either the coagulant dose or the pH is fixed as the other is varied across the jars. Titrations were performed before each experiment to determine the amount of acid or base required to achieve a target pH at a given coagulant dose.

5.5. Visualizing the Effects of Water Quality Parameters

The effects of water quality parameters on coagulation efficiency were visualized using contour plots of the measured response variables (e.g., filtered turbidity removal). In total, 128 contour plots were generated. For discussion purposes, waters were grouped into low and high pairs for each water quality parameter. For example, to compare the effects of increasing raw water SUVA on coagulation efficiency, waters 1 – 8 (Table 5.2) were placed in the low SUVA group while waters 9 – 16 were placed in the high SUVA group. A similar approach to the one shown in Figure 3.13 was used to extract data from each water's contour plot and compile it into either a "low" or "high" dataset. The dataset from each group was analyzed, and all datapoints that did not meet the filtered turbidity criterion ($\leq$0.3 NTU, or at least 90% removal) were rejected; thus, each water group consisted of only coagulation conditions that met the removal criterion. Figure 5.6 shows a scatter plot of the effective coagulation conditions of waters with a low SUVA (2 L/mg-

m). Every point on the plot represents a coagulation condition where the filtered turbidity criterion was achieved. Semi-transparent symbols were used such that when multiple symbols overlapped, they appeared relatively opaque. As a result, darker symbols denote common regions where the applied coagulation conditions were effective at reducing the filtered turbidity to ≤0.3 NTU with multiple waters.

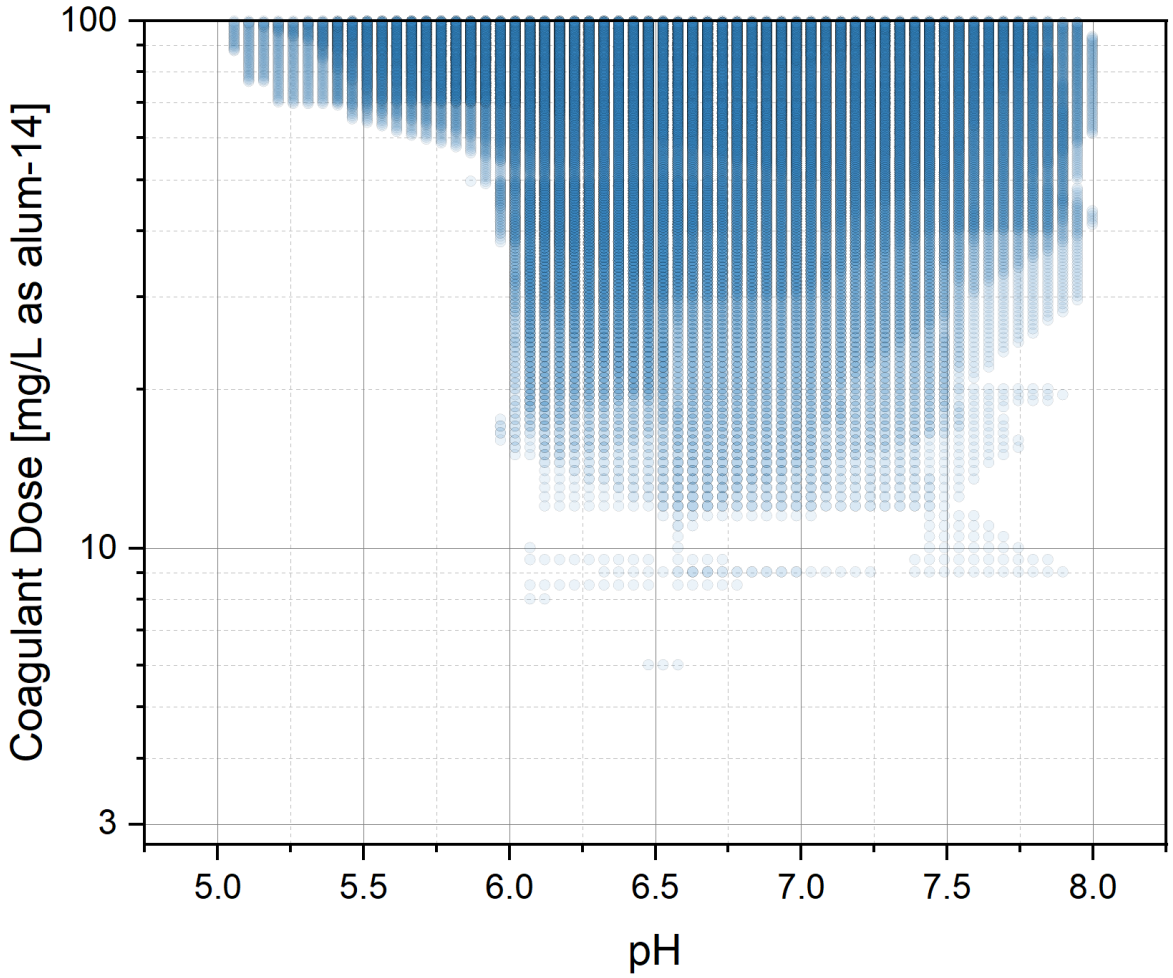

Figure 5.6. Scatter plot of effective filtered turbidity removals for low SUVA waters (8 waters)

Multivariate kernel density (KD) plots were used to create heatmaps to represent regions where effective coagulation conditions were concentrated. KD plots are estimates of the underlying probability density function of a given dataset. In other words, KD plots describe the

relative likelihood or probability that a continuous variable would take on a given value. In this case, a KD plot of all the combined effective coagulation conditions for a group of waters would highlight regions where an effective coagulation condition is likely to be found.

5.6. Combined Boundary of Effective Coagulation

Figure 5.7 shows two-dimensional (2D) and three-dimensional (3D) density plots for all the 16 waters combined. As a reminder, the filtered turbidity cut-off used here was only done for discussion purposes and to simplify the presentation of the results. Blank (white) regions on the KD plots should not be interpreted as regions of ineffective coagulation. Similarly, darker regions do not necessarily imply better coagulation. Rather, darker colors represent the probability that a given coagulation condition (coagulant dose and pH) will be effective for any of the 16 waters. All coagulation conditions on the density scale produced a filtered turbidity below 0.3 NTU (just not for every water). Readers are encouraged to refer to the online interactive data visualization app that was created for the purpose of comparing the raw data, i.e., all contour levels for all the conditions investigated (Alansari 2021a).

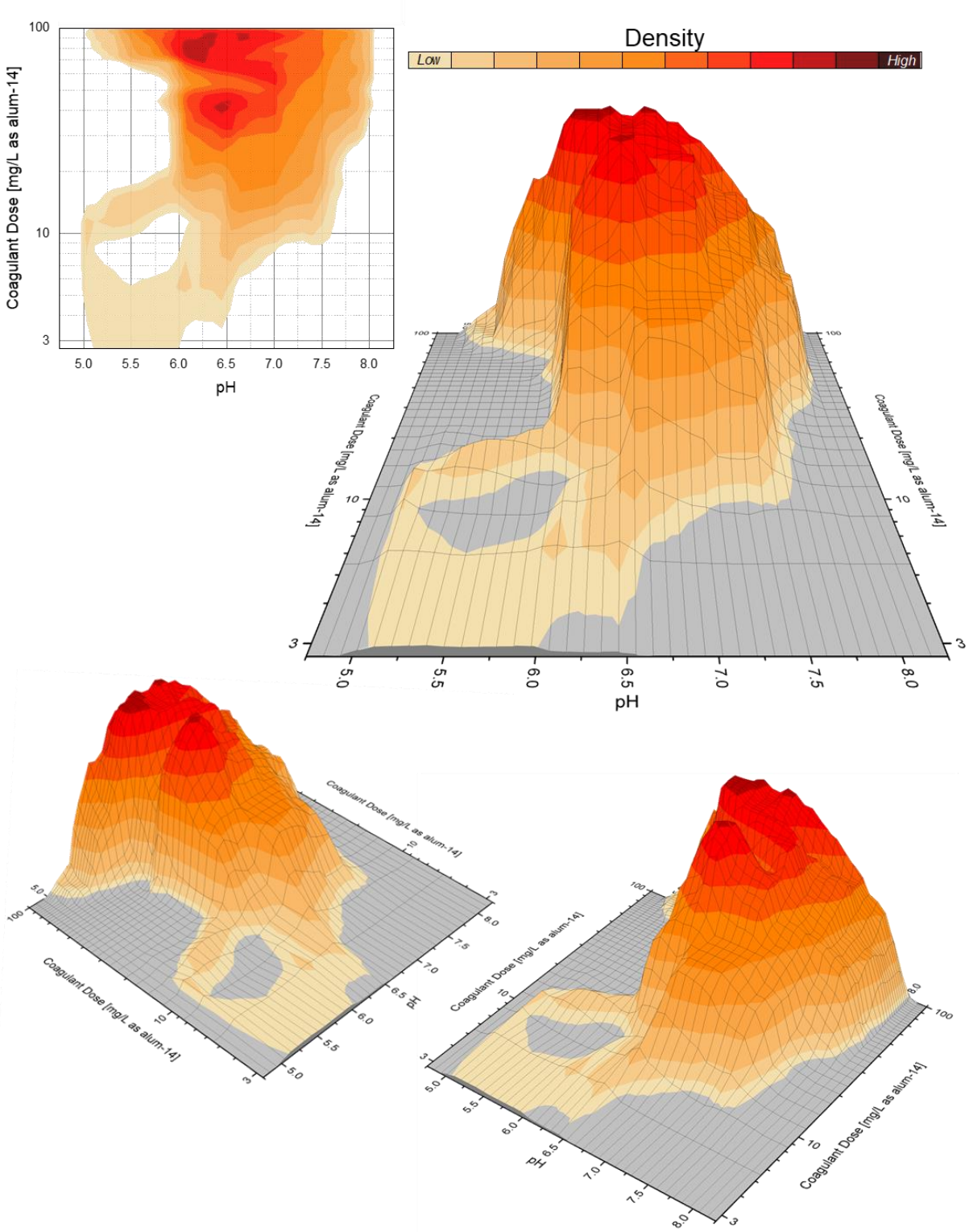

Figure 5.7. Combined filtered turbidity kernel density plot (16 waters)

The highest density region was found between 30 and 100 mg/L as alum-14 and between pH 6.0 and pH 7.0 (dark orange – maroon region) – which coincided with region mainly attributed to the sweep flocculation coagulation mechanism. The occurrence of overlapping coagulation conditions in this region implied that the coagulant dose and pH were relatively independent of water quality parameters or stoichiometry with negatively charged contaminants. Low density (beige – light orange) and separated regions in the low pH and dose range (pH<6.5 and <20 mg/L as alum-14) were attributed to the charge neutralization mechanism. The low density and separation of these zones were likely due to the stoichiometric nature of the charge neutralization mechanism with respect to water quality. As a result, finding effective coagulation conditions would be relatively more difficult and likely very dependent on exact water quality in these low-density regions compared to high-density regions. The most notable feature on the 3D density plot was the rapid change in density at approximately pH 6.0 and a coagulant dose above 20 mg/L as alum-14. This effect could be attributed to a shift in the coagulation mechanism from charge neutralization (pH<6.0) to sweep flocculation (pH>6.0).

The features observed in the combined, filtered turbidity removal KD plot (Figure 5.7) resulted from the main and interaction effects of water quality parameters on coagulation. By combining the waters into groups where one of the four parameters is controlled, the main effects of increasing the controlled water quality parameter on coagulation conditions can be visualized (e.g., waters low in turbidity versus water high in turbidity). Interaction effects can be visualized by controlling multiple water quality parameters simultaneously (e.g., increasing both turbidity and alkalinity one at a time versus simultaneously). Visualizing interactions is best done using the online interactive data visualization app (Alansari 2021a).

5.7. Effects of SUVA

To visualize the effects of SUVA on coagulation conditions, waters were grouped into low SUVA (2.0 L/mg-m) and high SUVA (5.0 L/mg-m) categories. Figure 5.8 shows the effects of increasing the raw water's SUVA on the filtered turbidity removal KD plots. The extension of the removal boundaries into the charge neutralization zone (lower-left quadrant) was clearly an effect of high SUVA (right-panel) due to the absence of coagulation conditions in the low SUVA group (left-panel). On the other hand, SUVA did not appear to substantially affect the coagulation conditions in the sweep flocculation zone since the size and shape of the high-density region remained the same. These results suggested that SUVA was primarily an essential factor (in terms of filtered turbidity removal) when the predominant mechanism was charge neutralization.

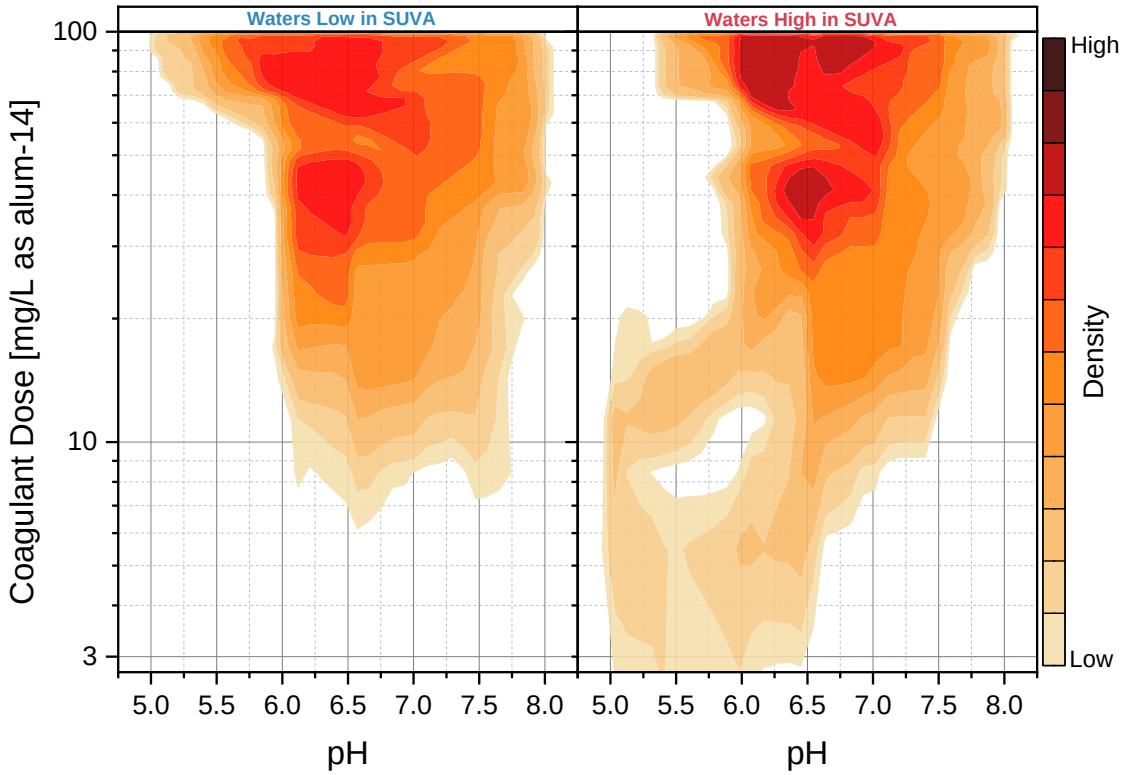

Figure 5.8. Effects of SUVA on effective coagulation conditions

5.8. Effects of Turbidity

Waters were grouped into low turbidity (3 NTU) and high turbidity (30 NTU) categories to study the effects of increasing raw water turbidity on effective coagulation conditions (Figure 5.9). In general, the results showed that increasing raw water turbidity had minor or negligible effects on coagulation conditions in the sweep flocculation zone (>30 mg/L as alum-14). The nearly identical high-density boundaries in Figure 5.8 and Figure 5.9 indicated that neither factor had a significant effect on coagulation conditions in this region.

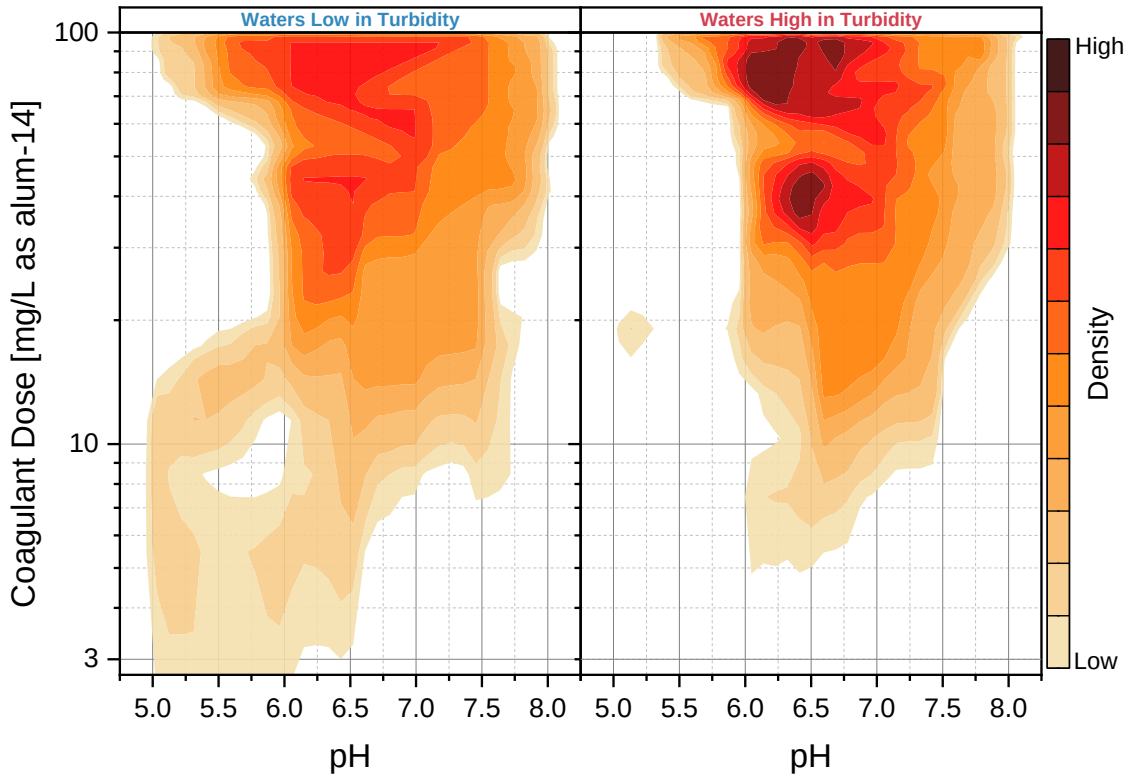

Figure 5.9. Effects of turbidity on effective coagulation conditions

The most notable feature was the absence of the low-density boundaries in the charge neutralization zone (lower-left quadrant) of the high turbidity KD plot (right-panel). The occurrence of coagulation conditions in the charge neutralization zone was found to be a feature of waters high in SUVA (Figure 5.8). The combined effects of high SUVA and turbidity could

have negatively impacted destabilization efficiency, which contributed to the absence of the low-density boundary. However, a close examination of each water's contour plot revealed that the absence of low-density boundaries in the charge neutralization zone was simply an artifact of the selected filtered turbidity criterion – i.e., the contour plots of the low and high turbidity waters were very similar. Figure 5.10 compares the effects of increasing raw water turbidity on filtered turbidity results in a pair of similar waters (waters 13 and 15 in Table 5.2). The orange contours represent the boundaries of the 0.3 NTU filtered turbidity criterion. In the high raw water turbidity case (right-panel), the 0.3 NTU contour did not extend into the charge neutralization zone – which was consistent with the results observed in the KD plot of Figure 5.9. Conversely, the low and high turbidity results were very similar compared to the 0.4 NTU contours; therefore, it can be reasonably argued that particles were destabilized (hence, the turbidity reduction), despite not meeting the filtered turbidity criterion. It is also worth mentioning that the filtered turbidity results were acquired using a column with only 3-inches of filter media at a loading rate of 4.5-5 gpm/ft^2.

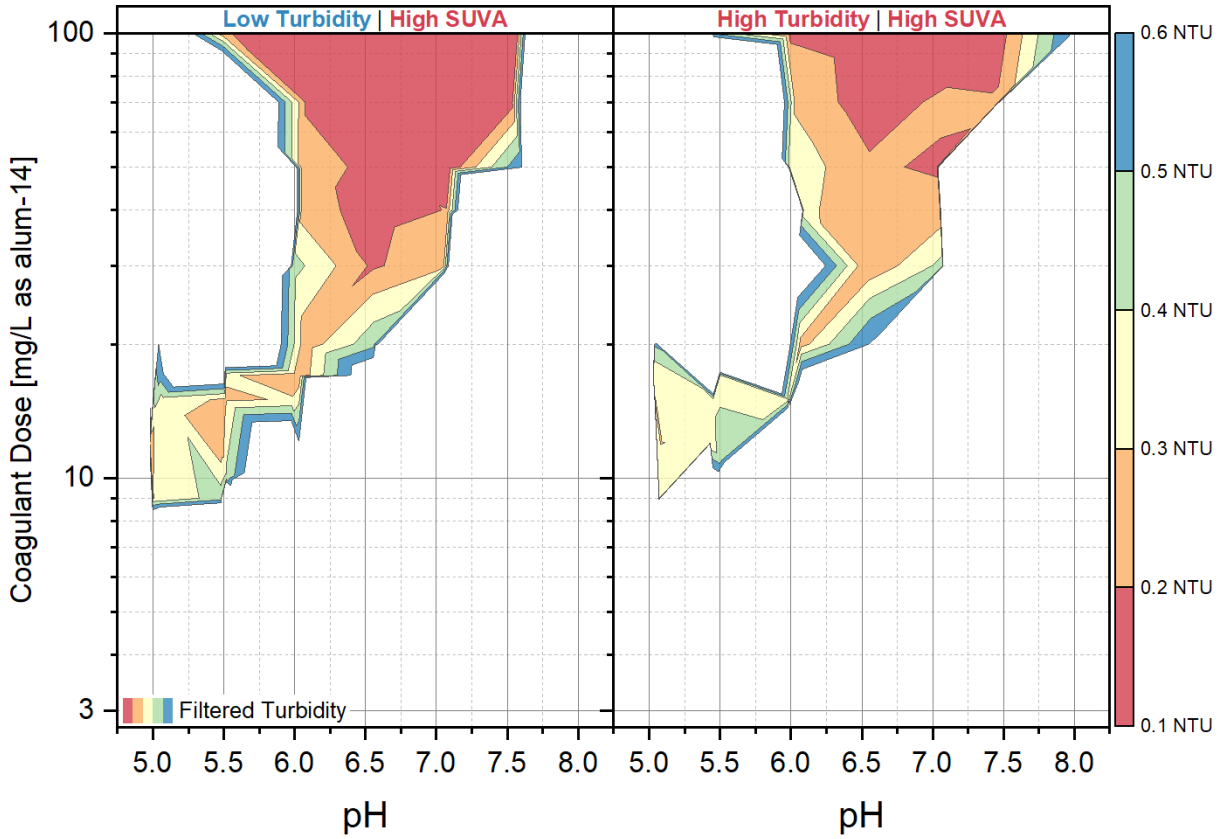

Figure 5.10. Comparing turbidity effects on a pair of similar high SUVA waters

5.9. Effects of Alkalinity

Figure 5.11 shows the effects of increasing the raw water alkalinity from 25 to 140 mg/L as $CaCO_3$ on the effective coagulation conditions. The combined KD plot (Figure 5.7) showed a characteristic vertical boundary at pH 6.0, where the density increased rapidly. A second vertical boundary at pH 6.5 below 20 mg/L as alum-14 was observed in the low alkalinity KD plot (left-panel); however, the density increase with increasing pH was not as drastic as the boundary at pH 6.0. Increasing raw water alkalinity primarily impacted conditions above 20 mg/L as alum-14 and pH 7.0 (top-right quadrant), which had the effect of narrowing and concentrating the high-density regions to pH 6.0 – 7.0. Examining the individual contour plots of the high alkalinity waters

revealed that the right right-edge of the removal boundary shifted to the left (lower pH) with increasing alkalinity.

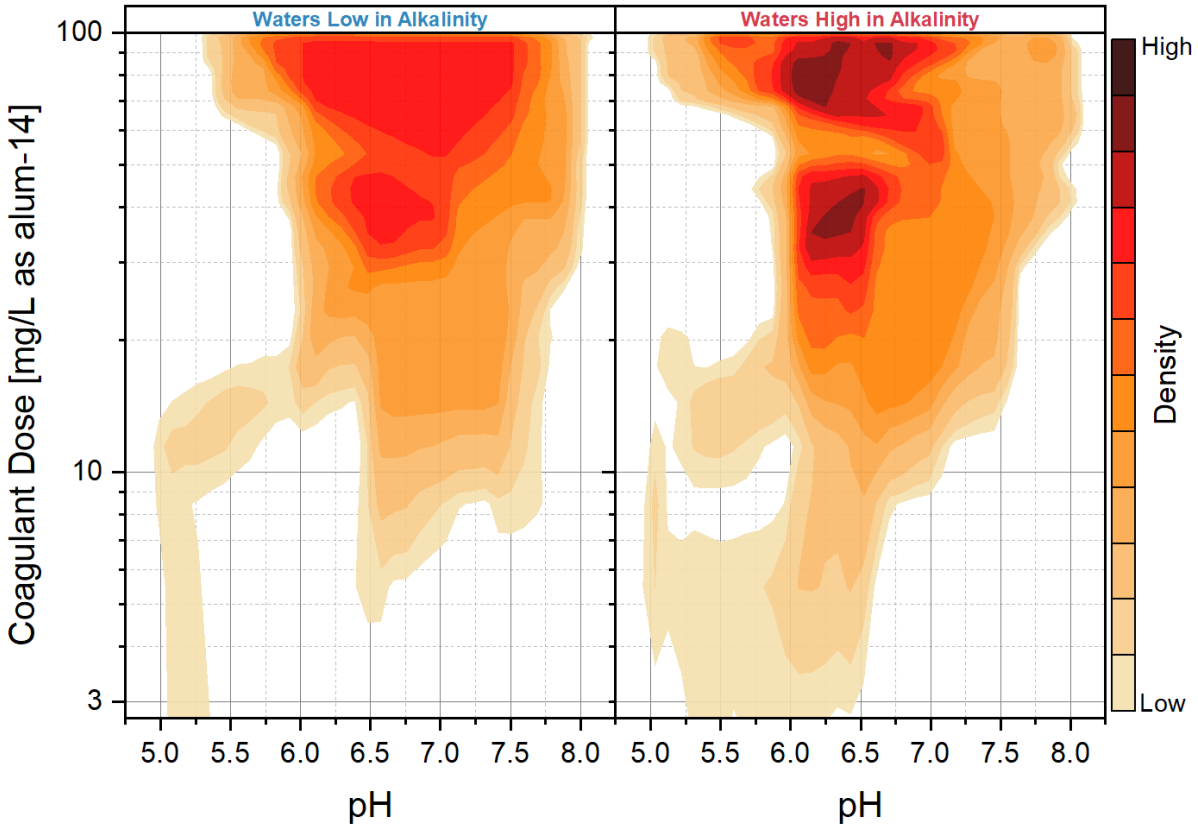

Figure 5.11. Effects of alkalinity on effective coagulation conditions

5.10. Effects of DOC

Waters were grouped into low DOC (2 mg/L) and high DOC (8 mg/L) categories to study the effects of increasing raw water DOC on effective coagulation conditions. Figure 5.12 compares the KD plots of the low and high DOC groups. The results showed that effective coagulation boundaries were highly dependent on the DOC concentration. Increasing raw water DOC generally had the effect of shifting the boundaries up (i.e., higher dose) and to the left (i.e., lower pH) from the green line in the left panel to the blue line in the right panel. High-density boundaries (dark orange – maroon) were generally broad with the low DOC group (left-panel) whereas the high-

density boundaries with the high DOC group was narrow and concentrated between pH 6.0 – 6.5 and above 20 mg/L as alum-14. The most notable feature was the extent of negative impact on coagulation conditions above pH 6.5 and below 30 mg/L as alum-14 represented by the grey boxes in each panel. Similarly, low-density boundaries in the charge neutralization zone (lower-left quadrant) shifted up (higher dose) with increasing raw water DOC.

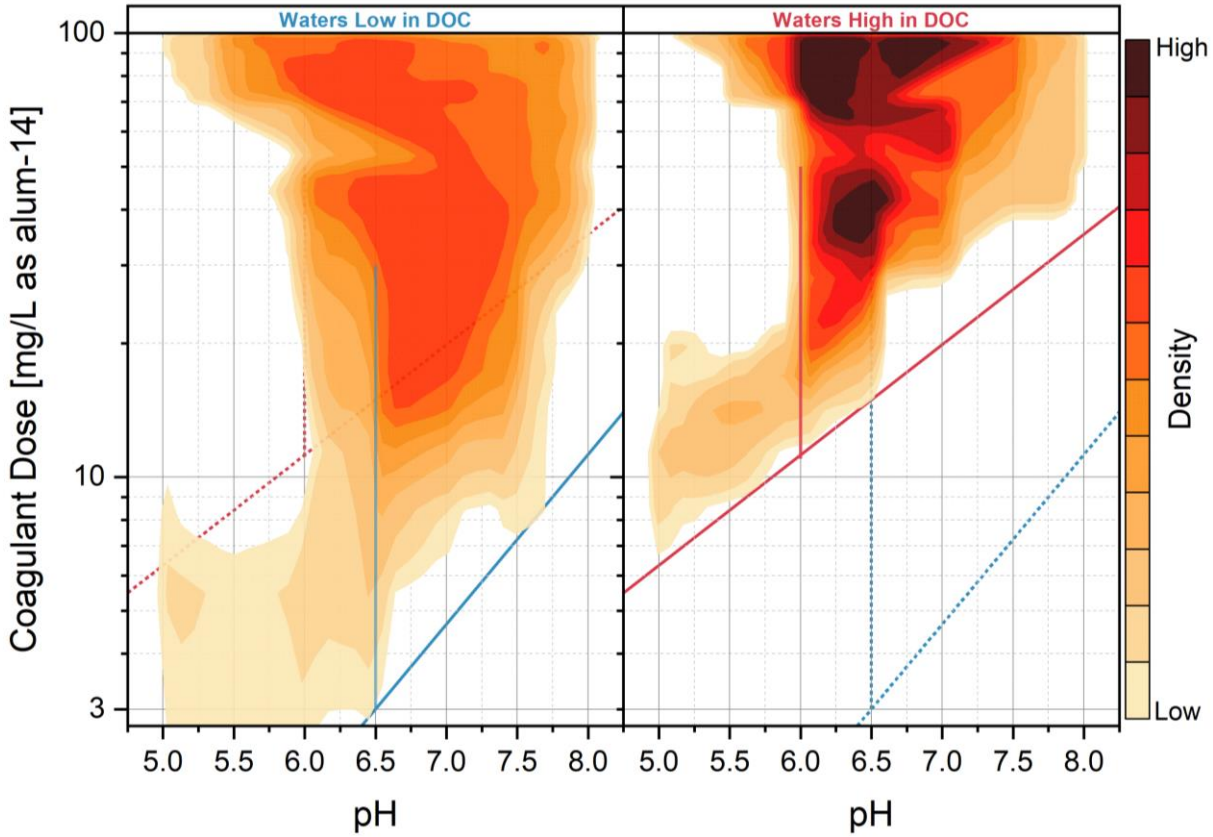

Figure 5.12. Effects of DOC on effective coagulation conditions

5.11. Interactions Between Water Quality Parameters

In the previous section, each water quality parameter was individually varied, and its main effects on the effective coagulation boundaries (≤0.3 NTU) were visualized (e.g., Figure 5.8). The interaction effects of multiple water quality parameters on coagulation conditions can be visualized by simultaneously controlling each parameter. The simplest form of an interaction is a two-way

interaction in which two out of four water quality parameters are controlled (e.g., DOC-alkalinity, SUVA-turbidity, etc.). Based on the number of water quality parameters investigated, a total of six unique combinations of any two controlled water quality parameters was possible. Each water quality parameter had two levels (low and high); therefore, considering all possible combinations of parameters and their levels results in 24 unique conditions. Three-way interactions can be thought of as two-way interactions that are varied across a third variable—for example, the effects of increasing raw water turbidity on waters low in DOC and alkalinity. There were 32 unique conditions possible that included three-way interactions. Unfortunately, there was no practical way of including and discussing all two-way and three-way interaction conditions; however, it is possible to visualize all cases using the interactive online data visualization app (Alansari 2021a).

Results from varying a single factor at a time showed that DOC and alkalinity were the only water quality parameters that had a sizeable impact on the sweep flocculation zone; therefore, the discussions here were limited to interactions involving both DOC and alkalinity. Two-way interaction effects of DOC and alkalinity were visualized using filtered turbidity removal KD plots. The groups included: (1) waters low in DOC and alkalinity, (2) water low in DOC and high in alkalinity, (3) waters high in DOC and low in alkalinity, and (4) water high in DOC and alkalinity. Each group included four waters with similar DOC and alkalinity levels (but varying SUVA and raw water turbidity). The results were plotted in a two-by-two grid where the rows represented DOC levels, and the columns represented alkalinity levels (Figure 5.13). In general, the location and size of the boundaries was found to be primarily determined by the concentration of DOC. Increasing the raw water DOC concentration shifted the boundary of effective coagulation conditions to higher doses and lower pH levels, regardless of the raw water alkalinity. A similar trend was observed when comparing interactions involving DOC/SUVA and DOC/turbidity

(Appendix E). High alkalinity generally caused the high-density boundaries to shift towards a lower pH and the low-density boundaries to extend further into the lower-left quadrant. At the same time, high alkalinity reduced the size of the high-density boundaries that were above 30 mg/L as alum-14, particularly with waters high in DOC.

Unfortunately, there was no practical method of visualizing three and four levels of interactions as this would have required 48 different plots. Readers are encouraged to refer to the online interactive data visualization app that was created to compare the raw data, i.e., all contour levels for all the conditions investigated (Alansari 2021a).

In summary, coagulation efficiency is directly dependent on water quality parameters. Edzwald and Benschoten (1990) concluded that NOM (not turbidity) controlled coagulation demand. The results showed that the "center of mass" of the effective coagulation boundaries was largely dictated by the concentration of the raw water DOC. SUVA determined the extent to which effective coagulation conditions extended into the charge neutralization zone. High alkalinity generally affected coagulation conditions in the sweep flocculation zone. Finally, turbidity generally had minimal impact on coagulation conditions at the studied levels. Some of the trends could be explained by the interactions between the water quality parameters; however, it was not possible to completely isolate all the effects of water quality parameters.

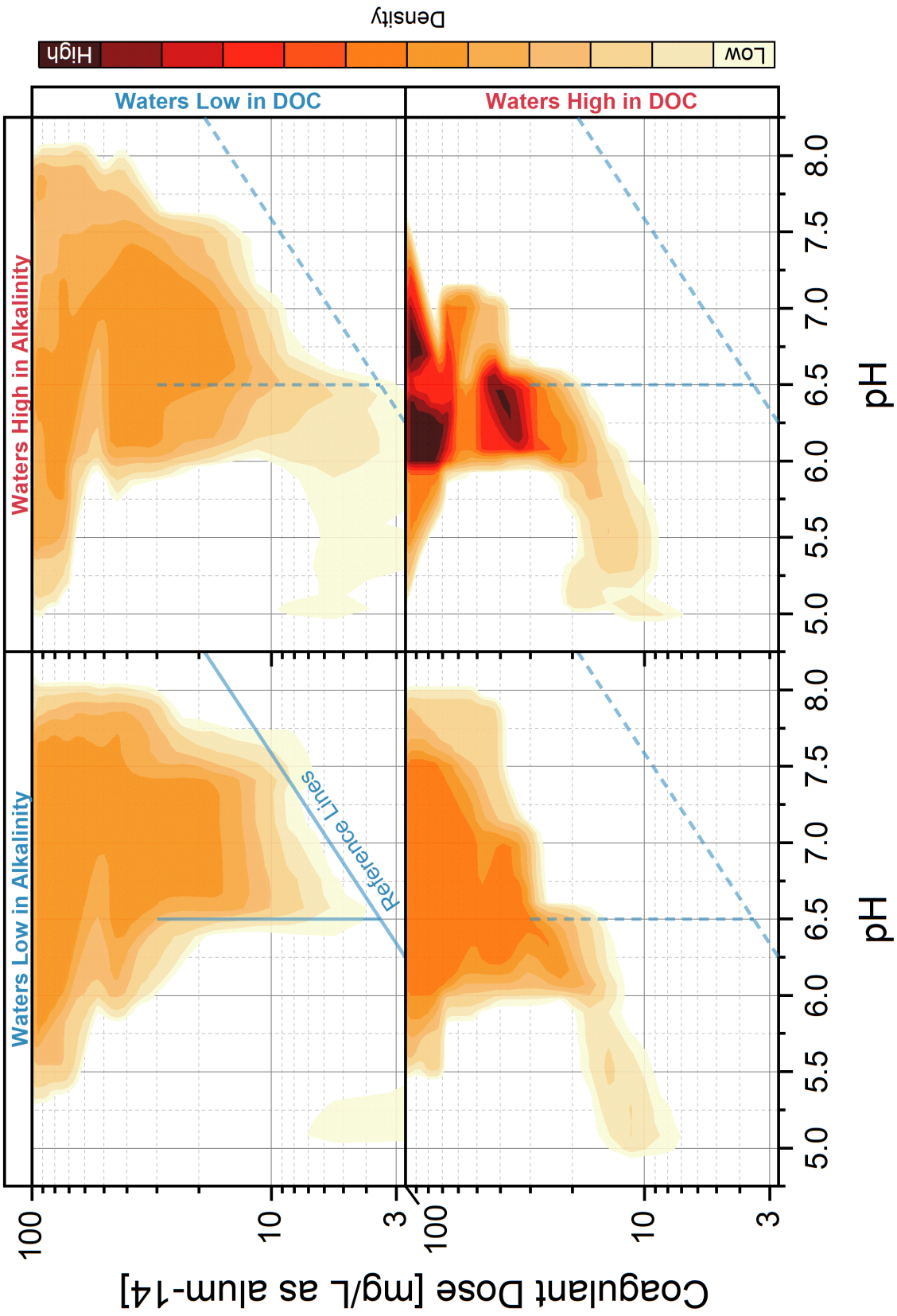

Figure 5.13. Two-way interactions of DOC and alkalinity

5.12. The Universal Coagulation Boundary

Combined jar test results (Figure 5.7) showed a significant overlap of coagulation conditions between 30 – 100 mg/L as alum-14 and pH 6.0 – 7.0. The high density of overlapping coagulation conditions suggested that water quality parameters had little impact on coagulation efficiency. Thus, this range could be regarded as a "universal" boundary for effective coagulation. It is also possible that waters with characteristics in the range of those investigated here (shown in Table 5.2) would find an effective coagulation condition in the red – maroon region. The green boundary shown in Figure 5.14 represents the high-density boundary that was extracted from the combined KD plot.

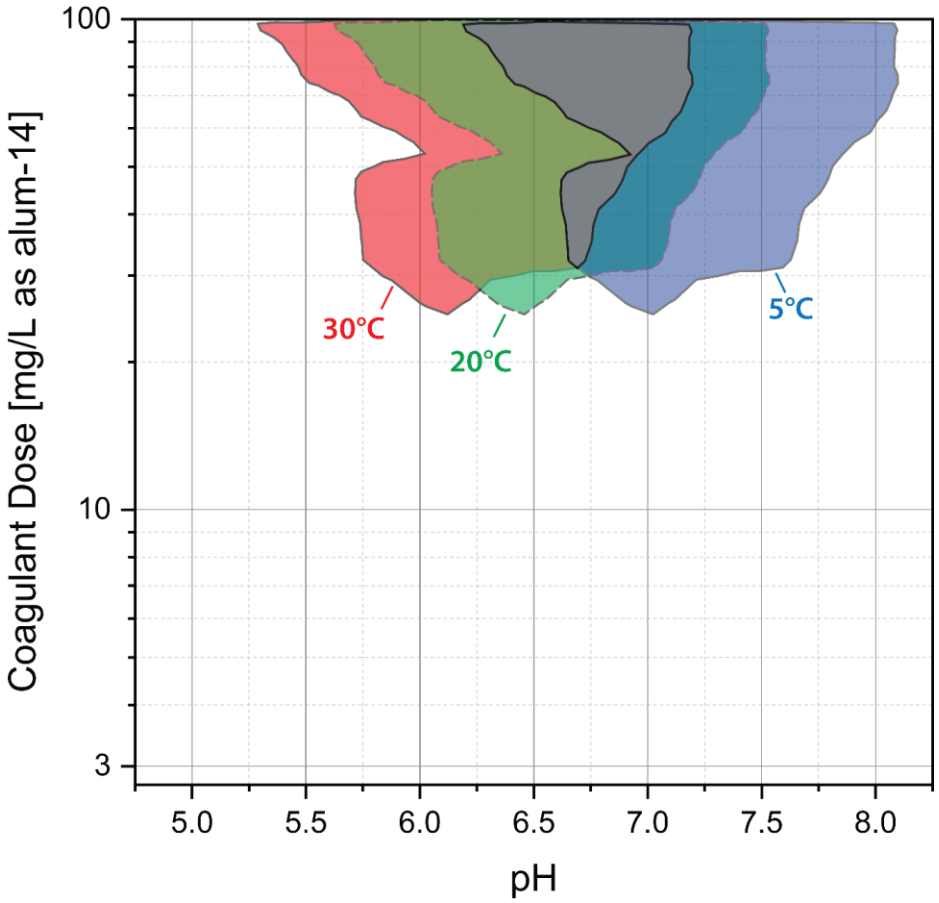

Figure 5.14. Universal coagulation boundary

Van Benschoten and Edzwald (1990a) found that the effects of temperature on the solubility of $Al(OH)_{3(s)}$ precipitate in deionized water could be accounted for by the changes in the OH^- concentration. All experiments were performed at approximately 20°C. Using the ion product of water (pK_w, Table 2.3), the pH could be adjusted to various temperatures by keeping pOH constant. For example, a water with a pH of 6.5 at 20°C has an approximate pOH of 7.7, based on a pK_w of 14.2. At 5°C, the pK_w is 14.7; therefore, the adjusted pH of the water would be 7.0 with a constant pOH. As a result, the universal boundary for effective coagulation could be temperature shifted using the approach described above. The major assumptions were that the boundaries would follow the equilibrium of the hydrolysis reactions, and the performance of the filters would not be significantly impacted by temperature. The red and blue boundaries were temperature adjusted to 30°C and 5°C, respectively. In theory, a treatment plant could operate in the gray boundary (the overlap between 30°C, 20°C, and 5°C) all year without needing to adjust their coagulation conditions, assuming their water quality parameters fall within the range of parameters investigated in this study. Hypothetically, while it could be possible to achieve good removals in the universal coagulation boundary with waters similar to those investigated here, the total chemical costs can be 10 – 20 times higher than what can be achieved with an optimized coagulation condition. The universal boundary could serve as an emergency protocol for operators to ensure effective treatment with rapidly changing water quality and deteriorating performance. The universal boundary could also serve as a starting point for operators to optimize their coagulation conditions via jar tests.

CHAPTER 6: MODELING COAGULATION

Modeling the coagulation process has historically been nearly impossible because water is a chemically complex medium that varies spatially and temporally. There are also many competing and interacting factors that influence the overall efficiency of the process. Moreover, the relationships between the process variables are complex and non-linear. The use of synthetic waters addressed some of these challenges by controlling the contents of the water and minimizing any spatial or temporal variability between experiments. Using a strategic and novel (next-generation) jar test procedure and a design of experiments approach, the main and interaction effects of water quality parameters on coagulation efficiency can be captured and visualized. The contour and KD plots provided a qualitative measure of the effects of water quality parameters on coagulation and shed some light on their interactions. A rough estimate of the response of the coagulation process to water quality changes can be made based on a qualitative analysis of the plots in the previous section. For instance, if the DOC concentration of the raw water doubled, then the minimum effective coagulant dose is expected to increase. On the other hand, a quantitative model of coagulation would theoretically allow operators and engineers to accurately predict the response of the coagulation process at their conditions and visualize operational boundaries.

6.1. Basics Modeling Approaches

Predictive models in the field of drinking water treatment are usually empirical in nature – i.e., they are based on experimental data and one's understanding of the relationships between the experimental parameters. They generally assume that a linear relationship exists between the process variables (inputs and outputs); thus, they are obtained by fitting a linear equation to the

data using an iterative process (i.e., linear regression). The basic form of a linear regression equation is shown in Equation 4:

$$y = \beta_0 + \beta_1 x_1 + \beta_2 x_2 + \cdots + \beta_n x_n \quad (4)$$

where:

y = dependent variable
β_0 = intercept
β_n = coefficient
x_n = independent variable

To account for curvature, quadratic ($\beta_n x_n^2$) and cubic ($\beta_n x_n^3$) terms can be added to the expression above. Similarly, interactions are included by computing the products of the independent variables. For example, the product of x_1 and x_2 describes the two-way interactions between the variables ($\beta_{12} x_1 x_2$).

Several studies have been published that used linear regression techniques to model coagulation (Bazer-Bachi et al. 1990; van Leeuwen et al. 1999; Trinh and Kang 2011; Zainal-Abideen et al. 2012). For example, van Leeuwen and coworkers conducted jar tests to determine the optimal alum dose using over 30 different water samples (van Leeuwen, Chow, Bursill and Drikas 1999). The authors did not control coagulation pH in their jar tests. A linear regression model was generated that calculated the alum dose from raw water turbidity, alkalinity, UV_{254}, and raw water pH. The authors reported that the model predictions were within ± 10 mg/L of the actual doses determined from jar tests. Most of the studies referenced above produced regression models with a very high coefficient of determination values (R^2>0.9). It is worth mentioning that most of the studies validated the accuracy of their model based on the same data (water) and experimental method that was used to fit the models.

To fit a model to a dataset, the values of the coefficients (β_n) in Equation 4 are adjusted such that the error between the actual and the predicted values are as small as possible. In the field of data analytics and modeling, fitting an equation to a dataset is referred to as model training, while the data being modeled is called the training data. Standard model performance metrics include the mean square error (MSE), root mean square error (RMSE), and mean absolute error (MAE). The most widely used performance metric is the RMSE (Géron 2019). RMSE measures the standard deviation of the residuals (difference between predicted and actual values) and has the same unit as the actual value – in this case, the RMSE would be "%" since filtered turbidity removal was expressed as a percentage. The true test of a model is its ability to make predictions on new data accurately. The error between the actual values of the new data and the model predictions is called the generalization error. If the generalization error was high while its training error was low, then the model is said to be overfitting the training data. Conversely, a generalized model should perform well on the training data as well as new data. Common strategies to minimize overfitting include (1) using simple models (e.g., a linear model instead of high-degree polynomials) and (2) using a validation dataset to check the performance of the model during training (Géron 2019).

Figure 6.1 shows a parallel coordinate plot of the filtered turbidity removals obtained from the extended jar test study with 16 waters (1,632 datapoints). Parallel coordinate plots are useful for visualization multivariate or high-dimensional datasets to determine the relationships between the variables. In this case, all process variables were carefully controlled (i.e., coagulation conditions, mixing parameters, and water quality parameters). Mixing parameters were not a factor since the jar test procedure employed a standardized mixing program. As a result, the jar test filtered turbidity removals were assumed to be only a function of the four water quality parameters

(i.e., DOC, SUVA, alkalinity, and turbidity) and the applied coagulation conditions (i.e., coagulant dose and coagulation pH). The purpose of Figure 6.1 was simply to highlight the complexity of coagulation process. Even when water quality and coagulation factors are controlled, it was still not possible to identify any discernable patterns in the removals. A model of the coagulation process should theoretically capture all the trends and complexities observed in Figure 6.1.

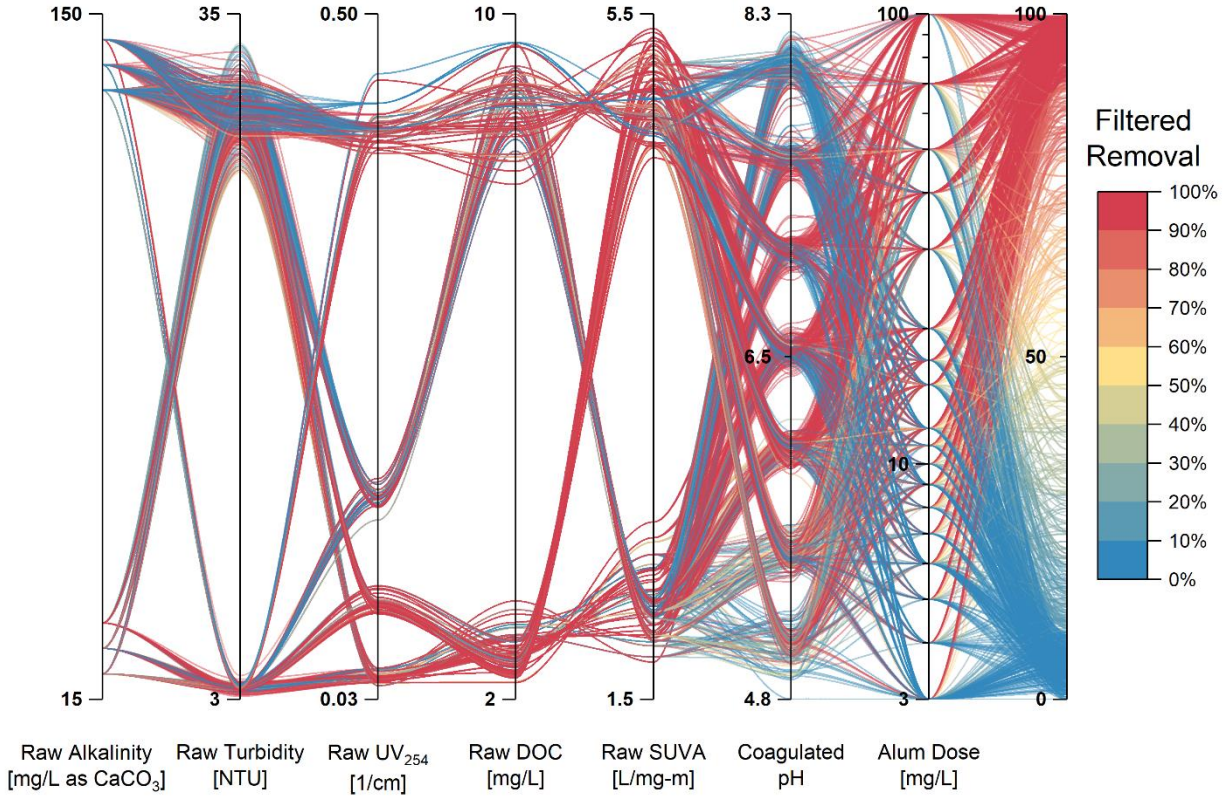

Figure 6.1. Parallel coordinate plot of all filtered turbidity removal data

6.2. Modeling Coagulation Using Basic Regression Models

Regression models were trained using *Python 3.7* and *scikit-learn 0.24.0,* an open-source library of data analytics tools and machine learning algorithms (Pedregosa et al. 2011). The jar test filtered turbidity dataset set was split into two separate sets: a training set that contained 15 waters used to train the model and a test set that contained 1 water to evaluate the model. Multiple regression models were trained, and their performance was validated using the test dataset. The performance metrics used were RMSE and R^2. Regression models included linear regression, decision trees, and gaussian process regression. Each model's hyperparameters (model training parameters) were tuned to minimize the RMSE. Descriptions of the regression models are available in the *scikit-learn 0.24.0* online documentation. Results of the regression models were summarized in Table 6.1.

Table 6.1. Summary of regression model results

Model Type	**No. of Coefficients**	**RMSE[(a)] [%]**	**$R^{2(b)}$**
Linear regression	7	37	0.43
+ 2-way interactions	22	32	0.44
+ 2nd° polynomials	27	29	0.54
+ 3rd° polynomials	77	32	0.46
+ 3-way interactions	42	33	0.41
+ 2nd° polynomials	47	30	0.51
+ 3rd° polynomials	77	32	0.46
Decision trees	-	31	0.51
Gaussian process regression	-	28	0.64

[a] Root mean square error of test dataset (lower is better).
[b] Coefficient of determination between predicted and actual values from test dataset

The performance of the investigated regression models was generally very poor. The RMSE values ranged between 28 – 37%, while the R^2 values ranged between 0.41 – 0.64 for the test dataset. Figure 6.2 shows a scatter plot of the predicted removals versus the actual jar test removals. The top panel shows the best performing linear regression (based on RMSE and R^2),

while the bottom panel shows the results obtained from the gaussian process regression model. All the predicted data points from a perfectly accurate regression model would fall on the solid diagonal line – i.e., the predicted values are all equal to the actual values. Datapoints below the diagonal line indicate that the model underestimated the removal, while datapoints above the line indicate that the model overestimated the removals.

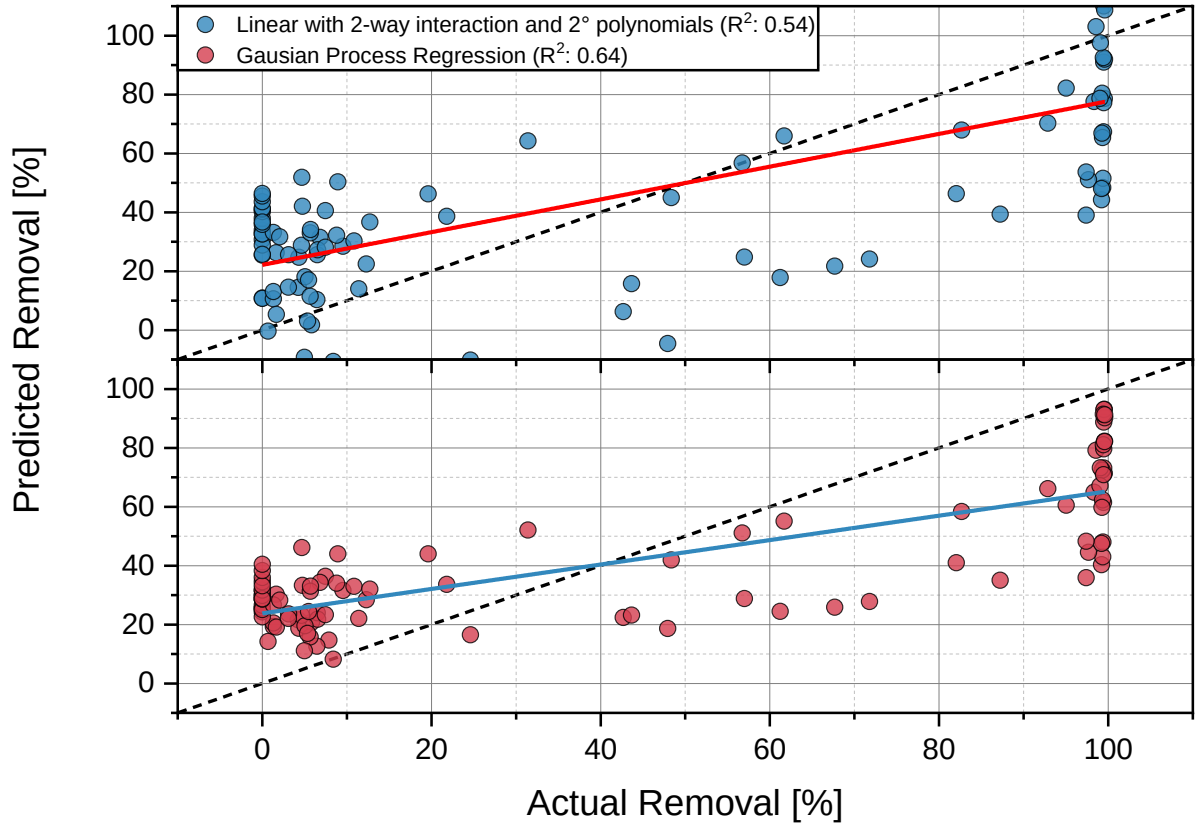

Figure 6.2. Performance of the trained regression models

Figure 6.3 compares the predicted and actual values of the test dataset using the linear regression model with two-way interactions and 2nd degree polynomials and the gaussian process regression model. The performance of the models was evaluated by comparing the actual contour plot (left panel) to the predicted contour plots of the filtered turbidity removals. It was apparent that the model performed poorly since the contour plots of the predicted results looked nothing

like the actual contour plot, even when ignoring the possibility of overfitting and using complex models such as 3-way interactions with third-degree polynomials and 77 trainable coefficients. It can be concluded that the investigated regression models were too simple to model the underlying coagulation processes; therefore, they were underfitting the training data, which resulted in significant prediction errors.

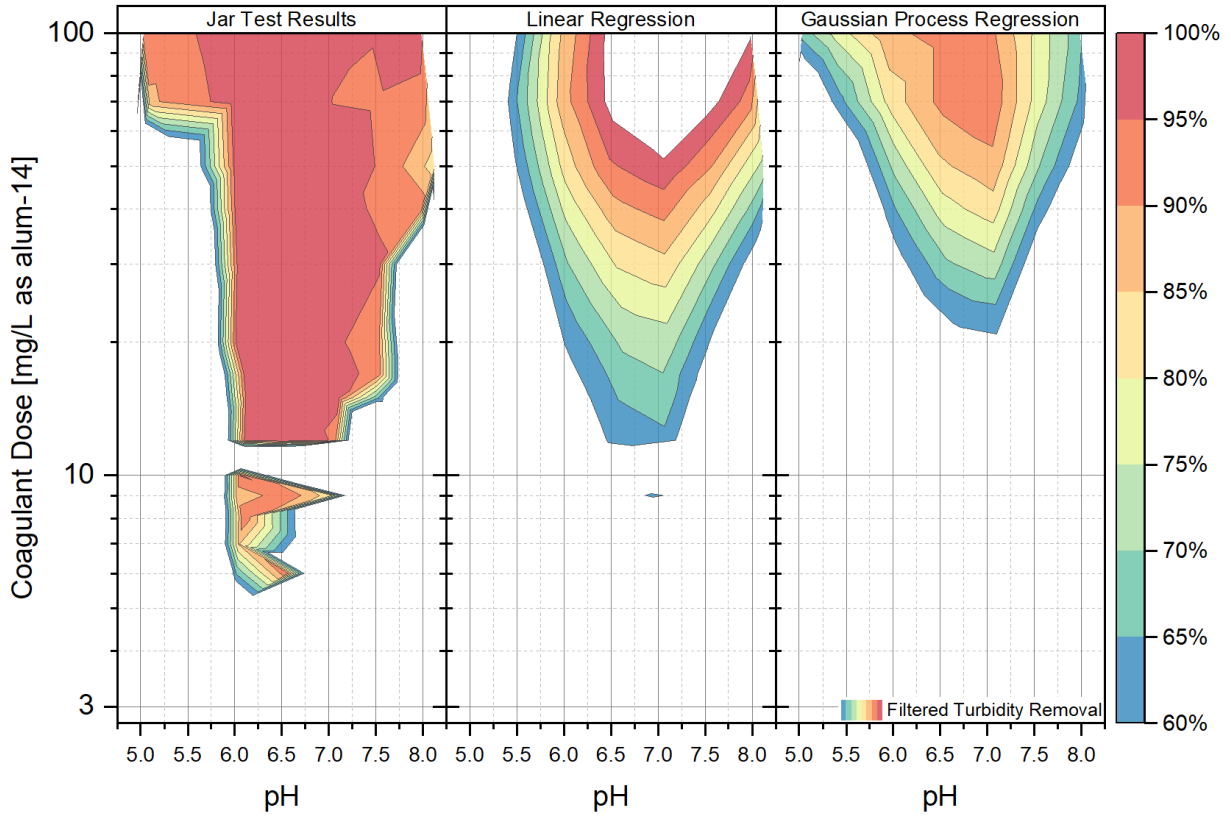

Figure 6.3. Comparison of jar test results and regression model predictions

The proper implementation of regression models requires some inferences regarding the relationships between the factors and the response variable. For example, the KD plots from the previous section showed that an increase in DOC generally increased the effective coagulant dose; however, that was only applicable to conditions where the coagulant dose was low. Similarly, the impact of increasing DOC on turbidity removals was typically worse with high alkalinity waters compared to low alkalinity waters. Although the combined effects of changing multiple water

quality parameters can be visualized, the underlying coagulation mechanisms are not well understood and not linearly related. The removal of a contaminant depends on the interactions between water quality parameters and coagulation conditions and the predominant coagulation mechanism – i.e., charge neutralization or sweep flocculation.

6.3. Artificial Neural Networks

In recent years, models based on artificial neural networks (ANNs) have gained considerable attention from the drinking water treatment research community (Li et al. 2021). ANNs fall under the machine learning subfield of artificial intelligence (AI). Mathematical and statistical models such as linear regression, support vector machines, etc., also fall under the machine learning subfield. A basic neural network is comprised of an input layer, a hidden layer, and an output layer. Each layer contains an array of interconnected units called neurons (modeled after biological neurons) that perform simple mathematical operations. An in-depth description of machine learning algorithms and neural networks can be found in the textbook written by Géron (2019). In summary, ANNs are trained to model a process by adjusting the weights and biases of the neurons iteratively to minimize the prediction error (Figure 6.4). ANNs are ideal for modeling problems where the underlying process is too complex for the traditional model and not well understood.

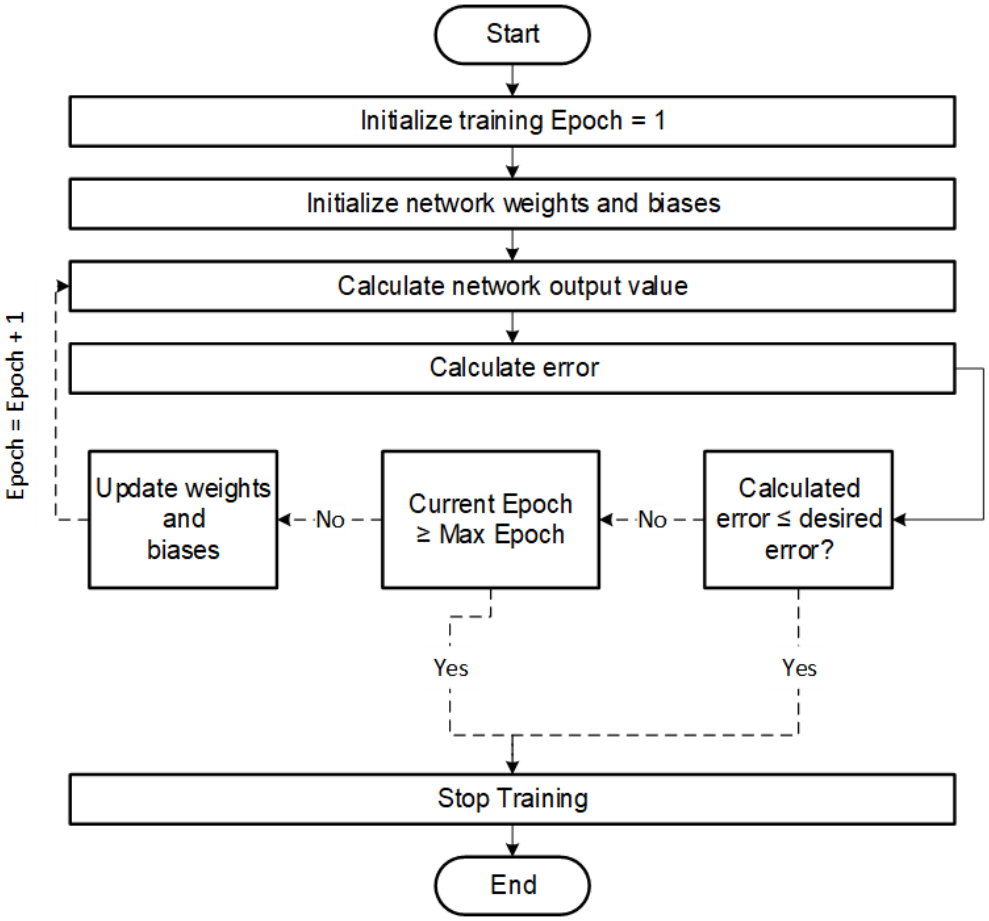

Figure 6.4. The basic process of training a neural network

Most ANN applications in drinking water treatment have been in control systems to automate the selection of an "optimal" coagulant dose at a given treatment facility (Gagnon, Grandjean and Thibault 1997; Baxter, Stanley and Zhang 1999; Fabris et al. 2013). The models are trained using a plant's historical data to make predictions on new data accordingly. Unfortunately, this approach produces site-specific models (cannot be used at a different facility). In principle, one can argue that what is being modeled is the water treatment plant staff/operators' behavior as they respond to changes in the process instead of the coagulation process itself. Historical data usually contains some variability; however, it is much harder to distinguish and

model the combined effects of the interacting coagulation factors from this type of data since multiple factors are varying simultaneously.

On the other hand, Maier, Morgan, and Chow (2004) used ANNs to model coagulation from jar test results instead of plant historical data. The authors reported that their model performed well with their test dataset; however, they could not scale their model to full-scale processes. They attributed this not to the modeling technique but rather to jar test results (which were used to develop the model) not directly scaling to the full-scale process. ANNs can model practically any complex process; however, their relevance and practical application depend on the type and quality of data that is used to train the neural network.

With the right data, models can be generated that essentially "understand" the underlying coagulation mechanisms and how each factor and its relationship to other factors impact coagulation efficiency. Furthermore, these models would not be limited to a specific location, process, water type, or output parameter.

6.4. Modeling Coagulation Using Deep Neural Networks

Modeling filtered turbidity removals using neural networks was performed using the *Keras* open-source artificial neural network library for *Python 3.7* (Chollet 2018). Figure 6.5 shows the fully connected neural network trained to predict removals based on coagulation conditions and water quality parameters. This type of ANN architecture is considered to be a deep neural network (DNN) is part of the deep learning subcategory of machine learning. DNNs have multiple layers between the input and output layers and are ideal for modeling very complex non-linear relationships. In this case, there were two hidden layers, with each layer containing 28 neurons/units. For training and evaluating the network, the dataset was split into three sets: (1) a

training dataset (14 waters), (2) a validation dataset (1 water), and (3) a testing dataset (1 water). The validation dataset was used to evaluate the model's performance during the training and tuning stages to prevent overfitting and minimize the generalization error (Géron 2019).

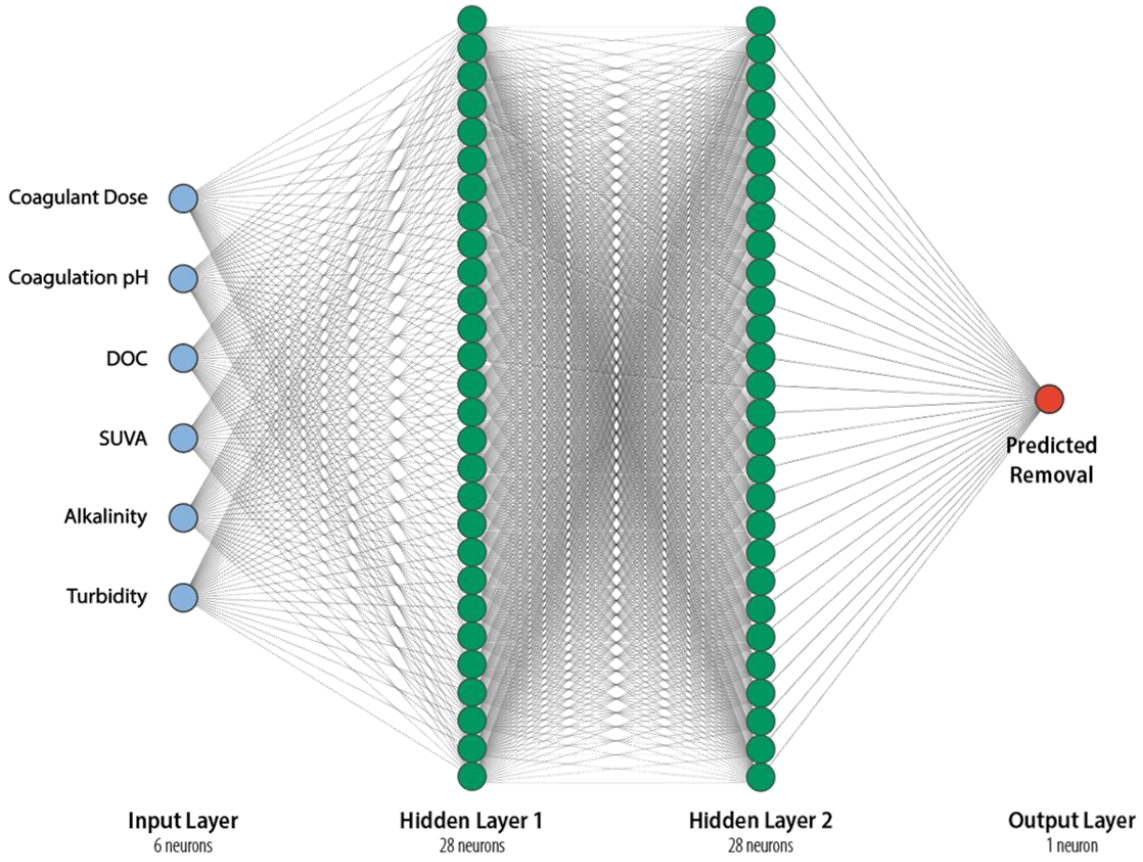

Figure 6.5. Filtered turbidity removal neural network

Figure 6.6 is a scatter plot of the removals predicted using the trained neural network versus the actual jar test results. The plot also included the predictions from the linear regression model for comparison purposes. The RMSE and R^2 values of the trained neural network (on the test dataset) were 9.6% and 0.88, respectively. The performance of the trained neutral network was substantially better than the performance of the linear model.

Figure 6.7 compares the jar test results and the trained neural network predictions. The predicted contour plot was nearly identical to the contour plot obtained from the jar test results. In

particular, the model correctly predicted the position of the vertical boundary (at pH 6.0), where coagulation rapidly transitions from being ineffective to effective. The model also correctly predicted the small boundary of effective coagulation below 10 mg/L as alum-14. The model slightly underestimated the removal in the range between pH 6.0 and 6.5 and 10 – 30 mg/L as alum-14 and slightly overestimated the removal in high pH (>7.5) and high dose region (>30 mg/L as alum-14).

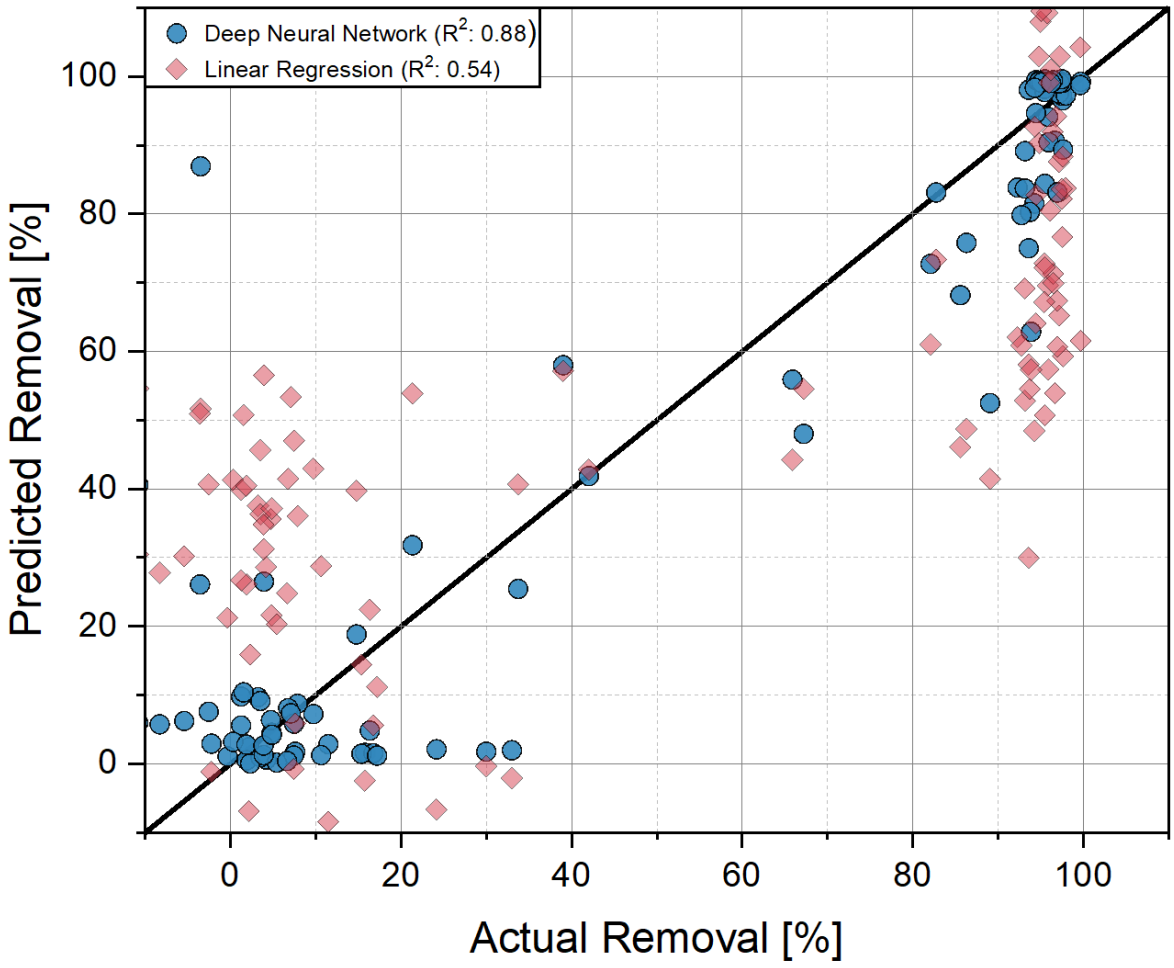

Figure 6.6 Performance of the trained deep neural network

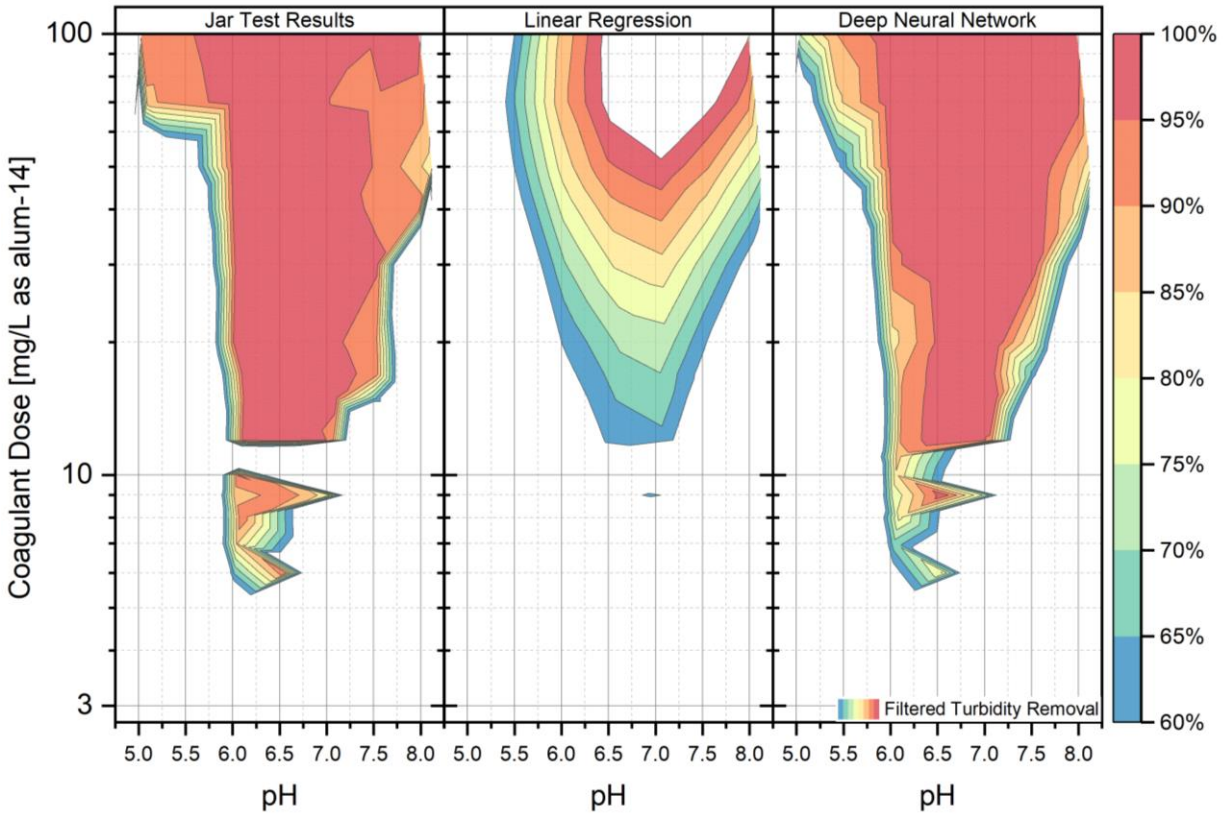

Figure 6.7. Comparison of jar test results and neural network model predictions

More importantly, the model responded to changes in raw water quality parameters in a predictable manner. Figure 6.8 shows the response of the neural network to an increase in the raw water SUVA. A qualitative analysis of the effects of increasing the SUVA on effective coagulation conditions (Figure 5.8) showed that SUVA had the effect of extending the lower boundaries further into the lower-left quadrant of the contour plot. In this case, the model produced a similar effect when the raw water SUVA was increased by a factor of 2. Similarly, jar test results showed that SUVA did not have any noticeable impact on the removal boundaries in the sweep coagulation region (high dose and pH), which the model predicted a similar response here as well. In general, the model also correctly predicted the response to changes in raw water DOC, alkalinity, and turbidity.

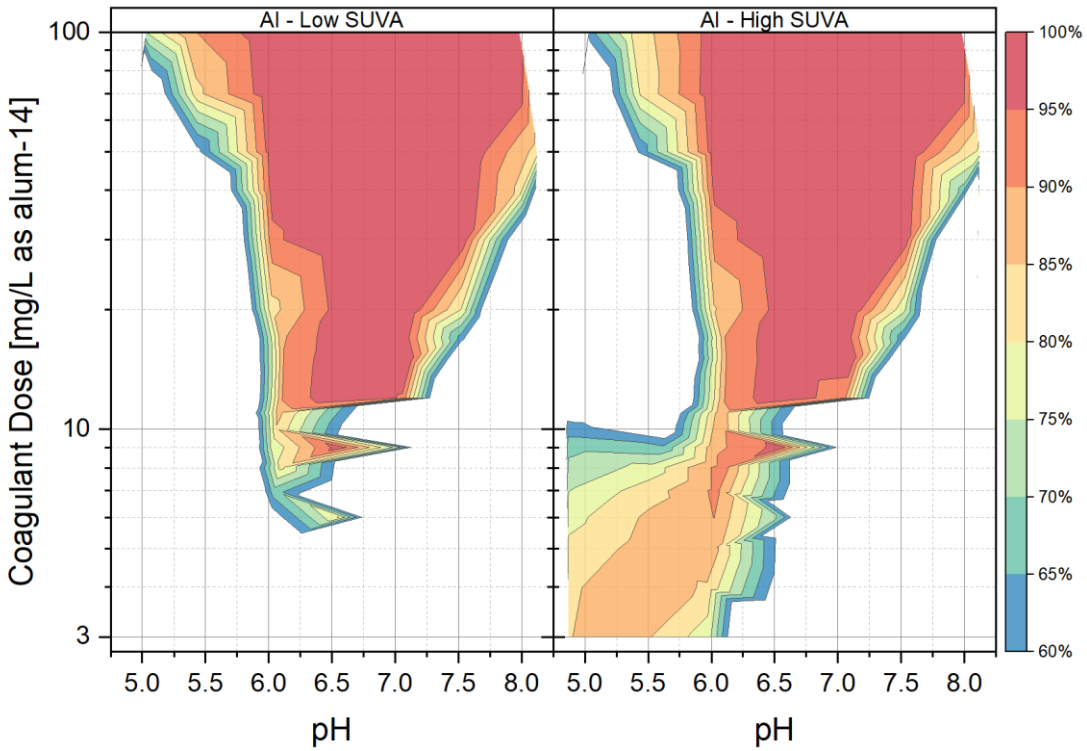

Figure 6.8. Response of the neural network to an increase in SUVA

6.5. Predicting Real-World Removals

The trained neural network's performance was evaluated by comparing the predicted and actual filtered turbidity removals at several full-scale drinking water treatment plants. Water quality data from 9 different utilities located in North Carolina (NC) were obtained using the NC Drinking Water Watch online database and the state's regulatory agency. Only treatment plants that used aluminum-based coagulants and reported UV_{254} data were considered. The complied dataset included raw and filtered water turbidity, alkalinity, TOC/DOC, UV_{254}, water temperature, coagulant dose, and pH (Table 6.2). It should be noted that this was a rudimentary evaluation of the model's performance. The assumption here was that if the model accurately predicted the filtered turbidity removal at the plant's conditions, it was probable that the predicted contour plot was also accurate. To properly evaluate the neural network's performance, 17 jar tests would have to be performed with each water to generate the contour plots.

Table 6.2. Data acquired from local drinking water treatment plants

Plant No.	Condition	Turbidity [NTU]	Alkalinity [mg/L as $CaCO_3$]	DOC [mg/L as C]	SUVA [L/mg-m]	Temp. [°C]	Dose [ppm]	pH
1	Warm	9.0	29	3.0	0.6	29	40	6.6
	Cold	14	24	4.0	3.0	11	40	6.6
2	Warm	6.5	18	1.5	0.3	26	39	6.6
	Cold	9.2	20	1.8	0.8	10	31	6.9
3	Warm	1.9	20	6.5	4	32	154	6.0
	Cold	5.5	16	6.9	4.2	17	111	6.0
4	Warm	4.4	188	8.1	4.2	25	122	7.6
	Cold	9.2	20	6.7	4.2	17	37	7.6
5	Warm	5.9	32	6.0	5	27	40	6.9
	Cold	2.1	34	6.1	4.2	17	46	6.2
6	Warm	4.0	27	6.1	5.4	28	66	6.1
	Cold	41	26	7.1	5.4	14	60	6.3
7	Warm	25	17	1.7	5.1	26	24	6.6
	Cold	32	16	2.9	4.8	13	38	6.8
8	Warm	260	6	6.8	2.2	26	39	6.6
	Cold	3.0	11	0.5	3.4	10	18	6.8
9	Warm	1.8	17	1.7	7.6	25	10	7
	Cold	1.3	13	0.5	9.6	5	10	7.3

The neural network was trained using data acquired from jar tests performed at 20±2°C; therefore, to account for temperature effects, the predictions were pH-shifted based on the assumption that the removal boundaries would shift with the solubility limit of the coagulant (Van Benschoten and Edzwald 1990b). As a result, the performance of the model was evaluated under cold weather and warm weather conditions at each utility. Water temperatures in the warm weather cases ranged from 23 – 32°C, whereas the cold weather temperatures ranged from 5 – 17°C. Additionally, data were split based on whether the neural network would have to interpolate or extrapolate to make predictions with respect to the range of the water quality parameters that were used to train the model. In general, it was assumed that the model would have to extrapolate with waters that contained more than three parameters that were considerably outside of the range of the neural network training dataset.

Table 6.3 compares the predicted and actual filtered turbidity removals at the investigated conditions. The model interpolated in 13 of the 18 total cases, whereas the model extrapolated in the remaining cases. Examples of the contour plots generated under interpolation and extrapolation conditions are shown in Appendix F. The results showed that in the cases where the model made predictions by interpolation, the error between the predicted and actual filtered turbidity removals ranged between -1.1 and 1.4%. The prediction error was higher in most cases with cold weather conditions compared to warm weather conditions. On the other hand, the prediction error was relatively high (-2.9 – 99%) in most extrapolation cases. This was expected since the waters fell entirely outside the range of parameters the model was trained on; however, one of the critical features of DNNs is that they can adapt to new data. This means that the neural network can be trained on new data as it becomes available and improve its general applicability to more waters.

Table 6.3. Summary of actual and predicted filtered turbidity removals

[1]	Water Source	Condition	Actual Removal [%]	Predicted Removal [%]	Error [%]
Interpolation	Plant 1	Warm Weather	99.4	99.6	-0.2
		Cold Weather	99.8	98.4	1.4
	Plant 2	Warm Weather	99.4	99.5	-0.1
		Cold Weather	99.7	99.2	0.5
	Plant 4	Cold Weather	98.4	99.5	-1.1
	Plant 3	Warm Weather	98.6	99	-0.4
		Cold Weather	99.6	98.9	0.7
	Plant 5	Warm Weather	99.2	99.2	0.0
		Cold Weather	94.8	94.3	0.5
	Plant 6	Warm Weather	98.3	98	0.3
		Cold Weather	99.8	99.1	0.7
	Plant 7	Warm Weather	99.9	99	0.9
		Cold Weather	99.9	98.5	1.4
Extrapolation	Plant 8	Warm Weather	99.9	0.87	99.1
		Cold Weather	96	82.7	13.9
	Plant 4	Warm Weather	96.4	99.2	-2.9
	Plant 9	Warm Weather	87.8	86.3	1.7
		Cold Weather	93.8	77.8	17.1

[1] The network interpolates when the water quality parameters fall within the trained model parameters and extrapolates when the water quality parameters fall outside the trained model parameters.

Based on these preliminary analyses, it seemed that the DNNs were capable of modeling the complex underlying process to make relatively accurate predictions – in this case, turbidity removals in a full-scale process – as long as the raw water quality parameters are within the range of the parameters used in the training set. The same DNNs can be trained to predict DOC removals in the same way they were trained to predict turbidity removals. The ultimate goal of modeling coagulation was not to replace jar tests but to eliminate the need for trial-and-error testing and reduce the probability of overfeeding the coagulant. AI models can help operators and consultants optimize coagulation conditions at water treatment facilities by allowing them to visualize their coagulation operational boundaries, identify global optimums, and make informed decisions based

on a set of desired performance criteria. This would lead to improved system performance, lower overall operating costs, and higher quality water.

CHAPTER 7: SUMMARY AND CONCLUSIONS

This research aimed to develop an accurate computer model for coagulation with aluminum sulfate with practical, real-world applications. This meant bridging the gap between coagulation theory and coagulation practice. In this study, well-established practical guidelines and theories were scrutinized, compared, and tested to guide the reader to a new level of understanding coagulation and ultimately accurately modeling it.

7.1. Standardizing the Jar Test Procedure

A jar test procedure was developed that used: (1) a standardized mixing program that did not need to be calibrated to any drinking water treatment process, (2) a single-variable optimization approach, and (3) granular media filtration instead of settling for optimizing coagulation conditions. The single-variable optimization approach was critical for studying the effects of coagulation factors on the efficiency of coagulation. Ultimately, the results showed that filtered turbidity was a superior performance metric to settled water turbidity, which is used in conventional jar testing.

- The key findings were as follows:

    1. Filtered water turbidity was only a function of the applied coagulant dose and coagulation pH and was largely unaffected by the jar test mixing parameters. However, settled water turbidity was a function of floc size and the jar test mixing parameters

2. The results of the filtered water turbidity were directly scalable from the jar test to the full-scale, while settled water turbidity results did not scale or agree with the full-scale results
3. Optimal coagulation boundaries based on filtered water turbidity were relatively broader, occurred at a significantly lower dose (by a factor of 1.1 – 2.5), and were less sensitive to minor changes in pH. Optimal coagulation boundaries based on settled water turbidity were smaller, separated, occurred at relatively higher doses, and were more sensitive to minor pH changes
4. The possibility of overfeeding the coagulant is reduced considerably by using filtered water turbidity

7.2. Creating Synthetic Waters

A new method was developed to create synthetic waters based on a target raw water dissolved organic carbon (DOC) concentration, specific ultraviolet absorbance (SUVA), turbidity, and alkalinity using relatively low-cost and readily available materials.

- The use of synthetic waters had two main advantages:

1. Water quality parameters can be tightly controlled, which permitted their exclusion as a factor when studying the effects of other factors such as coagulation conditions (i.e., dose and pH) and mixing parameters
2. Each water quality parameter could be independently controlled to quantify their individual effects on the coagulation efficiency

7.3. Advanced Coagulation Optimization

Advanced data analysis and visualization techniques were utilized to visualize and capture the main and interaction effects of multiple coagulation parameters on the efficiency of coagulation. Contour plots were used to visualize the effective coagulation boundaries as a function of the applied coagulant dose and coagulated pH. The effects of SUVA, DOC, alkalinity, and turbidity were isolated and visualized utilizing bivariate kernel density estimation and heatmaps. A multi-parameter optimization approach was developed to identify a total of 22 possible optimum coagulation conditions for a single water.

- Two search algorithms were developed that used different optimization strategies:
    1. An algorithm that minimized the total chemical cost
    2. An algorithm that prioritizes the robustness of the selected condition

7.4. Charge Neutralization Versus Sweep Flocculation

An operational distinction for charge neutralization and sweep flocculation was established. Charge neutralization conditions generally occurred below both 20 mg/L as alum-14 and pH 6.5. Results showed that a common vertical boundary existed where the coagulation mechanism rapidly transitioned between charge neutralization and sweep flocculation.

- The key findings were as follows:
    1. The pH at which the boundary occurred was primarily a function of the raw water's DOC and alkalinity. At the investigated low DOC and low alkalinity levels, the boundary occurred at pH 6.5 and shifted to pH 6.0 when either the DOC or the alkalinity levels increased.

2. A contour plot of the total available positive charge as a function of coagulant dose and pH showed that positively charged aluminum species were theoretically present in varying proportions up to pH 7.25 at 20° C.
3. The importance of producing particles or floc with a near-neutral zeta potential was found to be overstated. Turbidity removals ≤0.3 NTU were achieved in the zeta potential range of -40 to 20 mV

7.5. The Importance of Mixing

Using the standardized jar test procedure and a synthetic water to control all relevant factors, the effects of mixing parameters on the coagulation process were studied. In general, destabilization was proven to be simply a function of the applied coagulation conditions and largely independent of the applied mixing intensity and time. A minimum G-value of 20 s^{-1} was sufficient to produce filterable floc provided that there were at least 9 minutes of mixing.

- The specific findings concerning rapid mix were as follows:

1. Rapid mixing had no discernable positive impact on coagulation in jar tests or the full-scale processes studied
2. Prolonged rapid mixing (longer than 1 minute) could have a negative impact on floc size since flocculation could occur during the rapid mix stage
3. The theory that coagulation reactions were over in 7 seconds was refuted

- The specific findings concerning flocculation were as follows:

1. Flocculation time, intensity, and scheme (i.e., tapered or single-stage) did not have any discernible effect on jar test filtered turbidity removals
2. A minimum mixing time of 1 minute was required under sweep flocculation, while a minimum mixing time of 9 minutes was required for charge neutralization
3. There were no observed advantages to using a tapered flocculation scheme instead of a single-stage scheme (e.g., G-value of 20 s-1) when the jar test performance was compared based on filtered turbidity removals

7.6. The Effects of Water Quality Parameters

Consistent with prior research, the range of effective coagulation conditions was controlled by natural organic matter.

- The key findings were as follows:
    1. The raw water DOC concentration largely dictated the location, size, and shape of the effective coagulation boundaries.
    2. SUVA determined the extent to which effective coagulation conditions extended into the charge neutralization region.
    3. High alkalinity generally affected coagulation conditions in the sweep flocculation zone.
    4. Turbidity had minimal impact on coagulation conditions at the studied levels, particularly in the sweep flocculation region.
    5. A universal effective coagulation zone was identified that was generally independent of water quality parameters under the tested conditions. A universal effective alum dose of approximately 31 mg/L as alum-14 at pH 6.7 would

theoretically work with any water within the tested range of water quality parameters between the temperatures of 5 and 30°C.

7.7. Modeling coagulation

- Simple regression models are not capable of modeling all the complex underlying non-linear behaviors of the coagulation process
    1. The regression models considered ranged from linear regression models to advanced regression models based on machine learning techniques such as gaussian process regression
    2. When tested on new data (i.e., data that was not used in model training), the RMSE ranged between 28 – 37%, while the R^2 values ranged between 0.41 – 0.64.
- Deep neural networks were capable of learning the underlying patterns of the coagulation process and modeling its response to changing conditions
    1. The trained deep neural network consisted of 2 hidden layers, with each layer being made up of 28 neurons/units
    2. The RMSE and R^2 values of the trained neural network (on the test dataset) were 9.6% and 0.88, respectively
    3. The trained neural network model was able to generate a contour plot with reasonable accuracy simply based on the DOC, SUVA, alkalinity, and turbidity of the raw water
    4. The trained neural network predicted full-scale filtered turbidity removals within ±1.4% at 11 different facilities under cold and warm water conditions

7.8. Future Work and Recommendations

Deep neural networks appear to be ideal for solving many of the complex problems that have baffled engineers and scientists for over a century. The neural network in this study was trained on only 16 synthetic waters; yet, proved to be capable of predicting full-scale turbidity removals with acceptable accuracy. The model input parameters were only raw water turbidity, alkalinity, DOC, SUVA, and temperature. At this stage, the model predictions should be considered qualitative, where they could be used to identify effective coagulation boundaries and predict the response to changing water quality conditions. The current neural network could potentially eliminate the need for "trial-and-error" optimization for water treatment facilities, and jar tests would only be needed to validate the predictions.

Neural networks "learn" by example. The training data dictates their prediction accuracy and conditions under which they can be applied. There is no reason a deep neural network provided with a suitable and extensive dataset could not be trained to model coagulation with any water and any coagulant type accurately. There practically are no limitations on what a deep network could model. Modeling drinking water coagulation is no longer an impossible feat. The same neural network can be trained to predict DOC removals, type and volume of pH adjusting chemicals required, total chemical costs, disinfection by-products formation, and much more. This endeavor would require a renewed interest (and investment) in coagulation research and a collective effort from the research community, regulators, consulting engineers, and industry. The recent advancements in the field of CFD coupled with models based on AI like deep neural networks could make it possible for drinking water treatment processes to be designed and modeled computationally in the near future, much in the same way that has been done for several decades in wastewater treatment.

REFERENCES

Alansari, A. (2020a). "+3Sense." from https://www.amiralansari.com/3sense.

Alansari, A. (2020b). "Alum Equilibrium." from https://www.amiralansari.com/solubility.

Alansari, A. (2020c). "Flocculation Modeling App." 2020, from https://www.amiralansari.com/flocculation.

Alansari, A. (2020d). "Jar Test Procedure." 2020, from https://www.amiralansari.com/jartest.

Alansari, A. (2021a). "Coagulation Revisted." 2021, from http://coagulation.amiralansari.com.

Alansari, A. (2021b). "PMetrics." from https://www.amiralansari.com/pmetrics.d

Alansari, A., M. Selbes, T. Karanfil and J. Amburgey (2015). "Optimization of coagulation pretreatment conditions in a ceramic membrane system." Journal-American Water Works Association **107**(12): E693-E701.

Alansari, A., M. Selbes, T. Karanfil and J. Amburgey (2016). "Removal of Disinfection By-product Precursors Using Hybrid Coagulation–Ceramic Membrane Systems." Journal-American Water Works Association **108**(10): E513-E522.

Allerdings, D., G. Forster, E. Vasyukova and W. Uhl (2015). "The practical influence of rapid mixing on coagulation in a full-scale water treatment plant." Water Sci Technol **71**(4): 566-571.

Amirtharajah, A. and K. M. Mills (1982). "Rapid-mix design for mechanisms of alum coagulation." Journal-American Water Works Association **74**(4): 210-216.

Amirtharajah, A. and C. R. O'melia (1990). Coagulation processes: destabilization, mixing, and flocculation. Water Quality and Treatment: A Handbook of Community Water Supplies. New York, NY, McGraw-Hill**:** 1990.

Amirtharajah, A. and S. L. Trusler (1986). "Destabilization of particles by turbulent rapid mixing." Journal of Environmental Engineering **112**(6): 1085-1108.

Barr, P. (2007). "Treatment Optimization-Providing More Effective Multiple-barrier Protection." Journal - American Water Works Association **99**(12): 40-43.

Baruth, E. E. (2004). Water treatment plant design, ASCE.

Baxter, C. W., S. J. Stanley and Q. Zhang (1999). "Development of a full-scale artificial neural network model for the removal of natural organic matter by enhanced coagulation." Journal of Water Supply: Research and Technology—AQUA **48**(4): 129-136.

Bazer-Bachi, A., E. Puech-Coste, R. Ben Aim and J. Probst (1990). "Modélisation mathématique du taux de coagulant dans une station de traitement d'eau." Revue des sciences de l'eau/Journal of Water Science **3**(4): 377-397.

Benjamin, M. M. and D. F. Lawler (2013). Water quality engineering: Physical/chemical treatment processes, John Wiley & Sons.

Bernhardt, H. and H. Schell (1993). "Effects of Energy Input during Orthokinetic Aggregation on the Filterability of Generated Flocs." Water Science and Technology **27**(10): 35-65.

Black, A. and S. Hannah (1961). "Electrophoretic studies of turbidity removal by coagulation with aluminum sulfate." Journal - American Water Works Association **53**(4): 438-452.

Black, A. P., A. M. Buswell, F. A. Eidsness and A. L. Black (1957). "Review of the Jar Test." Journal (American Water Works Association) **49**(11): 1414-1424.

Black, A. P. and A. L. Smith (1962). "Determination of the Mobility of Colloidal Particles by Microelectrophoresis." Journal (American Water Works Association) **54**(8): 926-934.

Black, A. P. and M. R. Vilaret (1969). "Effect of particle size on turbidity removal." Journal AWWA **61**(4): 209-214.

Bratby, J. (2016). Coagulation and flocculation in water and wastewater treatment, IWA publishing.

Brink, D. R., S. I. Choi, M. Al-Ani and D. W. Hendricks (1988). "Bench-Scale Evaluation of Coagulants for Low Turbidity Water." Journal-American Water Works Association **80**(4): 199-165.

Brown, P. L. and C. Ekberg (2016). Hydrolysis of metal ions, John Wiley & Sons.

Budd, G. C., A. F. Hess, H. Shorney-Darby, J. J. Neemann, C. M. Spencer, J. D. Bellamy and P. H. Hargette (2004). "Coagulation applications for new treatment goals." Journal-American Water Works Association **96**(2): 102-113.

Ching, H.-W., M. Elimelech and J. G. Hering (1994). "Dynamics of coagulation of clay particles with aluminum sulfate." Journal of Environmental Engineering **120**(1): 169-189.

Chollet, F. (2018). "Keras: The python deep learning library." Astrophysics Source Code Library: ascl: 1806.1022.

Committee, A. C. (1989). "Committee report: Coagulation as an integrated water treatment process." Journal-American Water Works Association **81**(10): 72-78.

Conley, W. R. and R. H. Evers (1968). "Coagulation control." Journal-American Water Works Association **60**(2): 165-174.

Crittenden, J. C., R. R. Trussell, D. W. Hand, K. J. Howe and G. Tchobanoglous (2012a). Coagulation and Flocculation. MWH's water treatment: principles and design, John Wiley & Sons.

Crittenden, J. C., R. R. Trussell, D. W. Hand, K. J. Howe and G. Tchobanoglous (2012b). MWH's water treatment: principles and design, John Wiley & Sons.

Crozes, G., P. White and M. Marshall (1995). "Enhanced coagulation: its effect on NOM removal and chemical costs." Journal - American Water Works Association **87**(1): 78-89.

Czitrom, V. (1999). "One-Factor-at-a-Time versus Designed Experiments." The American Statistician **53**(2): 126-131.

Davis, C. C. and M. Edwards (2017). "Role of Calcium in the Coagulation of NOM with Ferric Chloride." Environmental Science & Technology **51**(20): 11652-11659.

Dempsey, B. A., H. Sheu, T. T. Ahmed and J. Mentink (1985). "Polyaluminum Chloride and Alum Coagulation of Clay-Fulvic Acid Suspensions." Journal-American Water Works Association **77**(3): 74-80.

Dentel, S. K. and K. M. Kingery (1989). "Using streaming current detectors in water treatment." Journal-American Water Works Association **81**(3): 85-94.

Dentel, S. K., J. J. Resta, P. V. Shetty and T. A. Bober (1988). "Selecting Coagulant, Filtration, and Sludge-Conditioning Aids." Journal-American Water Works Association **80**(1): 72-84.

Dentel, S. K., A. V. Thomas and K. M. Kingery (1989). "Evaluation of the streaming current detector—II. Continuous flow tests." Water Research **23**(4): 423-430.

Driscoll, C. T. and R. D. Letterman (1988). "Chemistry and Fate of Al(III) in Treated Drinking Water." Journal of Environmental Engineering **114**(1): 21-37.

Edwards, G. A. and A. Amirtharajah (1985). "Removing color caused by humic acids." Journal-American Water Works Association **77**(3): 50-57.

Edzwald, J. (1993). "Coagulation in drinking water treatment: particles, organics and coagulants." Water Science Technology **27**(11): 21-35.

Edzwald, J. and G. S. Kaminski (2009). "A practical method for water plants to select coagulant dosing." Journal of the New England Water Works Association **123**: 15-31.

Edzwald, J. K. (2013). "Coagulant mixing revisited: theory and practice." Journal of Water Supply: Research and Technology-Aqua **62**(2): 67-77.

Edzwald, J. K. (2014). "Coagulation and Mixing: History and Present Versus Sustainable Practice." Journal of the New England Water Works Association **128**(4): 301.

Edzwald, J. K. (2020). "Aluminum in Drinking Water: Occurrence, Effects, and Control." Journal-American Water Works Association **112**(5): 34-41.

Edzwald, J. K., W. C. Becker and K. L. Wattier (1985). "Surrogate parameters for monitoring organic matter and THM precursors." Journal-American Water Works Association **77**(4): 122-132.

Edzwald, J. K. and J. E. Tobiason (1999). "Enhanced coagulation: US requirements and a broader view." Water Science and Technology **40**(9): 63-70.

Edzwald, J. K. and J. E. Van Benschoten (1990). Aluminum coagulation of natural organic matter. Chemical water and wastewater treatment, Springer**:** 341-359.

Fabris, R., C. Chow, R. Dexter, J. Colton, J. Knoblauch and M. Drikas (2013). "Feed-forward coagulant control using online UV/Vis monitoring." Water Science and Technology: Water Supply **13**(2): 420-426.

Fox, K. R. and D. A. Lytle (1996). "Milwaukee's crypto outbreak: investigation and recommendations." Journal - American Water Works Association **88**(9): 87-94.

Gagnon, C., B. P. A. Grandjean and J. Thibault (1997). "Modelling of coagulant dosage in a water treatment plant." Artificial Intelligence in Engineering **11**(4): 401-404.

Géron, A. (2019). Hands-on machine learning with Scikit-Learn, Keras, and TensorFlow: Concepts, tools, and techniques to build intelligent systems, O'Reilly Media.

GLUMRB (2018). Recommended Standards for Water Works. St. Paul, MN, Minnesota's Bookstore Communications Media Division.

Graham, B. W. (1939). "Factors in Coagulation." Journal - American Water Works Association **31**(1): 67-73.

Gregory, D. and K. Carlson (2003). "Relationship of pH and floc formation kinetics to granular media filtration performance." Environmental science technology **37**(7): 1398-1403.

Gregory, J. (2005). Particles in water: properties and processes, CRC Press.

Gregory, J. (2009). "Monitoring particle aggregation processes." Adv Colloid Interface Sci **147-148**: 109-123.

Griffith, J. D. and R. G. Williams (1972). "Application of Jar-Test Analysis at Phoenix, Ariz." Journal of American Water Works Association: 825-830.

Haarhoff, J. and J. L. Cleasby (1988). "Comparing Aluminum and Iron Coagulants for In-line Filtration of Cold Water." Journal-American Water Works Association **80**(4): 168-175.

Han, M. and D. F. Lawler (1992). "The (relative) insignificance of G in flocculation." Journal-American Water Works Association **84**(10): 79-91.

Hannah, S., J. Cohen and G. Robeck (1967). "Control Techniques for Coagulation-Filtration." Journal - American Water Works Association **59**(9): 1149-1163.

Hayden, P. L. and A. J. Rubin (1973). Studies on the Hydrolysis and Precipitation of Aluminum (III), Ohio State University. Water Resources Center.

Hendricks, D. (2016). Fundamentals of water treatment unit processes: physical, chemical, and biological, Crc Press.

Herman, L. D. (1984). "Coagulation Program Selection." Opflow **10**(3): 6-7.

Hudson, H. E. and E. G. Wagner (1981). "Conduct and uses of jar tests." Journal - American Water Works Association **73**(4): 218-223.

Hudson Jr, H. (1975). "Residence times in pretreatment." Journal-American Water Works Association **67**(1): 45-52.

Ives, K. (1979). A NEW CONCEPT OF FILTERABILITY.

Jarvis, P., B. Jefferson and S. A. Parsons (2005). "How the natural organic matter to coagulant ratio impacts on floc structural properties." Environmental science technology **39**(22): 8919-8924.

Jarvis, P., B. Jefferson and S. A. Parsons (2006). "Floc structural characteristics using conventional coagulation for a high doc, low alkalinity surface water source." Water Res **40**(14): 2727-2737.

Jenny, R. M., O. D. Simmons, M. Shatalov and J. J. Ducoste (2014). "Modeling a continuous flow ultraviolet Light Emitting Diode reactor using computational fluid dynamics." Chemical Engineering Science **116**: 524-535.

Jiao, R., R. Fabris, C. W. K. Chow, M. Drikas, J. van Leeuwen, D. Wang and Z. Xu (2017). "Influence of coagulation mechanisms and floc formation on filterability." J Environ Sci (China) **57**: 338-345.

Jiao, R., H. Xu, W. Xu, X. Yang and D. Wang (2015). "Influence of coagulation mechanisms on the residual aluminum--the roles of coagulant species and MW of organic matter." J Hazard Mater **290**: 16-25.

Johnson, P. N. and A. Amirtharajah (1983). "Ferric chloride and alum as single and dual coagulants." Journal-American Water Works Association **75**(5): 232-239.

Jones, S. E. and J. T. Lennon (2015). "A test of the subsidy–stability hypothesis: the effects of terrestrial carbon in aquatic ecosystems." Ecology **96**(6): 1550-1560.

Kan, C., C. Huang and J. R. Pan (2002). "Time requirement for rapid-mixing in coagulation." Colloids Surfaces A: Physicochemical Engineering Aspects **203**(1-3): 1-9.

Kawamura, S. (1973). "Coagulation considerations." Journal-American Water Works Association: 417-423.

Kawamura, S. (1975). "Design and Operation of High-Rate Filters-Part 1." Journal (American Water Works Association) **67**(10): 535-544.

King, C. (2017). The Utilization of Granular Media Filtration and Rapid Flocculation in a Modified Jar Test Procedure for Drinking Water Treatment. J. Amburgey, J. Bowen and O. Keen, ProQuest Dissertations Publishing.

Knocke, W. R., S. West and R. C. Hoehn (1986). "Effects of Low Temperature on the Removal of Trihalomethane Precursors by Coagulation." Journal - American Water Works Association **78**(4): 189-195.

Langelier, W. F. (1921). "Coagulation of water with alum by prolonged agitation." Engineering news record **86**(22): 924-928.

Langelier, W. F. (1982). "Teaching, Research, and Consultation in Water Purification and Sewage Treatment, University of California at Berkeley, 1916-1955" an oral history conducted 1970 by Malca Chal. M. Chall. Berkeley, University of California.

Langelier, W. F. and H. F. Ludwig (1949). "Mechanism of flocculation in the clarification of turbid waters." Journal - American Water Works Association **41**(2): 163-181.

Lawler, D. F. (1993). "Physical aspects of flocculation: from microscale to macroscale." Water Science and Technology **27**(10): 165-180.

LeChevallier, M. W. and W. D. Norton (1992). "Examining Relationships Between Particle Counts and Giardia, Cryptosporidium, and Turbidity." Journal (American Water Works Association) **84**(12): 54-60.

Lennon, J. T., S. K. Hamilton, M. E. Muscarella, A. S. Grandy, K. Wickings and S. E. Jones (2013). "A source of terrestrial organic carbon to investigate the browning of aquatic ecosystems." PLoS One **8**(10): e75771.

Letterman, R. D. and C. T. Driscoll (1988). "Survey of Residual Aluminum in Filtered Water." Journal - American Water Works Association **80**(4): 154-158.

Letterman, R. D., J. Quon and R. S. Gemmell (1973). "Influence of rapid-mix parameters on flocculation." Journal-American Water Works Association **65**(11): 716-722.

Letterman, R. D., M. Tabatabaie and R. S. Ames Jr (1979). "The effect of the bicarbonate ion concentration on flocculation with aluminum sulfate." Journal-American Water Works Association **71**(8): 467-472.

Letterman, R. D., S. Vanderbrook and P. Sricharoenchaikit (1982). "Electrophoretic mobility measurements in coagulation with aluminum salts." Journal-American Water Works Association **74**(1): 44-51.

Li, L., S. Rong, R. Wang and S. Yu (2021). "Recent advances in artificial intelligence and machine learning for nonlinear relationship analysis and process control in drinking water treatment: A review." Chemical Engineering Journal **405**: 126673.

Li, T., Z. Zhu, D. Wang, C. Yao and H. Tang (2006). "Characterization of floc size, strength and structure under various coagulation mechanisms." Powder Technology **168**(2): 104-110.

Logsdon, G., A. Hess, M. Chipps and A. Rachwal (2002). Filter maintenance and operations guidance manual, American Water Works Association Research Foundation.

Mahmoud, H. (2012). Disinfection of Low UV Transmittance Fluids: Fundamentals and Applications. Doctor of Philosophy, The University of Western Ontario.

Maier, H. (2004). "Use of artificial neural networks for predicting optimal alum doses and treated water quality parameters." Environmental Modelling & Software **19**(5): 485-494.

Malinaro, A., J. Rhoades, W. Pennock and F. Gutierrez (2019). "Take a Mixed Approach to Mixing." Journal - American Water Works Association **111**(5): 72-74.

Matsui, Y., A. Yuasa, Y. Furuya and T. Kamei (1998). "Dynamic analysis of coagulation with alum and PACl." Journal-American Water Works Association **90**(10): 96-106.

McCurdy, K., K. Carlson and D. Gregory (2004). "Floc morphology and cyclic shearing recovery: comparison of alum and polyaluminum chloride coagulants." Water Res **38**(2): 486-494.

Milne, C. J., D. G. Kinniburgh, W. H. van Riemsdijk and E. Tipping (2003). "Generic NICA-Donnan model parameters for metal-ion binding by humic substances." Environ Sci Technol **37**(5): 958-971.

Montgomery, D. C. (2017). Design and analysis of experiments. Hoboken, NJ, John Wiley & Sons, Inc.

Morris, J. K. and W. R. Knocke (1984). "Temperature Effects on the Use of Metal-Ion Coagulants for Water Treatment." Journal-American Water Works Association **76**(3): 74-79.

Nordstrom, D. K. and H. M. May (1996). "Aqueous equilibrium data for mononuclear aluminum species." The environmental chemistry of aluminum **2**: 39-80.

Pedregosa, F., G. Varoquaux, A. Gramfort, V. Michel, B. Thirion, O. Grisel, M. Blondel, P. Prettenhofer, R. Weiss and V. Dubourg (2011). "Scikit-learn: Machine learning in Python." the Journal of machine Learning research **12**: 2825-2830.

Pernitsky, D. J., R. E. Cantwell, E. Murphy, N. Paradis, J. Boutilier and G. Bache (2011). "Use Zeta Potential to Improve Direct Filtration Operation." Opflow **37**(2): 20-23.

Polaczyk, A. L. (2010). Micro- to macroscale modeling of drinking water treatment and distribution. 3439271 Ph.D., The University of North Carolina at Charlotte.

Polaczyk, A. L., J. E. Amburgey, A. Alansari, J. C. Poler, M. Propato, V. R. J. C. Hill, S. A. Physicochemical and E. Aspects (2020). "Calculation and uncertainty of zeta potentials of microorganisms in a 1: 1 electrolyte with a conductivity similar to surface water." **586**: 124097.

Randtke, S. J. (1988). "Organic Contaminant Removal by Coagulation and Related Process Combinations." **80**(5): 40-56.

Reckhow, D. A. and P. C. Singer (1984). "The Removal of Organic Halide Precursors by Preozonation and Alum Coagulation." Journal - American Water Works Association **76**(4): 151-157.

Riddick, T. M. (1961). "Zeta potential and its application to difficult waters." Journal - American Water Works Association **53**(8): 1007-1030.

Robidoux, M., P. del Giorgio and A. Derry (2015). "Effects of humic stress on the zooplankton from clear and DOC-rich lakes." Freshwater Biology **60**(7): 1263-1278.

Rossini, M., J. G. Garrido and M. Galluzzo (1999). "Optimization of the coagulation–flocculation treatment: influence of rapid mix parameters." Water Research **33**(8): 1817-1826.

Semmens, M. J. and A. Staples (1986). "The nature of organics removed during treatment of Mississippi River water." Journal-American Water Works Association **78**(2): 76-81.

Shin, J. Y., R. F. Spinette and C. R. O'Melia (2008). "Stoichiometry of coagulation revisited." Environ Sci Technol **42**(7): 2582-2589.

Sillanpää, M., A. Matilainen and T. Lahtinen (2015). Chapter 2 - Characterization of NOM. Natural Organic Matter in Water. M. Sillanpää, Butterworth-Heinemann**:** 17-53.

Singer, P. C., J. J. B. III, G. M. Palen and A. E. Scrivner (1981). "Trihalomethane formation in North Carolina drinking waters." Journal AWWA **73**(8): 392-401.

Singley, J. (1981). Coagulation Control Using Jar Tests. Proc. 1981 AWWA Ann. Conf., St. Louis.

Skaf, D. W., V. L. Punzi, J. T. Rolle and K. A. Kleinberg (2020). "Removal of micron-sized microplastic particles from simulated drinking water via alum coagulation." Chemical Engineering Journal **386**: 123807.

Smith, O. M. (1920). "The Removal of Clay and Silica from Water." Journal - American Water Works Association **7**(3): 302-314.

Spicer, P. T., S. E. Pratsinis, J. Raper, R. Amal, G. Bushell and G. Meesters (1998). "Effect of shear schedule on particle size, density, and structure during flocculation in stirred tanks." Powder Technology **97**(1): 26-34.

Stumm, W. and C. R. O'Melia (1968). "Stoichiometry of coagulation." Journal-American Water Works Association **60**(5): 514-539.

Teefy, S. (1996). Tracer studies in water treatment facilities: a protocol and case studies, American Water Works Association.

Teefy, S., J. Farmerie and E. Pyles (2011). Operational control of coagulation and filtration processes. AWWA manual ; M37. Denver, American Water Works Association.

TeKippe, R. J. and R. K. Ham (1970). "Coagulation testing: a comparison of techniques—Part 1." Journal-American Water Works Association **62**(9): 594-602.

Thurman, E. M. (1985). Organic geochemistry of natural waters. Dordrecht ; Boston

Hingham, MA, USA, M. Nijhoff ;

Distributors for the U.S. and Canada, Kluwer Academic.

Trinh, T. K. and L. S. Kang (2011). "Response surface methodological approach to optimize the coagulation–flocculation process in drinking water treatment." Chemical Engineering Research and Design **89**(7): 1126-1135.

Tseng, T., B. D. Segal and M. Edwards (2000). "Increasing alkalinity to reduce turbidity." Journal-American Water Works Association **92**(6): 44-54.

USEPA (1998). "Stage 1 Disinfectants and Disinfection Byproducts Rule. Final Rule." Fed. Reg. **63**(241): 69389.

USEPA (2002). "National primary drinking water regulations: Long Term 1 Enhanced Surface Water Treatment Rule. Final rule." Fed Regist **67**(9): 1811-1844.

Vadasarukkai, Y. S. and G. A. Gagnon (2015). "Application of low-mixing energy input for the coagulation process." Water Res **84**: 333-341.

Vadasarukkai, Y. S. and G. A. Gagnon (2017). "Influence of the Mixing Energy Consumption Affecting Coagulation and Floc Aggregation." Environ Sci Technol **51**(6): 3480-3489.

Van Benschoten, J. E. (1988). Speciation and fate of aluminum in water treatment, ProQuest Dissertations Publishing.

Van Benschoten, J. E. and J. K. Edzwald (1990a). "Chemical aspects of coagulation using aluminum salts—I. Hydrolytic reactions of alum and polyaluminum chloride." Water Research **24**(12): 1519-1526.

Van Benschoten, J. E. and J. K. Edzwald (1990b). "Chemical aspects of coagulation using aluminum salts—II. Coagulation of fulvic acid using alum and polyaluminum chloride." Water Research **24**(12): 1527-1535.

van Leeuwen, J., C. W. K. Chow, D. Bursill and M. Drikas (1999). "Empirical mathematical models and artificial neural networks for the determination of alum doses for treatment of southern Australian surface waters." Journal of Water Supply: Research and Technology—AQUA **48**(3): 115-127.

Vik, E. A., D. A. Carlson, A. S. Eikum and E. T. Gjessing (1985). "Removing aquatic humus from Norwegian lakes." Journal-American Water Works Association **77**(3): 58-66.

Wagner, E. G. and H. E. Hudson (1982). "Low-dosage high-rate direct filtration." Journal - American Water Works Association **74**(5): 256-261.

White, M. C., J. D. Thompson, G. W. Harrington and P. C. Singer (1997). "Evaluating criteria for enhanced coagulation compliance." Journal-American Water Works Association **89**(5): 64-77.

Yonkin, M. C., C. A. Cotton, W. D. Simcoe and L. Sealey (2005). Validation of the city of Albany, New York's UV facility the devil is in the details. 2005 Water Quality Technology Conference, WQTC 2005, November 6, 2005 - November 10, 2005, Quebec City, QC, Canada, American Water Works Association.

Yu, W.-z., J. Gregory, L. Campos and G. Li (2011). "The role of mixing conditions on floc growth, breakage and re-growth." Chemical Engineering Journal **171**(2): 425-430.

Zainal-Abideen, M., A. Aris, F. Yusof, Z. Abdul-Majid, A. Selamat and S. I. Omar (2012). "Optimizing the coagulation process in a drinking water treatment plant -- comparison between traditional and statistical experimental design jar tests." Water Sci Technol **65**(3): 496-503.

APPENDIX A: NEXT-GENERATION JAR TEST PROCEDURE

The jar test apparatus used during experimentation was a six-jar programmable jar tester (Phipps & Bird, Richmond, VA, model PB-900™). All experiments were performed at room temperature (20°C ±1.5°C). The standard mixing program consisted of a rapid mix stage followed by three-stage tapered flocculation. The jar tester was programmed to execute the following mixing program: rapid mix at 300 rpm (~600 s^{-1}) for 1 minute; stage 1 flocculation at 70 rpm (~70 s^{-1}) for 5 minutes; stage 2 flocculation at 50 rpm (~46 s^{-1}) for 5 minutes; and stage 3 flocculation at 30 rpm (~24 s^{-1}) for 10 minutes.

Each jar was filled with 2.2 L of raw water using a graduated cylinder. A volume of 10 mL was wasted from each jar at the start of the experiment to flush out any potential remnant particles from the sample lines. Jar tests always began with a titration stage in which the volumes of the pH adjusting chemicals (0.1N HCl or 0.1N NaOH) required to hold the pH constant at a given coagulant dose were determined. Titrations were performed on a 200 mL sample collected from each jar using a graduated cylinder. During the titration stage, the jars were continuously mixed at 100 rpm to prevent the particles from settling. A pH meter (Accumet® AR15, Thermo Fisher Scientific, Waltham, Mass.) equipped with a glass-body electrode (Accumet® 13-620-223A, Thermo Fisher Scientific, Waltham, Mass.) was used for pH measurements. The electrode was standardized daily with pH 4.0, 7.0, and 10.0 buffer solutions. The following steps outline the titration process:

1. Measure and record the pH of the raw water
2. Add the corresponding volume of coagulant and record the pH
3. Incrementally add acid/base until the target pH is achieved
4. Record the volume of pH adjusting chemical used

Stock solutions of aluminum sulfate (alum) were prepared by dissolving aluminum sulfate octadecahydrate powder (≥98% aluminum sulfate, Sigma-Aldrich Co. LLC, St. Louis, Mo.) in DI water. The target concentration of the stock alum solution was 10 g/L (811 mg/L as Al). After completing the titration stage, the combined volume of the coagulant and pH adjusting chemical was wasted from their corresponding jars to ensure that the final volume of water in all the jars remained constant. The pH adjusting chemical determined from the titration step was added immediately before starting the mixing program (jar test). The pH of the water after adding the acid/base was measured to record the pH before coagulation. The coagulant was simultaneously dosed into the jars at the start of the rapid mix stage using syringes mounted above the jars. The pH after coagulation was measured by collecting a 200 mL sample from each jar at the end of the rapid mix stage. In general, a difference of ±0.2 from the target pH was considered acceptable in this study. Coagulated water zeta potential samples were collected at the end of the rapid mix stage and analyzed immediately. It should be noted that zeta potential sample run times were generally between 3 – 5 minutes; therefore, the last sample was processed approximately 20 minutes after collection.

Settled water turbidity samples were collected after a 20-minute settling period at the end of the mixing program. Approximately 10 mL of water was wasted from each jar to flush out any remnant particles from the sample lines before collecting settled water turbidity samples. Filtration was performed using a novel filtration apparatus designed and built by the authors. The filter stand consisted of six identical filters constructed using clear 2" diameter schedule 40 PVC pipe (Figure C1). Each filter was filled with 3-inches of crushed recycled glass (VitroClean VF25, Trivitro Corp., Seattle, WA) filter media. The effective size (ES), uniformity coefficient (UC), and porosity of the filter media were 0.45 mm, 1.45, and 0.48, respectively.

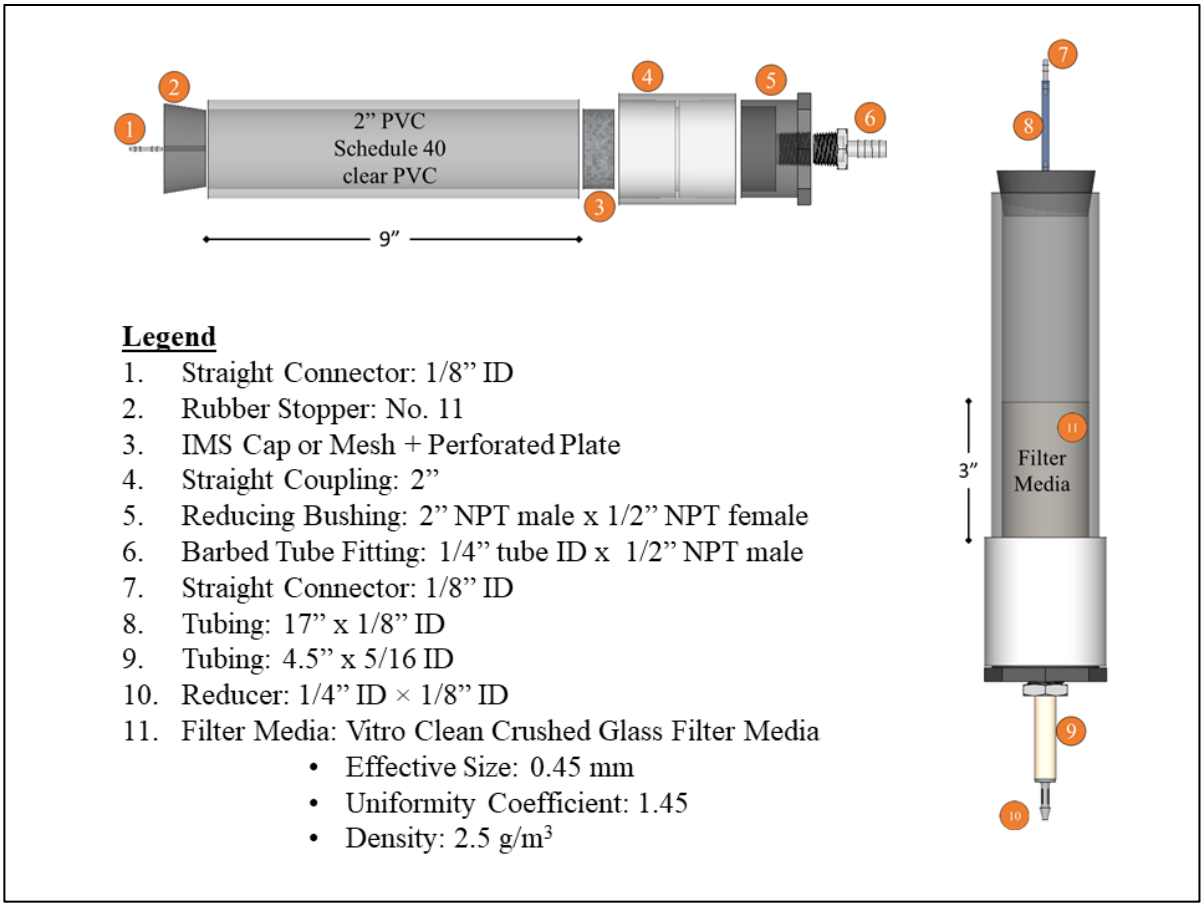

Figure C1. Filter column

The total volume of water in each filter column was approximately 250 mL. Prior to each jar test, each column was backwashed (40 – 50% bed expansion) for approximately 1 minute and filled with DI water. Care was taken to ensure that the filter column and lines were filled entirely with water as preliminary experiments showed that air bubbles negatively impacted the hydraulics and could potentially break-up the floc during filtration. The water filtered by gravity at a rate of approximately 4.5 – 5 gpm/ft^2. Detailed construction plans for the filter columns and the filter stand can be found online (Alansari 2020d). Filtered turbidity, UV_{254}, and DOC samples were collected 2 minutes after the start of filtration to account for the dead volume in the filter (Figure C2). UV_{254} and DOC samples were processed and analyzed immediately. The final pH of the water

and temperature were measured and recorded at the end of the experiment to determine whether the measured parameters drifted over the course of the experiment.

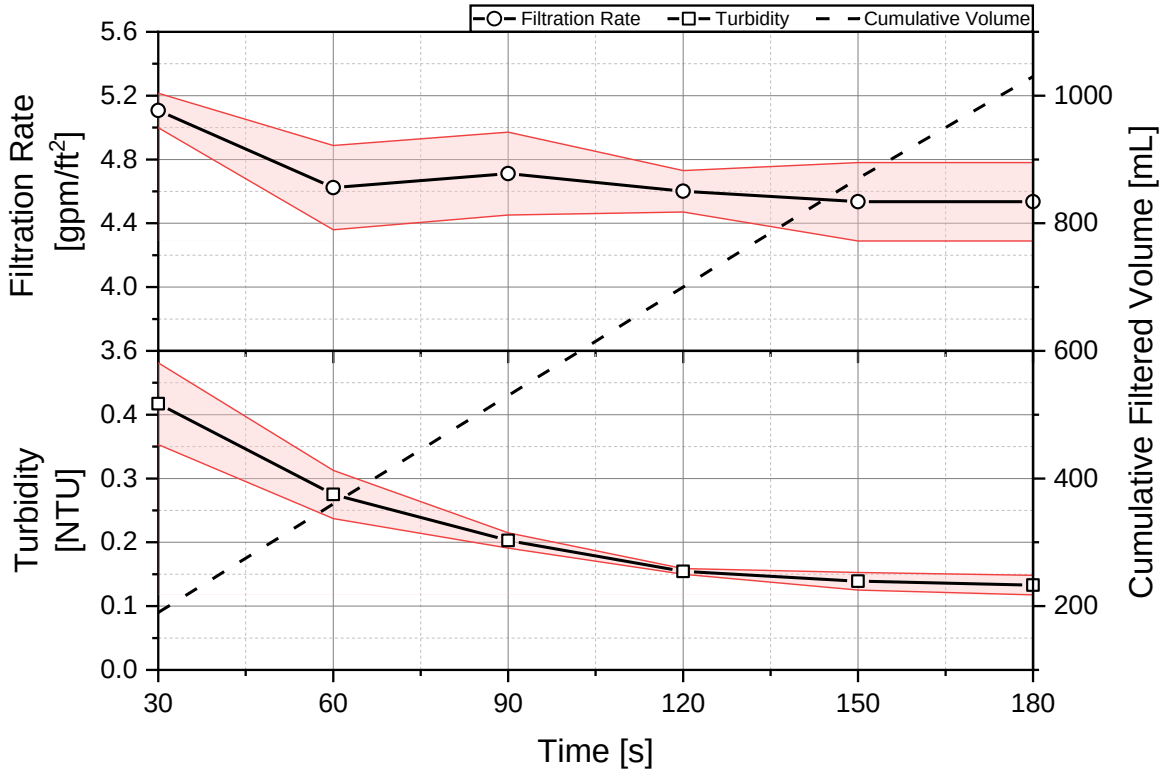

Figure C2. Average (n=12) filtration rate and filtered water turbidity of the filter columns (Note = red bands represent the standard deviation about the mean)

APPENDIX B: CREATING SYNTHETIC WATERS

Synthetic waters are created by combining deionized (DI) water and surrogates for natural turbidity, alkalinity, dissolved organic carbon (DOC), and specific ultraviolet absorbance at 254nm (SUVA). Organics were added by combining varying proportions of instant coffee and SuperHume® to achieve desired DOC and SUVA levels. SuperHume® (Eco Lawn and Garden SuperHume®, Burnsville, MN) is a commercial liquid soil additive that contains 17% humic acid, 13% fulvic acid, and 4% humics obtained from Leonardite shale. The use of instant coffee and SuperHume® as surrogates for organics has been reported previously in the literature (Yonkin et al. 2005; Mahmoud 2012; Lennon et al. 2013; Jenny et al. 2014; Jones and Lennon 2015; Robidoux, del Giorgio and Derry 2015).

Solutions of instant coffee were freshly prepared for each synthetic water batch by dissolving instant coffee (Maxwell House, Kraft-Heinze) in ultrapure water to achieve a final concentration of 8 g/L. The SuperHume® had to be filtered through a coffee filter followed by an 8-μm and a 3-μm poly-carbonate membrane (TSTP02500, MilliporeSigma, Burlington, MA) to remove large clumps of sediment and improve its consistency. Stock solutions of SuperHume® were prepared by diluting the filtrate using ultrapure water to achieve a final concentration of 2% SuperHume® by volume. Instant coffee and SuperHume® have a SUVA of approximately 1.8 and 9.0 L/mg-m, respectively. Standard curves and empirical equations were developed for the instant coffee and SuperHume® solutions to determine the volumes needed for a desired DOC concentration and SUVA (Figure B1). By varying the proportions of each surrogate solution, the SUVA of the synthetic water can be adjusted to any valve in the range of 1.8 and 9.0 L/mg-m (Figure B2).

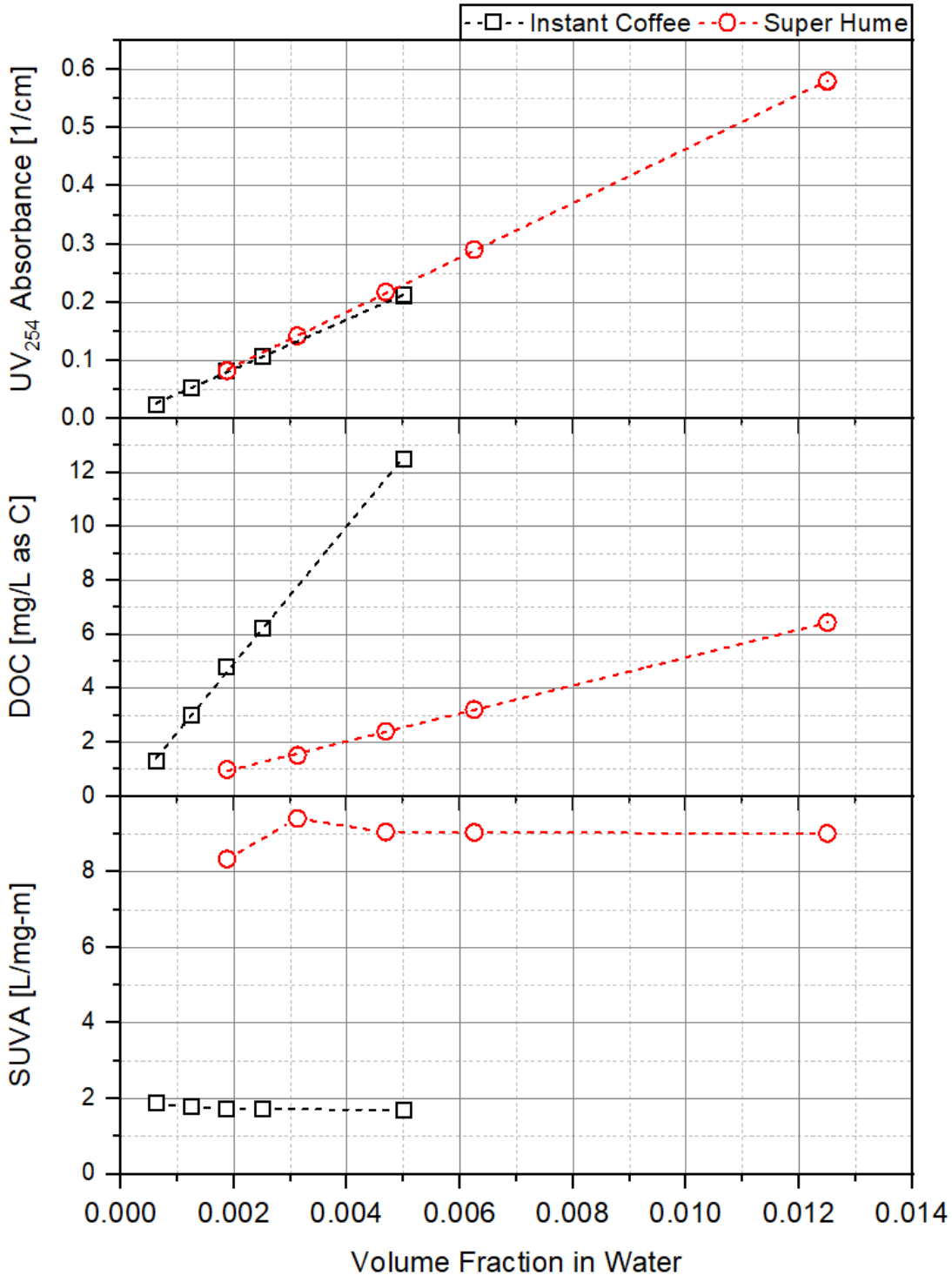

Figure B1. Properties of organic surrogates

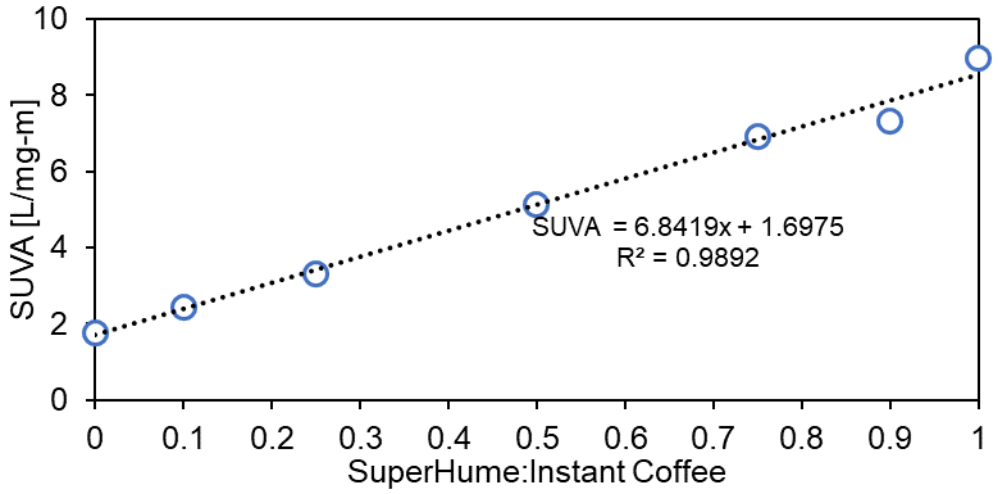

Figure B2. Surrogate organics SUVA measurements

The procedure for calculating the volumes of SuperHume® and instant coffee that would be required to achieve a target DOC and SUVA given a batch volume is outlined below:

Steps for Calculating the Volumes of SuperHume® and Instant coffee

Calculating volume of SuperHume® required

$$SH\ [mL] = 2.43x10^{-4} * BV * (DOC * SUVA - 2.2DOC + 2.13) \quad \text{(B.1)}$$

where: SH = volume of 2% SuperHume® required (mL)
BV = volume of batch (mL)
DOC = desired DOC concentration of final solution (mg/L as C)
SUVA = desired SUVA of final solution (L/mg-m)

Calculating volume of instant coffee required

$$MH\ [mL] = -5.51x10^{-5} * BV * (DOC \cdot SUVA - 8.8 * DOC - 1.9255) \quad \text{(B.2)}$$

where: MH = volume of instant coffee solution (8 g/L) required (mL)

Example Calculation

Batch Volume = 27 [L]; Desired DOC = 5 [mg/L]; Desired SUVA = 2.0 [L/mg-m]

Step1: Required volume of 2% SuperHume® (equation C.1)

$$SH = -2.43x10^{-4}\ x\ 27{,}000\ [mL]\ x \left(\left(5\left[\frac{mg}{L}\right] x2 \left[\frac{L}{mg \cdot m}\right]\right) - \left(2.2 * 5\left[\frac{mg}{L}\right]\right) + 2.13\right)$$

$$SH = 7.41\ [mL]$$

Step 2: Required volume of 8g/L solution of instant Coffee (equation C.2)

$$MH = -5.51x10^{-5}x27{,}000\ [mL]x \left(\left(5\left[\frac{mg}{L}\right] x2 \left[\frac{L}{mg \cdot m}\right]\right) - \left(8.8x5\left[\frac{mg}{L}\right]\right) - 1.9255\right)$$

$$MH = 53.5\ [ml]$$

Required volumes of SuperHume® and instant coffee are 7.41 [mL] and 53.5 [mL], respectively.

The source of natural turbidity or particles in the synthetic water was primarily from kaolin (K7375, MilliporeSigma, St. Louis, Mo). Both instant coffee and SuperHume® contributed to some turbidity as well; therefore, the amount of kaolin required depended on the amount of organics added to the synthetic water. Stock suspensions of kaolin were prepared using DI water to achieve a final concentration of 5 g/L. The procedure for calculating the required volume of kaolin is outlined below:

Steps for Calculating the Volume of Kaolin

1) **Calculate concentrations of instant coffee and SuperHume® added**

$$Instant\ Coffee\ \left[\frac{mg}{L}\right] = \frac{volume\ added\ [mL] * Stock\ concentration\ \left[\frac{mg}{L}\right]}{Batch\ Volume\ [mL]} \quad \text{(B.3)}$$

$$SuperHume^{®}[\%] = \frac{volume\ added\ [mL] * Stock\ concentration\ \left[\frac{mg}{L}\right]}{Batch\ Volume\ [mL]} \quad \text{(B.4)}$$

2) **Calculate turbidity from organics**

$$Organics\ Turb.[NTU] = 0.024 * Instant\ Coffee\ \left[\frac{mg}{L}\right] + 66.54 * SuperHume^{®}[\%] + 0.19573 \quad \text{(B.5)}$$

3) **Calculate turbidity from kaolin**

$$Kaolin\ Turb.[NTU] = Desired\ Turb\ [NTU] - Organics\ Turb\ [NTU] \quad \text{(B.6)}$$

4) **Required concentration of kaolin**

$$Kaolin\ \left[\frac{mg}{L}\right] = -0.0056 * Kaolin\ Turb^2 + 0.857 * Kaolin\ Turb + 0.0114 \quad \text{(B.7)}$$

5) **Required volume of kaolin in jar**

$$Kaolin\ [mL] = \frac{kaolin\left[\frac{mg}{L}\right] * Jar\ Volume\ [mL]}{stock\ concentration\ \left[\frac{mg}{L}\right]} \quad \text{(B.8)}$$

Example Calculation

Batch Volume = 27 [L]; Desired Turbidity = 3 [NTU]; Volume of SH added = 7.41 [mL]; Volume of instant coffee added = 53.5 [mL]; Jar Volume = 2.2 [L]

Step 1: Calculate concentrations of instant coffee and SuperHume® added (equation C.3)

$$Instant\ Coffee\ \left[\frac{mg}{L}\right] = \frac{53.5\ [mL]\ x\ 8{,}000\ \left[\frac{mg}{L}\right]}{27{,}000\ [mL]} = 15.85\ \left[\frac{mg}{L}\right]$$

$$SuperHume^{®} = \frac{7.41\ [mL]\ x\ 2[\%]}{27{,}000\ [ml]} = 5.489\ x\ 10^{-4}\ [\%]$$

Step 2: Calculate turbidity from organics (equation C.4)

$$Organics\ Turb\ [NTU] = \left(0.024x15.85\left[\frac{mg}{L}\right]\right) + (66.54x5.489x10^{-4}[\%]) + 0.19573 = 0.6126\ [NTU]$$

Step 3: Calculate turbidity from kaolin (equation B.3)

$$Kaolin\ Turb\ [NTU] = 3\ [NTU] - 0.6126\ [NTU] = 2.387\ [NTU]$$

Step 4: Calculate required concentration of kaolin (equation B.4)

$$Kaolin\ \left[\frac{mg}{L}\right] = (-0.0056x2.387[NTU]^2) + (0.857x2.387[NTU]) + 0.0114 = 2.025\ \left[\frac{mg}{L}\right]$$

Step 5: Required volume of kaolin in each jar (equation B.5)

$$Kaolin\ [mL] = \frac{2.025\left[\frac{mg}{L}\right]x\ 2{,}200\ [mL]}{5{,}000\left[\frac{mg}{L}\right]} = 0.891\ [mL]$$

Required volume of 5g/L solution of kaolin in each jar = 0.891 [mL]

Stock solution of sodium bicarbonate (15 g/L in DI water) were used to add alkalinity to the synthetic water (S233-3, Thermo Fisher Scientific, Waltham, Mass.). It should be noted that the empirical equations obtained from the standard curves have an accuracy of ±20%, primarily due to the variability in the stock solutions. A correction factor had to applied to the equations for every new batch of stock solution to account for this variability. Fresh batches of water were prepared on the day of each experiment in a 7-gallon high-density polyethylene (HDPE) container. The water was then allowed to equilibrate for at least 3 hours before experimentation. All ingredients, except for kaolin, were added directly to the container and mixed thoroughly. Kaolin was added directly to each jar to minimize turbidity variations between the jars.

APPENDIX C: FLOC CHARACTERIZATION EXPERIMENT

Water was continuously cycled through the photometric dispersion analyzer at a rate of 30 mL/min via peristaltic pump (Masterflex, Cole Parmer, Vernon Hills, IL) placed downstream of the instrument (Figure D1). An overhead mixer (Power Control-Visc IKA Eurostar, Staufen, Germany) equipped with a 2" (51 mm) diameter propeller (Lightnin A100, SPX Flow, Charlotte, NC) mixed the water in a 2 L jar (B-KER^2, Phipps and Bird, Richmond, VA). The impeller was placed at a depth of 10 cm (measured from the bottom of the jar).

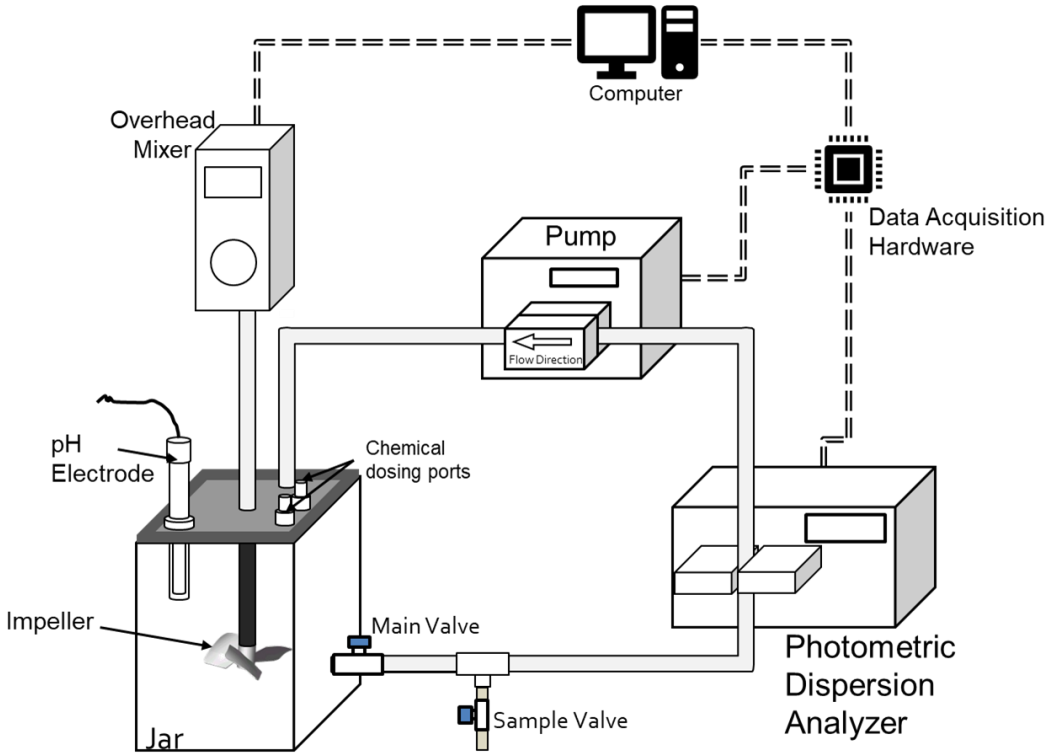

Figure D1. Photometric dispersion analyzer setup

Due to the normal fluctuations (noise) of the flocculation index signal, a minimum/maximum cannot merely be based on absolute values; therefore, *OriginPro*'s built-in *Rise Time* tool was used to extract the maximum FI and formation times objectively. The algorithm

used a histogram method to identify the low and high states of the signal, followed by a linear search to calculate the time intervals at which the $t_{10\%}$ and $t_{90\%}$ values occurred. A screenshot of the application of this tool is shown in Figure D2. Settled and filtered water turbidity were collected and measured at the end of the mixing program.

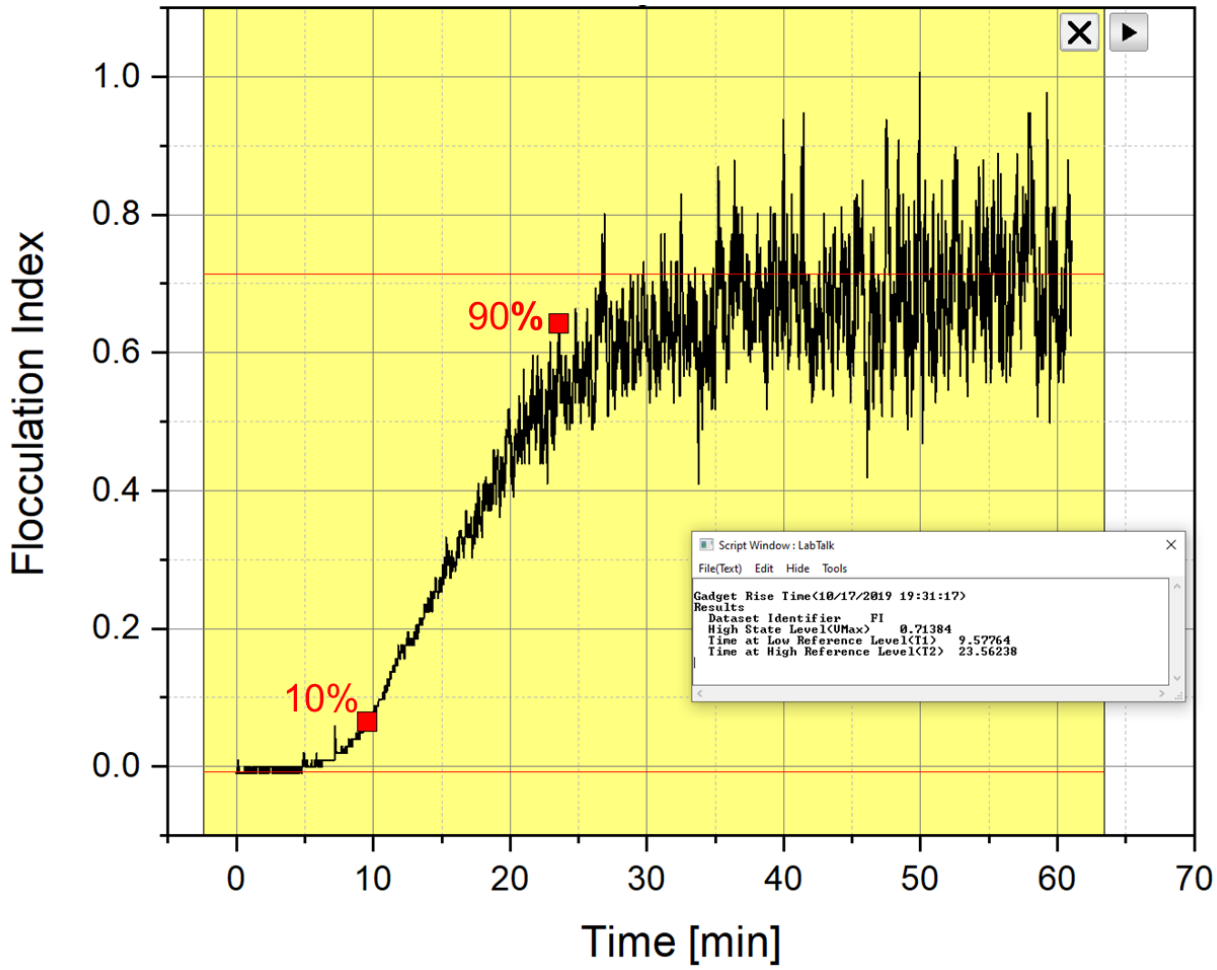

Figure D2. OriginPro 2019 Rise Time Tool

APPENDIX D: CHEMICAL COST CALCULATIONS

Table F1. Average treatment chemical costs in the US

Chemical	Grade	$/dry ton
Aluminum Sulfate	48.5%	$ 319
Sodium Hydroxide	50%	$ 500
Sulfuric Acid	93%	$ 160

Scaling up alum costs

$$Cost\ \left[\frac{\$}{Mgal}\right] = Alum\ Dose\left[\frac{mg}{L}\right]\ x\ 3{,}785{,}000\ \left[\frac{L}{Mgal}\right]\ x\ Cost\ \left[\frac{\$}{dry\ ton}\right] x\ 1.1023\ x10^{-9}\left[\frac{dry\ ton}{mg}\right]$$

Scaling up sulfuric acid costs

$$Acid\ Cost\ \left[\frac{\$}{Mgal}\right] = \left(\begin{array}{c}\left(\frac{Vol.\ of\ acid\ added\ [L]\ x\ Stock\ conc.\ [M]}{Jar\ Volume\ [L]}\right) x\ \left(\frac{n\ of\ acid}{n\ of\ H_2SO_4}\right) \\ x\ MW_{H_2SO_4}\ \left[\frac{g}{mol}\right] x\ 1000\ \left[\frac{mg}{g}\right]\ x\ 3{,}785{,}000\ \left[\frac{L}{Mgal}\right]\ x\ Cost\ \left[\frac{\$}{dry\ ton}\right] x\ 1.1023\ x10^{-9}\left[\frac{dry\ ton}{mg}\right]\end{array}\right)$$

Scaling up sodium hydroxide costs

$$Base\ Cost\ \left[\frac{\$}{Mgal}\right] = \left(\begin{array}{c}\left(\frac{Vol.\ of\ base\ added\ [L]\ x\ Stock\ conc.\ [M]}{Jar\ Volume\ [L]}\right) x\ \left(\frac{n\ of\ base}{n\ of\ H_2SO_4}\right) x\ MW_{NaOH}\ \left[\frac{g}{mol}\right] \\ x\ 1000\ \left[\frac{mg}{g}\right]\ x\ 3{,}785{,}000\ \left[\frac{L}{Mgal}\right]\ x\ Cost\ \left[\frac{\$}{dry\ ton}\right] x\ 1.1023\ x10^{-9}\left[\frac{dry\ ton}{mg}\right]\end{array}\right)$$

Example Calculation

Alum dose = 10 mg/L; HCl volume = 5.4 mL; HCl concentration = 0.1 M

Step 1: Calculate cost of alum

$$Alum\ Cost\ = 10\left[\frac{mg}{L}\right]\ x\ 3{,}785{,}00\ \left[\frac{L}{Mga}\right]\ x\ 319\ \left[\frac{\$}{dry\ ton}\right]\ x\ 1.1023\ x\ 10^{-9}\left[\frac{dry\ ton}{mg}\right] = 13.3\ \left[\frac{\$}{Mgal}\right]$$

Step 2: Calculate cost of sulfuric acid

$$Acid\ Cost$$
$$= \left(\frac{0.054\ [L]\ x\ 0.1\ [M]}{2\ [L]}\right)\ x\ \left(\frac{1}{2}\right)\ x\ 98\left[\frac{g}{mol}\right]\ x\ 1000\left[\frac{mg}{g}\right]\ x\ 3{,}785{,}00\ \left[\frac{L}{Mga}\right]\ x\ 319\ \left[\frac{\$}{dry\ ton}\right]\ x\ 1.1023\ x\ 10^{-9}$$
$$= 8.83\ \left[\frac{\$}{Mgal}\right]$$

Step 3: Total Cost

$$Total\ Cost\ = 13.3\ \left[\frac{\$}{Mgal}\right] + 8.83\ \left[\frac{\$}{Mgal}\right] = 22.1\ \left[\frac{\$}{Mgal}\right]$$

APPENDIX E: TWO-WAY INTERACTIONS OF WATER QUALITY PARAMETERS

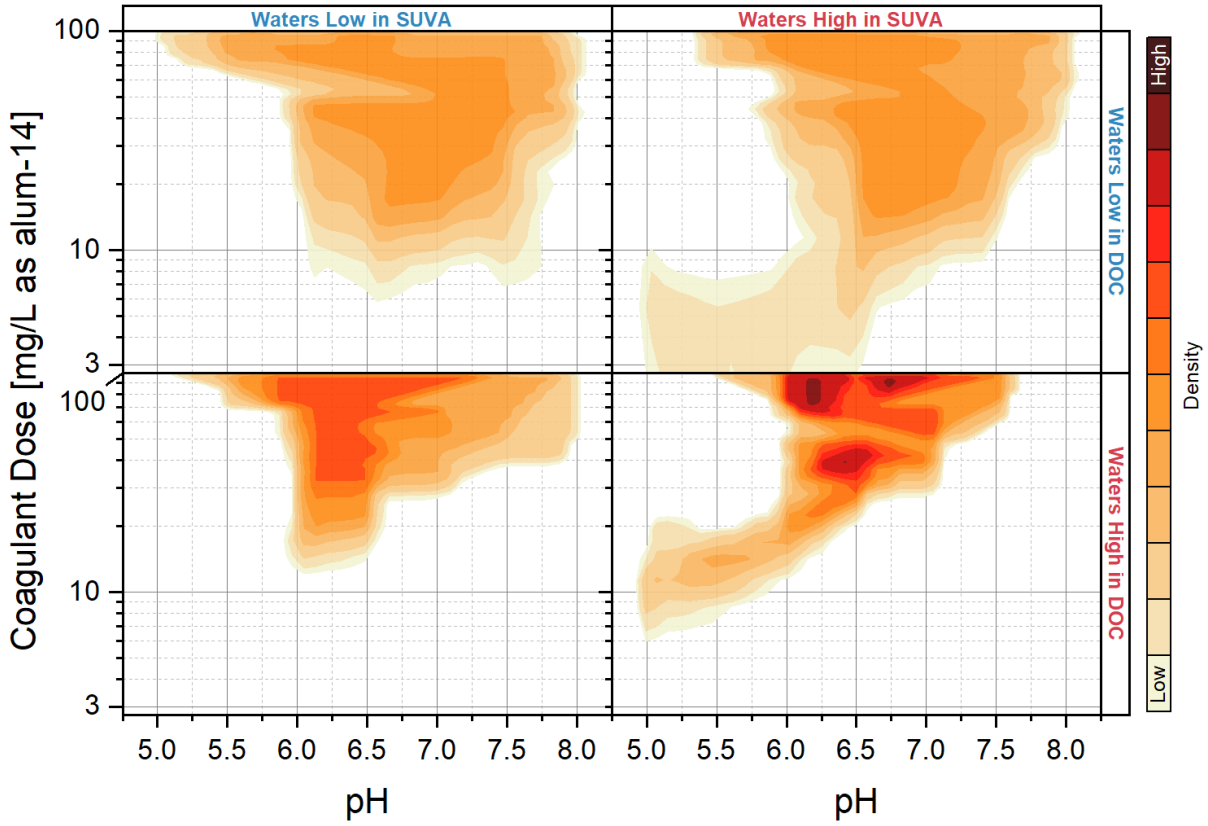

Figure E1. Combined effects of DOC and SUVA on effective coagulation conditions

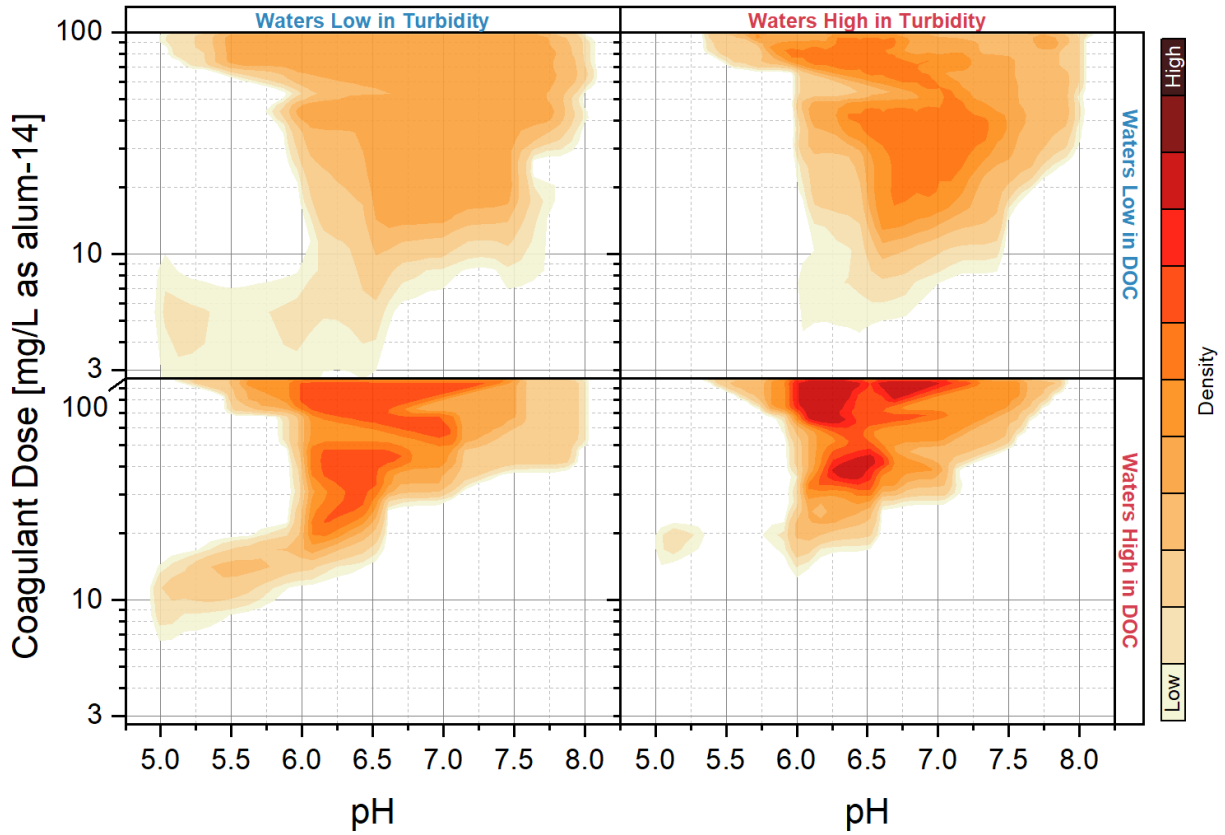

Figure E2. Combined effects of DOC and turbidity on effective coagulation conditions

APPENDIX F: PLANT DATA

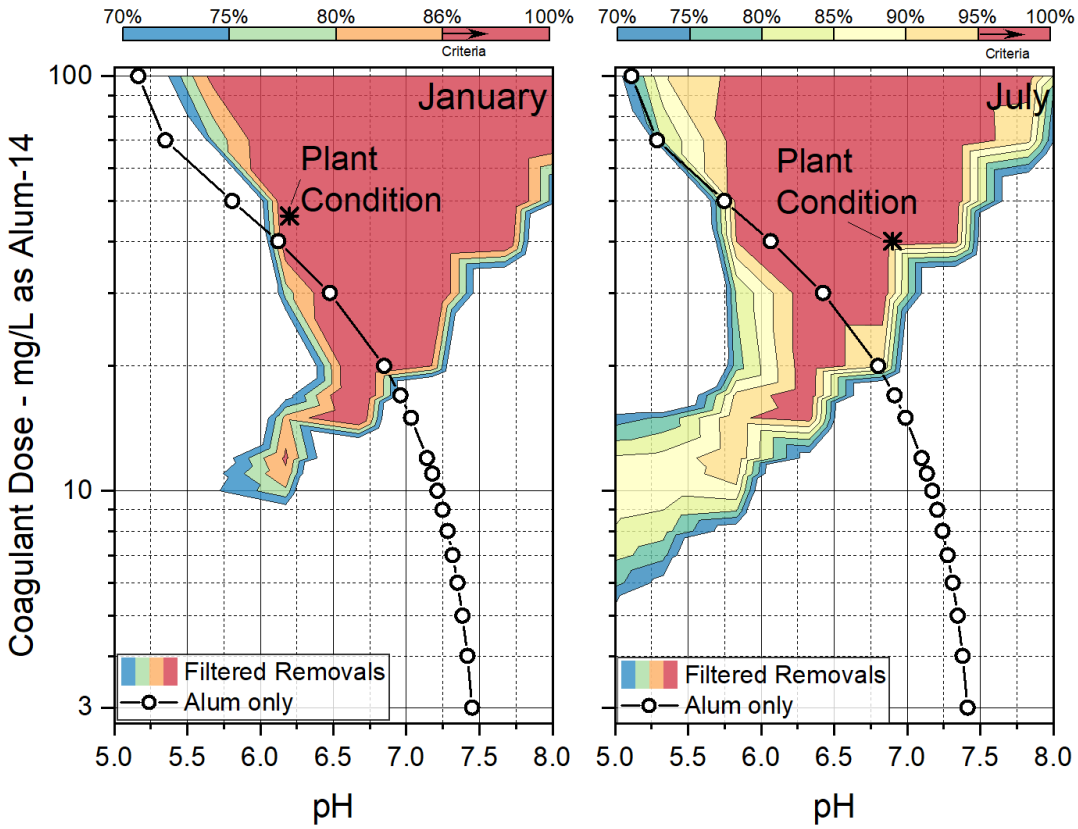

Figure F1. Predicted filtered turbidity removals for Plant 6 (interpolation)

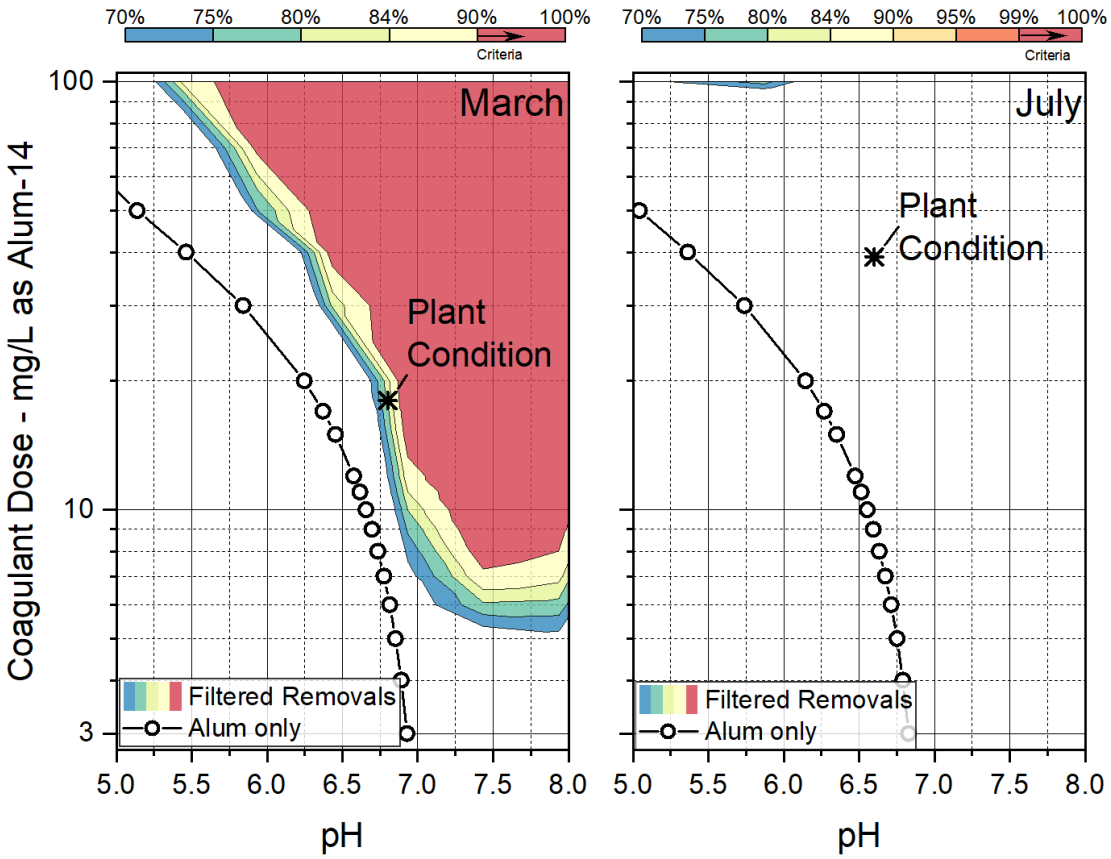

Figure F2. Predicted filtered turbidity removals for Plant 8 (extrapolation)